Österreichische Beiträge zu Meteorologie und Geophysik

ISSN 1016-6254

Heft 14

PROCEEDINGS OF THE 7TH INTERNATIONAL MEETING ON ALPINE GRAVIMETRY VIENNA 1996

edited by
Bruno Meurers
Zentralanstalt für Meteorologie und Geodynamik, Wien

Wien 1996

Österreichische Beiträge zu
Meteorologie und Geophysik

Heft 14

PROCEEDINGS OF THE 7TH INTERNATIONAL MEETING ON ALPINE GRAVIMETRY VIENNA 1996

edited by Bruno Meurers

Wien 1996

Zentralanstalt für Meteorologie und Geodynamik, Wien

Publ.Nr. 373

ISSN 1016-6254

IMPRESSUM

Herausgeber: Peter Steinhauser
Zentralanstalt für Meteorologie und Geodynamik
Hohe Warte 38, 1190 Wien
Austria (Österreich)
Siegfried J. Bauer
Institut für Meteorologie und Geophysik, Universität Graz
Helmut Pichler
Institut für Meteorologie und Geophysik, Universität Innsbruck

Redaktion: Peter Steinhauser

für den Inhalt verantwortlich: Bruno Meurers

Druck: Robitschek & Co. Ges.m.b.H.
Schloßgasse 10-12, A-1050 Wien

Verlag: Zentralanstalt für Meteorologie und Geodynamik, Wien

Preface

The 7th International Meeting on „Alpine Gravimetry" was held in Vienna on April 11 - 12, 1996, organized by the Institute of Meteorology and Geophysics (University of Vienna). The meeting took place in the new University Campus UZA II, which offered quite good facilities and a pleasant atmosphere to the participants. Scientists from 6 countries (Austria, Czechia, Germany, Hungary, Slovakia and Slovenia) attended this meeting and contributed to an interesting program by 25 oral presentations. Similar to former meetings the main topics were concerned with gravity investigations especially in high mountainous areas, theoretical and practical aspects of gravity interpretation and with instrumental problems of absolute and relative gravimetry. Of course, the areas of interest were not restricted to the Alps, just contrary most of the contributions dealed with investigations in quite different parts of Europe (Bohemian Massif, Western Carpathians, Pannonian Basin, Scandinavian Caledonides) and even of South America (Central Andes). Maybe it is necessary to change the workshop title of future meetings to address more properly the whole field of gravimetric research.

The meeting started with gravity field interpretation. G.Walach (MU Leoben) and H.J.Götze (FU Berlin) acted as chairpersons of the first two sessions regarding this topic. Local problems as well as and regional aspects were discussed including geodynamics and tectonics of crust and upper mantle in the Central Andes and in different european orogenies. At the end of the first afternoon session P.Varga (GGKI, Sopron) presented his interesting paper about laboratory gravimetry which was formerly scheduled at Friday afternoon and had to be shifted due to personal reasons. The following session was dedicated to the interdisciplinary research of physical geodesy and geophysics. H.Lichtenegger (TU Graz) presided over this third session dealing with the interpretation of the local geoid in Hungary and with the projected new geoid computation in Austria including reports about preparatory activities. This „Geoid 2000" solution and also a new Bouguer gravity map of Austria will hopefully be open for discussion during the next meeting. The last two sessions were guided by H.Granser (OMV) and F.Weber (MU Leoben). They were concerned with 3-D gravity field modeling, physical filtering, theoretical aspects of special interpretation methods, GPS based coordinate determination in gravity surveying and instrumental problems in high precision gravimetry. The meeting was closed by a review of gravimetry in engineering and environmental geophysics.

The present proceedings contain all manuscripts received before mid of July 1996. The former deadline of 31 May had to be postponed on request of several authors. Fortunately only one paper is missing. The contributions are arranged in the same order as presented during the meeting.

Again I wish to express my cordial gratitude

- to all participants, who contributed to a successful meeting with their presentations and fruitful discussions,
- to the authors for preparing camera ready manuscripts,
- to the chairmen, who took care for exactly holding the program schedule and often introduced valuable stimulation into the discussion,
- and last, but not least, to all colleagues having supported the organization, and to the Central Institute of Meteorology and Geodynamics for publishing these proceedings in a special issue of "Österreichische Beiträge zu Meteorologie und Geophysik".

Vienna, July 1996 Bruno Meurers

Contents and Program:

A) No paper available.

B) Only abstract available. Parts of this contribution are submitted for publication already. References are given at the end of the abstract.

[c] Only abstract available.

GRAVITY FIELD AND GEOID AT THE SOUTH AMERICAN ACTIVE MARGIN (20° to 29° S)

Hans-Jürgen Götze and Andreas Kirchner

Institut für Geologie, Geophysik und Geoinformatik, FU Berlin, Haus N, Malteserstraße 74-100, D-12249 Berlin, Germany; Email: hajo@zedat.fu-berlin.de

Abstract:

Most recently the MIGRA group with participants from Chile, Argentina and Germany has surveyed some 3.500 new gravity observations in an Andean Geotraverse covering N-Chile and NW-Argentina between 64°- 71° W and 20° - 29° S. MIGRA is an international gravity research group which was established under the umbrella of the "Collaborative Research Center" "Deformation Processes in the Andes" at Freie Universität Berlin (Germany). Oil and mining industry gravity data were reprocessed and included into the MIGRA data base which contains more than 15.000 gravity data at present. Due to severe logistical problems (terrain access, no maps, no levelling lines etc.) the overall error of the calculated gravity anomalies results of approximately 4 - 5 mGal which is about 1% compared with the magnitude of ca. 450 mGal of the Bouguer anomaly. Under the framework of the interdisciplinary research project CINCA (**C**rustal **I**nvestigations Off- and Onshore **N**azca/**C**entral **A**ndes) gravity surveys of the MIGRA group has been extended to the Pacific ocean. In summer 1995 MIGRA took part in the "CINCA" offshore experiment SO - 104 of the german research vessel "Sonne" between the latitudes 20° S and 24° S.

The entire data base which includes point data and 10 km * 10 km data grids of free-air-, different types of Bouguer- and isostatic-residual anomalies are presented here in maps of the isostatic residual field along with a preliminary interpretation by 3D density modelling. Constraints were mainly taken from modelling results of the seismic research group (C4) of the "Collaborative Research Center 267". In addition to this our interpretation benefits from intensive discussions with project C1 (Structural evolution in the magmatic arc).

KEY WORDS: Gravity field, geoid, tectonics, 3D modelling, offshore gravity, Central Andes.

INTRODUCTION

From 1993 to 1996 the international MIGRA group with participants from Chile, Argentina and Germany has surveyed some 3.500 new gravity observations in an Andean geotraverse covering N-Chile and NW-Argentina between 64°- 71° W and 20° - 29° S. MIGRA is a Spanish acronym for "**M**ediciones **I**nternacionales de **GR**avedad en los **A**ndes" (Götze and Schmidt, 1993). Including reprocessed older data of Freie Universität Berlin, South American universities, oil and mining industry, now there is a data base of about 15.000 gravity values available, which can be used together with other geophysical and geological information for an interdisciplinary interpretation of the structure and evolution of the Central Andes (Götze et al. 1995; Götze and the MIGRA group 1996). In summer 1995 MIGRA took part in the "CINCA" offshore experiment of the german research vessel "Sonne" between the latitudes 20° S to 24° S. The offshore gravity data are connected with the onland survey and linked to the IGSN 71 to draw a complete gravity picture of this ocean-continent transition.

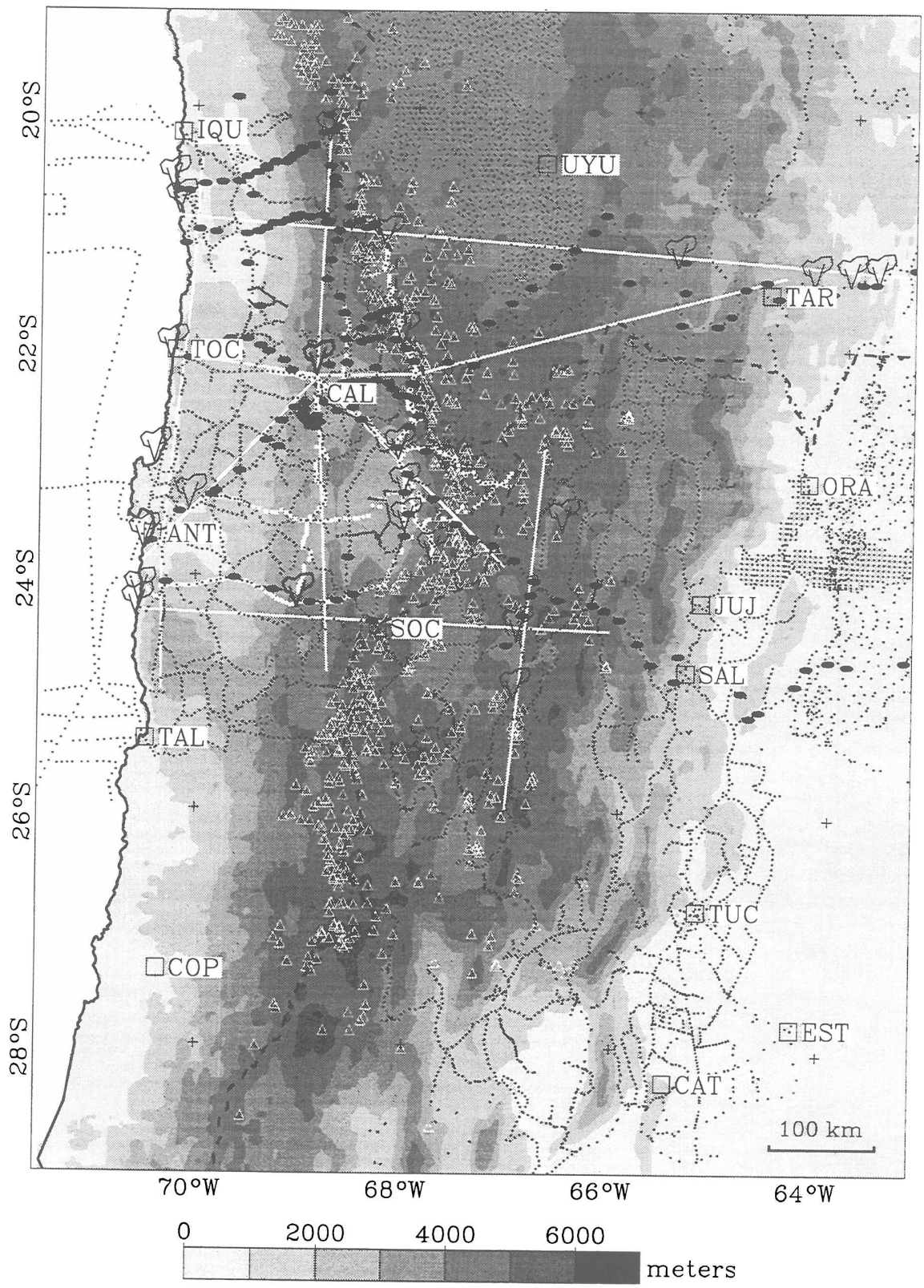

Figure 1: Topography and geophysical database of the Collaborative Research Center 267 in the Central Andes between latitude 20 ° and 29° S. The topography grid has been taken from Isacks (1988). Volcanoes present the magmatic arc (white triangels). Seismic refraction lines and shot points (white lines) are shown together with magnetotelluric (black ellipses) and gravity sites (black dots). IQU = Iquique, CAL = Calama, ANT = Antofagasta, TAL = Taltal, UYU = Uyuni, TAR = Tarija, ORA = Orán, SOC = Paso Socompa, JUJ = Jujuy, SAL = Salta, TUC = Tucumán, CAT = Catamarca.

The previous network of gravity data in the Central Andes [e.g. Dragicevic, 1970] was only coarse-meshed and suitable for regional gravity field interpretations. In 1982, the departments of Earth Sciences at Freie and Technische Universität Berlin launched a Research Unit entitled "Mobility of Active Continental Margins". It was the project's intention to provide more insight into lithospheric structures and the evolution of the Central Andes in a segment between 20° and 26° latitude south. An interdisciplinary approach comprised a variety of geophysical, geological, and petrological studies [Reutter et al., 1994]. Both gravity field research and reprocessing of older data were done under this project.

This Research Unit was the "pathfinder" of a second scientific project, the "Collaborative Research Center 267, (SFB 267)" called "Deformation Processes in the Central Andes" which was established at the Freie and Technische Universität Berlin, GeoForschungsZentrum Potsdam and the University Potdam. It is financed by the Deutsche Forschungsgemeinschaft, the Universities, and the GeoResearchCenter and concentrates interdisciplinary geoscientific research on the Central Andes crossing the fields of geology, geophysics, geodesy, remote sensing, mineralogy and geochemistry. Under the umbrella of this longterm project, 17 task groups are aiming at a better understanding of the crustal processes acting at this convergent plate margin by both laboratory and field campaigns. Among the task groups of "SFB 267" we work towards data aquisition, processing and interdisciplinary interpretation of potential fields including the geoid. In particular, the gravity group focuses on the following subjects: (1) construction of a modern gravity data base tied to international standard networks by reprocessing existing data and complementing them with new field surveys, and (2) interdisciplinary interpretation of gravity. As in the case of other foreign research programs, successful work in this difficultly accessible region is possible only through the assistance and incorporation of South American colleagues. Toward this end, MIGRA combines and concentrates forces of experts from both the European and South American sides.

ONSHORE FIELD WORK AND REDUCTIONS

The investigated region covers a 900 km x 1.000 km area in the central part of the Andean orogenic system (Figure 1). The young Andean orogen between 20° - 29° S comprises different structures which have evolved on a Precambrian-Paleozoic basement (e.g. Reutter et al., 1994). This belt of ancient rocks was also described as the border of the "Faja Eruptiva Occidental". Two of our gravity surveys obtained structural information with new stations covering the northern and southern edges of this belt, near Calama (Chile) and in the southern Argentinean Puna respectively. The investigated area is characterized by its enormous topography and remoteness, by its aridity, low population density and limited infrastructure. Other difficulties limiting our field work were the lack of topographic maps and geodetic networks in some regions. The spacing of stations amounts to approximately 5 km along all passable tracks aside from some local areas with a higher station density. To complete this data base we included gravity observations from different sources (Table 1). With the exception of some inaccessible regions in the "Eastern" and "Western Cordillera", the gravity coverage for the region is fairly uniform. All measurements are tied to the IGSN71 gravity datum at base stations in Oran/Argentina, Iquique/Chile and Tucumán/Argentina (Götze et al. 1994; Götze and the MIGRA group 1996).

The large size of the area and the severe logistical problems did not always allow us to determine the drift of the gravity meters by repeating the measurements at each station. However, even when we used bad tracks, the drift of the LaCoste & Romberg instruments (model G) rarely exceeded 0.1 mGal per day. Only about 35% of the gravity sites could be tied directly to benchmarks, such as levelling lines or trigonometric heights, so we used altimeters for height determinations. To improve the quality of our barometric measurements, we calculated time-dependent drift corrections as it is usually done for gravity measurements, using as many benchmarks and repeated measurements as possible.

Number	Source	State
873	YPFB (Santa Cruz, National Oil Company)	Bolivia
462	IGM (Instituto Geográfico Militar, La Paz)	Bolivia
4100	FU Berlin/UdChile (1981 - 1985)	Germany
3500	FU Berlin/UdChile (1993 - 1996)	Germany
2120	CODELCO (Santiago); National Copper Mining Company; high station density	Chile
3427	ENAP (Santiago); National Oil Company; high station density	Chile
344	BGI (Bureau Gravimétrique International, Toulouse)	France
311	YPF (Buenos Aires, National Oil Company)	Argentina
53	Geodetic Institute, University of Buenos Aires	Argentina

Table 1: Data sources of the "Central Andes" gravity data base.

Moreover, the profiles with common altimeter stations of several days were tied together in order to eliminate systematic errors. The scales of the barometers have been calibrated on levelling lines with an altitude difference of about 2.000 m. Error estimations showed that even in the worst case the accuracy was better than 20 m, giving an error in the Bouguer anomaly of about 4 mGal, which is less than 1% of the overall magnitude of more than 450 mGal (Figure 2).

The basis of the calculation of gravity anomaly values are the following equations:

$$CBA = g_{abs} - \gamma_h + \delta g_{top} + \delta g_{bou} \qquad \textit{complete Bouguer anomaly} \quad (1)$$

$$FA = g_{abs} - \gamma_h \qquad \textit{complete Free-air anomaly} \quad (2)$$

with:

g_{abs} : absolute gravity at station (measured) tied to the ISGN71 datum,
γ_h : normal gravity at station level h; Normal Gravity Formula of 1967,
δg_{top} : true 3D topographic reduction,
δg_{bou} : Bouguer reduction.

For the terrain correction (up to 167 km around all stations), a method including calculations of the earth´s curvature developed for gravity investigations in the Alps was used, after adapting it to the special situation in the Central Andes. Reduction density was 2.67 g/cm^3 and a digital terrain model (Isacks, 1988) was used to calculate true 3D terrain corrections for each gravity station including the reprocessed gravity sites of older surveys. For different morphological units we obtained the following typical values of topographic reduction: Longitudinal valley and Chaco region: 0.5 - 1 mGal, Coastal, Pre- and Western Cordillera, Altiplano/Puna and Subandean Belt: 1 - 10 mGal and steep coast and Eastern Cordillera: 10 - 25 mGal.

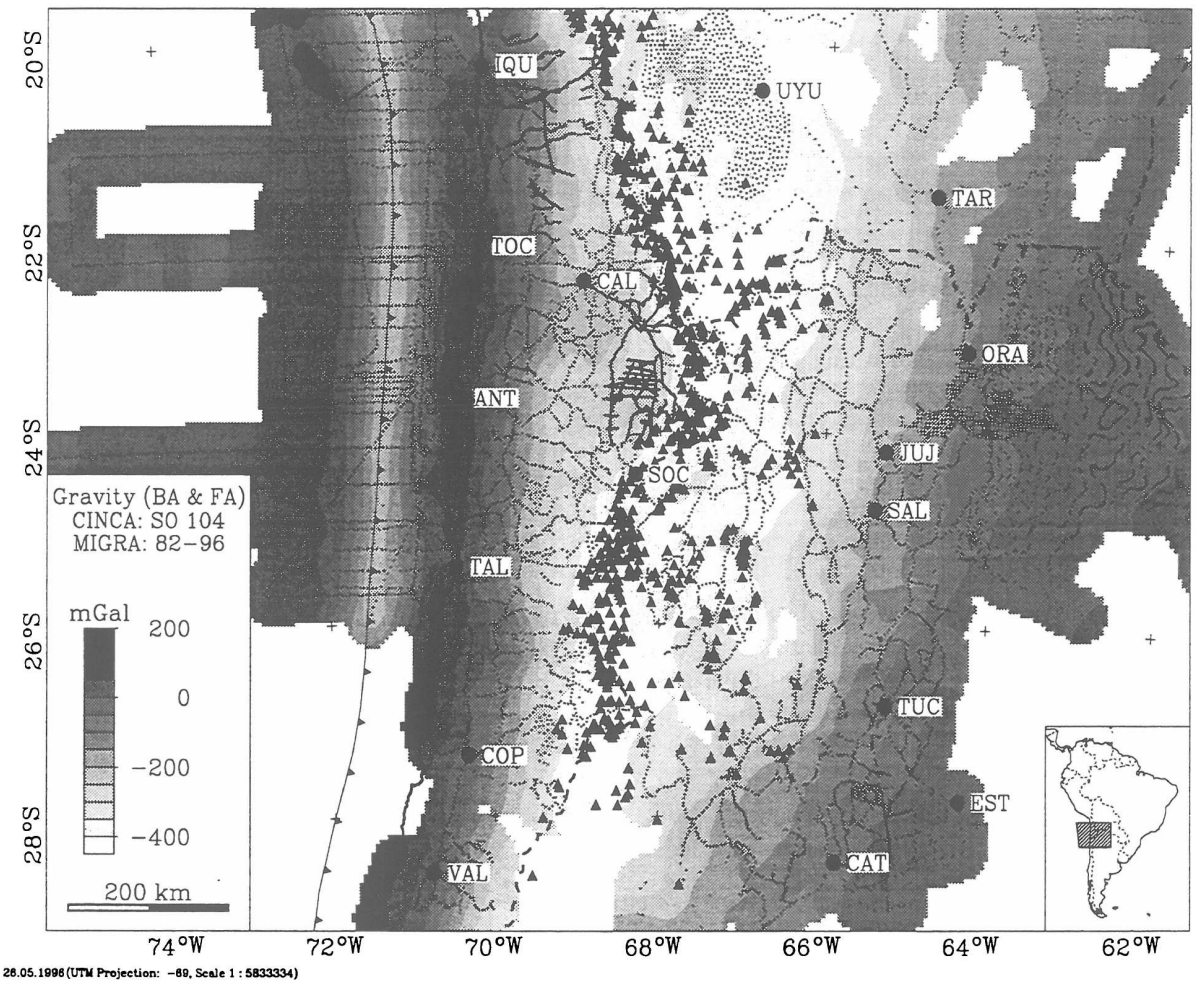

Figure 2: The Bouguer anomaly of the Central Andes with 10 mGal contour lines. In the offshore area the Bouguer anomaly was replaced by Free air anomalies. We merged results of the CINCA 1995 campaign of the german research vessel SONNE with results of the onland gravity research of MIGRA.

OFFSHORE GRAVITY AND DATA ACCURACY

Gravity data at sea were collected along continous survey lines (some 8.000 km) during the CINCA offshore experiment SO - 104 of the german research vessel "Sonne". The average density of observational sites amounts of about 15 observations per km. Gravity survey of cruise SO - 104 was tied to the Chilean National Gravity network of the "Departamento Geofísico, Universidad de Chile, Santiago" at reference stations in Valparaiso, Antofagasta and Iquique. The drift of the KSS31/32 onboard gravity sensor was low and amounts to -0.048 mGal/day, or -1.44 mGal/month, respectively. The overall drift of the gravity meter was determined to be 0.47 mGal per 92 days.

Further information about the accuracy of the offshore survey provide the so called "misties". Misties are crossover errors if the gravity readings of two crossing lines are compared. Assuming that this accuracy depends mainly on the gravity sensor several methods have been invented to minimize crossover errors (e.g. Prince and Forsyth, 1984). It has also been argued that misties are frequently caused by bad positioning (Fritsch and Roeser, 1986). Anyway, statistical treatments of misties at intersections of survey lines reveals the precision of the

offshore gravity measurements including auxiliary physical quantities. On the 1st leg of cruise S0-104 about 44 intersections have been obtained. Some 80 % of gravity misties were less than 1 mGal and about 80 % of the water depth misties were less than 9 m. These data show the high precision of both gravity and waterdepth measurements on cruise So 104/1. The 2nd leg of the survey was characterized by a more complicated topology of crossing profiles due to the wide angle reflection experiments which required gravity measurements at the same line for three times. Therefore, a more sophisticated algorithm has been used to estimate crossover errors. In total, the accuracy of the gravity survey is truly better than 1 mGal, and accuracy of water depth determinations are better than 10 m (Fritsch, pers. comm.).

GRAVITY ANOMALIES AND GEOID

Onshore the Bouguer anomaly drops down to a regional minimum of about - 450 mGal in the area of the recent volcanic arc, related to crustal thickening by isostatic compensation. The effect of isostatic compensation of topography was calculated assuming the model of Vening-Meinesz with the following parameters: density contrast of the earth's mantle and crust ΔRHO = 0.35 g/cm^3, a normal crustal thickness of 35 km and a flexural rigidity of 10 ^{23} Nm. The gravity effect of the isostatic compensation root was eliminated from the Bouguer gravity and the resulting anomaly serves as a residual field (Fig. 3).

The most interesting features of this field (Figure 3) are:

(1) Positive values in the area of the forearc with isolated complexes parallel to the coastline. They are regionally caused by the presence of the dense subducting plate (gravity effect of about 50 mGal; density contrast: 0.05 g/cm^3) and locally by uplifted jurassic batholiths intruded into the "Formación La Negra". Most surprisingly the belt of positive residual gravity continues north of Taltal in the shelf area offshore South America.

(2) The NNW-SSE striking positive anomaly from Calama (CAL) by the Salar de Atacama to southern Puna extending from the forearc region via the recent volcanic arc into the backarc region of NW Argentina. We explain this gravity maximum by a highly metamorphic and high-density Paleozoic/Precambrian structure, the "Faja Eruptiva Occidental", which is oblique to the N-S orientation of the recent volcanic belt.

(3) Local minima along the recent volcanic arc point to reservoirs of partly molten material at depths of 15 - 20 km.

(4) Minima following a line from Ollagüe (OLL) to Calama (CAL) along 69° W, are caused by the Eocene volcanic arc with low-density volcanic material in the upper crust.

(5) Alternating gravity highs and lows in the backarc region east of 67° W are observed in wide areas of the Argentine Puna and the Eastern Cordillera with a general NE-SW trend. The minima point to the position of mesozoic basins which are located in the

Argentine Puna and extend northward to the territory of Bolivia. Gravity highs correlate with outcrops of Precambrian/Paleozoic basement in the Puna and Eastern Cordillera. 3D forward modelling of both gravity and gravity potential (geoid) can explain that most of the observed geoid anomaly (undulation) of 50 - 60 m is caused by Andean topography and isostatic roots. However, also density inhomogeneities in the downgoing slab and in the asthenospheric wedge contribute to undulations of the Earth's geoid in the Central Andes. All 3D density modelling has been proven by the results of refraction seismics (e.g. Wigger et al., 1994; Schmitz 1993, 1994).

3D MODELLING

A large scaled 3D density model was constructed to investigate the regional structure and density distribution of the Andean lithosphere. The modelled area reaches from 12° to 35° S and from 57° to 79°W comprising large parts of both the Nazca Plate in the West and the Brasilian Shield east of the Andean orogen as a reference lithosphere. The principal parts of the model are the downgoing Nazca Plate, Andean crust, continental lithosphere with Brasilian shield crust and an astenospheric wedge.

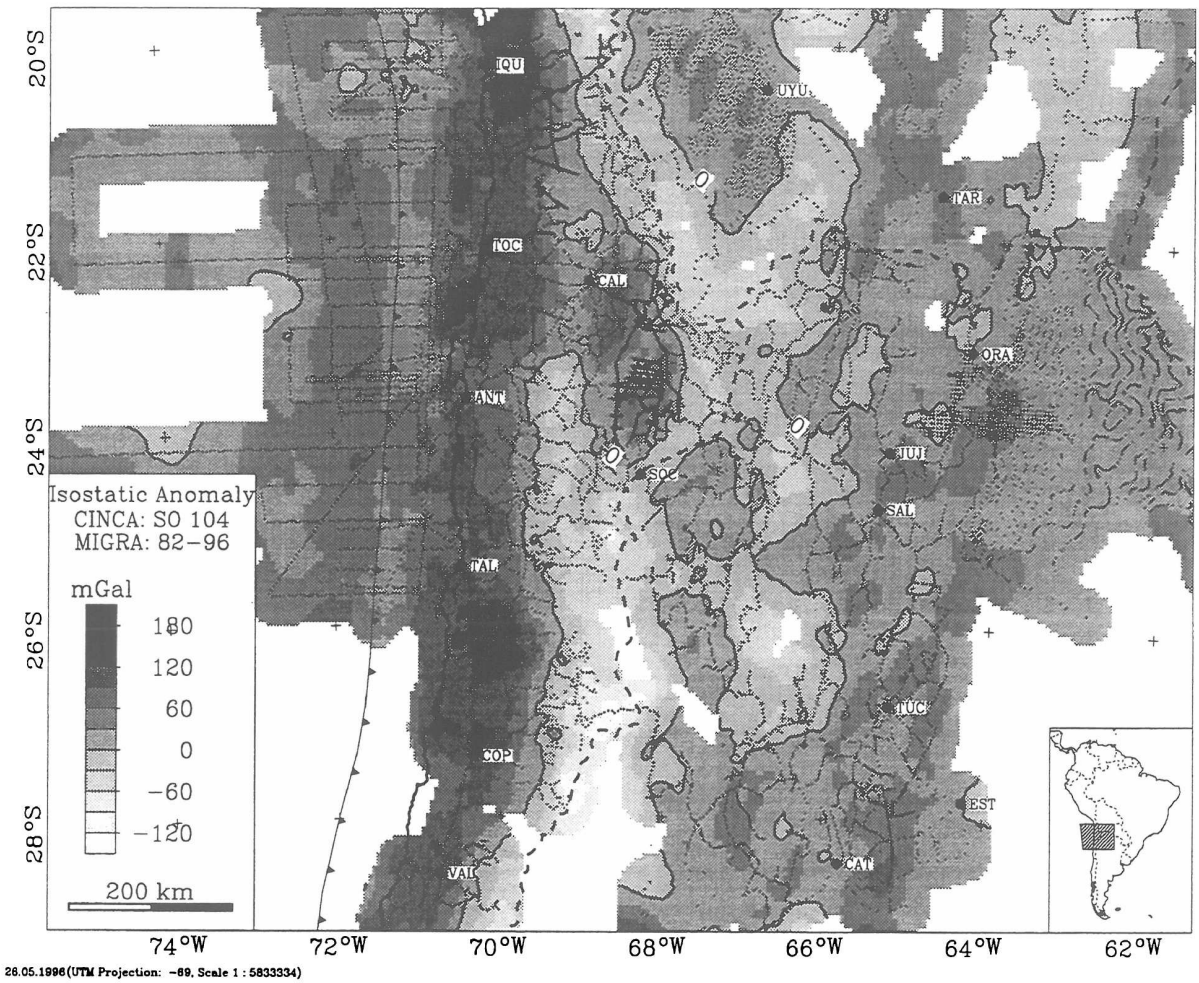

Figure 3: Residual gravity field of the Central Andes. Color shades contour gravity by 10 mGal intervals. Gravity stations are shown and the 0 - mGal contour line.

The model resembles the new results of refraction seismics based on two WE and two NS trending ray tracing models at 24° and 23.5° and 68° and 69° W respectively as described above. Additionally, a balanced cross section at 21° S according to earlier refraction seismics (Schmitz, 1994) was included. As a preliminary study the velocities of seismic models were directly converted into densities by using e.g. the Nafe & Drake relationship or similar velocity-density relationships. Initial model geometry was slightly modified by the use of interactive computer graphics to verify regional trends implied by the Bouguer gravity field and the topography-reduced geoid. Fig. Y shows the major crustal parts of the density model at 23.5° S.

In the forearc a 10 km thick upper crust with a density of 2.85 g/cm^3 tops a 20 km thick high-density lower crust material (2.95-2.93 g/cm^3), followed by parts with reduced density (2.93-2.90 g/cm^3) which are interpreted as serpentinized Pre-Andean mantle material. In the Precordillera the upper crust thickens to about 20 km with its density decreasing to 2.77 g/cm^3. It can be followed to the recent arc with the same thickness and again decreasing density (2.73 g/cm^3). Towards the back arc the upper crust base rises to 15 km, its density increasing to Precordilleran values. The Coastal Cordilleran high-density material can also be pursued in WE direction with decreasing densities down to 2.86 g/cm^3 and its base reaching 40 km as it passes beneath the recent arc. There is a low-density zone of 2.70 g/cm^3 underneath the volcanic chain between 20 and 35 km depth resembling the LVZ detected by refraction seismics.

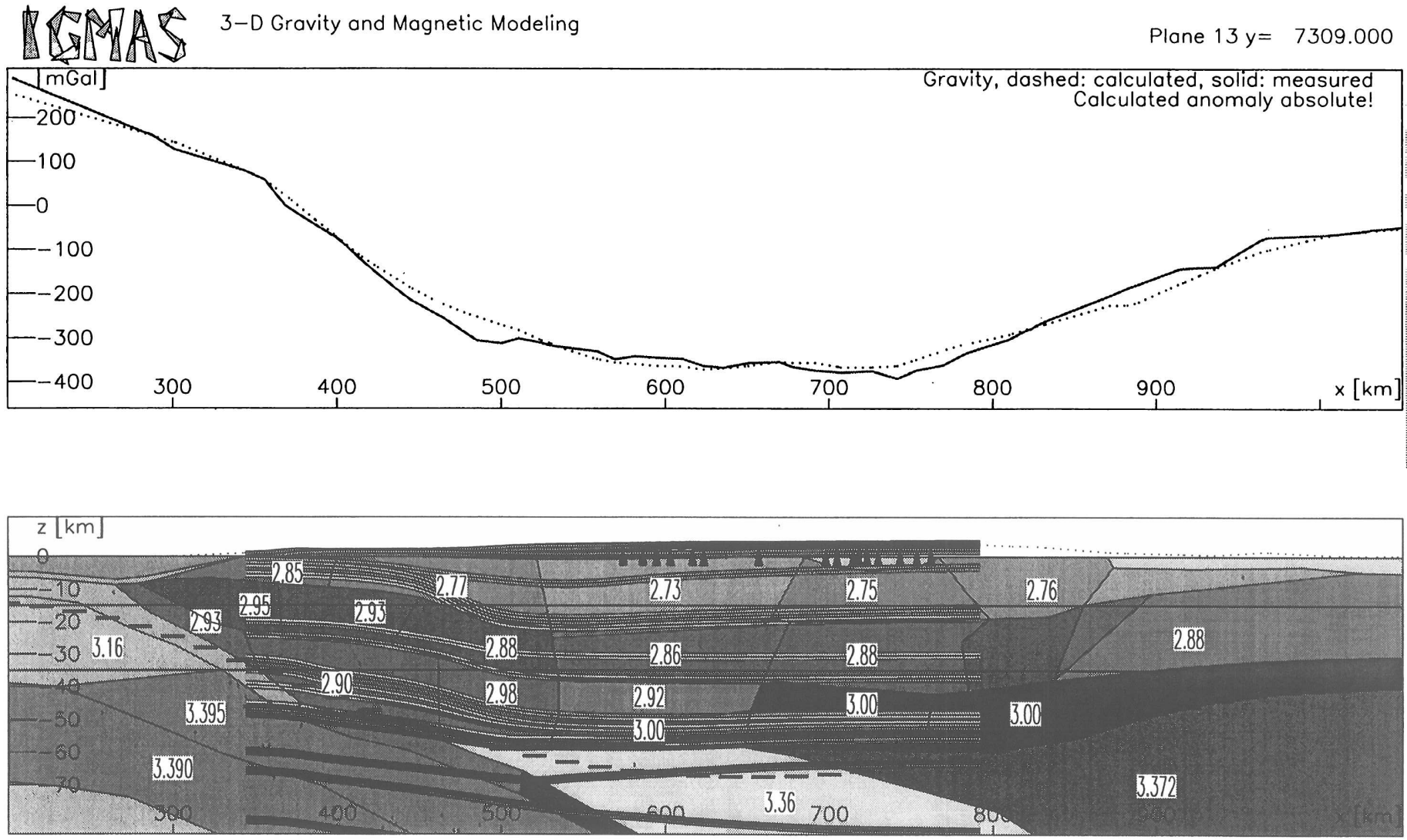

Figure 4: A cross section of the 3D density model along latitude 24° S. The image contains the density domains and shows the constraints that were used from seismics research and seismology (e.g. Schmitz 1994; Wigger et al., 1994). The assymetry of the gravity field reflects the different crustal behavior of Andean crust in the forearc with a high density distribution and in the backarc with lower density.

Lower crustal bodies are modelled with a density of 2.98-3.00 g/cm^3 below 40 km placing the "gravimetric" moho to a depth of approximately 60 km according to 2D ray tracing models. A seismically implied second low-density zone is modelled between 44 and 50 km with a density of 2.92 g/cm^3.

The Brasilian shield crust consists of a 4-6 km thick sedimentary cover (2.45 g/cm^3) followed by a 2.88 g/cm^3 mid crustal body and a lower crust down to 40 km with a thickness of 10~km and a density of 3.00 g/cm^3. The shield crust lies on top of the continental lithosphere modelled with a density of 3.37 g/cm^3.

The shape of the subducting Nazca Plate is inferred from results of Cahill, 1992 and earthquake hypocenters of the PISCO 94 seismic catalogue (Asch, Rudloff, Graeber, pers. comm.). For definition of the descending angle in the forearc there are moho observations by refraction seismics between 21° and 24° S. The transition of a 2.90 g/cm^3 oceanic crust to a 3.5 g/cm^3 eclogite layer on top of the downgoing slab, which starts at about 50 km and is completed at 70 km depth, is simulated by a model body with a density of 3.15 g/cm^3 of oceanic crustal thickness within this depth range. In the model we present here the subducting Nazca Plate is modelled down to 670 km with a mean density contrast to the surrounding asthenosphere of 0.02 g/cm^3.

The model also contains an asthenospheric wedge with a density of 3.36 g/cm^3 filling the space between the slab and the shield lithosphere. According to studies on Andean magmatism (Kay, 1994) and P-wave attenuation (Whitman, 1992) it reaches the crustal root beneath the recent arc with an alongstrike change of geometry.

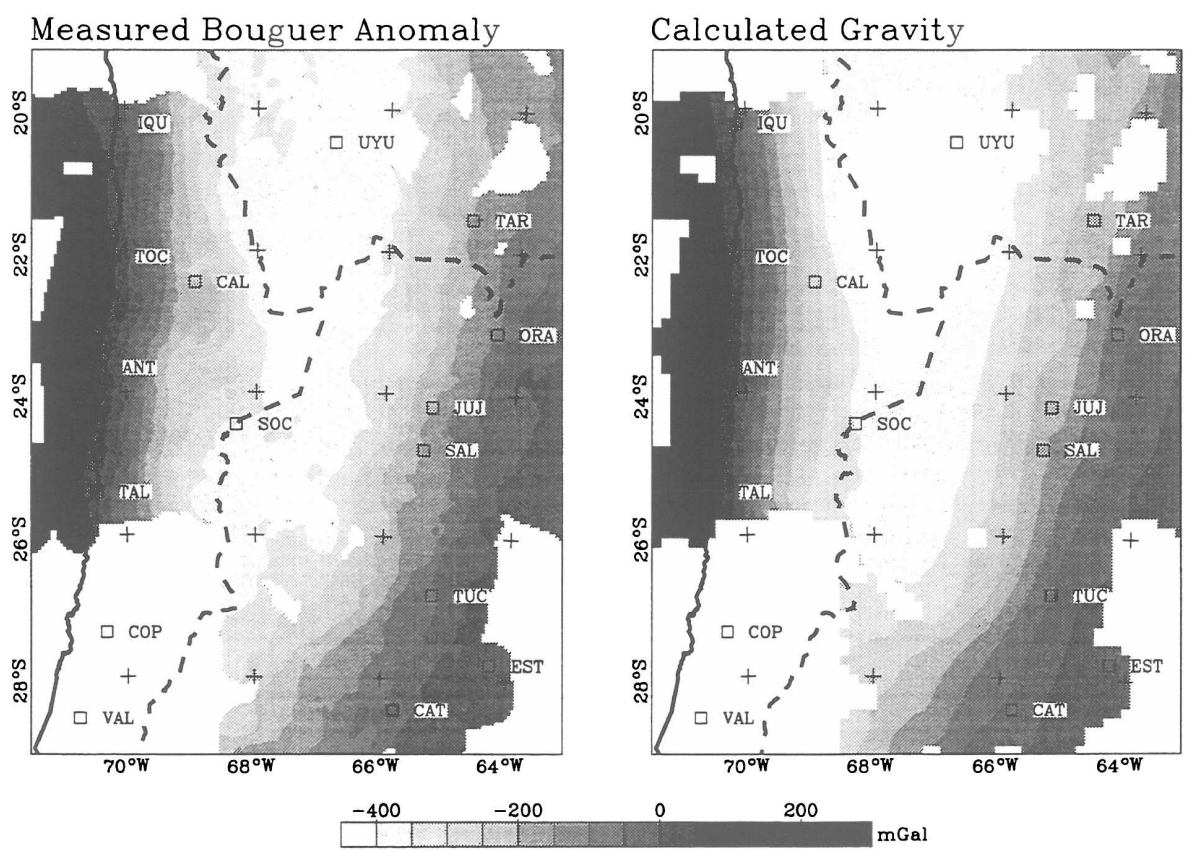

Figure 5: Comparison of 3D modelling results with the measured gravity data base in the Central Andes. The fit of both measured and modelled field is fairly good and reflects the coincidence of the density model and the results of other geophysical methods.

SFB 267
MIGRA
Gravity Group, D3
Elevation, Isostasy
and Gravity

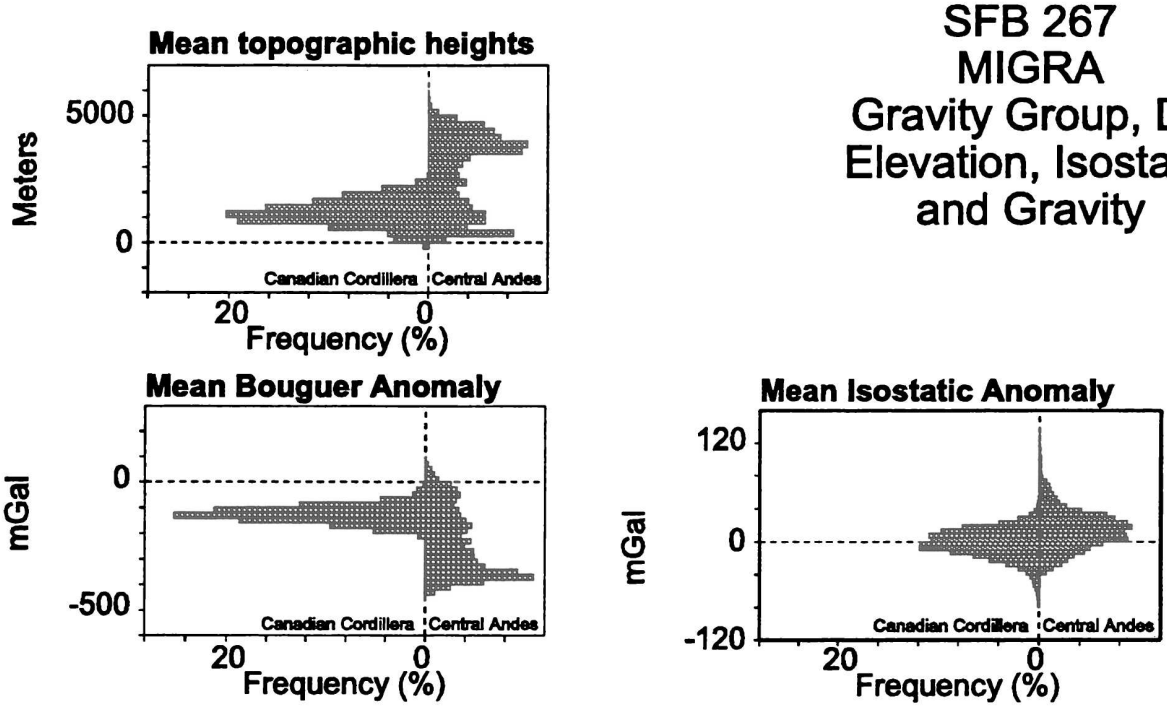

Topographic profiles and Moho

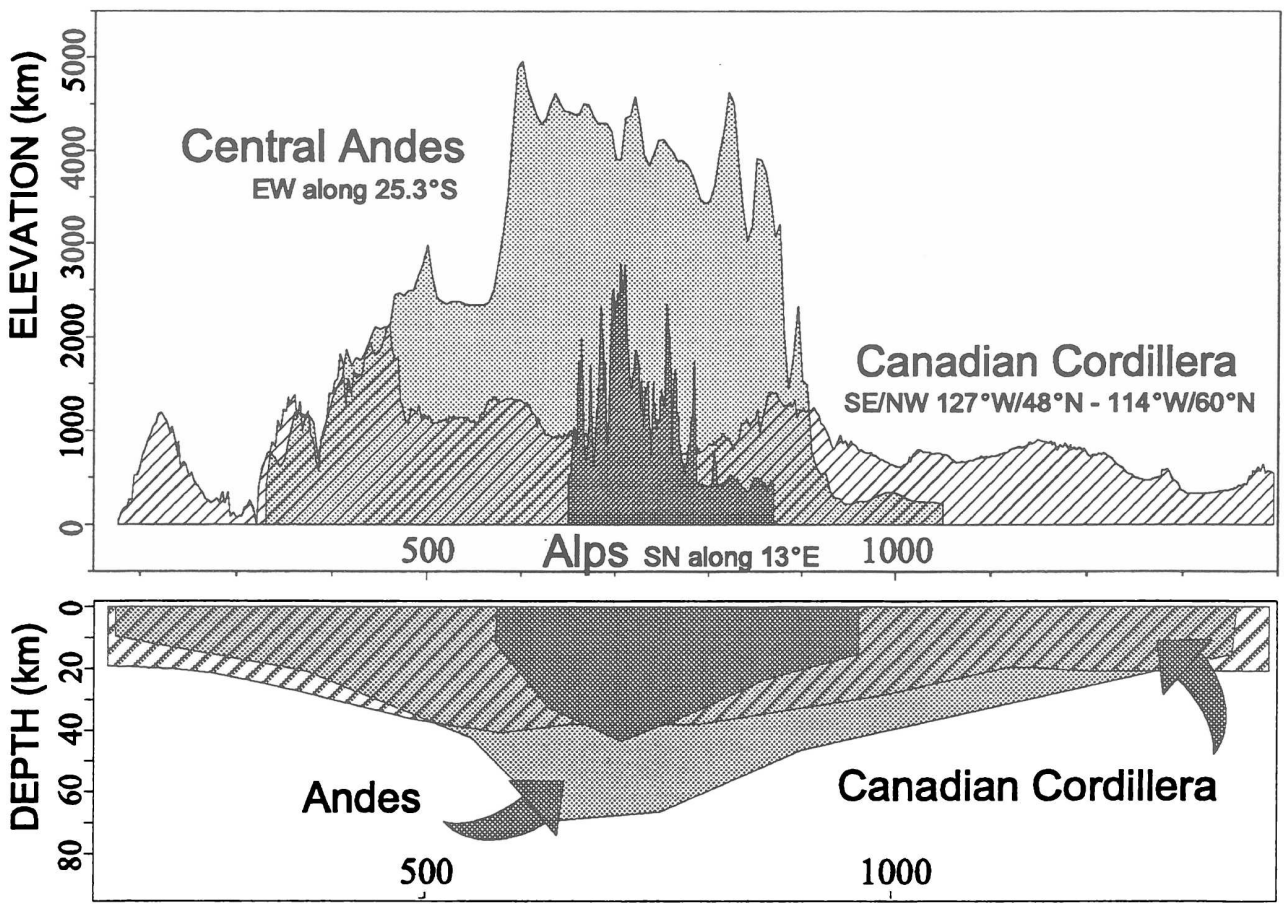

Figure 6: A comparison of mean topography, Bouguer gravity, isostatic anomaly and Moho depth along three profiles (Central Andes, Eastern Alps and Canadian Cordillera). The figure underlines the extraordinary role the Andes play among the other orogenies of the world.

CONCLUSIONS

The updated gravity data base will play an important role in both local investigations of applied geophysics and regional interdisciplinary interpretations concerning the evolution and present state of active continental margins. Modern 3D modelling techniques of both geoid and gravity in combination with Geoscientific Information System facilities can provide new inside into the physical behavior of the crust-mantle system and its recent geometry. A preliminary statistical comparison (Figure 6) of mean topography, Bouguer gravity and isostatic field is shown together with three typical vertical cross-sections of the topography and Moho surface of the Andes, the Alps and the Canadian Cordillera. The gravity field seems to be a sensitive indicator which is linked to many processes contributing to the tectonic framework of young orogenies.

MIGRA data sets are available via FTP for non commercial applications of universities and governmental agencies. You may contact H.-J. Götze at Freie Universität Berlin (Germany) under "hajo@zedat.fu-berlin.de" or refer to the "Gravity Research Group´s" Home page on the WWW for further information: http://userpage.fu-berlin.de/~wwwgravi.

ACKNOWLEDGEMENT

The support with maps and geodetic information by the following institutions is gratefully acknowledged: Institutos Geográficos Militares in Santiago, Buenos Aires and La Paz, Yacimientos Petrolíferos Fiscales of Argentina and Bolivia, Empresa Nacional de Petróleo, and CODELCO both from Chile. This paper presents results of the 1995 "CINCA" offshore experiment SO - 104 of the german research vessel "Sonne". Processing and interpretation of gravity data are part of a joint project of the gravity research group at Bundesanstalt für Geowissenschaften und Rohstoffe (Hannover) and the gravity research project D3 of the SFB 267 which is funded by the Deutsche Forschungsgemeinschaft (DFG) and Freie Universität Berlin. This paper contributes also to the IGCP 345.

REFERENCES

Dragicevic, M., Carta gravimétrica de los Andes meridionales e interpretación de las anomalías de gravedad de Chile central. *Publ. 93*, Dep. de Geofis. y Geod., Univ. de Chile, Santiago, 1970

Fritsch, J. and H.A. Roeser 1988. On the accuracy of gravity measurements at sea. Geologisches Jahrbuch, E 42, 195 - 208.

Götze, H.-J. und S. Schmidt, 1993. El que conocio el desierto no lo olvida - jamas. In: VERTIENTE, Revista de la Facultad de Ingenieria y Ciencias Geologicas, Universidad Catolica del Norte, Antofagasta, Chile, 9, No. 9, ISSN 0716-1964, pp. 6 - 10.

Götze, H.-J., Lahmeyer, B., Schmidt, S. and Strunk, S., 1994. The Lithospheric Structure of the Central Andes (20°-26°S) as inferred from Quantitative Interpretation of Regional Gravity. In: Tectonics of the Southern Central Andes (Eds.: Reutter, Scheuber, Wigger), pp. 7-21, Springer Verlag Heidelberg.

Götze, H.-J., M. Schmitz, P. Giese, S. Schmidt, P. Wigger, G. Schwarz, M. Araneda, G. Chong D. and J. Viramonte, 1995. Las estructuras litosféricas de los Andes Cantrales australes basados en interpretaciones geofísicas. IGCP Special Volume, Revista Geológica de Chile, Vol 22, No. 2, 179-192.

Götze, H.-J. and the MIGRA group, 1996. Group updates gravity database for Central Andes. EOS Transactions, Electronic Supplement, American Geophysical Union, 5 pages. http://www.agu.org/eos_elec/95189e.html.

Isacks, B.L., 1988. Uplift of the Central Andean Plateau and Bending of the Bolivian Orocline. *Journ. Geophys. Res.*, Vol. 93, No. B4, 3211 - 3231.

Prince, R.A. and Forsyth, D.W. 1984. A simple objective method for minimizing crossover errors in marine gravity data. Geophysics, 49 (7), 1070-1083.

Reutter, K.-J., E. Scheuber and P. Wigger (Editors), 1994. *Tectonics of the Southern Central Andes*, Springer Verlag, Heidelberg, pp. 333.

Schmitz, M., (1993): Kollisionsstrukturen in den Zentralen Anden: Ergebnisse refraktionsseismischer Messungen und Modellierung krustaler Deformationen. Berliner Geowiss. Abh. (B), 20, pp. 1-127. Fachbereich Geowissenschaften der FU Berlin.

Schmitz, M., (1994): A balanced model of the Southern Central Andes. TECTONICS, 13, no.2, pp. 484-492.

Wigger, P.J., M. Schmitz, M. Araneda, M., G. Asch, S. Baldzuhn, P. Giese, W.-D. Heinsohn, E. Martinez, E. Ricaldi, P. Röwer and J. Viramonte, 1994. Variation of the crustal structure of the Southern Central Andes deduced from seismic refraction investigations. In: Tectonics of the Southern Central Andes (Eds.: Reutter, Scheuber, Wigger), Springer Verlag Heidelberg, pp. 23-48 .

INTERPRETATION OF LONG–WAVELENGTH GRAVITY ANOMALIES MAINLY IN THE WESTERN CARPATHIANS AND PARTLY IN THE SCANDINAVIAN CALEDONIDES AND THE EASTERN ALPS

Miroslav Bielik[1], Dan Dyrelius[2] and Robert J. Lillie[3]

[1] Geophysical Institute of the Slovak Academy of Sciences
[2] Department of Solid Earth Physics, University of Uppsala
[3] Department of Geosciences, Oregon State University

Abstract:

Summarization of the results which were obtained in frame of density modelling of the long-wavelength gravity anomalies over the different types of continental lithosphere in Europe is presented. The Western Carpathians, the Eastern Alps and the Scandinavian Caledonides represent continental collision regions and the Pannonian Basin characterize extensional type of continental lithosphere. In spite of different evolution of these European continental lithospheric parts this gravity study provides evidence for significant influence of the lithosphere – asthenosphere boundary upon the long-wavelength observed Bouguer gravity anomalies. Presented gravity models are consistent with different topography, thicknesses of sediments, crust and lower lithosphere. The results also indicate the interaction of asthenospheric, lithospheric and crustal processes and their mutual dependencies during formation of this continental collisional and extensional regions. Moreover, the research illustrates how is important an accuracy of determination of Moho discontinuity for density modelling of the lithospheric cross-sections.

Introduction

The Western Carpathians, the Scandinavian Caledonides and the Eastern Alps belong to the continental collision mountain belts. Although their evolutions and ages of collision are different, they provide an opportunity to study not only how the European crust varies in thickness due to passive margin development and continental collision, but also how the lithosphere – asthenosphere boundary has been affected by these processes.

Density modelling of the present lithosphere structure uses existing gravimetric, seismic, seismological, geothermal data, observed topography and bathymetry and other geophysical and geological observations. The contribution gives a review on the study of long-wavelegth gravity anomalies in mentioned collisional mountain belts. Some results have represented a part of single studies. For the purpose to give an integrate view some modified pictures are also used in this paper.

Simple models in local isostatic equilibrium show a configuration of topography, bathymetry, sedimentary, crustal and lithospheric thicknesses which are consistent with observed free air and Bouguer gravity anomalies. This analysis serves as a basis for refining

the cross-sections presented in the study. The general motivation for this study is to improve knowledge and understanding of continental crustal formation and evolution, with special emphasis on modelling the gross structure of the crust and lower lithosphere.

Geology

The Eastern Alps and the Western Carpathians are included in the northern branch of the young mountain belt stretching from the Alps to the Himalaya (Fig.1). They are the results of Mesozoic and Cenozoic continental collision between Europe and several continental fragments to the south, including Africa (Royden et al. 1988).

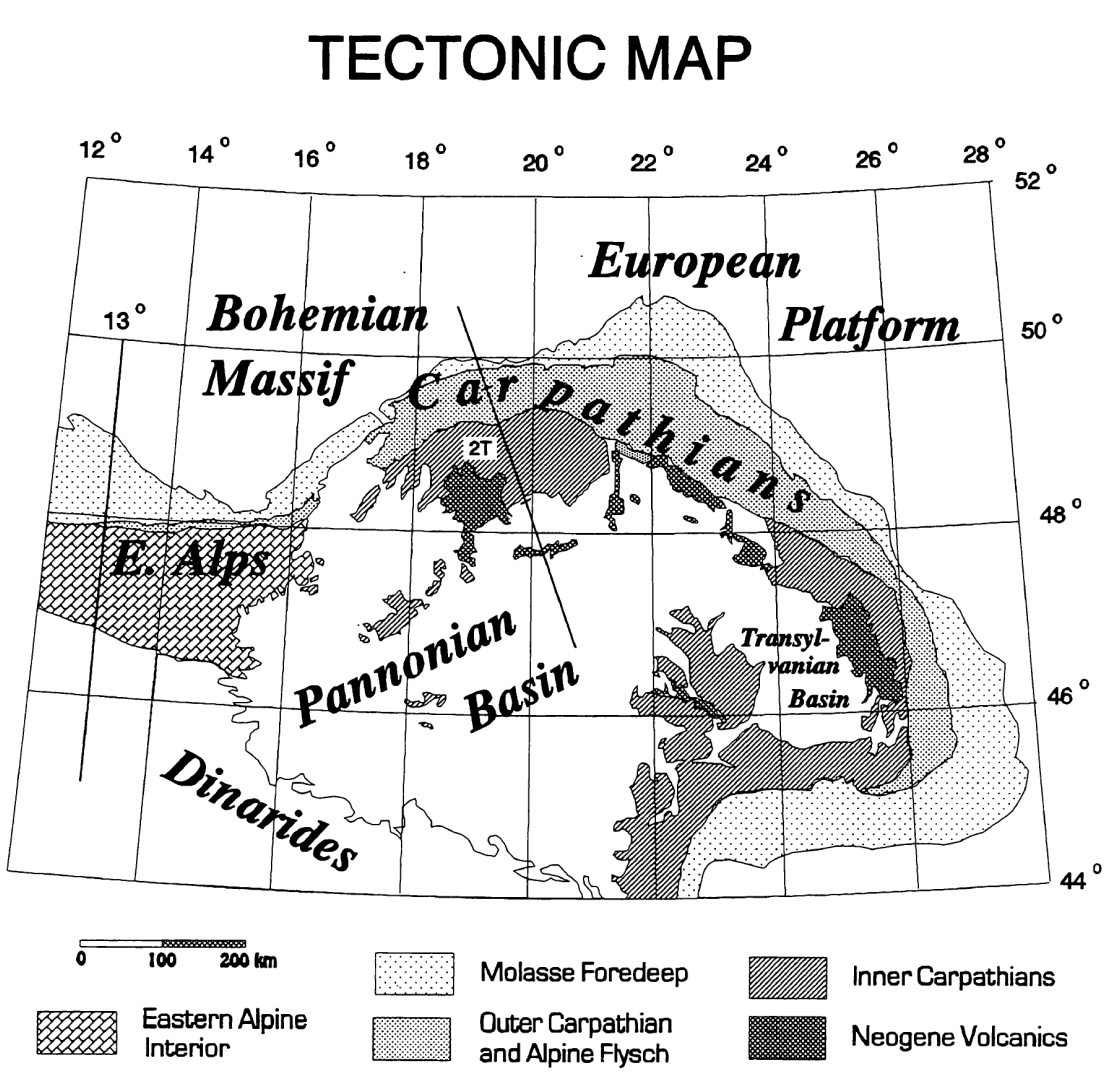

Fig. 1

The Western Carpathians

The fundamental feature of the mountains is its nappe structure (Andrusov 1968), which was formed from Cretaceous to Miocene. On the basis its geodynamic evolution the Western Carpathians are divided into the externides and the internides separated by very complicated tectonic suture of the Klippen Belt. The externides are formed by neo-Alpine accreation wedge of the flysch nappes which overthrust Carpathian foredeep covering flanks of the North European plate. The internides represent paleo and meso-Alpine consolidated part of the orogene, which is in principle divided into nappes of the fundament (Tatricum, Veporicum and Gemericum) and superficial nappes (Fatricum, Hronicum and Silicicum). The internides consist of the central Western Carpathians and the inner Western Carpathians. The fundamental driving mechanism neo-Alpine geodynamic evolution of the Western Carpathians was retreating subduction of the flysch basement of the externides towards the platform margin under overriding plate of the orogene (Royden 1993, Tomek et al. 1987) and kinematic processes which led to the Oligocene-Lower Miocene extrusion of the Western Carpathian and North Pannonian crustal fragments from the Alpine collision zone (Ratschbacher et al. 1991a,b). Characteristical elements of the Western Carpathians are extensive Tertiary volcanism and evolution intramountain basins, too (Lexa et al. 1993).

The Eastern Alps

The process of the Eastern Alpine evolution can be divided into five tectonic epochs (Dietrich et al., 1976). First tectonic subdivision of the Eastern and Southern Alps and formation of two different rift systems were in Permo-Triassic. During Liassic to Malm opening of the Penninic Ocean or Piemontais and separation of the Euroasian plate from the Austroalpine – Southalpine – Adriatic plate took place. Formation of ridge-type oceanic crust in the Penninic ocean started from Malm to Early Cretaceous. Senomanian to Eocene time is characterized by subduction of the Penninic oceanic lithosphere under the Austroalpine – Southalpine – Adriatic plate. Collision of the two continental plates and vertical uplift took place during Late Eocene to Miocene. After the end of alpine tectonic movements were formed the inneralpine neogene basins with miocene volcanics, interpreted as a result of alpine subduction. Young dislocations form a distinct lineament which is still partly active today.

The Scandinavian Caledonides

The Scandinavian Caledonides (Gee et al. 1985, Hurich et al. 1989) are a classic example of a deeply eroded, collisional orogenic belt. Early Paleozoic convergence and collision between the Laurentian and Baltic continents produced large-scale thrusting

of the sedimentary and crystalline rocks of the Baltic shelf and obduction of outboard eugeoclinal and oceanic terranes. Structural and petrologic data indicate that continent–continent collision resulted in intracontinental (A-type) subduction of the Baltic shelf beneath Laurentia. Present erosion levels expose Caledonide mid-crustal geology. The mid-Proterozoic crystalline basement and overlying lower Paleozoic strata have been defined previously as autochthonous crust. The latter interpretations suggest that crystalline rocks exposed in the windows are allochthonous.

The Caledonides generally consist of sequences of thrust sheets displaced west to east onto the Baltic shield. The upper thrust sheets, derived from eugeoclinal and oceanic terranes, have undergone several hundred kilometers of eastward translation. The general structure across the belt, as currently exposed, is a transition from relatively thin foreland thrust sheets in the east to steeply dipping complexes of infolded basement and cover in the west. Penetrative crystalline rocks generally interpreted as Baltic basement are exposed throughout the orogen in a series of antiformal windows.

Seismic reflection profiling in the Western Carpathians

An analysis of deep-seated structure and lithosphere of the Western Carpathians accelerated mainly after for realization deep seismic reflection profiles crossing the mountain belt. It was done in framework of the Czechoslovak project ČESLOKORP. Majority of the profiles of this project has so far been situated in the Western Carpathians and along the contact of the Western Carpathians with the Bohemian Massif. Until now, data have been obtained along more than 1000 km of profiles (Ibrmajer et al. 1994).

From geological point of view the Profile 2T and the Profile 3T are the most important. They belong to the specially conducted transects intersecting basic geological units of the Western Carpathians. The results proved the fundamental feature of the Western Carpathians – its nappe structure.

Profile 2T also brought a new insight into the understanding of the history of the Tertiary deformation processes in the Western Carpatians. The whole crust flexure of the lower European plate can be explained as a result of subduction movements when passive continental margin of the Krosno sea was subducted beneath the Carpathian-Pannonian plate (Tomek et al. 1989).

Profile 3T runs from Vienna basin over the Little Carpathians to the Danube Basin. The profile showed collisional and extensional samples like thrusts, normal and strike-slip faults, which were active at different times. It was interpreted long-angle normal faults beneath the Danube Basin. The thrust fault have been observed beneath 20 km of the profile. The transtensional sinistral strike-slip fault, running along the western margin of

the Malé Karpaty Mts., so called Záhorský fault is the youngest tectonic phenomenon in this section.

Local isostatic modelling

At the beginning of this study the simple gravity models which are kept in local isostatic equilibrium were calculated. For finding clues to the recent lithosphere structure in European region topography, bathymetry, free-air and Bouguer anomalies were used together. In case of the long-wavelength gravity anomalies it is useful to simplify models into elements which represent major density contrasts. The contrasts assumed are relative to „typical crustal" materials. Topography (–2.67 g/cm^3), sea (–1.87 g/cm^3), sediment (–0.20 g/cm^3), lower lithosphere (0.3 g/cm^3) and asthenosphere (0.27 g/cm^3) represent the major anomalous bodies in the lithospheric cross-sections (Lillie et al. 1994). The contrast for sediments is relative to upper crustal materials, while the lower lithosphere and asthenosphere density contrast are relative to the lower crust.

On the basis of local isostatic modelling the density contrast (–0.03 g/cm^3) between asthenosphere and lower lithosphere was estimated. This density contrast due to local isostatic equilibrium:

a) for approximately 9 km updoming of the Moho and 60 km shallowing of the lithosphere – asthenosphere boundary in the Pannonian Basin region as compared to „normal lithosphere" of the area;

b) for about 20 km thickenning of the crust and 70 km deepening of the lithosphere beneath the Eastern Alps;

c) for about 23 km crustal thickening and almost 100 km lithosphere deepening in the Caledonides. The values of crustal and lithosphere thicknesses quite agree with depths of these boundaries which were determined by seismic and seismological research (Babuška et al. 1988, Lillie et al. 1994, Horváth 1993).

The figure 2–4 shows the contributions of the major density anomalous zones to the long-wavelegth gravity anomalies in the Western Carpathians, Pannonian Basin, the Eastern Alps and Scandinavian Caledonides.. The models are in local isostatic equilibrium.

From analysis of these gravity contributions follows that total gravity anomalies can not be explained fully without considering large relief on the lithosphere – asthenosphere boundary. In the Western Carpathian – Pannonian Basin region, the Eastern Alps and Scandinavian Caledonides, the present topography including bathymetry in the Norwegian Sea and sedimentary thicknesses is not sufficient to compensate, isostatically the

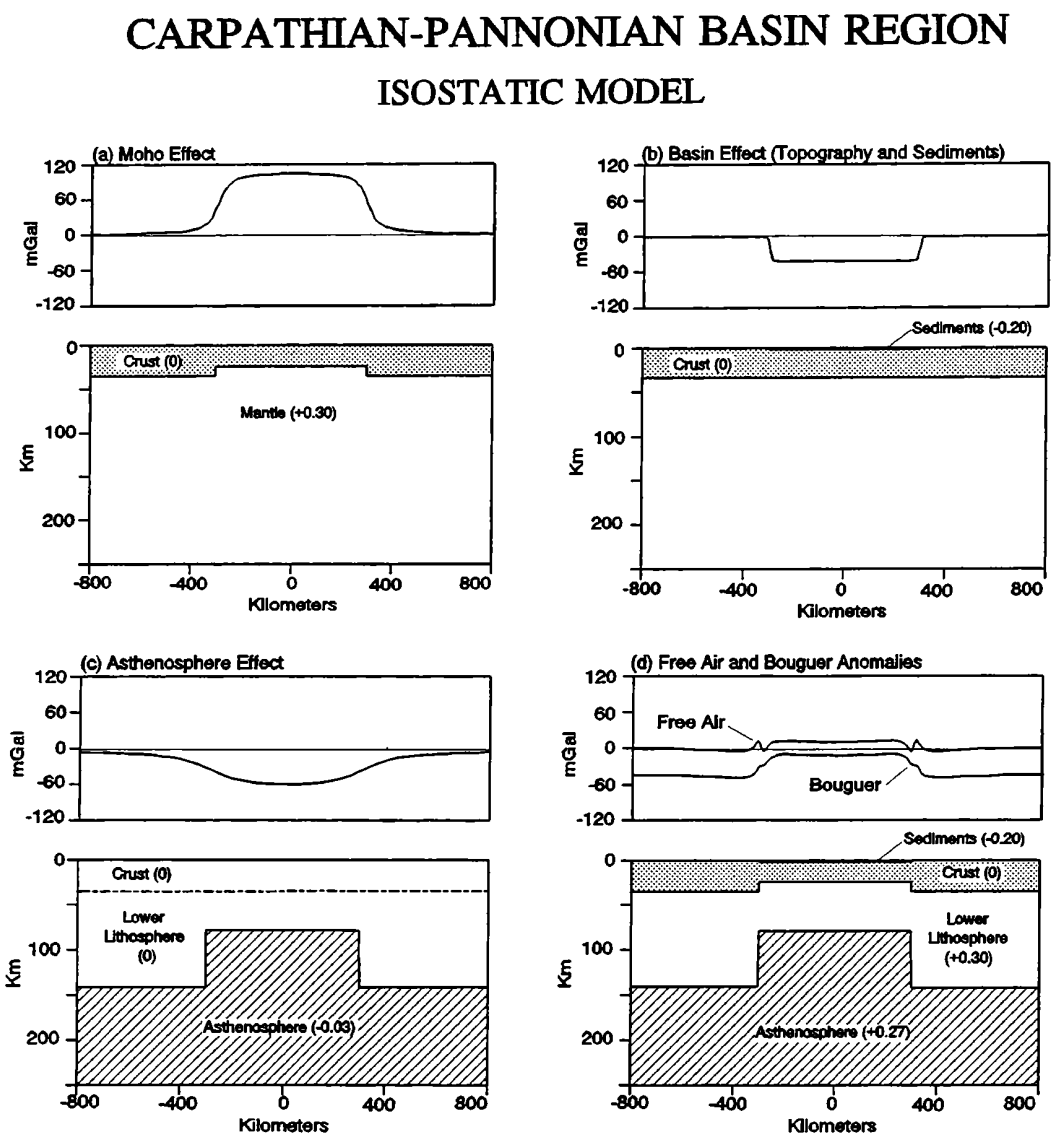

Fig. 2

crust-mantle boundary. It seems to be that influence of this boundary has a large scale range on the observed gravity anomalous field. This study is in accord with the results which were obtained by Hoernle et al. (1995). Their research gives seismotomographic and geochemical evidences for large-scale asthenosphere upwelling spreading from the Eastern Atlantic region (from about 500 km) towards NE to the Western, Central and Eastern Europe (to about 100 km and less). They also reason that asthenosphere shallowing must be taken into account in regional geophysical and geological studies of the lithosphere structure.

Lithospheric cross-sections

The study and perspective of the present lithospheric structure has been done along profiles extending perpendicularly across the Western Carpathians, the Eastern Alps and Scandinavian Caledonides.

The Western Carpathian Profile 2T (Fig. 1) runs along the line Tworog (Poland) – Battonya (Hungary). Its length is 500 km. The Slovak part of the profile is identical with the seismic reflection Profile 2T. From geological point of view the profile begins in the area of the Eastern European Platform (Poland), and towards the south east crosses the basic units of the Western Carpathians, to end in the Neogene of the Pannonian Basin.

The cross-section of the Scandinavian Profile 2 (Fig. 5) is identical with old the Blue

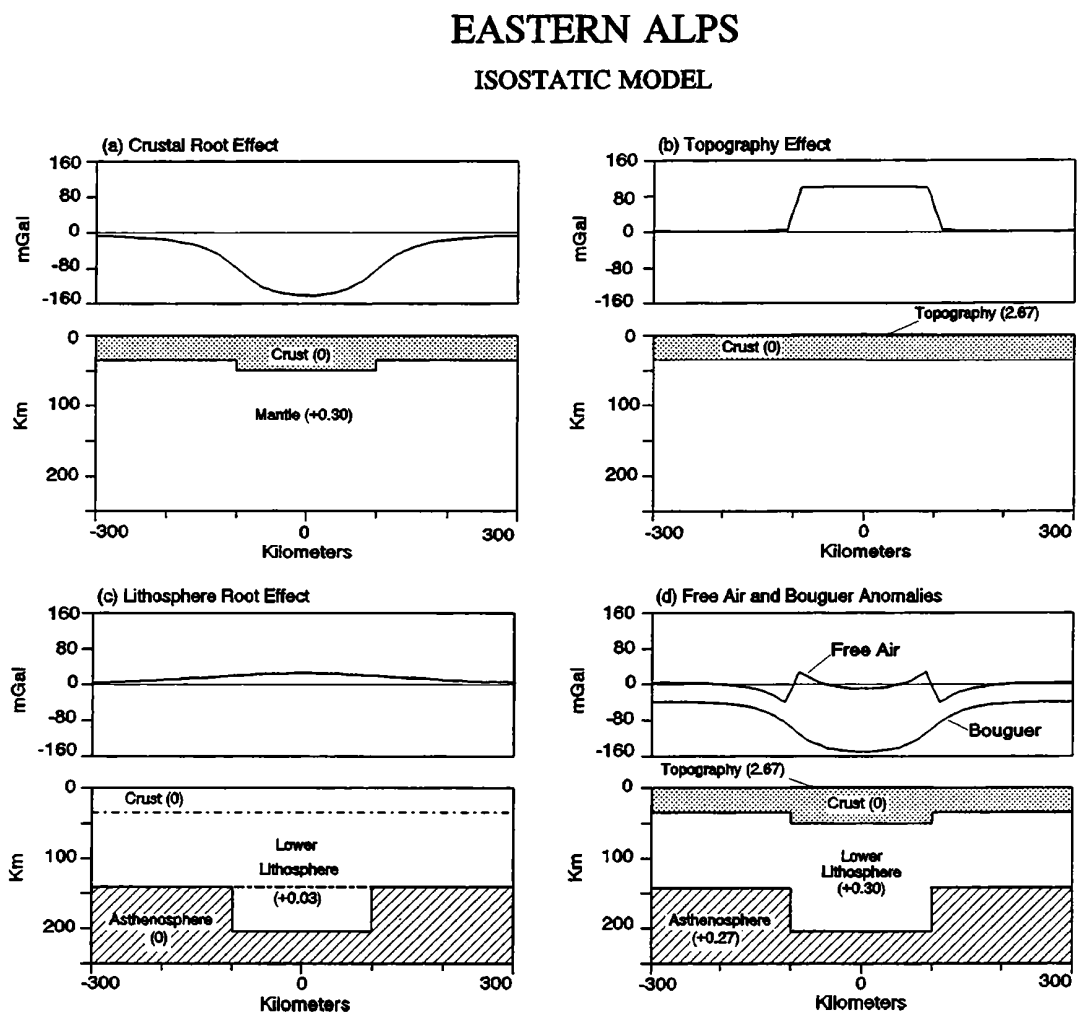

Fig. 3

Road Geotraverse (Hirschleber et al. 1975).

The lithospheric cross-section in the Eastern Alps was constructed along line 13° E longitude (Lillie et al. 1994).

The initial models showed that agreement between the observed and calculated gravity anomalies was not great, and it changes along the profile. For good correlation between the observed and calculated gravity anomalies, it was necessary to adjust the initial density model. On the basis of study of the contributions of individual anomalous zones and the validity of local isostatic equilibrium, it was found that the overall gravity field is most influenced by Moho. Substantially smaller gravity contributions mark other anomalous bodies. Therefore good correlation between observed and calculated gravity anomalies was obtained mainly by adjusting depths of Moho boundary. In the Norwegian sea, partly, the thicknesses of sediments were also corrected.

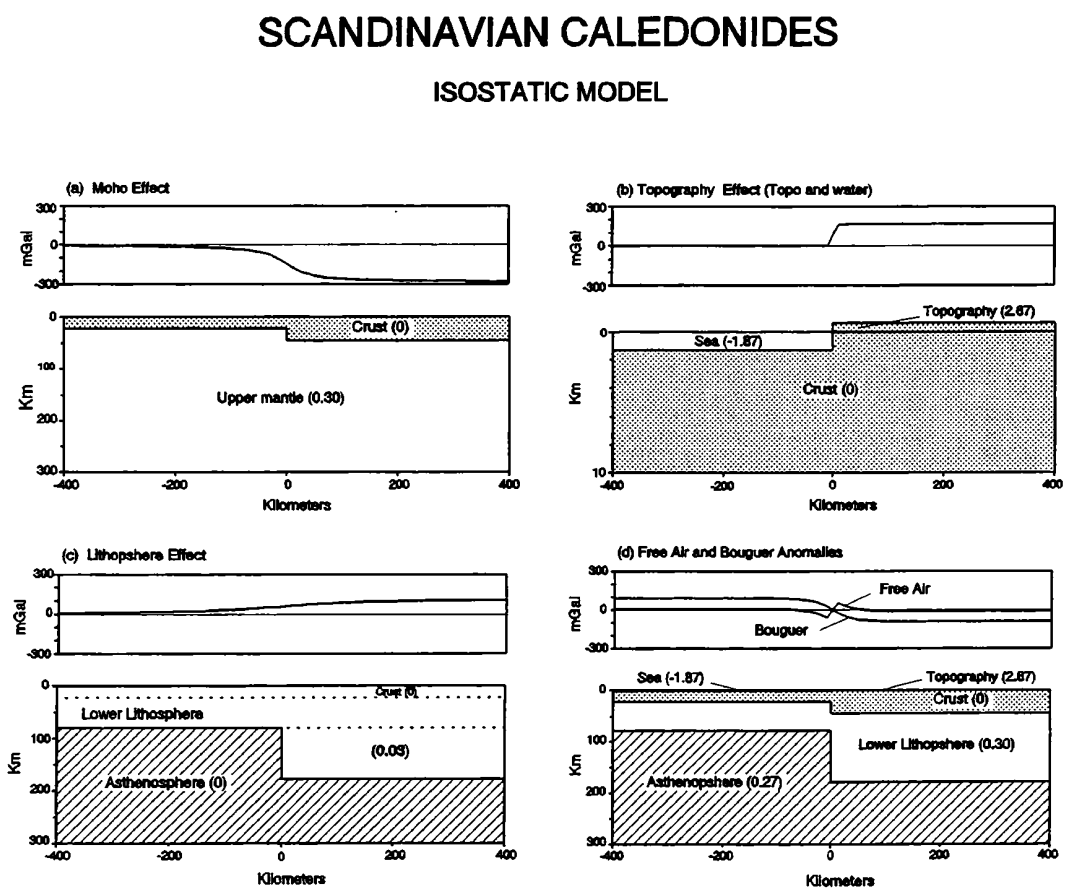

Fig. 4

The Carpathian gravity low (Fig. 6) is associated with underthrusting of the lower European plate under the upper the Carpathian – Pannonian plate, and its flexure as a result of loading of the passive margin of Krosno sea (Bielik 1995). The increase of the observed Bouguer anomaly towards the Pannonian Basin is connected with shallowing of the Moho

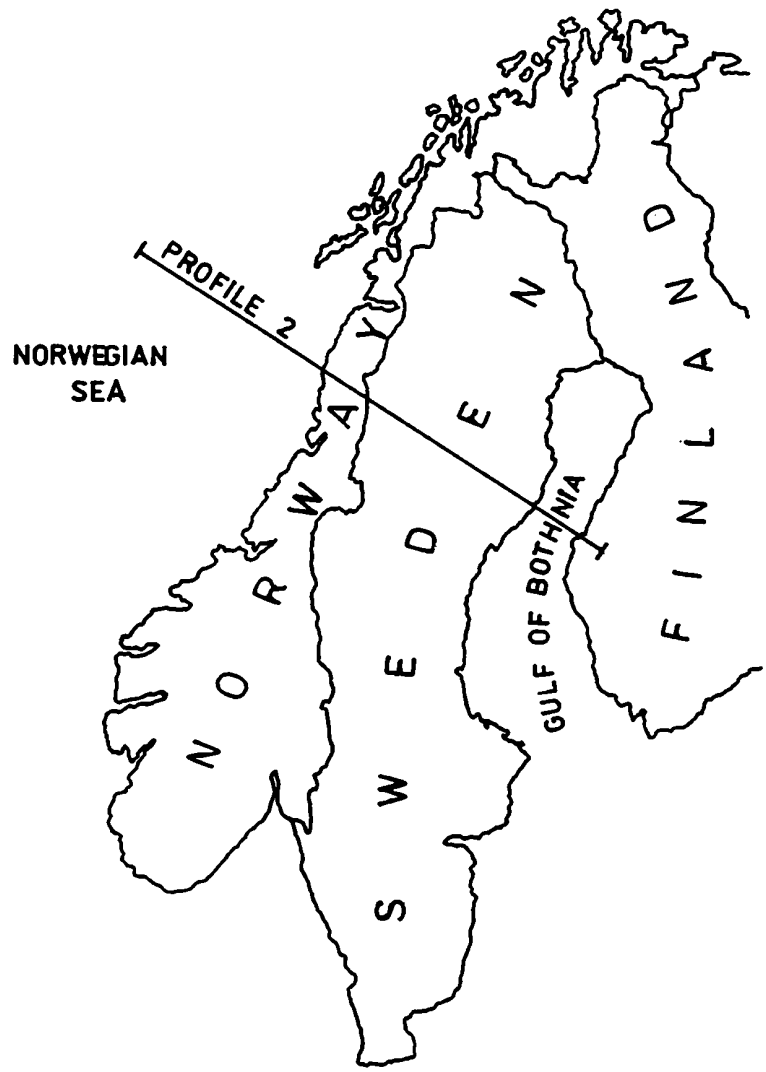

Fig. 5

boundary. In the Carpathian – Pannonian Basin both shallowing Moho and updoming of the asthenosphere is observed. This configuration is typical for extension area. Note that area of Moho shallowing is smaller than updoming of asthenosphere. It extends much more outward within the European craton (Lillie et al. 1994). The Eastern Alps gravity minimum (Fig. 7) is much broader than that observed for the Carpathians. It is connected with both the crust and lithosphere thicken beneath the highest topography of the Eastern Alps (Lillie et al. 1994). This interpretation is similar with results obtained by Kissling et al. (1983). The lithospheric root is nearly coincident with the crustal root, a small offset to the south of the crustal root, perhaps indicate of southward subduction. Note too, that without any adjustment of published thicknesses, there is close agreement between observed and calculated gravity anomalies.

The cross-section of Profile 2 (Fig. 8) shows changes in the topography, bathymet-

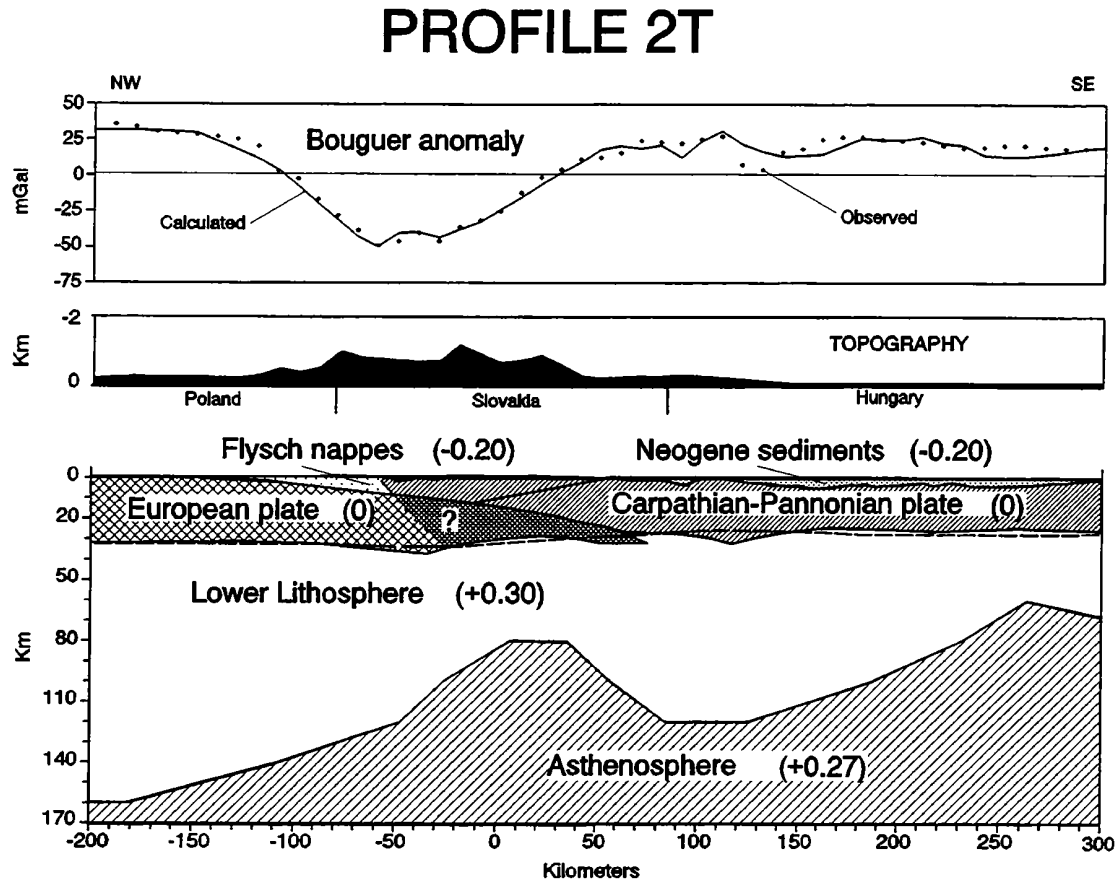

Fig. 6

ry, thicknesses of sediments, crust and lithosphere and free-air and Bouguer anomalies connected with the present structure of the Scandinavian Caledonides and its adjacent areas.

The results of interpretation of gravity field suggest that in the Caledonides the Moho depth deepens from 20–22 km in the Norwegian sea eastward to the Caledonian mountain belt (about 44–47 km). Note that the highest topography of Scandinavian Caledonides is not characterized by any significant crustal root if taking into account the gravity effect of the lithosphere – asthenosphere boundary. This conclusion is in accord with seismic results (Hirschleber et al. 1975, Kværna 1984, Lund 1979, Luosto 1991, Vogel 1976). They argued against older geophysical interpretations, which assumed the crustal root beneath the Caledonides. A sharp slope of Moho deepening beneath the boundary between the Norwegian sea and the Caledonides seems to be very real. Lithosphere thickening also occurs eastward. But the gradient of asthenosphere dipping is striking smaller than in case of Moho boundary.

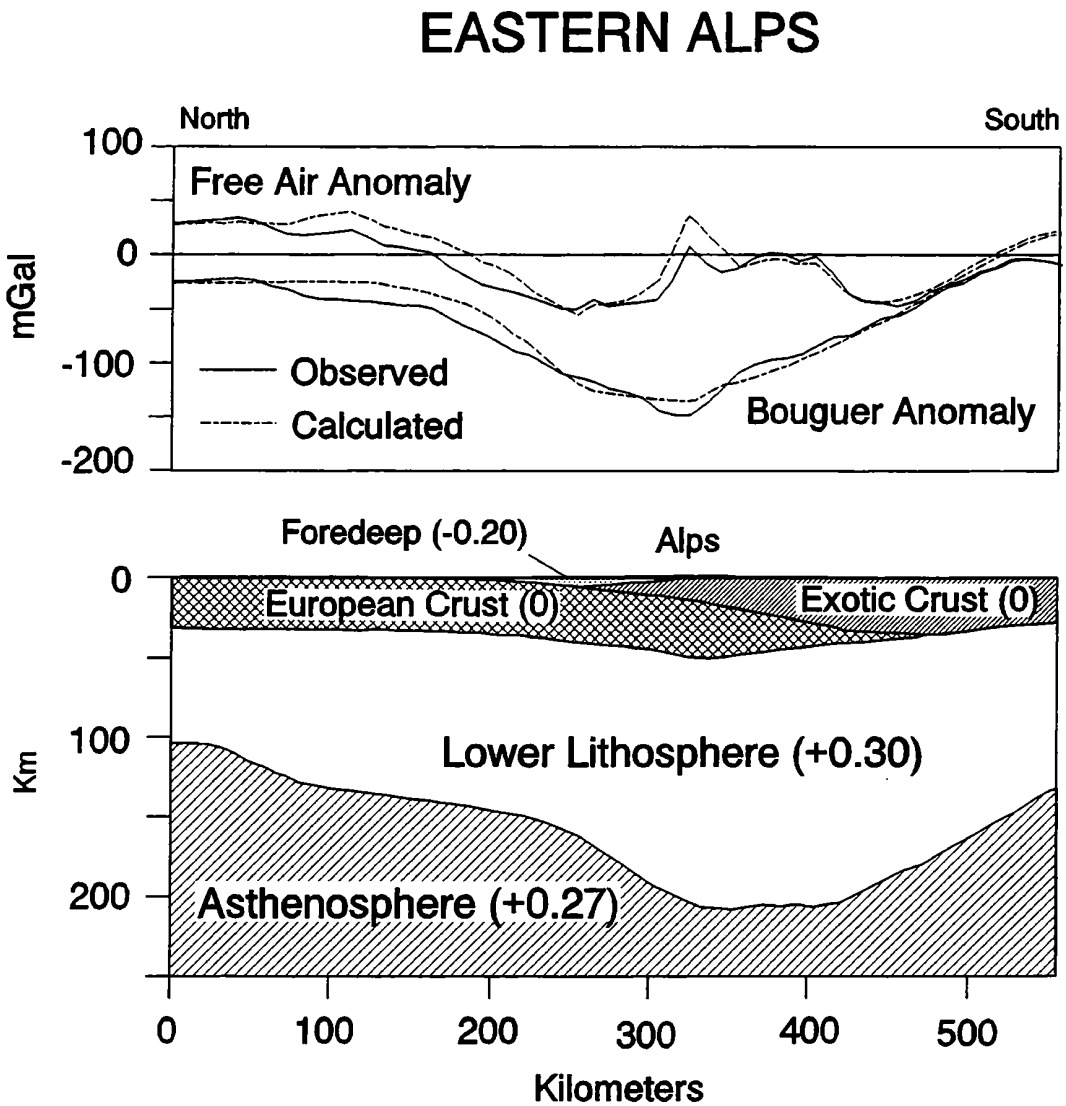

Fig. 7

Conclusions

Study of the gravity field in different areas in Europe has shown a significant influence of the lithosphere – asthenosphere boundary upon a gravity anomalies with long period. In regions where relief on the lithosphere – asthenosphere boundary is not large, or where the course is confined to narrow zone it may be possible to ignore the resulting, low - amplitude contribution in the modelling crustal structure. But if the lithosphere – asthenosphere boundary is located in relative small depths (from about 40–50 km to 120–150 km extension regions), or asthenosphere has large vertical relief and width, or gradient of its upwelling and/or deepping (collision and passive continental regions) is very large then the gravity effect would be taken into account in density modelling of long-wavelength

gravity anomalies.

The density contrast (–0.03 g/cm^3) was determined on the basis of models which are kept in local isostatic equilibrium and we are aware of a imperfection of this estimation. There is a possibility to discuss about quantitative estimation of density contrast between lithosphere and asthenosphere. Density can be affected by many conditions – rheology or mechanical properties of the lithosphere. But the negative density contrast is very probable. In spite of this imperfection, the determined gravity contrast is supported by other geophysical data. The seismic and geochemical evidence for large-scale mantle upwelling (large-scale low velocity region) beneath the Eastern Atlantic and Western and Central Europe were published by Hoernle et al. (1995). Moreover, beneath the lower lithosphere in the intra-Carpathian region it was found out the existence of positive residuals [i.e. the observed arrival times minus the theoretical arrival time of P-waves (Babuška et al. 1984,

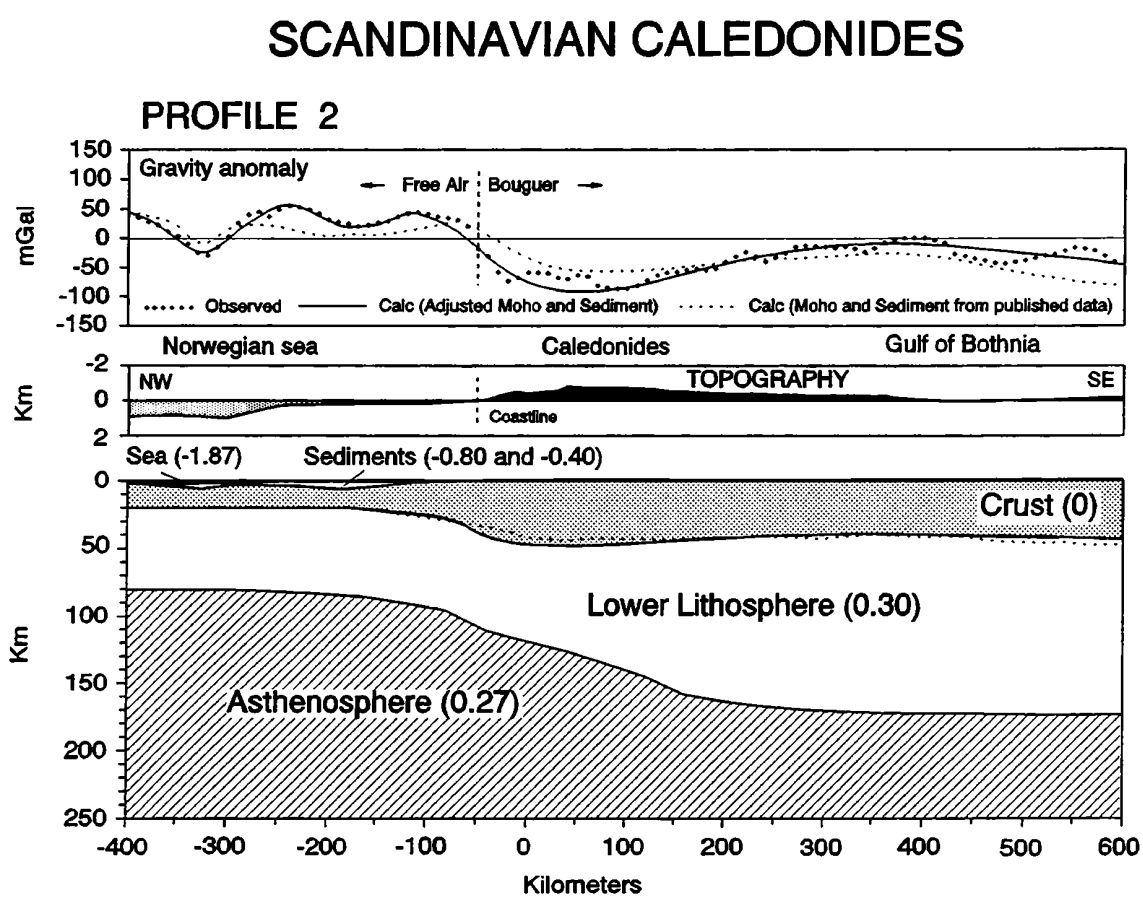

Fig. 8

1994)] and thus by relatively low P-wave velocities, zones of low resistivity (Adam 1992, Adam and Steiner 1993) and extreme of heat flow - probably characterizing partial melted asthenosphere (Čermák and Hurtig 1979, Majcin 1993). The zones of low S and P-waves was interpreted also along EGT geotraverse (Spakman 1986, Ansorge et al. 1992).

Moreover, this study revealed again that an accuracy of determination of Moho is the most important boundary for density modelling. It is known very well that influence of Moho has, in major cases, the largest gravity effect for observed Bouguer gravity anomalies. The conclusions of our gravity study in the Scandinavian Caledonides supported, for example, a decision to create CABLES project (Caledonian and Bothnian Lithosphere Elucidated by Seismics) in Sweden, which main goal is to define the Moho boundary in this mountain belt more precisely.

References

Ádám A., 1992. Crustal and Upper Mantle Research in Pannonian Basin by Electromagnetic Induction: A Review. Journal of China University of Geosciences, 3, 92–104.

Ádám A., Steiner T. 1993. Effect of deep-reaching tectonics on conductivity structure in the Pannonian Basin. Can magnetotelluric data constrain tectonic interpretations? Physics of the Earth and Planetary Interiors, 81, 1–8.

Andrusov D., 1968. Grundriss der Tektonik der Nördlichen Karpaten, Verlag Slovak Akad. Wiss., Bratislava, 188.

Ansorge J., Blundell D., Müller S., 1992. Europea's lithosphere – seismic structure. In: A continent revealed. The European Geotraverse. D. Blundell, R. Freeman, S. Müller (Editors). European science foundation. Cambridge University Press, 33–70.

Babuška V., Plomerová J., Šílený J., 1984. Spatial variation of P residuals and deep structure of the European lithosphere. Geophys. J. R. Astr. Soc., 79, 363–383.

Babuška V., Plomerová J., Petr V., Pěčová J., Praus O. 1994. Contribution of the MTS to the Study of Lithosphere in Central Europe, In: V. Bucha and M. Blížkovsky (Editors), Crustal Structure of the Bohemian Massif and the West Carpathians. Academia Praha – Heidelberg, 157–160.

Bielik M., 1995. Continental convergence in the Carpathian region by density modelling. Geologica Carpathica, 46, 3–12.

Čermák V., Hurtig E., 1979. Heat flow map of Europe 1:5 000 000. In: V. Čermák and L. Rybach (Editors), Terrestrial Heat Flow in Europe. Springer, 145–154.

Dietrich V. J., Essen F., 1976. Alpinische Gebirgsbildung in den Ostalpen: Ein Plattentektonisches Modell (Kurzfassung). Geologische Rundschau, 65, 2, 361–374.

Gee D. G., Sturt B. A., 1985. The Caledonide Orogen – Scandinavian and Related Area. Part 1. John Wiley & Son Ltd., 26–44.

Hoernle K., Zhang Y. S., Graham D., 1995. Seismic and geochemical evidence for large-scale mantle upwelling beneath the eastern Atlantic and western and central Europe, Nature, 374, 34–39.

Hirschleber H. B., Lund C. L., Meissner R., Vogel A., Weinrebe W., 1975. Seismic investigation along the Scandinavian "Blue Road" Traverse. J. Geophys., 41, 135–148.

Horváth F., 1993. Towards a mechanical model for the formation of the Pannonian Basin region. Tectonophysics, 226, 333–357.

Hurich C. A., Palm H., Dyrelius D., Kristoffersen Y., 1989. Deformation of the Baltic continental crust during Caledonide intracontinental subduction. Geology, 17, 423–425.

Ibrmajer J., Tomek Č., Koráb T., Dvořáková L., 1994. Deep Reflection Seismic Profiling in Czechoslovakia - the ČESLOKORP (Czechoslovak Crustal Reflection Profiling Project), In: V. Bucha and M. Blížkovský (Editors), Crustal Structure of the Bohemian Massif and the West Carpathians. Academia Praha – Heidelberg, 21–45.

Kissling E., Müller St., Werner D., 1983. Gravity anomalies, seismic structure and geothermal history of the Central Alps. Ann. Geophys., 1, 37–46.

Kværna T., 1984. Reinterpretation of seismic refraction profiles in the framework of Fennoscandian tectonic evolution. Thesis, Institute of Geophysics, University of Oslo, 135.

Lexa J., Konečný V., Kalinčiak M., Hojstričová V., 1993. Distribúcia vulkanitov karpatsko – panónskeho regiónu v priestore a čase, In: M. Rákus and J. Vozár (Editors), Geodynamický model a hlbinná stavba Západných Karpát. GÚDŠ Bratislava, 57–70.

Lillie R. J., Bielik M., Babuška V., Plomerová J., 1994. Gravity modelling of the lithosphere in the Eastern Alpine – Western Carpathian – Pannonian Basin region, Tectonophysics, 231, 215–235.

Lund C. L., 1979. Crustal structure along the Blue Road Profile in northern Scandinavian. Geologiska Föreningens i Stockholm Förhandlingar, 101, 191–204.

Luosto U., 1991. Moho depth map of the Fennoscandian Shield based on seismic refraction data. In: Structure and Dynamics of the Lithosphere. H. Korhonen, A. Lipponen (Eds.). Report S–25, Institute of Seismology, University of Helsinki.

Majcin D., 1993. Thermal stage of West Carpathian Lithosphere, Studia geoph. et geodaet., 4, 354–364.

Ratschbacher L., Merle O., Davy Ph., Cobbold P., 1991a. Lateral extrusion in the Eastern Alps. Part 1, Boundary conditions and experiments scaled for gravity. Tectonics, 10, 245–256.

Ratschbacher L., Frisch W., Lintzer H. G., Merle O., 1991b. Lateral extrusion in the Eastern Alps. Part 2, Structural analysis. Tectonics, 10, 257–271.

Royden L. H., 1988. Late Cenozoic tectonics of the Pannonian Basin system, In: L. H. Royden and F. Horváth (Editors), The Pannonian Basin: A study in Basin Evolution, Am. Assoc. Pet. Geol. Mem., 45, 27–48.

Royden L. H., 1993. The tectonic expression stab pull at continental convergent boundaries, Tectonics, 12, 303–325.

Spakman W. 1986. The upper mantle structure in the central European - mediterranean region. In: R. Freeman, St. Müller and P. Giese (Editors), 3th EGT Workshop: The Central segment, ESF, 215–221.

Tomek Č., Ibrmajer I., Koráb T., Biely A., Dvořáková L., Lexa J., Zbořil A., 1989. Crustal structure of the west Carpathians on deep reflection seismic line 2T. Mineralia Slov., 21, 2–26.

Vogel A., 1976. The Blue Road Geotraverse: The tentative synthesis of a lithospheric model. Geologiska Föreningens i Stockholm Förhandlingar, 98, 270–274.

GEOLOGICAL INTERPRETATION OF THE GRAVITY SURVEY IN THE SOUTH MORAVIA

Jiří Sedlák

Geofyzika a.s.

Zusammenfassung

GEOLOGISCHE INTERPRETATION DER SCHWEREMESSUNGEN IN SÜDMÄHREN

Im Artikel liegen die Ergebnisse der geologischen Interpretation der Schweredaten aus dem südlichen Teil der Tschechischen Republik vor. Das Interessengebiet liegt an der Berührungslinie des Böhmischen Massivs und der Westkarpaten. Die Interpretation des Schwerefeldes umfasst auch zwei quantitative Schwereschnitte, die den Bau der Depressionen von Nesvačilka und Vranovice lösen. Die ausgeprägten Linearstrukturen Richtung NW-SO entstanden durch eine Erosion in den südöstlichen Abhängen des Böhmischen Massivs. Nachher wurden sie von einer mächtigen Aufschichtung autochthonen Paläogens ausgefüllt und später von jüngeren Sedimentkomplexen des Molassenzone, Flyschzone und neogener Ausfüllung des Wiener Beckens überdeckt.

The study area is located in the southeastern portion of the Czech Republic. In terms of regional geology it encompasses the border area of the Bohemian Massif and West Carpathians (Fig. 1). The Bohemian Massif is in the surroundings of Brno represented by igneous rocks of the Brno Massif and its platform cover. Towards the south and southeast the massif plunges beneath the sedimentary sequences of the Carpathian Neogene Foredeep, Carpathian flysh nappes and the Vienna Basin. Average primary rock densities in main tectonic and regional geologic units in the area of interest are the following:

Granitoids of the Brno Massif	2.67 gcm^{-3}
Metabasite Zone of the Brno Massif	2.90 gcm^{-3}
Moravian Paleozoic	2.71 gcm^{-3}
Boskovice Furrow	2.68 gcm^{-3}
Flysh Nappes	2.45 gcm^{-3}
Neogene Deposits of the Carpathian Foredeep	2.30 gcm^{-3}
Neogene Deposits of the Vienna Basin	2.00 gcm^{-3}

The gravity map of the study area is shown on Fig. 2. During 1960's and 1970's the discussed territory of 4,000 sq km was covered by 16,000 data points. The Bouguer anomalies vary here from -42 mGal in the area of the Central Moravian Depression of the Vienna Basin to +32 mGal at the Metabasite Zone of the Brno Massif in the proximity of the city of Brno. Maximum gravity gradient of up to 150 E has been observed in Brno at the northeastern edge of the Metabasite Zone.

The metabasites of the Brno Massif account for a positive gravity anomaly trending generally to the north-north-east between Hustopeče and the western edge of Brno. The maximum of the anomaly (+32 mGal) coincides with the area of the plunge of the massif beneath the Carpathian Foredeep. The anomaly rapidly diminishes towards SSE and its relative amplitude in the vicinity of Hustopeče does not exceed +7 mGal. This configuration is brought about by increasing thickness of Carpathian sedimentary sequences.

The gravity effect of the Metabasite Zone corresponds with its expression in the map of magnetic anomalies. Numerous magnetite-rich outcrops have been identified within the limits of Brno. The decrease in the magnetic values towards SSE is less pronounced than that observed in the gravity map.

In addition to the density variations within the crystalline basement the gravity map reflects the configuration of the pre-Tertiary surface as well. The Neogene fill of the Vienna Basin and of the Carpathian Foredeep accounts for negative gravity anomalies of the northeastern trend. Perpendicular negative anomalies extending towards NW are associated with the Nesvačilka Depression (gravity minimum with the axis Brno - Hodonín, relative amplitude up to -8 mGal) and the parallel to it Vranovice Depression located further southwards. Both depressions are filled by autochthonous Paleogene deposits marked by low densities similar to those of Neogene formations.

On account of the higher thickness (up to 1,500 m) of the sedimentary fill and due to the situation of the depression at the northeastern edge of the Metabasite Zone of the Brno Massif the gravity effect of the Nesvačilka Depression is stronger. The position of the depression was most likely pre-determined by the structural configuration of the Precambrian basement. The southwestern edge of the depression coincides with the northeastern limit of the Metabasite Zone in the basement.

The gravity and seismic effect of the Vranovice Depression is less distinct. This could be explained by the presence of numerous transversal faults and by lower thickness of the Paleogene sedimentary fill at the same time. The gravity display is also influenced by the intersection of the southeastern part of the anomaly related to the Vranovice Depression and the anomaly of the Metabasite Zone in the deeper basement.

Quantitative interpretation of the gravity field has provided important information for the better understanding of the deep structure of the study area. It has been concluded that the Metabasite Zone in the area of the city of Brno plunges abruptly to the depth of 3 - 4 km (Dvořák, Rejl, Sedlák, Valeš 1992 and Sedlák, Šrámek 1995) while its width at the surface varies from 2.5 to 7.0 km. Further west the basic rocks dip more gently and build the basement of the granitoids of the western part of the Brno Massif, practically as far as the edge of the Boskovice Furrow. In this area the lower boundary of basic rocks has been identified in the depth of about 6 km. The author believes that the total width of the belt of basic rocks is in the range of 15 km. This includes both the steep and the gentle parts.

The author has constructed detailed gravity cross-sections A-A' and B-B' along the profiles Pohořelice - Slavkov (Fig. 5) and Mikulov - Ždánice (Fig. 6). This area is marked by a good level of the geological-geophysical knowledge based on abundant drilling results and seismic data. The cross-sections display the upper limit of the Metabasite Zone below Paleozoic - Tertiary sedimentary sequences in the depth from 1.5 - 2.7 km (A-A') or 5.5 - 6.6 km (B-B'). The lower boundary of metabasites occurs in the depth of 4.5 km and 9 km respectively. The total width of the zone is 15 to 23 km. The gravity effect of deeper structural levels is considered to be of secondary importance and has been included in the linear regional background (0.2 mGal/km). This was not taken into account in the calculations of gravity sections. The character of the gravity curve on both cross-sections has significantly been influenced by the presence of light autochthonous Paleogene sedimentary fill of the Vranovice and Nesvačilka Depressions. The cross-sections clearly substantiate the dominant position of the Nesvačilka Depression in the region and the importance of the tectonic configuration of the crystalline basement for the formation of this depression.

Both depressions have seen exploration for hydrocarbons (Adámek, Sedlák 1995). Commercial accumulations of oil and gas have been discovered primarily in the central portion of the Nesvačilka Depression. In 1991-1994 several segments of the Nesvačilka Depression were selected for high resolution gravity survey with the areal density of 25 data points/sq km.

References:

Adámek J., Sedlák J., 1995. Basement of Paleogenne Depressions of the South-Eastern Slopes of The Bohemian Massif. EAGE 57th Conference Glasgow.

Dvořák J., Rejl L., Sedlák J., Valeš V., 1993. Nové poznatky o hydrogeologicky výynamné struktuře v Brně. In B. Hamršmíd (editor) - Nové výsledky v terciéru Západních Karpat. Knihovnička Zemního plynu a nafty 15, 9-19. MND Hodonín.

Sedlák J., Šrámek J. 1995. Geofyzikální obraz řečkovicko-kuřimdké deprese. In B. Hamršmíd (editor) - Nové výsledky v terciéru Západních Karpat II. Knihovnička Zemního plynu a nafty 16, 9-14. MND Hodonín.

GEOLOGICAL MAP

Fig. 1

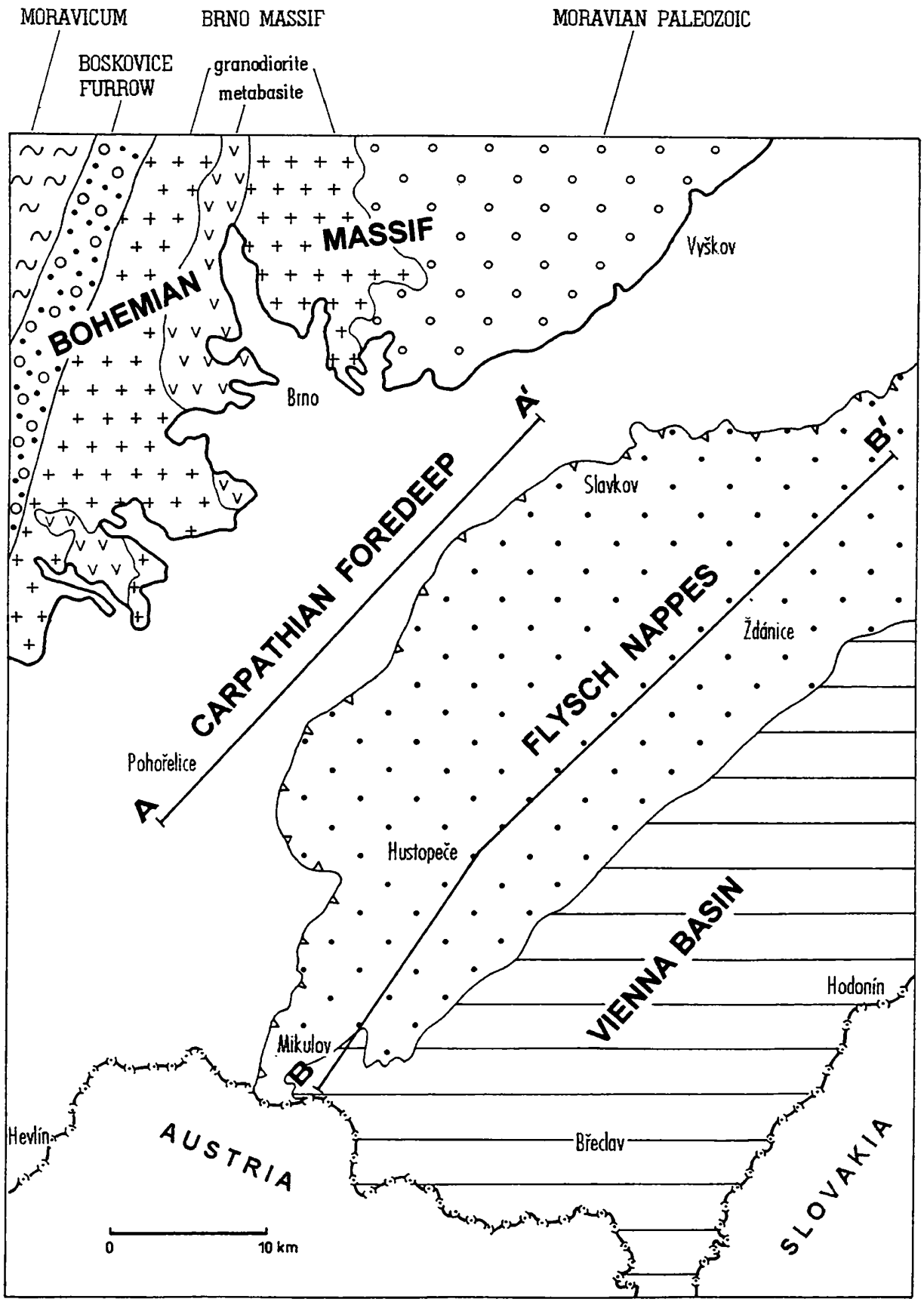

BOUGUER ANOMALY MAP

(contour interval 2 mGal)

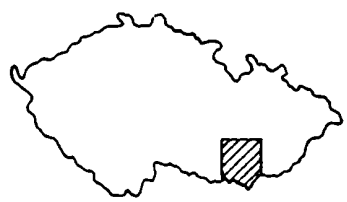

Fig. 2

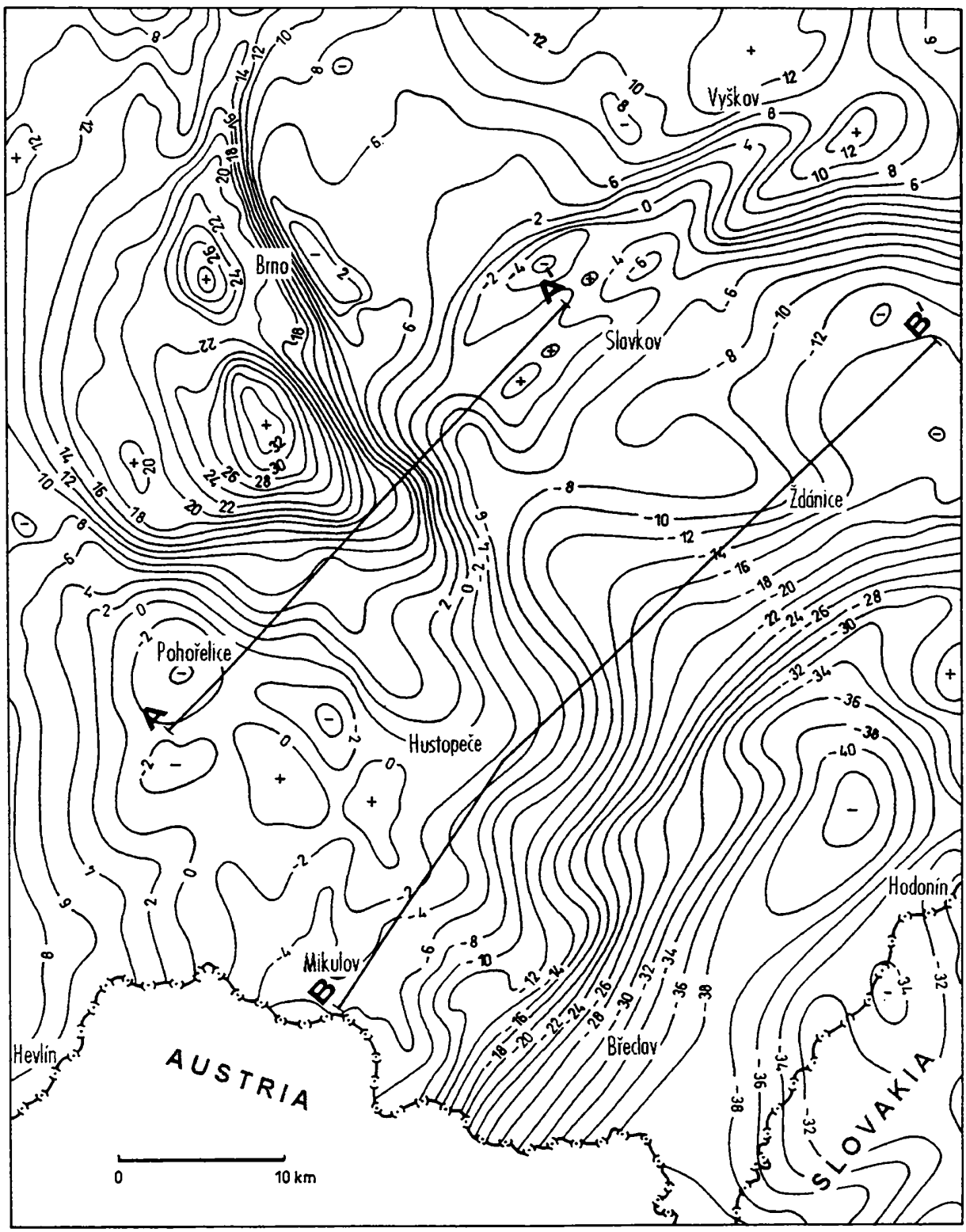

MAGNETIC INTENSITY MAP

Fig. 3

ΔZ - eastern part (contour interval 10 nT)
ΔT - western part (contour interval 25 nT)

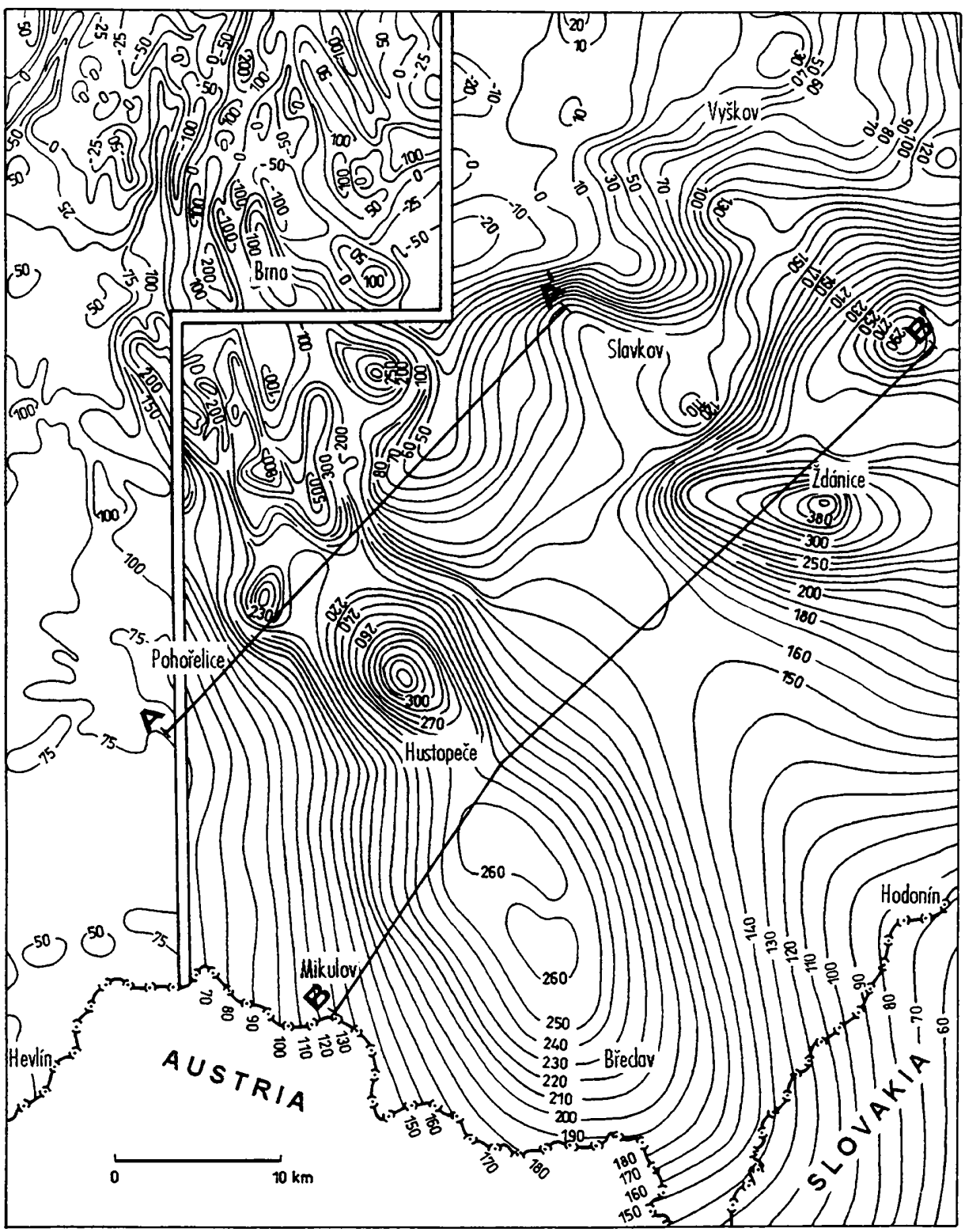

ISOPACH MAP OF PALEOGENE SEDIMENTS

Fig. 4

(Adámek J., Benada S., Ciprys V.)

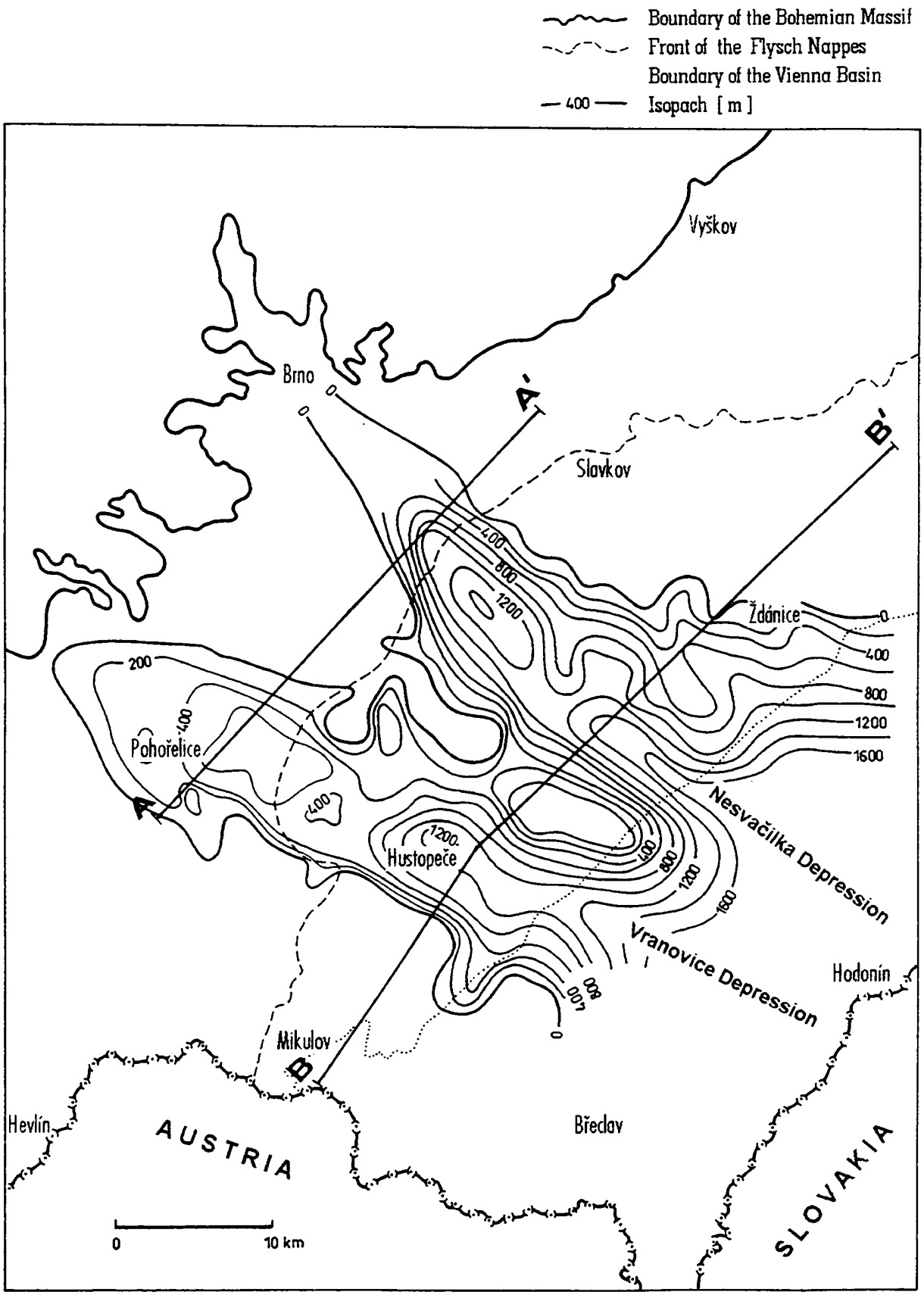

Legend (cross - sections A-A´ and B-B´):


neogene


autochtonous paleogene


flysh


mesozoic


carboniferous


devon - carbonates


devon - clastic sediments


gneiss


quartz diorite


granodiorite


granite


leucogranite


metabazite belt


basement complex undifferentiated

CROSS-SECTION A - A´

(Adámek J., Sedlák J.)

Fig. 5

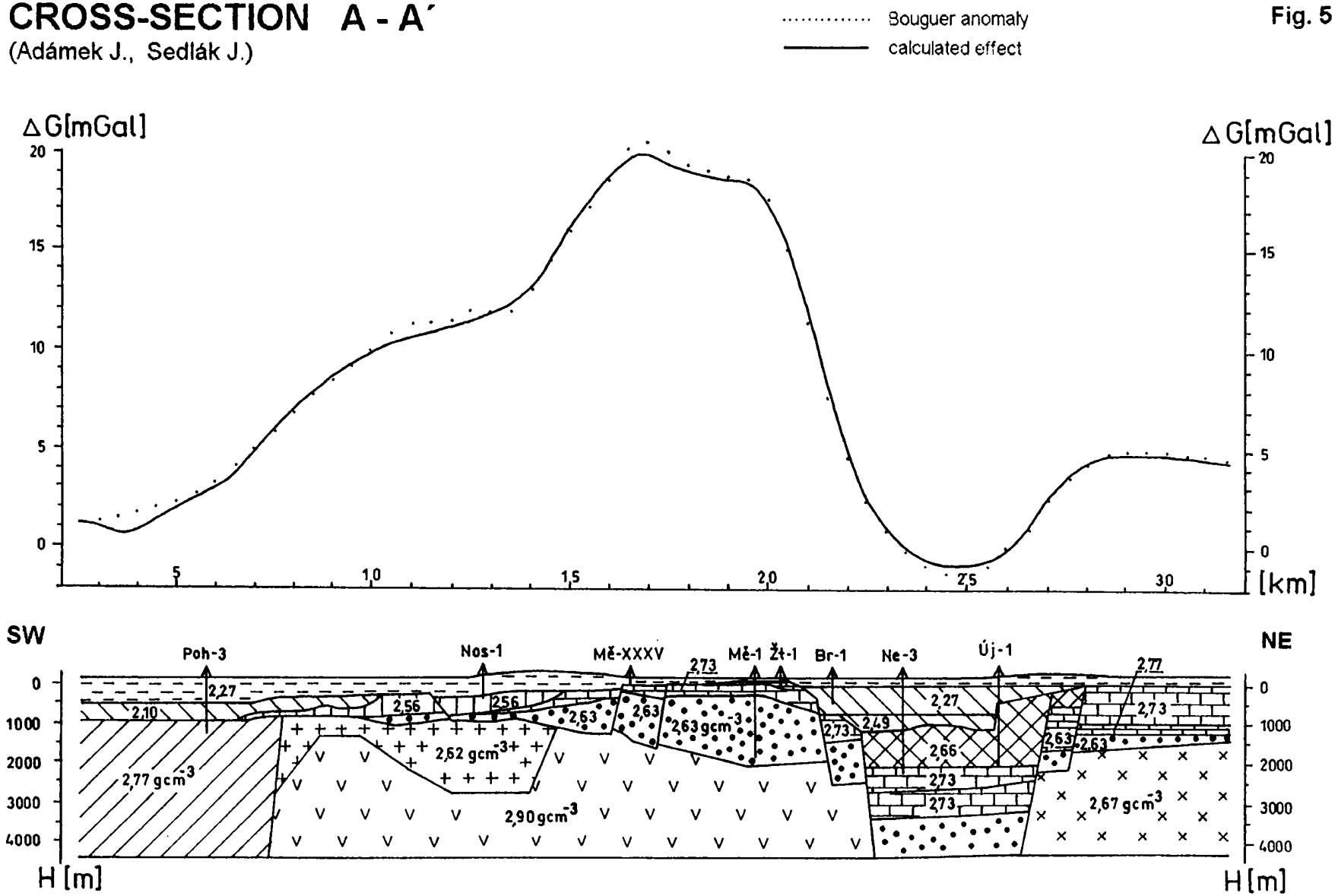

CROSS-SECTION B - B´

(Adámek J., Sedlák J.)

Bouguer anomaly
calculated effect

Fig. 6

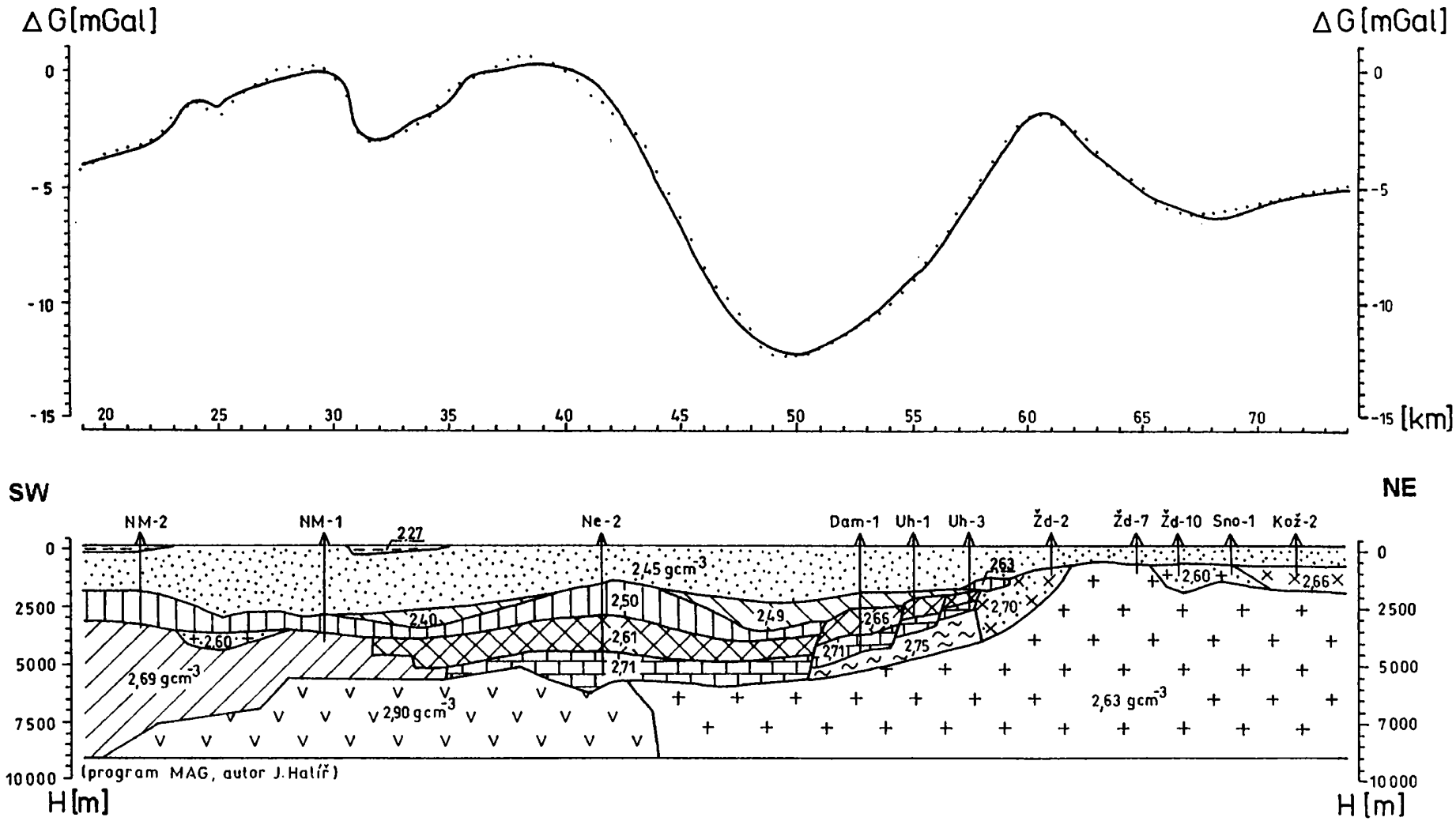

GRAVITY MAP OF THE WESTERN SLOVAKIA AND ITS POSSIBLE INTERPRETATION

Viktória Szalaiová [1] Jaroslav Šantavý[1] and Jozef Vozár [2]
1 Geocomplex a.s., Geologická 21, 822 07 BRATISLAVA, SLOVAKIA
2 Geological survey of Slovak republic, Mlynská dolina. 1, 817 04 BRATISLAVA, SLOVAKIA

Abstract:

The aim of this paper is short characterization of the expressive gravity anomalies in nw. part of Panonian basin as well as in Vienna and the Danube basin. The paper contents results of quantitative interpretation along two profiles, too. We call attention to Kolárovo anomaly problem as well, which is the most expressive structural phenomenon in the area of interest from demonstration intensity point of view. The total picture of the gravity field is presented by Bouguer anomaly map, residual anomaly map and by indication map of gravity horizontal gradients.

Key words:
gravity measurements, gravity anomalies, Bouguer anomalies, gradient, geophysical and geological interpretations, Danube basin

INTRODUCTION

In the area of study, great amount of the geophysical observations has been performed. From gravity measurements and interpretations, it is necessary to mention about works, concerning regional gravity mapping in 1 : 200 000 (Ibrmajer,J.,1963) and 1 : 25 000 (collective of authors) scales. During last years the field geophysical observations have been carried out with a target of direct prospecting for hydrocarbons (Mikuška,J.,et al 1992 - 1995). Moreover, some works have been realized in frame of "Maps of the geophysical indications and interpretations (MGII) " projects: MGII of Danube basin - NE (Panáček,A.,1987), MGII of Chojnická pahorkatina downs (Szalaiová,V., et al.,1994) and MGII of Tríbeč Mts. (Lanc,J., et al. 1995). In the northern part of the area, the interpretation of Danube lowland has been performed within DANREG project, which now terminated. In the year 1996 , the phase work "Synthesis of deep structure of the

Western Carpathians Mts. - western Slovakia region (Szalaiová,V., and Šantavý,J.,) was realized. In this study, the basic results of gravity surveys, performed for various purposes have been summarized. In the frame of "Bratislava - abiotic components of the environment (Hricko,J., et al. 1993) the detailed gravity measurements have been executed besides other geophysical observations.

PRE-TERTIARY BASEMENT OF THE DANUBE BASIN - SLOVAK PART

The map of Pre-Tertiary basement of Danube Basin - Slovak part (fig.1), constructed in accordance with the criteria, accepted by the participants of the DANREG, i.e. the GBA Vienna, the MÁFI Budapest and the Dionýz Štúr Institute of Geology Bratislava, displays the actual state of knowledge on Pre-Tertiary basement. Delineated Units of the Hungarian Central Mountains are separated in the north from the Central Western Carpathian Units by Rába - Hurbanovo fault belt. This is a new concept to explain the function of the Rába line and the Hurbanovo fault. The units within the Gabčíkovo depresion, which displays all the features typical for a "pull-apart" basin, are delineated different way . Within the framework of this space, the low metamorphosed volcanic and sedimentary sequences correlate well with the metamorphics of the Mihalyi phyllite formation as well as with the Paleozoic at Graz. The metamorphics and basic to ultrabasic rocks are considered to occur in the central part of the Gabčíkovo depression and are correlable to the problematic Penninic zone of the Western Carpathians. In the eastern part of the region, the Southern and Northern Veporicum are delineated, with a distinct differentiation of the two zones. This division refers to both, the crystalline rocks and the cover sequences. The Veporicum, as an entirety, is overlain by the Hronicum nappe and the Mesozoic nappe, correlable to the Silicicum. The Tatricum is, in a wider sense, divided in the map into three groups: The Malé Karpaty Mts., the Považský Inovec Mts. and Tríbeč Mts.. The cover sequences, wich occur within the Tatricum Unit, are delineated at the surface as well as inferred in the underlier. There is a separately delineated area in the region of the Považský Inovec and Tríbeč, underlain mainly by Permian and to a lesser extent by Triassic of the Hronicum nappes (the Malužiná formation). Of the whole Malužiná formation, the Permian basalts display the most distinct magnetic anomaly. Continuation of the cover sequences of the Tatricum of Malé Karpaty Mts. including the Vysoká nappe into the area of Pre-Tertiary basement is found within the Vienna basin (its southeastern part only). Contact of the Vysoká nappe with the Paleozoic of the Grauwacken-zone is tectonic (a fault). Continuation of the "Grauwackenzone" is continuous from the Austrian territory, but wedges out towards the northeast. The area underlain by higher nappes of the Malé Karpaty and Biele Karpaty

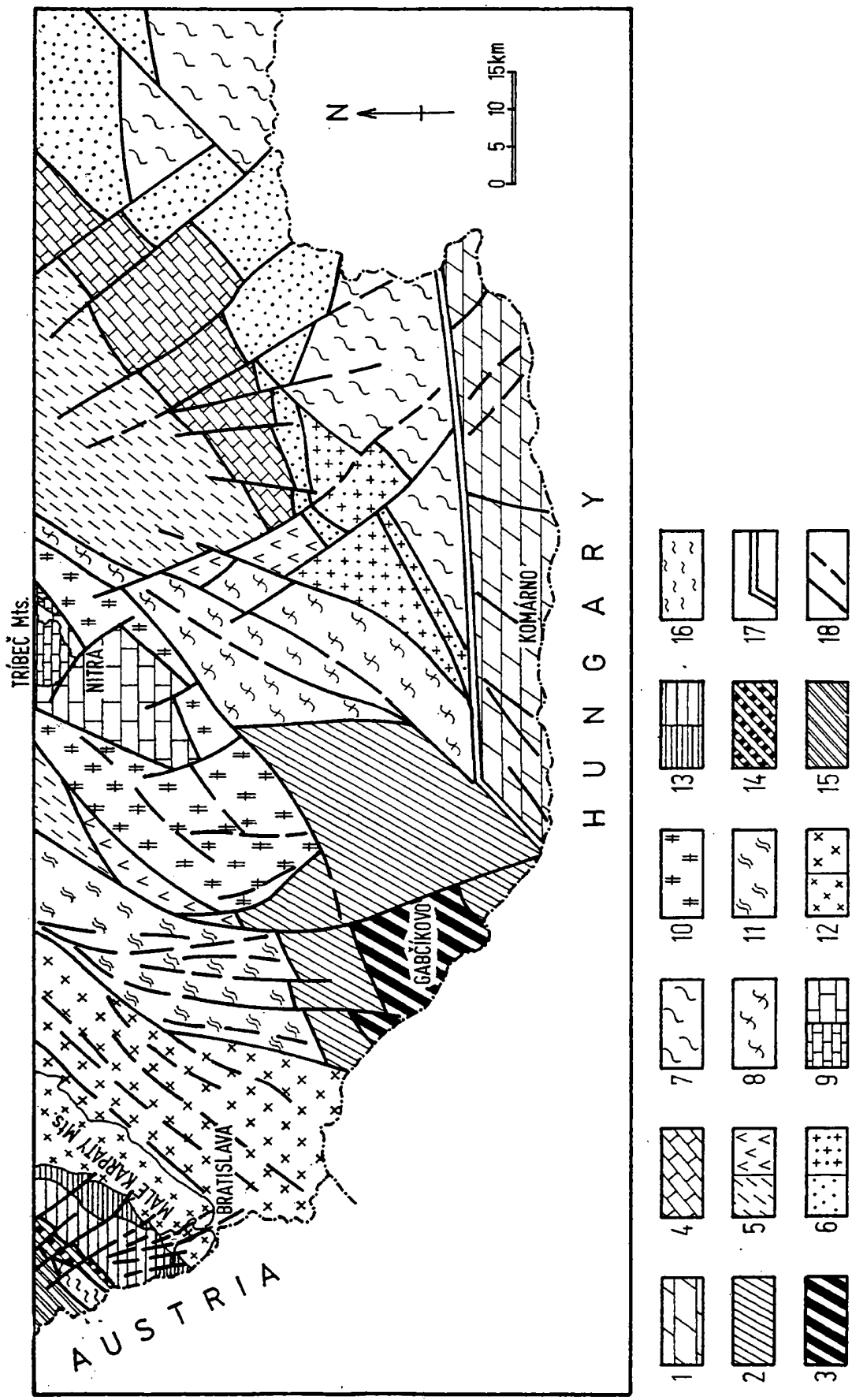

Fig. 1: Map of Pre-Tertiary basement of the Danube region on the territory of Slovak Republic (compiled by Vozár, 1994)

MAP OF PRE-TERTIARY BASEMENT OF THE DANUBE REGION ON THE TERRITORY OF SLOVAK REPUBLIK

Compiled by: J.Vozár,1994

Explanations:

1. Units of the Hungarian Central Mountains - prevailingly Mesozoic

2.-3. Units in the Gabčíkovo depression area

2. Undivided Paleozoic metasediments and metavolcanics - Mihalyi Formation

3. Ultrabasic rocks - ? basic metamorphic rocks correlated with the Penninic zone

4.-5. Units of the Inner and Central Western Carpathians

4. nappes of the Silicicum - prevailingly Triassic

5. nappes of the Hronicum - prevailingly Permian: a) sediments, b) volcanics - basalts, andesites

6.-7. Units of the Southern Veporicum

6.a. Late Paleozoic - Mesozoic envelope sequence, Revúca Gr.-Rimava and Slatviná Frms. correlated with Ipoly complex in Hungary

6.b. Inferred occurrences of the Southern Veporic, Early and Late Paleozoic with penetrations of Alpine granitoids (contact thermic metamorphism)

7. Early Paleozoic, prevailingly metamorphites with local occurrences of the envelope sequence (Late Paleozoic: Slatviná and Rimava Frms, Mesozoic: Tuhár development)

8.-13. Units of the Northern Veporicum and Tatricum

Northern Veporicum

8. Group of Rázdiel massif - Early Paleozoic (mestasediments, metavolcanics, mica schists, partly volcanics of the Skýcov and Slopňa Frms.), Mesozoic - prevailingly Triassic

9.-12. Tatricum

Group of the Tríbeč Mts.

9. Undivided Mesozoic - envelope sequence (prevailingly Triassic) of the Tríbeč Mts., Mesozoic partial nappe units overlying it (Krížna nappe) - a) at the surface, b) in the Pre - tertiary basement

10. Early Paleozoic: crystalline rocks, prevailingly granitoids of the Zobor massif (Tríbeč Mts.)

Group of the Považský Inovec Mts.

11. Early Paleozoic: crystalline rocks, mainly granitoids

Group of the Malé Karpaty Mts.

12. Early Paleozoic: granitoids (Bratislava and Modra massifs), metamorphites (metasediments and metavolcanics of Pezinok - Pernek and Harmónia Frms.)

13. Envelope unit of the Malé Karpty Mts.: Devín sequence - Mesozoic, partly Permian, Borinka sequence - Mesozoic, a) at the surface, b) in the Pre-Neogene basement

Nappe units in the basement of the Vienna basin - Slovak part

14.-15. Western Carpathian units

14. Mesozoic of the Vysoká nappe

15. Mesozoic of the Hronicum nappes

16. Eastern Alps - Paleozoic of the Grauwacken Zone

17. Raba - Hurbanovo fault - zone

18. Significant faults, faults, strike-slip faults, inferred faults

continues into the basement of the Vienna basin and they appear in a synthesized form in the map, covering but a small area.

QUALITATIVE INTERPRETATION

For qualitative interpretation of the field, the Bouguer anomaly (BA) map for 2.67 kg.dm^{-3} density (Fig.2) has been caltulated from regional gravity mappig (1 : 25 000 scale) data. These gravity measurements have been processed in individual technical reports. These reports content description of field works methodology, values of the measurements accuracy and short assessment of the gravity anomalies. The list of individual stages of the regional gravity mapping in 1 : 25 000 scales is presented in the report of Szalaiová,V., and Šantavý,J.,1996.

Besides Bouguer anomaly map following derived maps have been calculated: residual anomaly map for R = 4 000 m, regional map and map of horizontal gravity gradients, calculated for R = 4 000 m by Blakely´s method (see Fig.3a,b).

In Bouguer anomaly map (Fig.2) we can distinguished several intense regional anomalies. The possitive and negative anomalies regularly alternate. It is important to see nearly parallel courses of main anomaly axises, the positive or negative ones.

The positive gravity anomalies represent the Tatricum rocks complexes of core mountains: Malé Karpaty Mts., Považský Inovec and Tríbeč Mts.. The elevation of Pre-Tertiary basement in the Kolárovo surroundings, hidden so - called "Kolárovo anomaly" is caused by heavier rocks (with density of 2.9 - 3.0 kg.dm^{-3}) probably by alkaline ultramafic rocks as amphibolities (Bielik,M., et al. 1994). Bielik (1994) performed quantitative interpretation - modelling of the Kolárovo anomaly. This anomaly reaches the amplitude of +28 mGal in Bouguer anomaly map for density of 2.67 kg.dm. In stripped gravity map, after removal of Tertiary complexes effect, the amplitude increases up to +74 mGal. The correlation between gravity field amplitudes and basement depths after drillings, is good. This correlation is locally worser in Kolárovo, Komárno and Čalovo areas due to presence of deep alkaline body. The certain role plays the elevation presence of C and MOHO discontinuities in these places, too.

Another positive anomaly is located on the Medveďov - Šahy axis approx. It is affected by filted block of Hungarian Central Mts.. This block is frequently names as Pelsö unit, which is divided by Rába - Hurbanovo line from Tertiary fill of Danube basin. If is namely built by Mesozoic complexes. The possitive gravity anomaly, situated to the East of Štúrovo - Želiezovce - Levice line, is evoked by effect of the Pre-Tertiary rocks of Považský Inovec Mts.. In the map of Bouguer anomaly and in maps derivated, one can see sharp linear gradient of E - W direction in

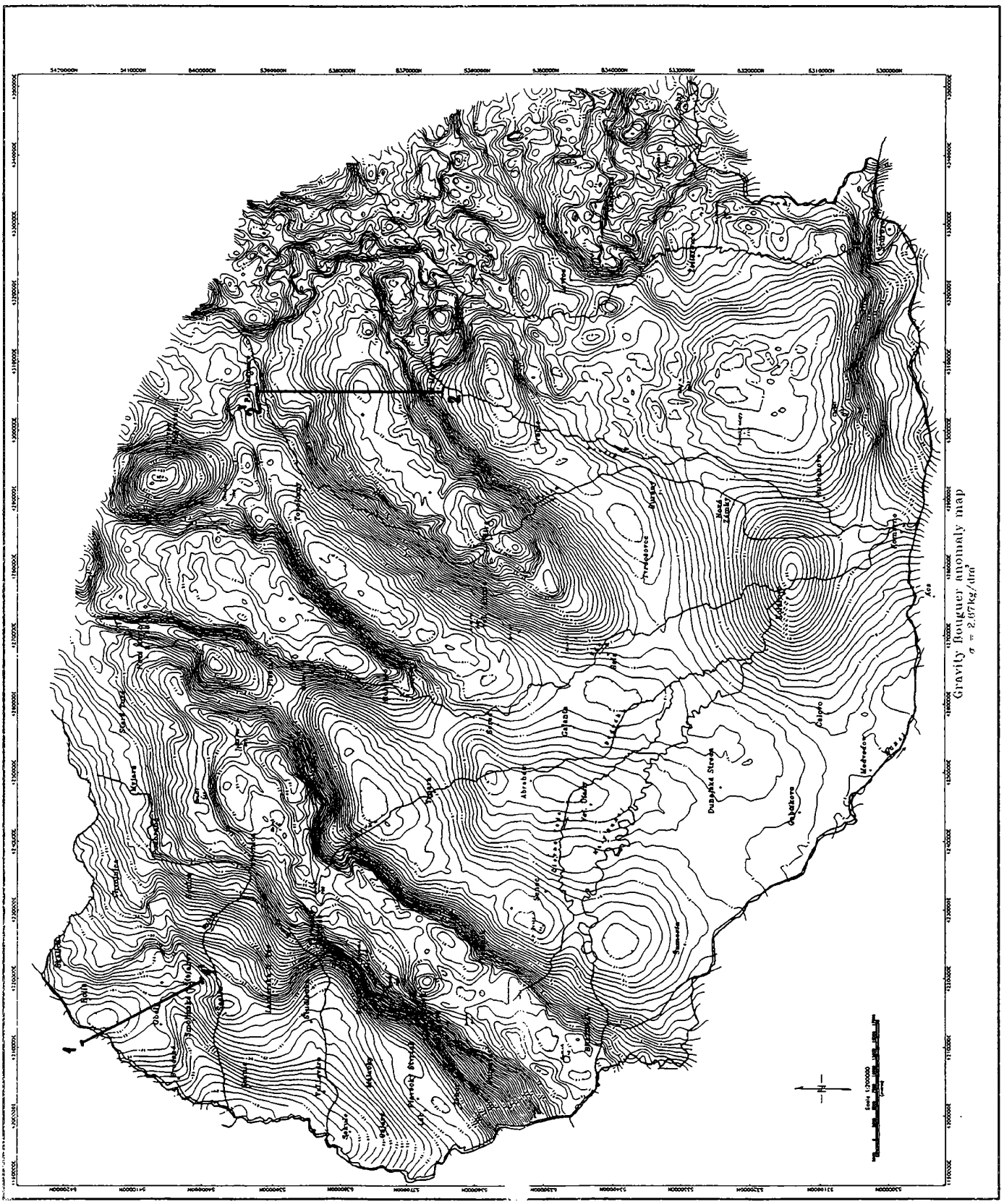

Fig.2

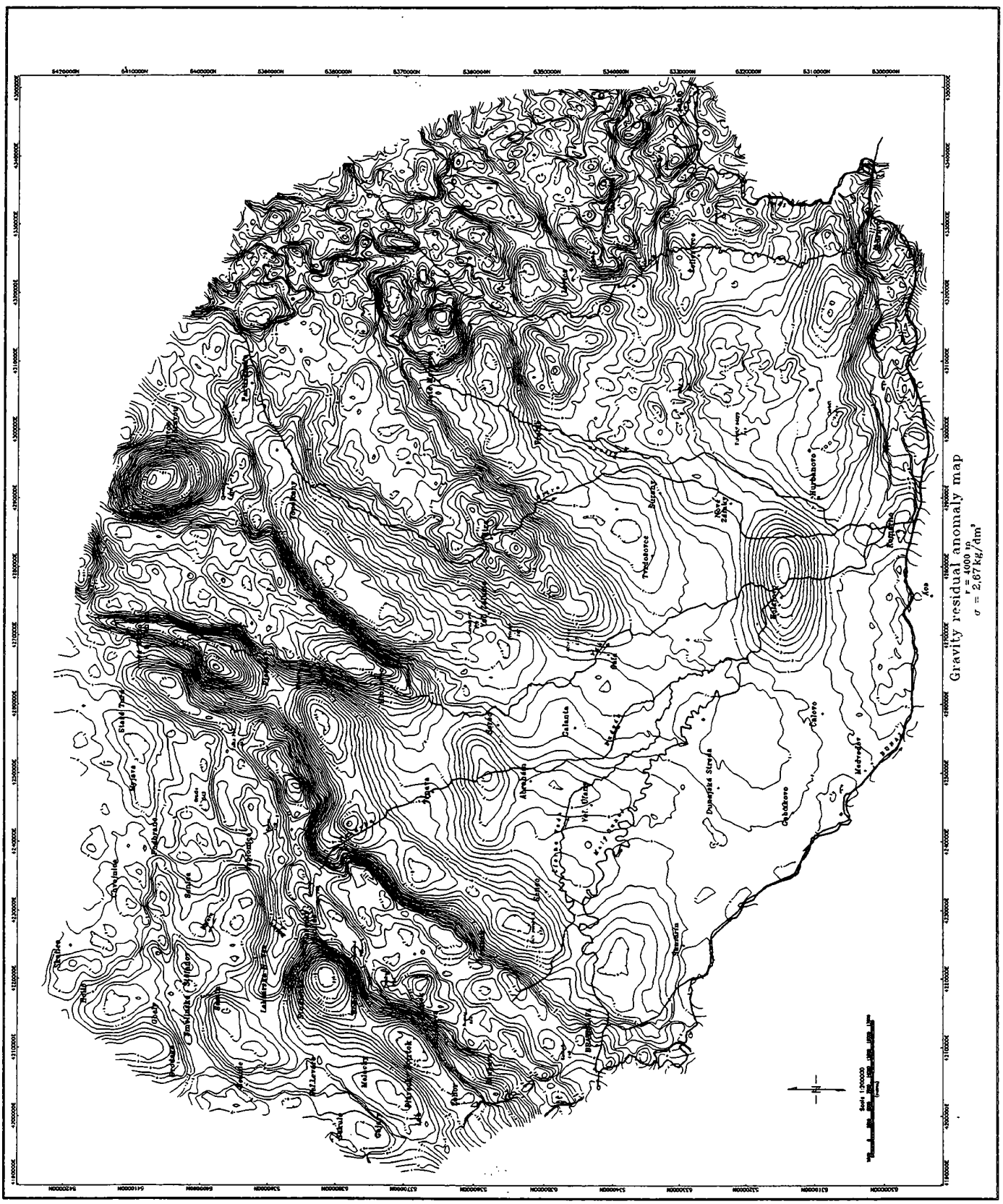

Fig.3a

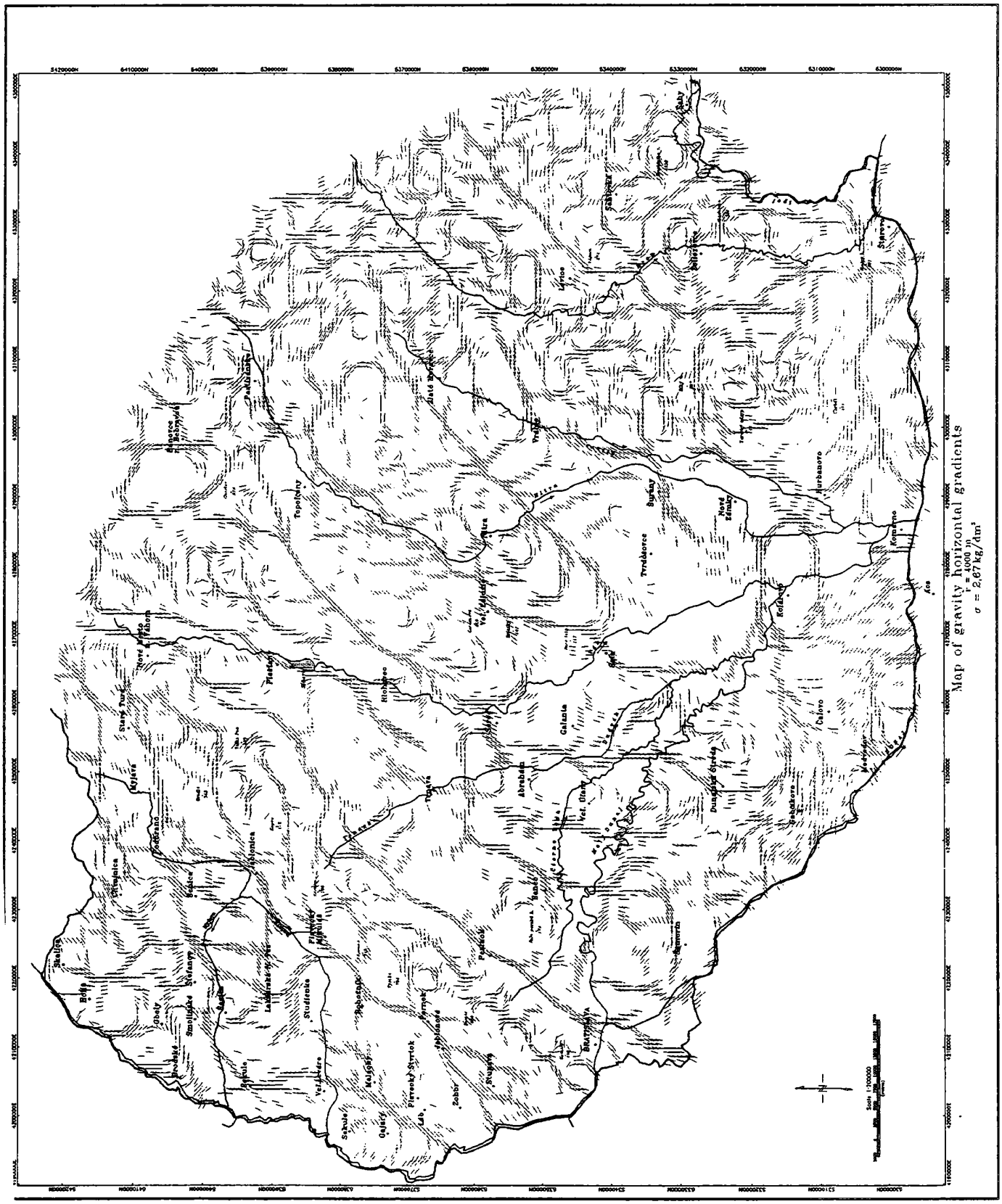

Fig.3b

north part of this anomaly. The gradient marks "strike - slip" tectonics between Abrahám and Trnava towns.

The negative gravity anomalies correspond to light rock complexes of Tertiary filling of the Danube basin, built mainly by gravely - sandy and clayey sediments. Accordingly, from intensity and geometry of the gravity field isolines, one can assumed thickness of the sedimentary complexes and their areal distribution. But it is no rule. This phenomenon will be explained in Gabčíkovo anomaly case. In its surroundings, as it is clear from Bouguer anomaly map, there is relatively positive anomaly, but from drilling results and seismic survey the Pre-Tertiary basement is at great depths. This phenomenon should be explained by presence of the neo-volcanics into Tertiary basin filling. This opinion confirms results of the magnetic observations (Gnojek,I., Putna,L., in Džuppa,P., 1993). The most expressive negative anomalies correspond with following depressions: Blatná, Rišňov, Bánovce, Komjatice and Dubnica. The gravity anomaly around Trnava town, which is a part of Blatná depression, has regional character and its source accordingly regional gravity map for R = 12 and 20 km, lies very deep (Plančár,J., in Fusán,O. et al, 1971). The neogene depressions among core mountains and depression on e. side of Tríbeč Mts., exhibit amplitude of -10 to -20 mGal, while in other part of the Danube basin in their continuation to the south is -2 to -6 mGal only.

The gravity field is affectes by presence of the heavy masses in basement (core). The MOHO - discontinuity is in whole area of interest in the same depth. We can state that morphology of the Pre-Tertiary basement geometry is very well reflexed in the gravity anomalies picture.

The faults in filling manifest in gravity field are expressive gravity gradients and sigmoidal bend of the isolines on greater distances. In the residual anomaly and horizontal gradients maps (Fig.3, Szalaiová,V., and Šantavý,J., 1996) one can see expressive demonstration of the density boundaries of NE - SW orientation, mainly corresponding with known tectonic lines. We can also see a large difference of density between Komárno lifted block and Dubnica platform. The picture around Levice town is more complicated. It is caused by neo - volcanics and mainly by decreased thickness of the Tertiary fill.

The Vienna basin is one of the regions which is well investigated by geophysical methods, mainly by seismic measurements. We will mention shortly about major gravity anomalies in this area.

The most expresive gravity anomaly (fig.4) is located in the area of Kúty depresion (up to -40.5 mGal). Its centre is in Kúty village surroundings. The depression is tectonically bounded. In the north, it is bounded by Hodonín - Gbely fault, which creates - together with Lužice - Brodské fault - the Hodonín - Gbely horst. The depression is limited by Svätý Ján fault.

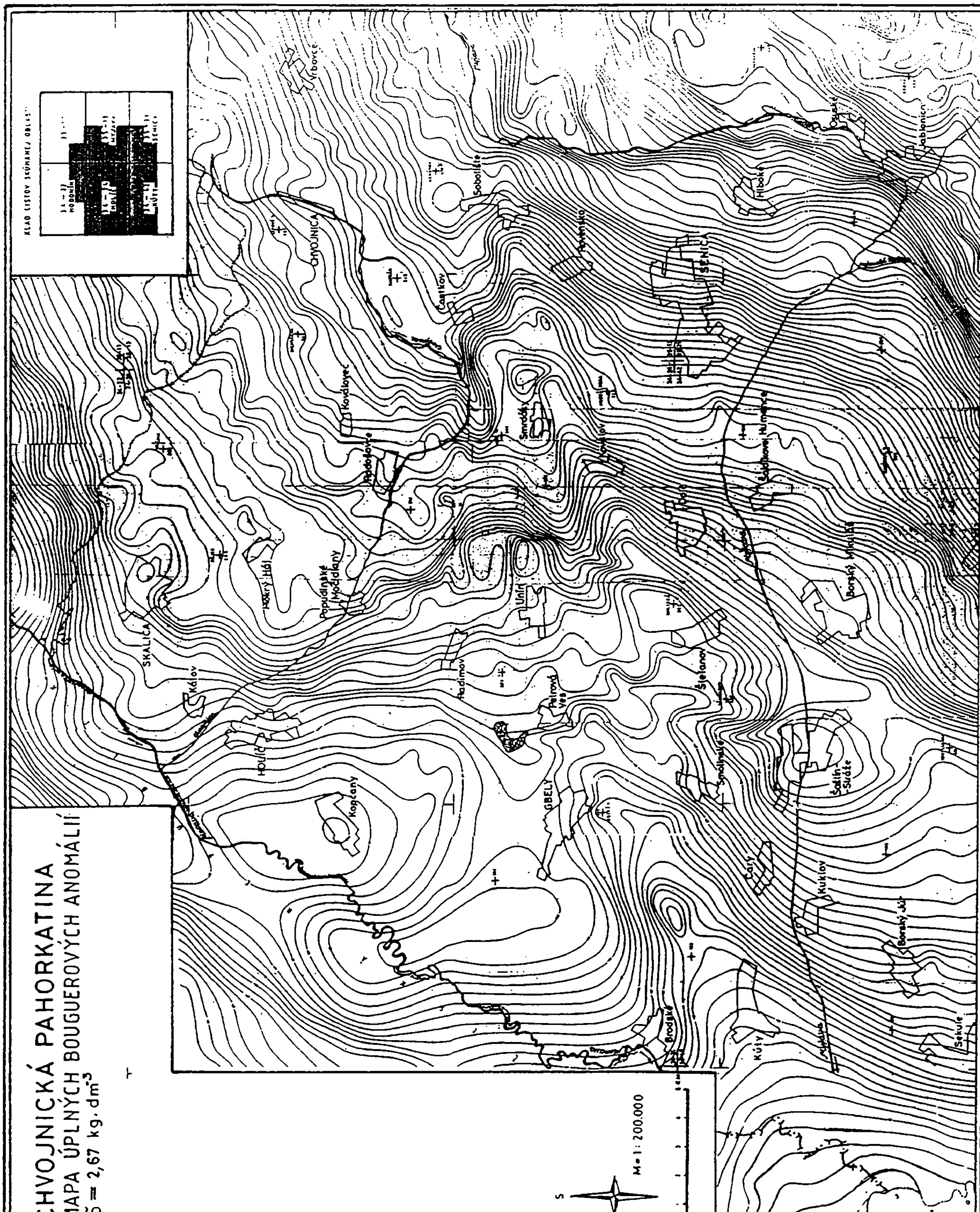
CHVOJNICKÁ PAHORKATINA
MAPA ÚPLNÝCH BOUGUEROVÝCH ANOMÁLIÍ
G = 2,67 kg.dm^{-3}
M = 1: 200.000
SENICA
SKALICA
CHVOJNICA
HOLÍČ
GBELY
Kopčany
Brodské
Kúty
Kuklov
Šaštín-Stráže
Smolinské
Štefanov
Petrova Ves
Radimov
Unín
Popudinské Močidľany
Kovalovec
Častkov
Sobotište
Hlboké
Jablonica
Osuské
Kopčany
Sekule
Borský Jur
Borský Mikuláš
Kátov
Mokrý Háj
Smrdáky
Vrbovce

Fig.4

Another expressive negative anomaly (-34.5 mGal) - Kopčany depression is situated near Kopčany village. We suppose its tectonic limitation, because it has in southern side the expressive gravity gradient . In South - West part of the area, around Šaštín - Stráže town, there is relatively positive anomaly (-24 mGal). Its North limitation is nonunambiguous by Bouguer anomaly map. This anomaly is affected by presence of the Choč unit rocks. They have higher natural density, which is proved by results of Ša -9, 10 and 11 boreholes. The Štefanov elevation coincides with Šaštín anomaly of the gravity field which has deep base and it influences the structural form of this area. Between Štefanov and Šaštín, the tectonic contact of flysch, nappe outher and Mesozoic nappes zones occurs. The areally large anomalies are in east and west of Smrdáky village. By interpretation (Tomek,Č.,1975) and drilling results, the basement is built by nappe outlier zone there. In the Bouguer anomaly map, the crossing of several tectonic lines is evident in this area.

The region west of Osuské village up to Šaštín - Stráže town is characterized by gravity gradient, which represents downthrow of the Neogene basement along tectonic lines of N - S course to the Brezovo depression. The downthrows along these faults are synsedimentary and that is why the thickness of the sediments on blocks of the same age could be different.

QUANTITATIVE INTERPRETATION

As examples of the quantitative interpretation we can show the profile which is interpretated in the Vienna basin - the part of Chvojnická pahorkatina downs (Fig.5) and the profile situated through the Tríbeč Mts. (Fig.6).

The profile in the Fig.5 passes from N - W direstion via the Gbely - Hodonín horst, Kopčany depression and continues S - E direction towards over the klippen belt zone. Practically it means the seismic profile 531/70, 75, which is lenghtened to borehole T -13A . We can gradually see the gradual downthrow of the structural elements of Gbely - Hodonín horst towards Kopčany depression. The profile 531/75 passes by the axis of Kopčany depression and characterizes its deeper part. In the region of Radimov it links with the profile 531/70, which continues to Štefanov elevation and towards Koválov depression. The surface of flysh horizont to the mentioned elevation rises gently from depth of 1250 m on dropped block of Jánsky fault up to approximatelly 600 m in the borehole Št - 205. In the section it is interpreted crossing the Farský and Jánsky fault.

The profile in the Fig.6 passes N - S direction aproximately from Partizánske town via Veľký Klíž village to Lovce village. It was found out by gravity regional mapping that there is expressive positive anomaly situated (BA for density 2.67 $kg.dm^{-3}$) with expressive gradient on the south side of Tríbeč Mts.. It is possible to interprete quantitatively this anomaly only in the case of presence of granite rocks of big thickness resp. by thinking of heavy block under the granite.

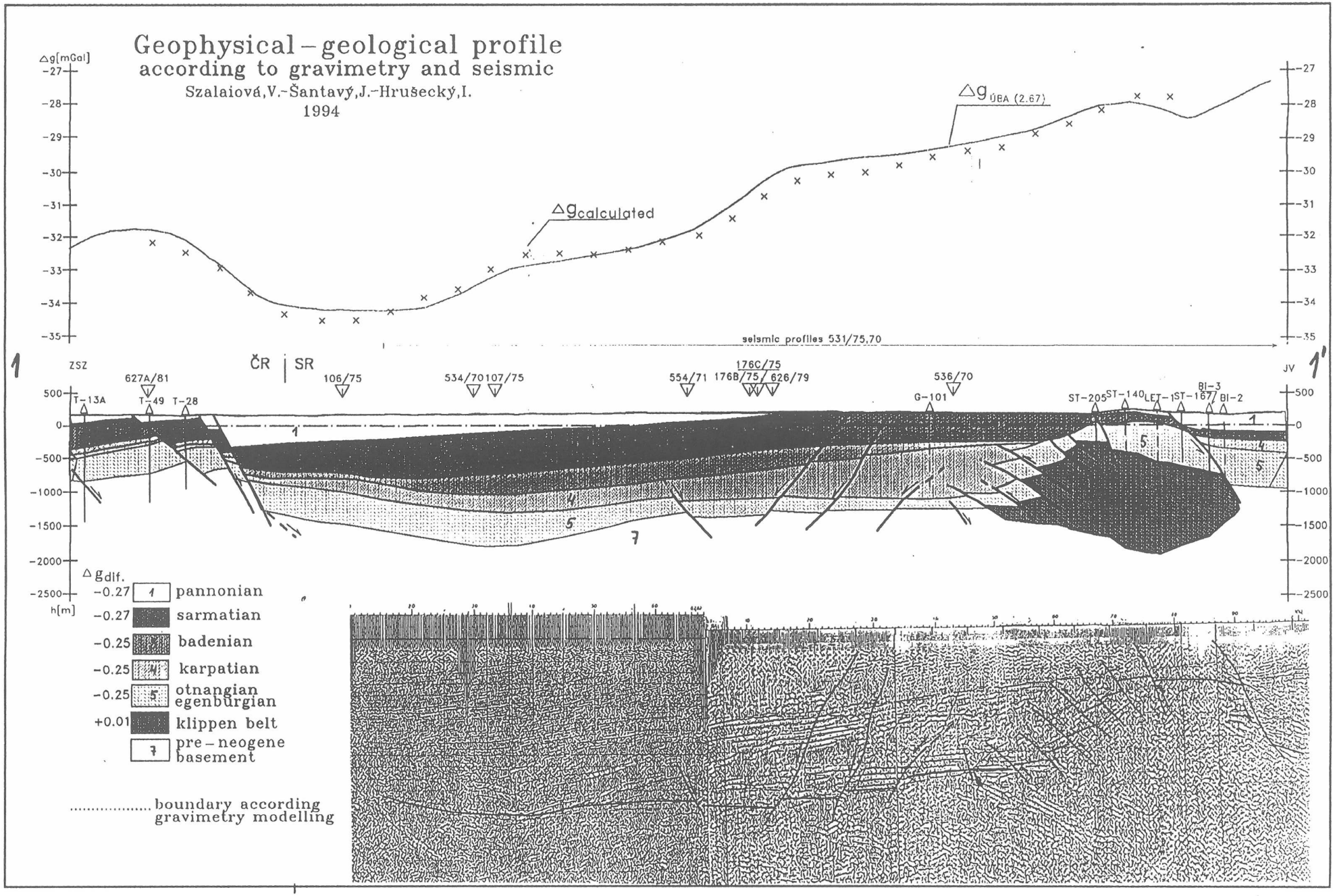
Geophysical – geological profile
according to gravimetry and seismic
Szalaiová,V.-Šantavý,J.-Hrušecký,I.
1994
Δg[mGal]
Δg ÚBA (2.67)
Δg calculated
seismic profiles 531/75,70
1
1'
ZSZ
JV
ČR
SR
627A/81
T-13A
T-49
T-28
106/75
534/70
107/75
554/71
176C/75
176B/75
626/79
536/70
G-101
ST-205
ST-140
LET-1
ST-167
BI-3
BI-2
h[m]
Δg dif.
-0.27 pannonian
-0.27 sarmatian
-0.25 badenian
-0.25 karpatian
-0.25 otnangian egenburgian
+0.01 klippen belt
pre – neogene basement
boundary according gravimetry modelling

Because we do not have the exact information about the thickness of granites in this region there are no information about any deep borehole, we interprete in a model the thickness of granit rock block aproximately 2000 m with density +0.03 $kg.dm^{-3}$ and it litologicaly could refer to quartz diorite. Under the diorite we interpreted the block with density +0.22 $kg.dm^{-3}$ (Šantavý,J.,Lanc,J. et al.1995). It is origin and the consistence is unknown, but it could be mice shist and amphibolite with thickness of 2500 m. Mentioned heavy block is supposed to be under the whole Tríbeč Mts. with continuing and wedging down into Komjatice depression in the south. In the west it wedging down into Topoľčany depression and towards the north is thickness decrease to 1500 m. Boundary on position 40.5 km refers to Skýcov deep line.

CONCLUSION AND DISCUSSION

In this article we tried to characterize the main gravity anomalies of the region of Podunajská panva basin. In the map BA there are the mountains which are built by crystalline complex of Tatricum and covering sequention , also as anomaly of the region of Kolárovo, which are probable sources of ultrabasic rocks. By interpretation the modeling the results about probable space decompose of the Kolárovo anomaly were obtained. It was found out that the anomal block is asymetric stretched in the course of east - west direction with the top border in the depth of 5 - 6 km and the lower border in the depth of 13 km. According to Bezák,V., et al. 1995 the Kolárovo anomaly is interpreted as suture of meliatikum unit used in disintegration orogene for the ascent of anomaly masses of astenosphere. The problem of Kolárovo anomaly interpretation was discussed by many experts and probably with knowledge increase and obtaining new exact information we will come back to this problem.

Besides Kolárovo anomaly it is need to notice the organization of positive and negative anomalies whith north - east direction, which is clear very well also in residual maps - the map of horizont gravity gradients and in the map of residual anomalies. In the map BA we can also follow probable strike slip of south block continuing of Považský Inovec Mts. between Abrahám village and Trnava town. We think it is interesting and the new results of interpretation would bring the modeling on seismic profiles measured by firm MAXUS DALLAS, which were realized for the oil - gas prospection.

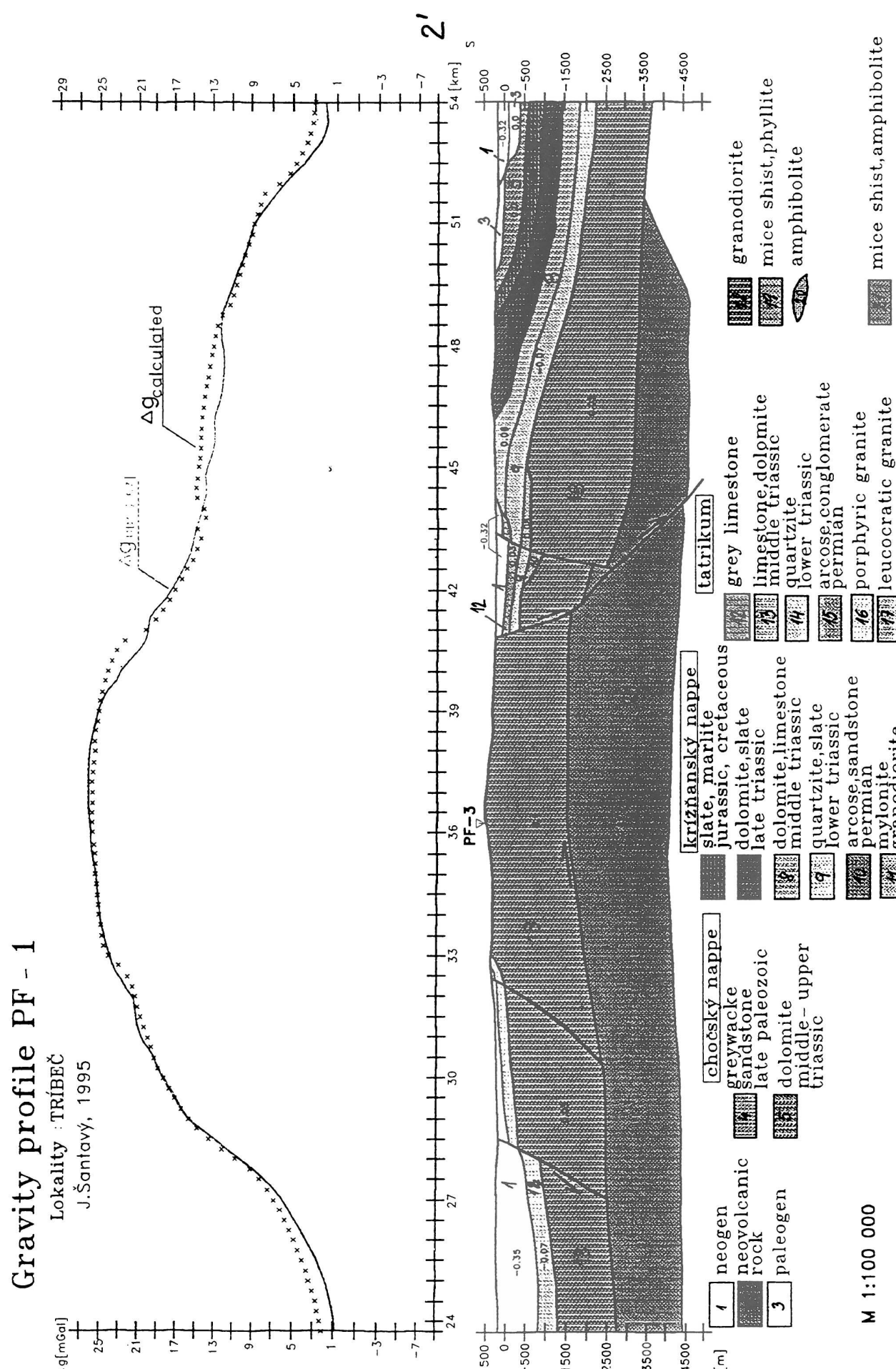
Gravity profile PF - 1
Lokality : TRÍBEČ
J.Šantavý, 1995
Δg[mGal]
Δg calculated
2
2'
J
S
54 [km]
PF-3
h[m]
M 1:100 000
krížňanský nappe
chočský nappe
tatrikum
neogen
neovolcanic rock
paleogen
greywacke sandstone late paleozoic
dolomite middle- upper triassic
slate, marlite jurassic, cretaceous
dolomite,slate late triassic
dolomite,limestone middle triassic
quartzite,slate lower triassic
arcose,sandstone permian
mylonite
granodiorite
grey limestone
limestone,dolomite middle triassic
quartzite lower triassic
arcose,conglomerate permian
porphyric granite
leucocratic granite
granodiorite
mice shist,phyllite
amphibolite
mice shist,amphibolite

Fig.6

References

Bezák,V.,Šefara,J.,Bielik,M.,Kubeš,P.,1995:Litosphery model of the West Carpathian, geophysical and geological interpretations. Mineralia Slovaca, No.27, p.169-178 (in Slovak)

Bielik,M.,Sitárová,A.,Marková,M.,Levashov,S.,1994:Interpretation of the Kolárovo gravity anomaly by the option method. Acta geologica Universitatis Comenianae, 50, p.37-43

Bílek,K.,Hrušecký,I.,1988:Investigation of geological built and oil-gas reservoir of lower Miocen of Gbely - Hodonín horst. VVNP Bratislava (in Slovak)

Džuppa,P.,et al. 1993: Geophysical investigation of Podunajská panva basin - DANREG. Manuscript. Geocomplex Bratislava (in Slovak)

Fusán,O., et al 1971: Geological model of basement of covered south parts of West Carpatian. Zborník geologických vied, Západné Karpaty edition. No 15., p. 173

Hricko,J., et al. 1993: Bratislava - environmental investigation. Abiotic component. Manuscript. Geocomplex Bratislava (in Slovak)

Ibrmajer,J. 1963: Regional gravity measurement in scale 1 : 200 000. Geofyzika Brno (in Czech)

Lanc,J., et al. 1995: Map of geophysical indications and interpretations of region Tríbeč. Final report. Geocomplex Bratislava (in Slovac)

Mikuška,J., et al. 1992 - 1995: Viedenská panva basin - direct finding out of oil - gas reservoirs. Nafta Gbely (in Slovak)

Panáček,A., et al. 1987: Map of geophysical indications and interpretations of region Podunajská nížina basin North - East part. Geocomplex Bratislava (in Slovak)

Szalaiová,V., et al. 1994: Map of geophysical indications and interpretations of region Chvojnícka pahorkatina hill. Final report. Geocomplex Bratislava (in Slovak)

Szalaiová,V.,Šantavý,J.,1995: Gephysical investigations od Slovakia - gravity measurements. Geocomplex Bratislava (in Slovak)

Szalaiová,V.,Šantavý,J.,1996 : Synthesis of deep built of West Carpathian. Region of West Slovakia. Stage report. Geocomplex Bratislava (in Slovak)

Tomek,Č. et al. 1975: Unique processing and interpretation of gravity measurements of Viedenská panva basin and adjoing inner flysh Carpatian. Manuscript. Geofyzika Brno (in Czech)

GRAVITY ANOMALIES CAUSED BY THERMOELASTIC DEFORMATIONS IN THE VICINITY OF MAGMATIC BODIES

Ladislav Brimich and Milan Hvoždara

Geophysical Institute of the Slovak Academy of Sciences

Abstract:

The paper presents theoretical formulae for the calculation of the steady-state thermoelastic deformation field due to magmatic bodies approximated by a three dimensional prism embedded in an elastic half-space. The formulae for the gravity anomaly due to non-uniform extension connected with thermoelastic deformation is derived as well. A set of figures presents the results of the pertinent numerical calculations. The results have shown that the main part of the negative gravity anomaly is due to the vertical elevation (doming) of the surface above the magmatic body. The free-air and Bouguer anomaly are of the order of $10^{-6}\,\mathrm{m\,s^{-2}}$, while the part due to extensional changes of the density is 3 orders less.

Introduction

The magmatic intrusion in the Earth's crust will cause a series of effects related to its mass as well as to the pressurization of the chamber due to overfilling or temperature changes. In the deformation modelling and prediction the most interesting effects are those which in principle could be detected on the surface before the eruption, including surface gravity changes and deformation. In consequence, the theoretical problem lies in calculating the gravitational potential and gravity changes, and the deformation produced on the Earth's surface by a magmatic intrusion in the crust.

Point source allows us to make adjustments and interpret data using simple models, although these present problems as ambiguities of the source solution (see e.g. Delaney and McTigue, 1994). The simplest model of volcanic intrusion is the classical model Mogi (1958); it represents a center of expansion buried at depth ζ in an elastic halfspace. Pressure changes within the magma chamber produce a deformation and gravity changes at the surface of the Earth. The effect of layering in an elastic medium was discussed by Rundle (1980, 1982, 1983). Gravitational effects are not significant for surface displacements and tilt. Rundle (1980) showed that gravitational effects in ground deformation become significant at wavelenghts larger than 1000 km, but have little relevance to deformation in the near-source region. The effect of vertical structure in gravitational media was discussed by Fernández and Rundle (1994), who show that the deviations of displacements in a layered medium from those in a homogeneous halfspace are more strongly affected by variations in elastic moduli than by changes in layer reference densities.

In the geodynamic theory, it is well-known that the thermoelastic stresses play a considerable role in the stress state of the lithosphere and its dynamics, especially in localities with pronounced positive geothermal anomalies (Combs and Hadley, 1997; Teisseyre, 1986). This is what spurred Hvoždara and Rosa (1980) to carry out a theoretical analysis of thermoelastic deformations of a homogeneous halfspace due to a point or linear source of heat, located at a particular depth in the halfspace. The theoretical formulae for the gravity anomaly due to non-uniform extension connected with thermoelastic deformations were derived by Hvoždara and Brimich (1995).

In Brimich et al. (1996) the computation of simple analytical models of surface displacements and gravity changes in layered elastic-gravitational medium and in an elastic halfspace with point source of heat is presented. The comparison of the radial and vertical components of the displacement and gravity changes indicates that the horizontal changes of these quantities are smaller for the thermoelastic model than for the elastic--gravitational.

This paper presents an advanced analysis, extended to the case of sources of heat uniformly distributed in a finite volume V of the halfspace, which corresponds to a model of magmatic body.

Thermoelastic deformation of the halfspace due to a point source of heat

It is proved (Nowacki, 1962) that the static non-uniform temperature field $T(x,y,z)$ in an elastic medium corresponds to the thermoelastic displacement field $\boldsymbol{u}$ which satisfies Lamé's equation:

$$(\lambda+\mu)\mathrm{graddiv}\boldsymbol{u}+\mu\nabla^2\boldsymbol{u}-\gamma\mathrm{grad}T=0, \tag{1}$$

where λ,μ are the Lamé elastic parameters, $\gamma=(3\lambda+2\mu)\alpha_T$, α_T being the thermal coefficient of the linear expansion, $\nabla^2\equiv\mathrm{divgrad}$ is the Laplace differential operator. We can see that the term $-\gamma\mathrm{grad}T$ plays the role of a body force in the equation of the elastic equilibrium (1). For the Carthesian components of the stress tensor σ_{ij} we have Duhamel – Neumann relations:

$$\sigma_{ij}=(\lambda\Theta-\gamma T)\delta_{ij}+2\mu e_{ij}, \qquad i,j=1,2,3 \tag{2}$$

where $\Theta=\mathrm{div}\boldsymbol{u}$, δ_{ij} being Kronecker symbol ($\delta_{ij}=1$, $i\neq j$, $\delta_{ii}=0$). Components of the strain tensor e_{ij} are defined as follows:

$$e_{ij}=\frac{1}{2}\left[\frac{\partial u_i}{\partial x_j}+\frac{\partial u_j}{\partial x_i}\right]. \tag{3}$$

The temperature field is considered to be static, i.e. in homogeneous medium it satisfies equation:

$$\lambda_T\nabla^2T=-s(x,y,z), \tag{4}$$

where λ_T is the heat conductivity and $s(x,y,z)$ gives the heat production per unit volume in the point (x,y,z).

Heat production of point source of heat located at the point $(0,0,\zeta)$ satisties equation:

$$s(x,y,z) = w\delta(x)\delta(y)\delta(z-\zeta), \tag{5}$$

w is the heat power of the source (in Watt). Then the temperature due to this source is axially symetric with respect to the z–axis and satisfies boundary condition $T(r,z)\,|_{z=0} = 0$. It is expressed by the formula:

$$T(r,z) = \frac{w}{4\pi\lambda_T}\left(R_1^{-1} - R_2^{-1}\right), \tag{6}$$

where $R_1 = [r^2 + (z-\zeta)^2]^{1/2}$, $R_2 = [r^2 + (z+\zeta)^2]^{1/2}$, $r^2 = x^2 + y^2$. The thermoelastic displacement u_T as the solution of Eq. (1) has the components:

$$\begin{aligned}(u_r)_T &= Ar\left\{R_1^{-1} + R_2^{-1} - 2\zeta z\ R_2^{-3} + 4\zeta(1-\nu)R_2^{-1}(R_2+\zeta+z)^{-1}\right\},\\ (u_z)_T &= A\left\{(z-\zeta)R_1^{-1} - (z+\zeta)R_2^{-1} - 2\zeta(1-2\nu)R_2^{-1} - 2\zeta z(z+\zeta)R_2^{-3}\right\},\end{aligned} \tag{7}$$

where $A = w\gamma[8\pi\lambda_T(\lambda+2\mu)]^{-1}$ and $\nu = \dfrac{1}{2}\dfrac{\lambda}{(\lambda+\mu)}$ being the Poisson ratio. The thermoelastic stress tensor has the components:

$$\begin{aligned}\sigma_{rr} = &-2\mu A\left\{(1+r^2R_1^{-2})R_1^{-1} - (1+r^2R_2^{-2})R_2^{-1} - \right.\\ &\left. - 2\zeta\left[4z + 2\zeta - 3z\zeta(z+\zeta)^2R_2^{-2}\right]R_2^{-3} + 4\zeta(1-\nu)R_2^{-1}\left[R_2+z+\zeta\right]^{-1}\right\},\end{aligned}$$

$$\begin{aligned}\sigma_{\varphi\varphi} = &-2\mu A\left\{R_1^{-1} - R_2^{-1} - 2\zeta\left[(2\nu-1)z + 2\nu\zeta\right]R_2^{-3} - \right.\\ &\left. - 4\zeta\,(1-\nu)R_2^{-1}(R_2+z+\zeta)^{-1}\right\},\end{aligned} \tag{8}$$

$$\begin{aligned}\sigma_{zz} = &-2\mu A\left\{(2-r^2R_1^{-2})R_1^{-1} - (2-r^2R_2^{-2})R_2^{-1} + \right.\\ &\left. + 2z\zeta\left[1 - 3(z+\zeta)^2R_2^{-2}\right]R_2^{-3}\right\},\end{aligned}$$

$$\sigma_{rz} = -6\mu Ar\left\{(z-\zeta)R_1^{-3} - \left[z - \zeta + 6z\zeta(z+\zeta)R_2^{-2}\right]R_2^{-3}\right\}.$$

The surface heat flow anomaly $q_z = \lambda_T\left[\dfrac{\partial T}{\partial z}\right]_{z=0}$ is:

$$q_z = \frac{w}{4\pi}\frac{2\zeta}{R_0^3}, \tag{9}$$

where $R_0 = (r^2+\zeta^2)^{1/2}$.

Thermoelastic deformation of the halfspace due to a finite volume source of heat

According to the principle of superposition we can employ the solution for the point source of heat such as the Green function, in order to calculate the effect due to the finite volume source of heat, i. e. for a certain magmatic body which occupies the volume V of the halfspace $z > 0$.

Let us suppose that the heat power due to the unit volume of the magmatic body is constant in the region V and equals to f_0. The temperature field outside the body is then given by the integral:

$$T(x,y,z) = \frac{f_0}{4\pi\lambda_T} \iiint_V \left[R_1^{-1} - R_2^{-1}\right] dV', \tag{10}$$

where now

$$\begin{aligned} R_1 &= \left[(x-x')^2 + (y-y')^2 + (z-z')^2\right]^{1/2}, \\ R_2 &= \left[(x-x')^2 + (y-y')^2 + (z+z')^2\right]^{1/2}, \end{aligned} \tag{11}$$

The calculation point $P \equiv (x,y,z)$, $z > 0$, a source location point $Q \equiv (x',y',z')$ is now an arbitrary point inside V. Formula (10) was generalized from (6) where we put general coordinates of a point source of heat and its heat power $w = f_0 dV'$ and then we integrated the temperature effect of all the point sources in V. In this way we can also obtain displacements and stresses, but first it is necessary to determine the Carthesian components of displacement (7) and stresses (8) which have been given in the „privileged" cylindrical coordinate system. In (7) and (8) we now replace w in the factor A by $f_0 dV'$ and integrate over the volume of the source region V to obtain the total effect for displacements and stresses. We denote the integrated values of displacements by U_x, U_y, U_z and the interated stress tensor components by S_{ij}, where $i,j = x,y,z$. Then we have:

$$U_x = B \iiint_V (x-x') \left\{R_1^{-1} + R_2^{-1} - 2z'zR_2^{-3} + 4(1-\nu)z'R_2^{-1}(R_2+z+z')^{-1}\right\} dV', \tag{12}$$

$$U_y = B \iiint_V (y-y') \left\{R_1^{-1} + R_2^{-1} - 2z'zR_2^{-3} + 4(1-\nu)z'R_2^{-1}(R_2+z+z')^{-1}\right\} dV', \tag{13}$$

$$U_z = B \iiint_V (z-z') \left\{R_1^{-1} - (z+z')R_2^{-1} - 2z'(1-2\nu)R_2^{-1} - 2z'z(z+z')R_2^{-3}\right\} dV', \tag{14}$$

where we introduced the factor $B = f_0\gamma[8\pi\lambda_T(\lambda+2\mu)]^{-1}$ instead of the factor A in formulae (7) and (8).

For the component of stress tensor we obtain:

$$S_{xx} = B \iiint_V A^{-1} \left[\sigma_{rr}\frac{(x-x')^2}{r^2} + \sigma_{\varphi\varphi}\frac{(y-y')^2}{r^2}\right] dV',$$

$$S_{yy} = B\iiint_V A^{-1}\left[\sigma_{rr}\frac{(y-y')^2}{r^2} + \sigma_{\varphi\varphi}\frac{(x-x')^2}{r^2}\right]dV',$$

$$S_{xy} = B\iiint_V A^{-1}(\sigma_{rr} - \sigma_{\varphi\varphi})\frac{(x-x')(y-y')}{r^2}dV', \tag{15}$$

$$S_{xz} = B\iiint_V A^{-1}\sigma_{rz}\frac{x-x'}{r}dV',$$

$$S_{yz} = B\iiint_V A^{-1}\sigma_{rz}\frac{y-y'}{r}dV',$$

$$S_{zz} = B\iiint_V A^{-1}\sigma_{zz}dV',$$

where σ_{rr}, σ_{rz} and σ_{zz} are given by (8).

We are mainly interested in the surface values of displacements and stresses. As regards the stress tensor we are interested in the principal stresses and the maximum shear stress. We performed this analysis on the $z = 0$ plane where S_{xz}, S_{yz} and S_{zz} are zero. According to the tensor analysis the formulae of the principal stresses in the x, y plane are given by the formula:

$$S_{1,2} = \frac{1}{2}(S_{xx} + S_{yy}) \pm \frac{1}{2}\left[(S_{xx} - S_{yy})^2 + (2S_{xy})^2\right]^{1/2}. \tag{16}$$

S_1 and S_2 being the maximum and minimum stresses, respectively. The maximum shear stress τ_{max} is given by the difference:

$$\tau_{max} = \frac{1}{2}(S_1 - S_2) = \frac{1}{2}\left[(S_{xx} - S_{yy})^2 + (2S_{xy})^2\right]^{1/2}. \tag{17}$$

(By application of (16) to the point source of heat at $x' = 0$, $y' = 0$, $z' = \zeta$ we can prove, in this simple case, that $S_1 = \sigma_{\varphi\varphi}$, $S_2 = \sigma_{rr}$ since $\cos\varphi = x/r$ and $\sin\varphi = y/r$). Directions α_1, α_2 of the principal stress are given by formulae:

$$\tan\alpha_1 = \frac{(S_1 - S_{xx})}{S_{12}},$$

$$\tan\alpha_2 = (S_2 - S_{xx})S_{12}, \tag{18}$$

$$\alpha_2 = \alpha_1 + \pi/2.$$

Thermoelastic displacements on the surface of the halfspace can be calculated by means of simplified formulae:

$$[U_x]_{z=0} = 4B(1-\nu)\iiint_V \frac{z'(x-x')}{R_0(R_0+z')}dV',$$

$$[U_y]_{z=0} = 4B(1-\nu)\iiint_V \frac{z'(y-y')}{R_0(R_0+z')}dV', \tag{19}$$

$$[U_z]_{z=0} = -4B(1-\nu)\iiint_V \frac{z'}{R_0}dV',$$

where $R_0 = R_1|_{z=0} = R_2|_{z=0} = [(x-x')^2 + (y-y')^2 + (z')^2]^{1/2}$. It is also interesting to evaluate the associated anomaly of the heat flow which is due to the temperature field (10). According to the expression $q_z = \lambda_T \left[\frac{\partial T}{\partial z}\right]_{z=0}$ we obtain:

$$q_z = \frac{f_0}{2\pi} \iiint_V \frac{z'}{R_0^3} dV'. \tag{20}$$

For non-zero components of the stress tensor we have:

$$S_{xx}|_{z=0} = 8B\mu \left\{ \nu \iiint_V \frac{(z')^2}{R_0^3} dV' + (1-\nu) \iiint_V \frac{z'}{R_0(R_0+z')} dV' - \right.$$
$$\left. - (1-\nu) \iiint_V \frac{(x-x')^2 z'(2R_0+z')}{R_0^3(R_0+z')^2} dV' \right\},$$

$$S_{yy}|_{z=0} = 8B\mu \left\{ \nu \iiint_V \frac{(z')^2}{R_0^3} dV' + (1-\nu) \iiint_V \frac{z'}{R_0(R_0+z')} dV' - \right.$$
$$\left. - (1-\nu) \iiint_V \frac{(y-y')z'(2R_0+z')}{R_0^3(R_0+z')^2} dV' \right\}, \tag{21}$$

$$S_{xy}|_{z=0} = -8B\mu(1-\nu) \iiint_V \frac{(x-x')(y-y')z'(2R_0+z')}{R_0^3(R_0+z')^2} dV'.$$

Components S_{zz}, S_{xz}, S_{yz} are zero at $z = 0$. Formulae (19)–(21) require calculation of triple integrals since $dV' = dx'dy'dz'$. If we suppose that $z' \in < z_1'; z_2' >$ then we can carry out the integration with respect to z' analytically.

By using Hook's low we can express the strain components for the surface of the Earth:

$$\varepsilon_{xx} = \frac{1}{2\mu} S_{xx} - \frac{\lambda}{\mu(6\lambda+4\mu)}(S_{xx}+S_{yy}),$$
$$\varepsilon_{yy} = \frac{1}{2\mu} S_{yy} - \frac{\lambda}{\mu(6\lambda+4\mu)}(S_{xx}+S_{yy}), \tag{22}$$
$$\varepsilon_{zz} = \frac{\lambda}{\mu(6\lambda+4\mu)}(S_{xx}+S_{yy}),$$
$$\varepsilon_{xy} = \frac{1}{2\mu} S_{xy}.$$

Dilatation $\Theta = \mathrm{div}\boldsymbol{u}$ can be expressed:

$$\Theta = \frac{1}{3\lambda+2\mu}(S_{xx}+S_{yy}). \tag{23}$$

In this formulae we have accounted that for the free surface of the Earth the stress tensor components S_{zz}, S_{xz}, S_{yz} are zero.

In calculating the perturbation of gravity due to a heat source, there are two principal reasons for the gravity change:

a) The free-air variation and Bouguer correction as the effect of vertical uplift of the surface above the heat source. This effect can simply be calculated as:

$$\Delta g_{TFB} = \left[\frac{\partial g_0}{\partial z} - 2\pi G\rho_0\right](u_z)_T, \tag{24}$$

where $\frac{\partial g_0}{\partial z} = +0.3086 \times 10^{-7}\, s^{-2}$ is the vertical gradient of normal gravity, $G = 6.67 \times 10^{-11}\,\mathrm{kg^{-1}m^3s^{-2}}$ is Newton's gravitational constant, ρ_0 is the density and $(u_z)_T$ is the z component of the displacement.

b) The change of density ρ_0 by increment $\Delta\rho_{\mathrm{TE}}$ due to the divergence of thermoelastic displacement u_T:

$$\Delta\rho_{\mathrm{TE}} = -\rho_0 \mathrm{div} u_T. \tag{25}$$

The gravity change Δg_{TE} due to the thermoelastic density change $\Delta\rho = -\rho_0 \mathrm{div} u_T$ can be expressed as $[\partial\varphi_{TE}/\partial z]_{z=0}$ where the perturbation potential satisfies the Poisson's equation:

$$\nabla^2\psi_{TE}(r,z) = 4\pi G\rho_0 \mathrm{div} u_T, \qquad z \geq 0 \tag{26}$$

and in the upper halfspace Laplace equation:

$$\nabla^2\psi_{0TE}(r,z) = 0, \qquad z < 0. \tag{27}$$

The divergence of the displacement components (7) is simply calculable and leads to result:

$$\mathrm{div} u_T = 2A\left\{R_1^{-1} - R_2^{-1} + 2(1-2\nu)\zeta(z+\zeta)R_2^{-3}\right\}. \tag{28}$$

The potential ψ_{TE} and ψ_{0TE} must fulfil the continuity boundary conditions at the surface $z = 0$:

$$[\psi_{TE}]_{z=0} = [\psi_{0TE}]_{z=0},$$

$$\left[\frac{\partial\psi_{TE}}{\partial z}\right]_{z=0} = \left[\frac{\partial\psi_{0TE}}{\partial z}\right]_{z=0} \tag{29}$$

The solution of this boundary–value problem showes that:

$$\left[\frac{\partial\psi_{TE}}{\partial z}\right]_{z=0} = \Delta g_{TE} = -8\pi G\rho_0 A(1-\nu)\frac{\zeta}{\sqrt{R^2+\zeta^2}}. \tag{30}$$

Numerical results and discussion

Results of deformation characteristics for the surface due to a point source of heat are plotted in Fig. 1. It showes surface displacements and stresses due to the point source of

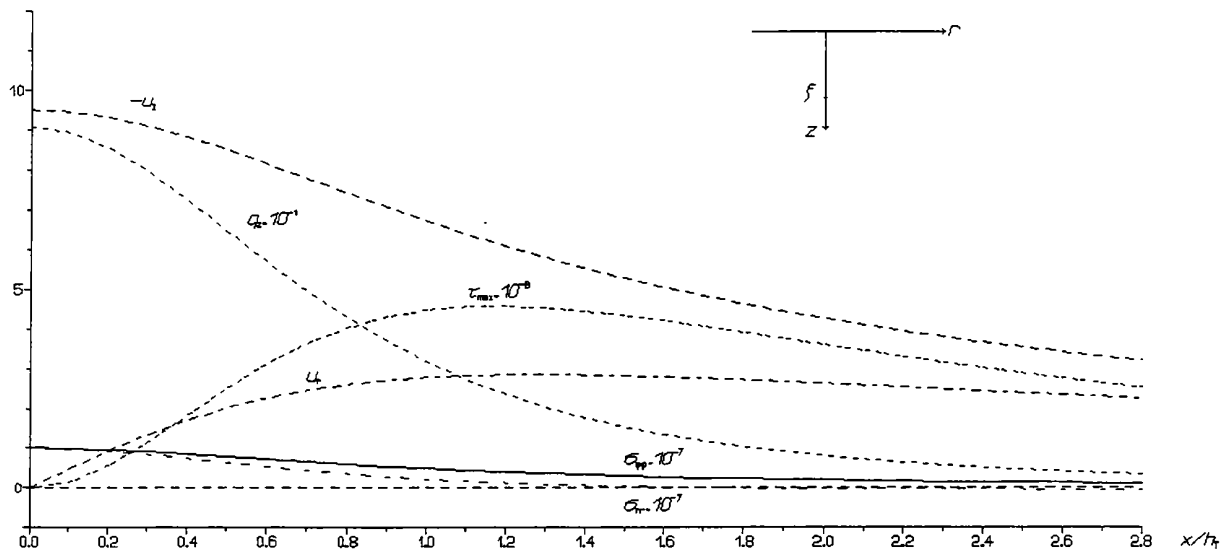

Fig. 1 Computed heat flow g_z and associated thermoelastic displacements u_r, u_z and stress characteristics σ_{rr}, $\sigma_{\varphi\varphi}$, τ_{max} on the surface of the halfspace in which the static point heat source is located, in the depth $\zeta = 50\,\mathrm{km}$, its heat power is $w = 6.6 \times 10^8\,\mathrm{W}$, Lamé elastic parameters of the halfspace are $\lambda = 7.5 \times 10^{10}\,\mathrm{Pa}$, $\mu = 6.075 \times 10^{10}\,\mathrm{Pa}$. The coefficient of linear thermal expansion is $\alpha_T = 10^{-6}\mathrm{K}^{-1}$, thermal conductivity $\lambda_T = 3\mathrm{W\,m}^{-1}\mathrm{K}^{-1}$ (g_z is in $\mathrm{m\,W\,m}^{-2}$, u_r, u_z in metres, stresses in Pascals).

heat in the depth $\zeta = 50\mathrm{km}$ of the elastic halfspace which gives the maximum surface heat flow anomaly $q_z|_{r=0} \doteq 42\mathrm{mW/m}^2$, i. e. about 1 H.F.U. We can see that the surface of the halfspace is swollen most in epicentre of the heat source (u_z is negative). The horizontal displacement u_r is zero in the epicentre, it increases to maximum at about $r \approx \zeta$ and then decreases slowly. On the surface of the halfspace $z = 0$ only σ_{rr} and $\sigma_{\varphi\varphi}$ are non-zero, since σ_{rz} and σ_{zz} are zero at this free boundary according to the theory of elasticity. The $\sigma_{\varphi\varphi}$ component is positive, i. e. the stress is expansive over the whole surface; σ_{rr} is positive only for $r \leq 1.7\zeta$, then it attains small negative values, i. e. the stress is compressive for $r \geq 1.7\zeta$. It can be easily shown that the stresses $\sigma_{\varphi\varphi}$ and σ_{rr} are principal on the surface $z = 0$, $\sigma_{\varphi\varphi}$ being the maximum and σ_{rr} minimum stress. The maximum shear stress is $\tau_{max} = \frac{1}{2}(\sigma_{\varphi\varphi} - \sigma_{rr})$. It attains its maximum at the circle $r \approx \zeta$ which is the region where circular faults can first arise.

We considered the magmatic body of a prismatic shape elongated vertically and horizontally which allows the numerical integration to be easily programmed. For the vertically elongated prisma of a square horizontal cross-section of the body we have: $\zeta' \in < -a/2;\, a/2 >$, $y' \in < -b/2;\, b/2 >$, $z' \in < z'_1, z'_2 >$, where $a = b = 4\,\mathrm{km}$, $z'_1 = h_T - c/2$, $z'_2 = h_T + c/2$, $c = 10\,\mathrm{km}$. For the horizontally elongated prisma we have chosen $a = b = 8\,\mathrm{km}$, $c = 2.5\,\mathrm{km}$ so the volume of the prisma was the same in both cases. The depth of the prismatic body centre was taken to be $h_T = 50\,\mathrm{km}$. We confined our calculations to determining surface deformation characteristics and associated heat flow anomaly

only. At the same time we also performed the calculation of deformation characteristics due to an equivalent point source of heat located in the depth $\zeta = h_T$, its heat power being $w = f_0 V$, where $V = abc$ is the volume of the body. The result of calculation have shown that both the pattern and values of the deformation field due to a column – like magmatic body and to the equivalent point source of heat are very close (within accuracy range of 10% for the depth $h_T = 50\,\mathrm{km}$). In our calculation we assumed the thermal conductivity of the lithosphere λ_T to be $3\,\mathrm{W\,m^{-1}K^{-1}}$, and for the heat power f_0 of the unit volume of the body we have chosen:

$$f_0 = 42.1(2\pi\, h_T^2)/V \tag{31}$$

in order to keep the same epicentral heat flow anomaly for the equivalent point source of heat for all prismatic models. Curves of the surface heat flow anomaly were calculated by means of formula (20). These curves of a well-known bell-like form can be seen in Figs 2a and 3a. The maximum of q_z is above the centre of body, it attains about $40\,\mathrm{m\,W\,m^{-2}}$ so the shape of the prisma is not clearly expressed in q_z curves. Here we have chosen the following Lame's elastic constants for our lithosphere model: $\lambda = 7.05 \times 10^{10}\,\mathrm{Pa}$, $\mu = 6.075 \times 10^{10}\,\mathrm{Pa}$. The coefficient of linear heat expansion λ_T was assumed to be $10^{-6}\,\mathrm{K^{-1}}$. The curves of U_x in Figs 2a and 3a illustrate the horizontal displacement on the surface for the profile $y = 0$, i. e. $\varphi = 0°$. We have found that values of the horizontal displacement $U_r = U_x \cos\varphi + U_y \sin\varphi$ [$\varphi = \arctan(y/x)$] differ from those of U_x less than by 1% for all profiles φ, clearly because of square cross-section of the prismas. The vertical displacement U_z is negative, so we plotted $-U_z$ for the profile $y = 0$. The values of $-U_z$ for other profiles φ are very close to the plotted one (within an accuracy range of 10%).

The field of the stress tensor is shown by curves of S_{max} and S_{min} (Figs 2a and 3a), which correspond to the principal stresses S_1 and S_2 given in (16). The values presented are multiplied by the factor 10^{-7}. The maximum shear stress (multiplied by the factor 10^{-6}) is given by the curve τ_{max}. The plotted curves are for the profile $y = 0$, $\varphi = 0°$, but these stress characteristics are almost axially symetric for our model.

We calculated the directions of principal stresses as well using (18). The direction of S_{max} is close to $\varphi + \pi/2$, i. e. S_{max} corresponds to σ_{rr}. The calculated values of $\sigma_{\varphi\varphi}$ and σ_{rr} for the equivalent point source are very close to the values of S_{max} and S_{min} for a finite-volume magmatic body. The stress S_{max} is positive (expansive) over the whole surface and S_{min} is positive for $r \leq 1.7h_T$. So in the epicentral region $r \leq 1.7h_T$ we can expect the system of tensile fractures perpendicular to direction of S_{max}. According to the fracture theory radial fractures and associated circular fractures can arise in this region. The most critical fracture region is at $r \approx h_T$, where τ_{max} attains its maximum. Such a system of radial and circular fractures is quite often observed in regions of recent or

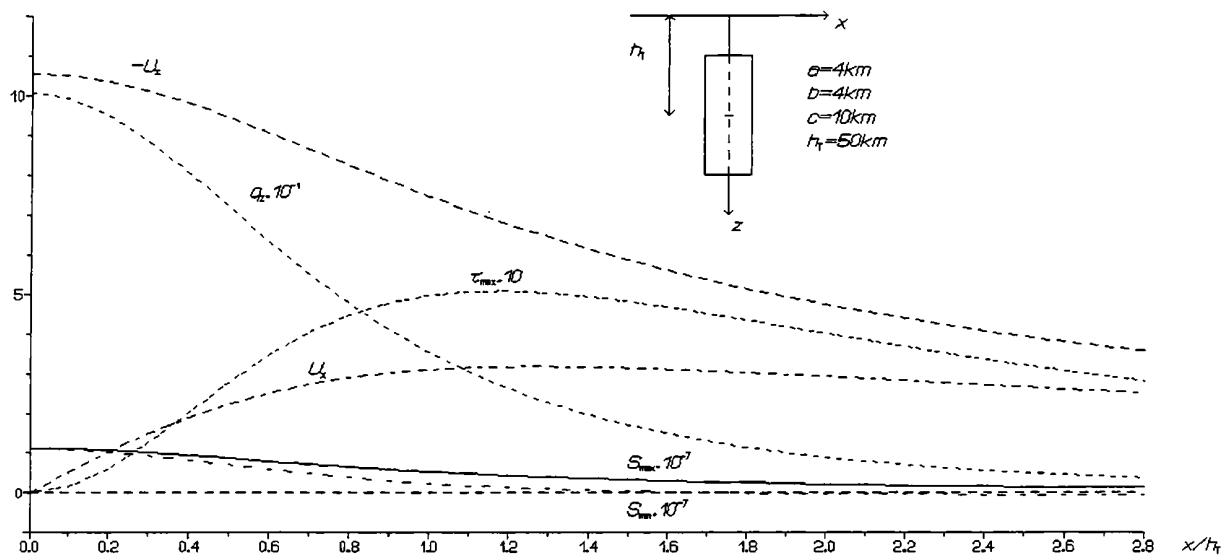

Fig. 2a

present magmatic activity.

The components of strain tensor on the Earth's surface calculated according to formulae (23) are plotted on Figs 2b and 3b. We can see that the principal components ε_{xx},

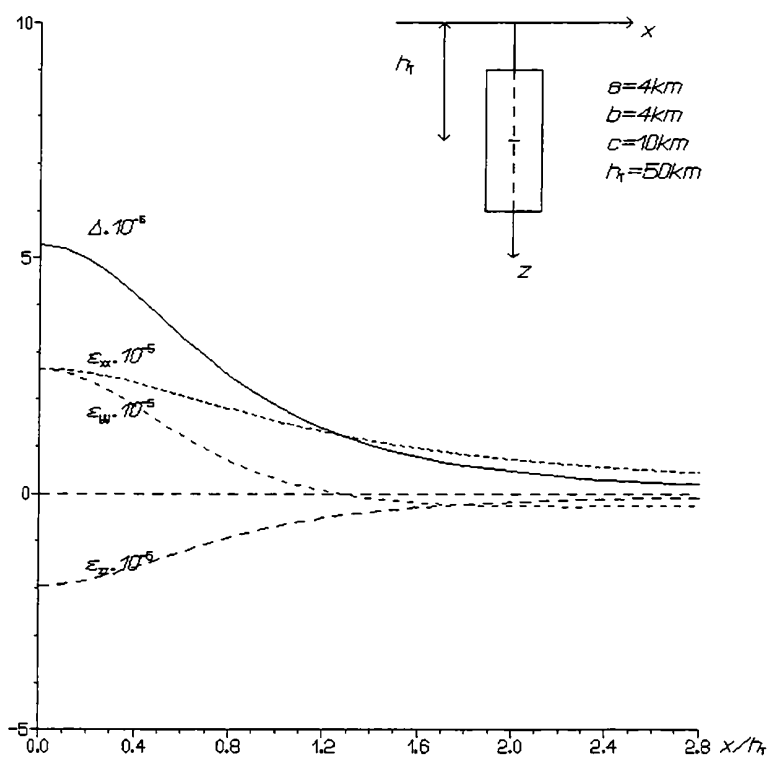

Fig. 2a,b Computed heat flow and thermoelastic deformation characteristics on the surface of the halfspace in which the finite-volume magmatic body (vertical prisma) is located, its centre being in the depth $h_T = 50\,\mathrm{km}$, heat power density $f_0 = 4.125 \times 10^{-3}\,\mathrm{W\,m^{-3}}$. Parameters of the halfspace are the same as in Fig. 1, g_2 is in $\mathrm{m\,W\,m^{-2}}$, u_x, u_z in metres, stresses in Pascals.

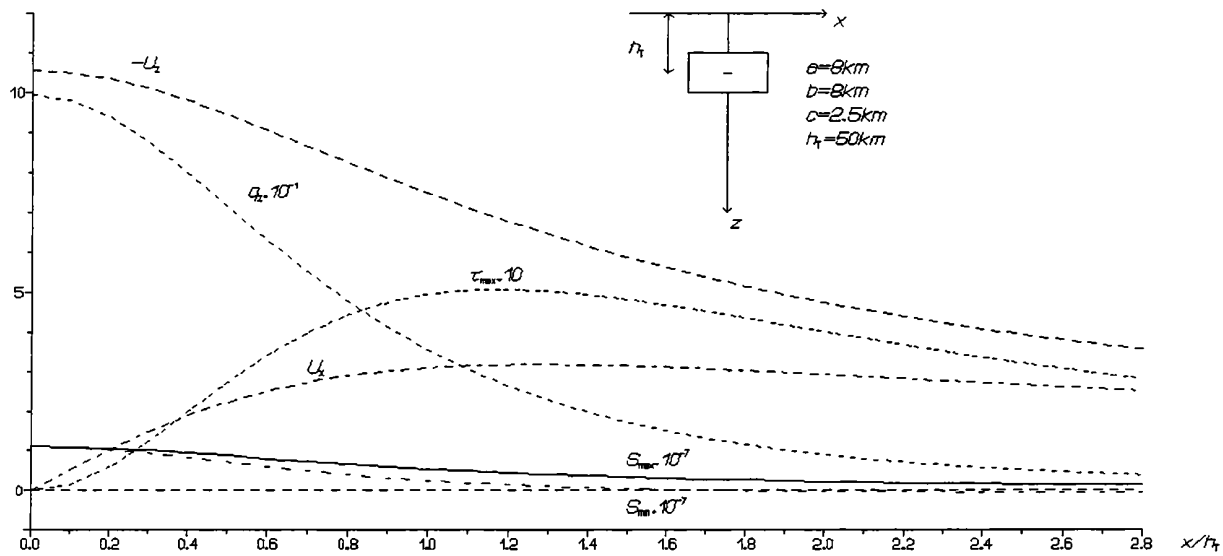

Fig. 3a

ε_{yy}, ε_{zz} attain the maximum values in the epicentral region of the body. They are of order 10^{-4} and are negligible in the horizontal distance $x \geq 1.2\,h_T$. It is interesting that the component ε_{xx} is negative in the distance $x \leq 1.5\,h_T$ which corresponds to compression. It is of order 10^{-5}.

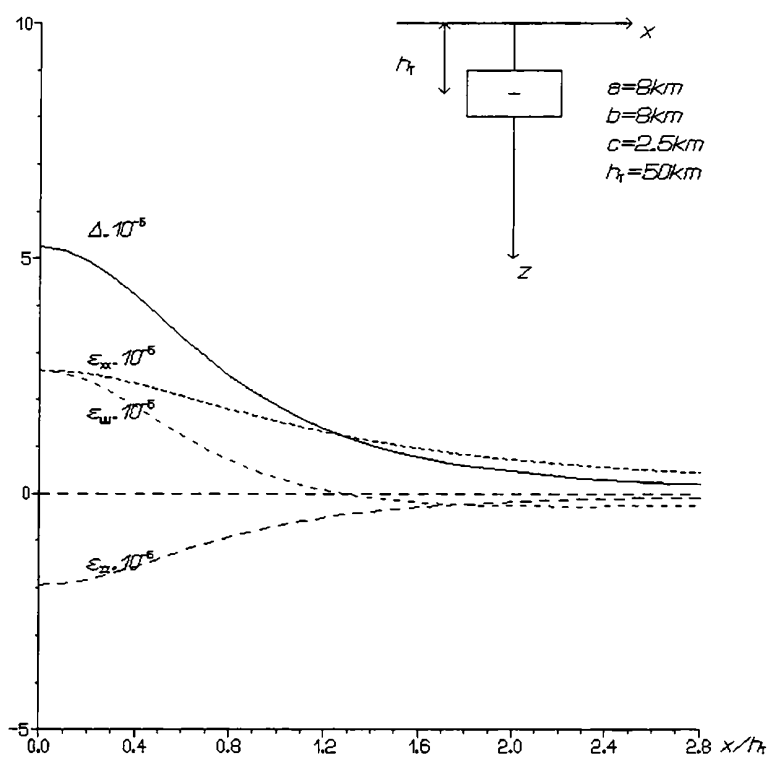

Fig. 3a,b The same as Figs 2a,b for the horizontal prisma.

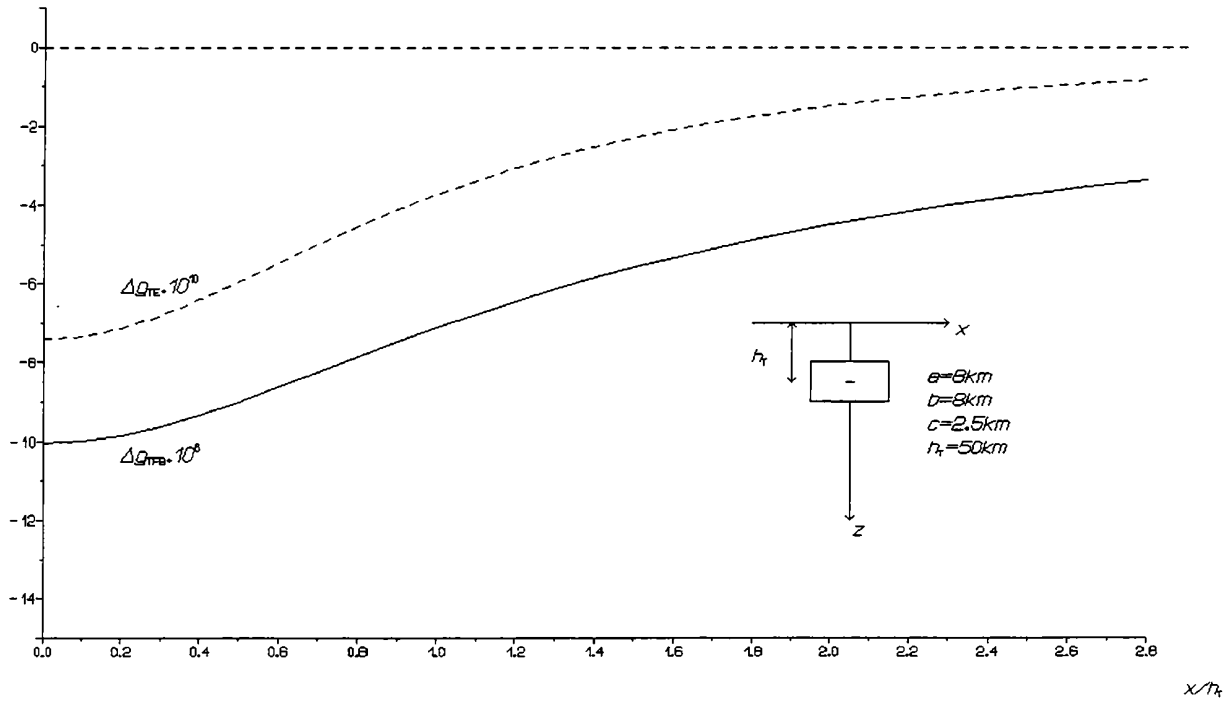

Fig. 4 Computed values of Δg_{TE} and Δg_{TEB} in $\mathrm{m\,s^{-2}}$.

In Fig. 4 we have plotted two curves of gravity anomaly connected with the thermoelastic deformation field. We can see that Δg_{TE} is of order $10^{-9}\mathrm{m\,s^{-2}}$ ($\simeq 0.1\,\mu$gal), but the free-air and Bouguer correction Δg_{TFB} is three orders greater $10^{-6}\mathrm{m\,s^{-2}}$ (0.1 miligal). Both of them are negative, which is in agreement with intuition. It is clear, that the sum of $\Delta g_{TE} + \Delta g_{TFB}$ is in essence equal to Δg_{TFB}, because the later is prevailing.

Conclusions

In this paper we present basic formulae and results of numerical calculation for simplified mathematical models of the static thermoelastic deformations (the magmatic body is approximated by both the point source of heat and the finite volume source).

Even though the models are a considerable idealization of the real situation (since e. g. we do not consider the gravity effect of magmatic mass transport more close to the surface), we have obtained useful results, which approximately agree with actual observations in geothermaly disturbed areas, e. g. Okube and Watanabe (1989). In the last cited paper we can find experimental data which show the vertical displacements (doming) of about –30 cm in the epicentral area. The observed negative gravity anomaly is about $8 \times 10^{-7}\mathrm{m\,s^{-2}}$ in the neigbourhood of the magmatic body however it changes to a positive values of about $3 \times 10^{-7}\mathrm{m\,s^{-2}}$. This change from negative to positive values can be explained by the mass density changes which are not considered in our paper. The

displacement direction and their values result in a pronounced dome in the epicentral region of the magmatic body. Horizontal displacement is directed radially away from epicentre. The surface stresses are positive (i. e. expansive) and in the epicentral region $x \leq h_T$ they attain values of about 10^{-3} of the shear modulus μ which is sufficient stress to produce tensile fractures and faults. A gravity anomaly of the order of tens of microgals connected with the thermoelastic deformation field offer a valuable tool for understanding the geodynamic processes connected with magmatic activity at an early stage. An additional gravity effect can be expected due to transport of magmatic material of density different from the crustal density (this effect is not subject of this paper).

These results are in good agreement with known patterns of the displacements, the stresses and the fault observed in the regions of near-surface igneous bodies (e. g. laccolithes or diapires) Park (1983). In summary, our theoretical analysis suggest that the combination of observations of surface deformations and gravity change are a powerful tool in the study of preparattory stages before volcanic activity. The theoretical results obtained in this paper were utilised in Majcin and Hvoždara (1995) for an approximation of slow diapiric heating of the lithosphere.

References

Brimich L., Fernández J., Granell R. D. Rr., Hvoždara M., 1996. Some comments on the effects of Earth models on ground deformation modelling. Studia geophys. et geod., 40, 14–24.

Combs J., Hadley D., 1977. Microearthquake investigations of the Mesa geothermal anomaly. Imperial Valley, California, Geophysics, 42, 17–25.

Delaney P. T., McTigue D. F., 1994. Volume of magma accumulation or withdrawal estimated from surface uplift or subsidence, with application to the 1960 collapse of Kilauea volcano. Bull. Volcanol., 56, 417–424.

Fernández J., Rundle J. B., 1994. Gravity changes and deformation due to a magmatic intrusion in a two-layered crustal model. J. Geophys. Res., 99, 2737–2746.

Hvoždara M., Brimich L., 1995. Theoretical models for gravity anomalies caused by thermoelastic deformations in the vicinity of magmatic bodies. Cahiers du Centre Européen de Géodynamique et de Séismologie, 8, 337–349.

Hvoždara M., Rosa K., 1980. Stresses and displacements due to a stationary point source of heat in an elastic halfspace. Studia geophys. et geod., 24, 51–59.

Majcin D., Hvoždara M., 1995. Gravity anomalies caused by magmatic activity in the East-Slovakian Basin. Cahiers du Centre Européen de Géodynamique et de Séismologie, 8, 329–336.

Mogi K., 1958. Relation between the erruptions of various volcanoes and the deformations of the ground-surface around them. Bull. Earthquake Res. Inst. Univ. Tokyo, 36, 99–134.

Okube S., Watanabe H., 1989. Gravity change caused by a fissure eruption. Geophys. Res. Lett., 16, 445–448.

Park R. G., 1983. Foundations of structural geology. Blackie, Glasgow and London.

Rundle J. B., 1980. Static elastic-gravitational deformation of a layered halfspace by point couple sources. J. Geophys. Res., 85, 5355–5363.

Rundle J. B., 1982. Deformation, gravity and potential changes due to volcanic loading of the crust. J. Geophys. Res., 87, 10729–10744.

Rundle J. B., 1983. Correction to „Deformation, gravity and potential changes due to volcanic loading of the crust". J. Geophys. Res., 88, 10647–10652.

Teisseyre R., 1986. Thermal stresse. In: R. Teisseyre (Ed.), Continuum Theories in solid Earth Physics, Elsevier, Amsterdam.

ÜBERSICHT DER SCHWEREMESSUNGEN IN DER TSCHECHISCHEN REPUBLIK

Jiří Sedlák

Geofyzika a.s.

Zusammenfassung

Dieser Beitrag enthält eine kurze aktuelle Übersicht der auf dem Gebiet der Tschechischen Republik durchgeführten regionalen Schweremessungen.

Schweremessungen 1:200 000

Bis 1956 wurden Schweremessungen auf 45 000 km² der Fläche der ehemaligen Tschechoslowakei durchgeführt. 1957 bis 1960 wurden auf den übrigen 83 000 km² der Fläche Ergänzungsmessungen im Maßstab 1:200 000 vorgenommen, und dadurch wurde das ganze Gebiet der Tschechoslowakei mit der Durchschnittsdichte 1 Punkt/5 km² umfaßt. Die durchschnittliche Entfernung zwischen zwei nebeneinander liegenden Schwerepunkten betrug 2,5 km. 1961 bis 1964 wurden die Daten verarbeitet und Schwerekarten 1:200 000 in Einzelblättern gedruckt. 1965 wurde schließlich unter der Führung des wissenschaftlichen Redakteurs J. Ibrmajer die übersichtliche gravimetrische Karte der Tschechoslowakei im Maßstab 1:500 000 herausgegeben.

Schweremessungen 1:25 000

1965 bis 1995 wurden auf dem Gebiet der heutigen Tschechischen Republik detaillierte Schweremessungen im Maßstab 1:25 000 durchgeführt. Die durchschnittliche Entfernung zwischen zwei nebeneinander liegenden Punkten betrug ca. 500 m, und das Gebiet wurde mit der Flächendichte von 4-5 Punkten/km² umfaßt. Bis heutzutage wurden Schweremessungen auf 75% der Fläche der Tschechischen Republik vorgenommen (Bild 1). Die Ergebnisse der Messungen und ihre Interpretation beinhalten 200 Etappenteilberichte. Im Laufe der Messungen wurden 250 000 neue

genaue Schwerepunkte vermessen. Die Qualität der Schweredaten überstieg den ursprünglichen Maßstab 1:200 000 nicht nur dank der Dichte der Messungen, sondern vor allem dank der besseren Geräteausstattung und der verbesserten Methodik der Datenverarbeitung, besonders im Rahmen der topographischen Korrekturrechnungen

Schwereuntersuchung im Maßstab 1:25 000 findet in der Praxis die größte Ausnutzung bei der Erforschung der Vorkommen von energetischen Rohstoffen (Erdöl, Erdgas, Kohle, Uran), von Erzen, in der hydrogeologischen und ingenieurgeologischen Erforschung und neulich auch bei der Erforschung für den Bedarf der Kernenergetik im allgemeinen. Die Ergebnisse der Schweremessungen können auch auf dem Gebiet der regionalen Planung und des Umweltschutzes verwendet werden.

Schweremessungen 1:10 000

1987 bis 1995 wurden auf die Erdöl und Erdgassuche gerichtete detaillierte Schweremessungen im Maßstab 1:10 000 durchgeführt. Zum großen Teil lagen sie im östlichen Teil der Tschechischen Republik. Es handelte sich um Messungen in ausgewählten Abschnitten des Molassenvorlandes, in der Flyschzone der Westkarpaten und im Wiener Becken. Es wurden an die 30 000 Schwerepunkte mit der Flächendichte von 25 Punkten/km^2 vermessen, so daß die durchschnittliche Entfernung zwischen zwei nebeneinander liegenden Punkten ca. 200 m betrug.

Zukünftig geplante Aktivitäten

Verwalter der Datenbasis der Schweremessungen ist Geofyzika a.s., mit dem Sitz in Brno. Gegenwärtig wird die elektronische Datenverarbeitung durchgeführt mit dem Ziel, die bestehende Schweredatenbasis im Einklang mit den internationalen Referenzstandards IGSN 71 und WGS 84 zu gestalten. Das Endziel der Arbeiten ist es, 1996 die neue gravimetrische Karte der Tschechischen Republik zu erstellen und zu drucken.

GEOFYZIKA Q. S.
P.O. BOX 62
612 46 BRNO
CZECH REPUBLIC

TSCHECHISCHE REPUBLIK

ÜBERSICHT DER SCHWEREMESSUNGEN 1:25 000

zu 1. 7. 1996

(5 Punkte/km^2)

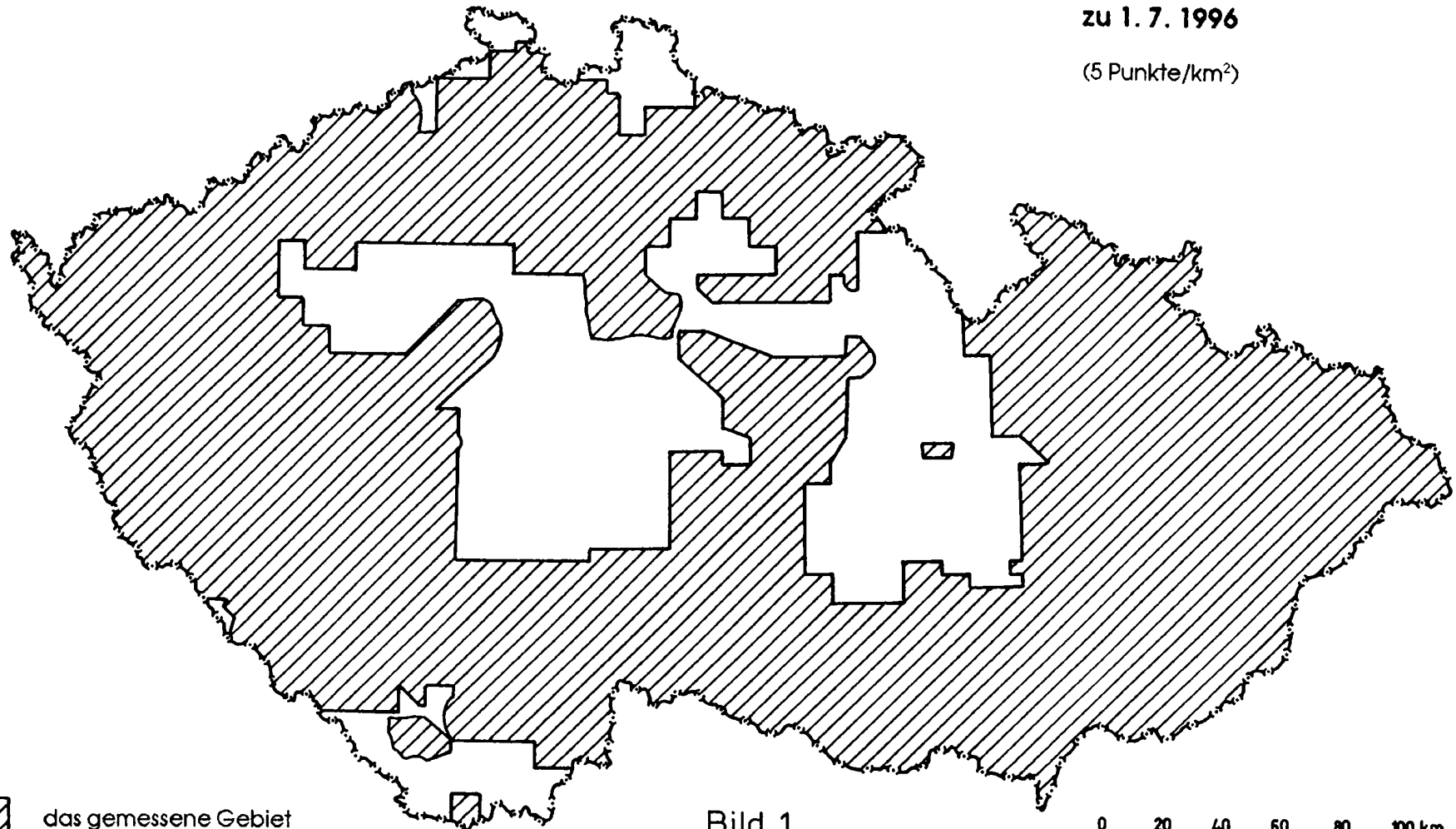

das gemessene Gebiet

0 20 40 60 80 100 km

Bild 1

ESTIMATE OF SALT DEPOSITS IN THE ALPINE AREA BY THE USE OF GRAVIMETRY

Alexander Radinger
Institute of Applied Geophysics, Joanneum Research, Graz

Abstract:

Gravimetry has always been a substantial part of applied geophysics and is therefore used for exploration as well as engineering surveys. There are a few points we will think about which are important for obtaining field data that can be used to produce a realistic model of the deposit. The estimate of volume and site of a salt deposit in the alpine area was used to think about the possibilities of gravimetry in similar surveys.

Dem Prinzip der Vielfalt der Methoden und deren Vernetzung verpflichtet, zieht der anwendende Geophysiker in geeigneten Fällen die Gravimetrie für prospektions- und ingenieurgeophysikalische Fragestellungen in Betracht. Wesentliche Voraussetzung für die Anwendung jeder geophysikalischen Technik, natürlich auch der Gravimetrie, ist ein Abschätzen der Möglichkeiten entsprechend den Anforderungen eines speziellen Falles (z.B. Salzprospektion). Es geht also darum, nicht nur einen gangbaren Weg für Durchführung, Auswertung und Interpretation gravimetrischer Messungen unter Berücksichtigung teilweise extremer Bedingungen im inneralpinen Bereich zu finden. Auch muß primär im Zuge der Planungsarbeiten eine realistische Abschätzung der zu erwartenden Signalamplitude durchgeführt werden.

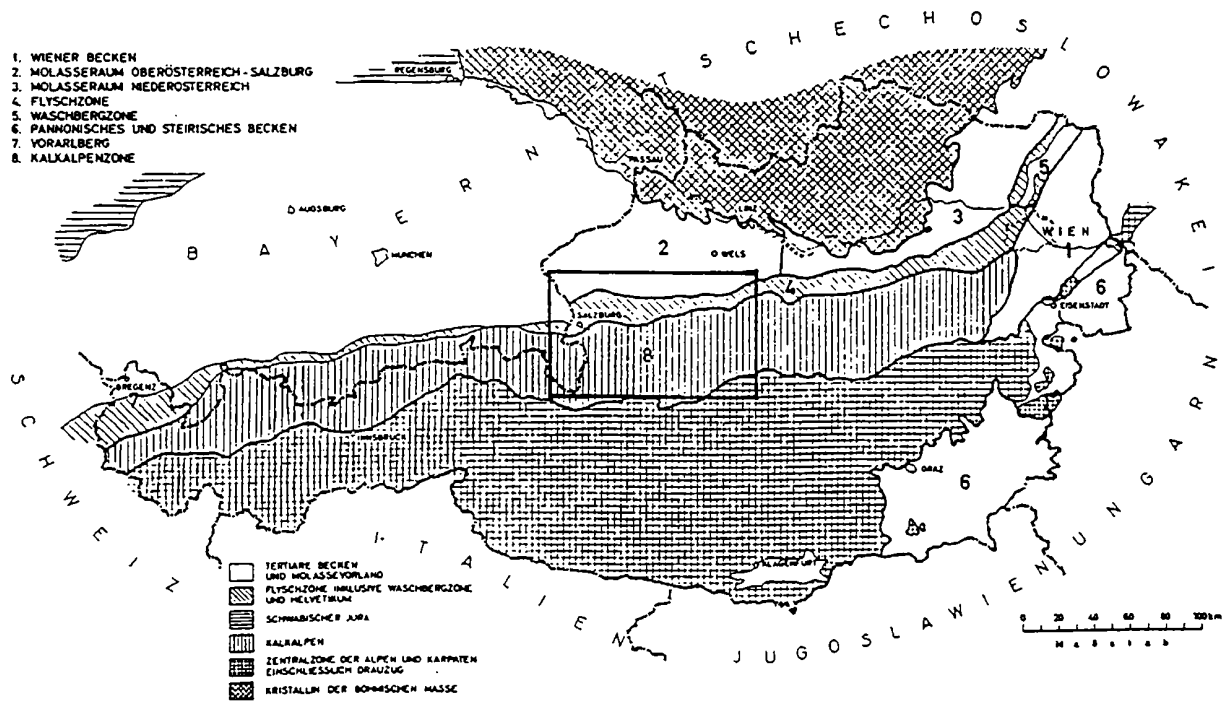

Abb. 1: Übersichtslageplan mit dem Untersuchungsgebiet

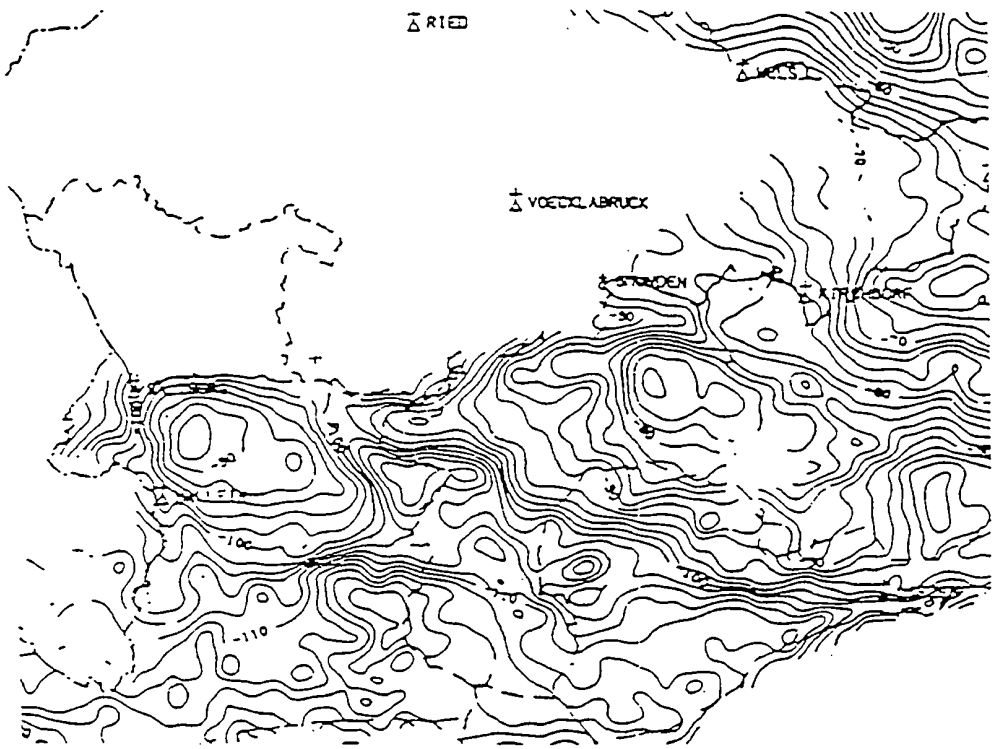

Abb. 2: Verlauf der Bougueranomalie in den nördlichen Kalkalpen (Zych, 1986)

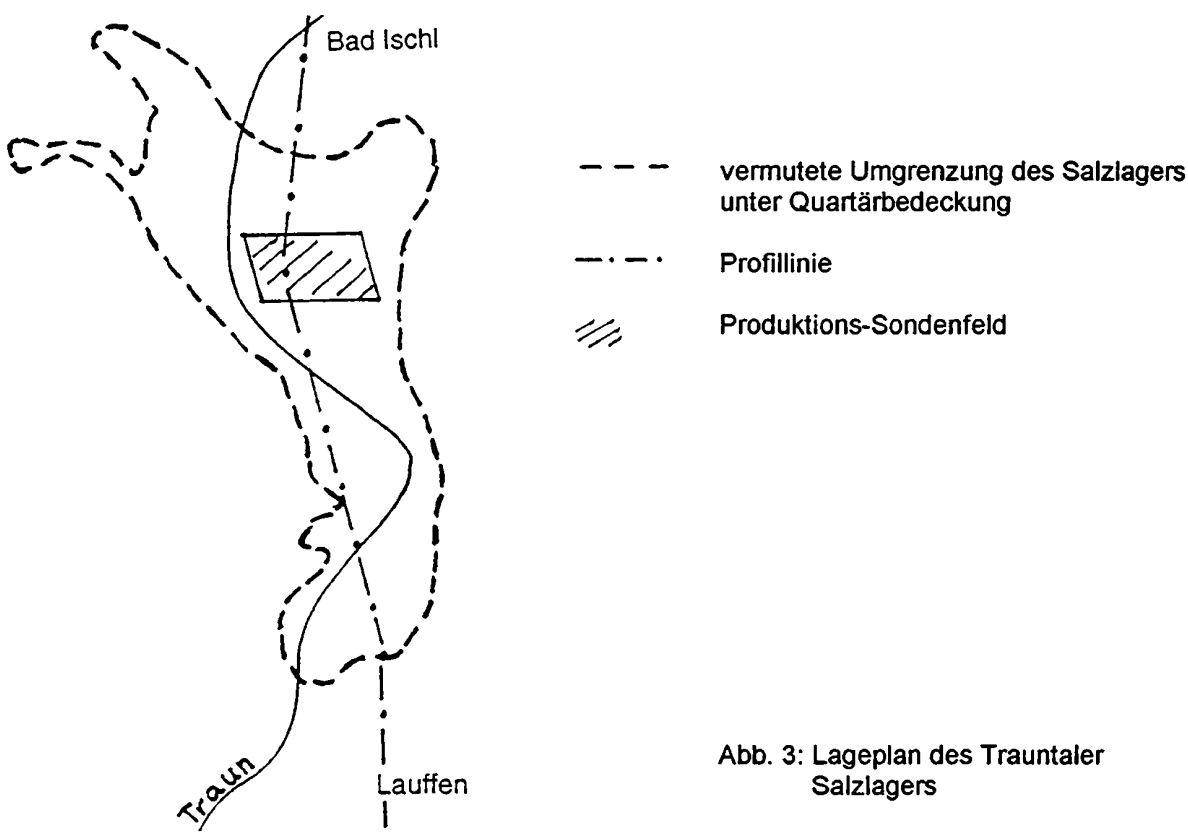

Abb. 3: Lageplan des Trauntaler Salzlagers

Als Fallstudie dient das Trauntaler Salzlager im Traun- und Ischltal. Die Anforderung an die Gravimetrie sei das Modellieren einer vermuteten Salzlagerstätte, an Hand einer gravimetrischen Detailuntersuchung. Ziel muß es sein, Lage und Volumen der Lagerstätte zu kennen, um eine Kosten- Nutzenrechnung für die Rohsolegewinnung anstellen zu können.

Für das vorliegende Prospekt und unter Berücksichtigung der im inneralpinen Bereich auftretenden starken Oberflächenreliefs und inhomogenen Dichteverteilungen, kommt der Planungsphase besondere Bedeutung zu. Es muß geklärt werden, welche bzw. ob die vom Auftraggeber vorgeschlagene Technik geeignet und zielführend ist. Es geht nicht darum einer speziellen Methode die Kompetenz abzusprechen, aber es muß doch gewährleistet sein, daß entsprechend der Zielsetzung die geeignetste Methode zum Einsatz kommt bzw., daß eine Kombination verschiedener Methoden (Komplexinterpretation) angestrebt wird.

Ausgangspunkt für das Prospekt sei eine großräumige, regionale Aufnahme der Schwere (Abb. 2). Andere Ergebnisse, wie bohrlochgeophysikalische Meßdaten stehen nur zum Teil zur Verfügung. Aufschlußbohrungen und Produktionssonden, die im Gebiet zwischen Bad Ischl und Lauffen niedergebracht wurden (Abb. 3), dienen als Randbedingungen für die Modellierung des Untergrundes.

Geologie:

Im höheren Perm wurde das sogenannte Haselgebirge mit seinen Salz- und Gipslagerstätten in den mittleren und östlichen Kalkalpen abgelagert. Als Haselgebirge bezeichnet man im alpinen Salzbergbau ein sedimentär gebildetes Gemenge aus fein zertrümmertem Ton, Anhydrit, Gips und Steinsalz als Grundmasse. Schauberger (1984) unterscheidet im Bereich der Salzberge vom Liegenden weg

a) Rotsalzgebirge
b) Grüntongebirge
c) buntes Salztongebirge: durchschnittlich 50 % Salzgehalt
d) Grausalzgebirge: durchschnittlich 60 % Salzgehalt

Das Trauntaler Salzlager besteht aus *buntem Salztongebirge* in Wechsellagerung mit *anhydritischem Grausalzgebirge.* In dieser Zusammensetzung ist es der Reichenhaller Salzfazies zuzurechnen.

Im unteren Teil der Lagerstätte herrscht meist das salzreiche Grausalzgebirge vor, was den Laugbetrieb erheblich erleichtert. Das Liegende des Salzlagers wird von der Überschiebungsbahn der das Salzlager einschließenden Hallstädter Decke über das Tirolikum (Neokom und Malmkalk) gebildet (Abb. 3). Das Gebiet um den Wolfgangsee (Ischltal) wurde von einem Zweig desTrauntalergletschers durchflossen. Wir finden daher heute eine zum Teil mächtige Grundmoränenbedeckeung (Sand, Ton, Kies, Schluff) von durchschnittlich 50m.

Ausgehend von diesen geologischen Vorstellungen und veröffentlichten Bohrergebnissen wird ein 2-D Modell des Untergrundes erstellt. Die Berechnung der Schwerewirkung beliebig geformter zweidimensionaler Körper mit polygonalem Querschnitt erfolgt basierend auf den Überlegungen Talwanis.

Der Versuch eine Salzlagerstätte wie die im Ischltal zu modellieren, wirft einige Fragen auf. Ist der Dichtekontrast zwischen den salzführenden Schichten und ihrer Umgebung groß genug, um verwertbare Signalamplituden zu erhalten? Im Idealfall würden wir einen Dichtekontrast von 0.4 - 0.5 g/cm^3 erwarten, der eine relativ scharf begrenzt negative Anomalie (Abb. 5) im Bild der Bougueranomalie hervorrufen würde.

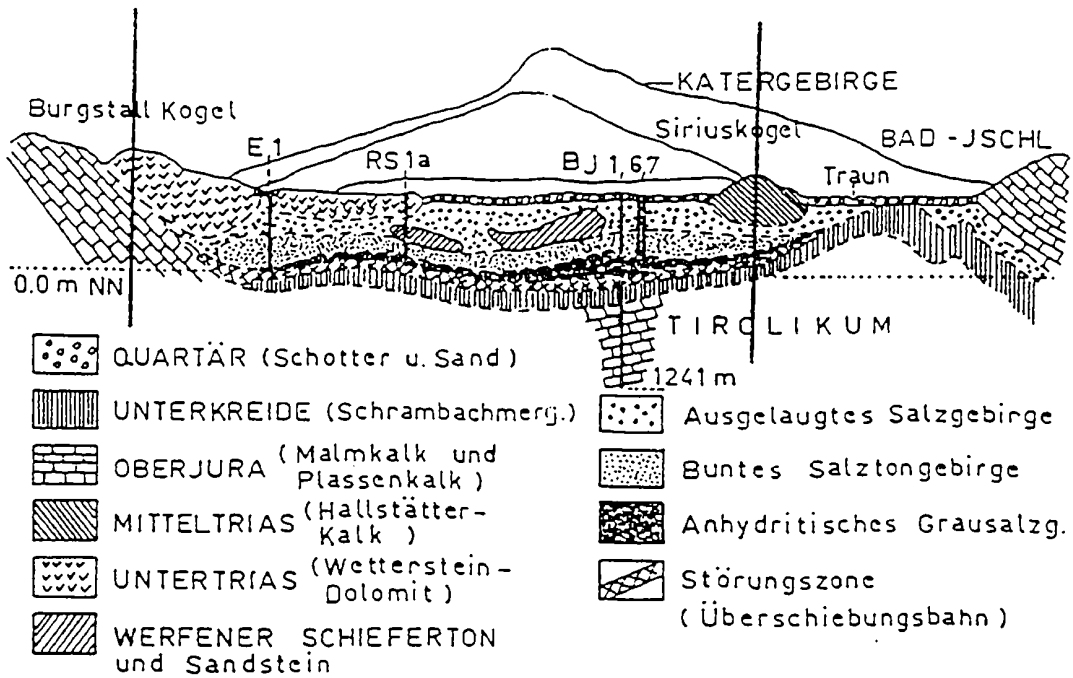

Abb. 4: Geologisches Tiefenprofil durch das Trauntal (Schauberger 1984)

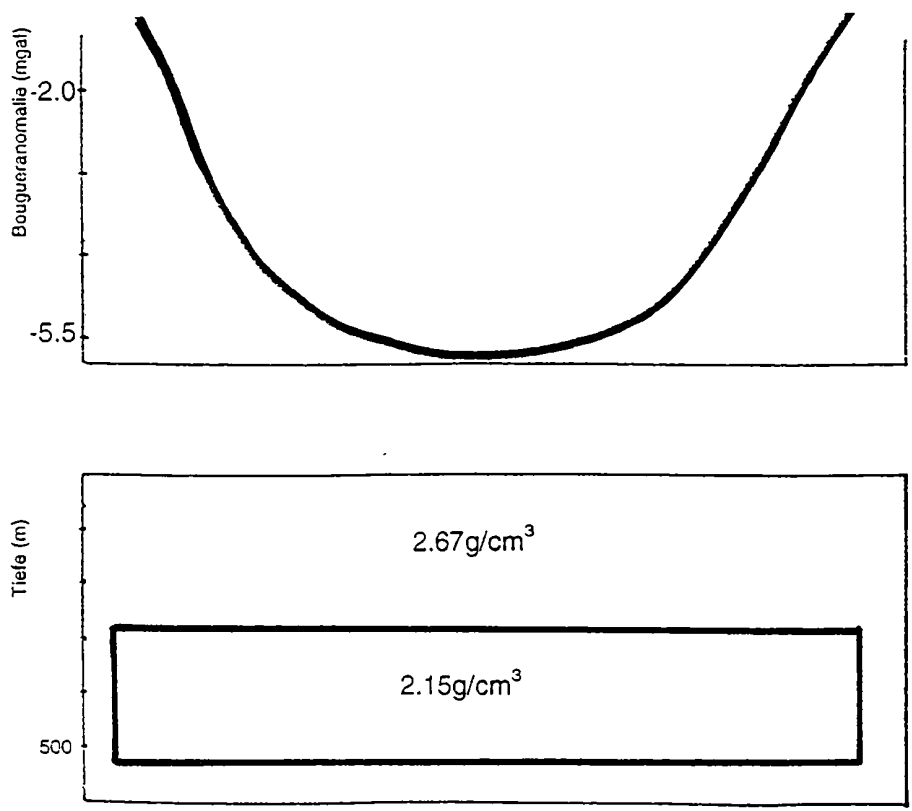

Abb. 5: Verlauf der Bougueranomalie über einem homogenem Salzkörper mit hohem Dichtekontrast gegenüber dem Umgebungsgestein.

Neben den schwierigen topographischen Verhältnissen im inneralpinen Bereich sind es zwei Dinge, die die Möglichkeiten der Gravimetrie zur Salzprospektion beeinträchtigen. Zum

einen die starken auch innerhalb der salzführenden Schichten auftretenden Dichteinhomogenitäten. Im vorliegenden Fall ist das anhydritische Grausalzgebirge mit relativ geringen Dichtewerten (ca. 2.2 g/cm^3) als Liegendes des Salzlagers vom bunten Salztongebirge überlagert, das zwar auch prospektionstechnisch interessierende Bereiche enthält, in Bezug auf die Dichte aber wesentlich geringere Kontraste zum Umgebungsgestein zeigt.

Zum anderen läßt der Typus des Trauntaler Salzlagers mit seinen Schmier- und Überschiebungshorizonten des Haselgebirges keine Vergleiche mit dem klassischen Salzstock zu, für dessen Auffindung die Gravimetrie im besonderen in Norddeutschland große Erfolge feiern konnte (Abb. 6).

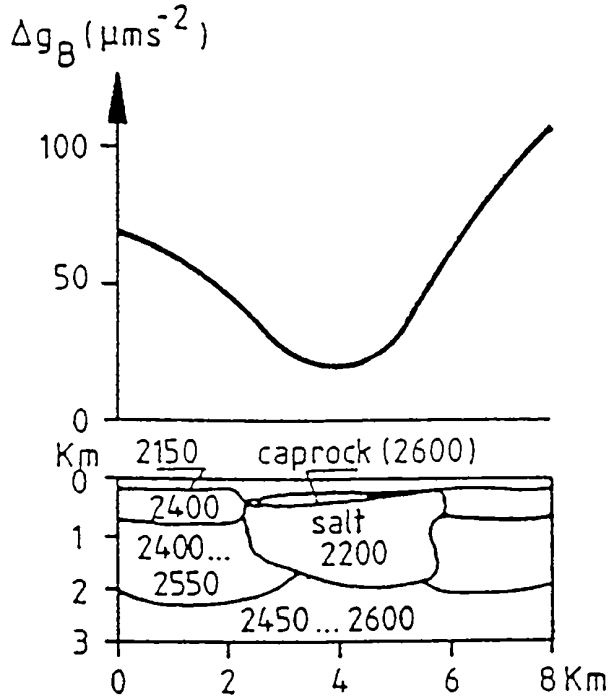

Abb. 6: Verlauf der Bougueranomalie über einem Salzstock in Norddeutschland (Torge 1989)

Abb. 7 zeigt den Verlauf der Bougueranomalie über dem Salzlager modelliert nach den geologischen Vorstellungen aus Abb. 4.

Dolomit	2.80 - 2.90 g/cm^3
Mergelkalk	2.65 - 2.73 g/cm^3
Gips	2.31 - 2.33 g/cm^3

Ausgelaugtes (Dolomit, Gips, Ton Gebirge)
buntes Salztongebirge (Salztone, Melphyr-, Tuffiteinlagerungen)
anhydritisches Grausalzgebirge (2.1 - 2.4 g/cm^3)

Morphologische und gesteinsphysikalische Parameter im Traun und Ischltal beeinflussen die Erfolgsaussichten gravimetrischer Detailuntersuchungen in hohem Maße. Ein gangbarer Weg wäre daher die Kombination mit anderen geophysikalischen Methoden. Man könnte die Gravimetrie mit großen Punktabständen anlegen, um rasch Vorinformationen zu erhalten. Diese könnten dann z.B. Ausgangspunkt für die Planung von reflexionsseismischen Profilen sein. Im Laufe des Jahres 1996 sind im Gebiet des Trauntaler Salzlagers gravimetrische Feldmessungen geplant, die die bisherigen Überlegungen ergänzen werden.

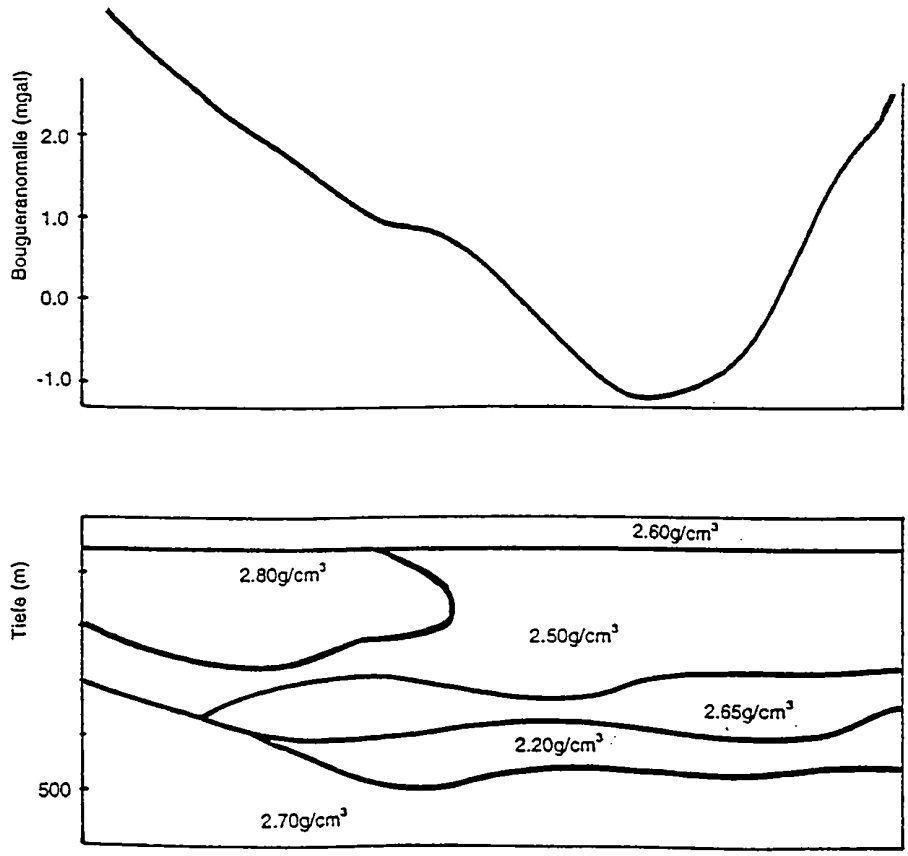

Abb. 7: Verlauf der Bougueranomalie über dem Trauntaler Salzlager bei geringen Dichtekontrasten Modellierung entsprechend Abb. 4

Literatur:

Torge W., 1989. Gravimetry. De Gruyter

Schauberger O., Neuhold R., Thomanek K., 1985. Die Entwicklung der Bohrlochsolegewinnung aus dem Trauntaler Salzlager in Bad Ischl. Berg- und Hüttenmännische Monatshefte, Heft 4

Militzer H., Schön J., Stötzner U., 1986. Angew. Geophysik im Ingenieur- und Bergbau. Deutscher Verlag für Grundstoffindustrie.

Zych D., 1988. 30 Jahre Gravimetermessungen der ÖMV Aktiengesellschaft in Österreich und ihre geologisch-geophysikalische Interpretation. Archiv für Lagerstättenforschung der GBA Wien, Band Nr.9.

LABORATORY GRAVIMETRY

LABORATORY CALIBRATION OF GRAVIMETERS AND PROBLEMS RELATED TO THE GRAVITATIONAL CONSTANT

Peter Varga

Geodetic and Geophysical Research Institute of the
Hungarian Academy of Sciences, Sopron, POB 5, H-9401 Hungary.

Abstract

Three severe problems of recent laboratory gravimetry are described. First of all the calibration of the gravimeters is discussed. On this basis a question of non–Newtonian gravimetry can be answered. Finally problems related to the gravitational constants G are described and a new method to determine its value is proposed.

1. INTRODUCTION

Laboratory gravimetry is concerned with experiments where the experimental conditions are under control, in contrast to observations where they are not. The experiments of this type can be done in rooms, in cavities under the Earth's surface. Instruments can be placed into carefully controlled enclosures and left undisturbed for long periods. Measurements which belong to the laboratory gravimetry are among others:

- observation of temporal variations of the gravity field
- determination of the gravitational constant
- determination of the absolute value of gravity
- calibration of gravimeters
- tidal gravimetry
- gravitational problems related to Earth rotation
- influence of external forces on the gravity field (e.g. hydrogeological effects; influence of air pressure)
- gravitational effect of the liquid core

The aim of present study is to discuss a possible way to obtain accurate and reliable calibration values for gravimeters in a laboratory.

On the basis of laboratory calibration it can be proved that the gravitational constant obtained in a laboratory has a more realistic value than that determined by means of the gravity field of big geological masses. Another experimental and theoretical considerations show that there is no realistic temporal variation – in geological time scale – of the gravitational constant G. The gravitational constant was the first fundamental constant

of physics. Nevertheless, its value is known with less accuracy. The torsion balance used in experiments to determine the value of G may not be the best way in which this unfavourable situation can be altered. Possibly the solution can be the use of the special gravimeter calibration device equipped with a heavy cylindrical ring (Varga 1989, Varga et al., 1995) with superconducting gravimeters calibrated along calibration lines where gravity values were determined by means of absolute gravimeters.

2. LABORATORY CALIBRATION OF GRAVIMETERS

Beside the gravimeter manufacturers the first high precision laboratory absolute calibration device was prepeared by Brein (1962). We can speak about three different calibration methods:

a. Parallel recording with two or more devices. In this case the gravity record of a well calibrated gravimeter is compared with the ones to be calibrated. The calibration obtained in this way, however, is not an absolute determination of the instrumental scale. The accuracy obtained with this method can reach 0.1 %. To make the calibration of this type absolute for the calibration an absolute ballistic instrument must be used. Up to the present with the use of them an accuracy better than 0.5 % was reached (Varga & Hegymegi, 1985; Hinderer et al., 1991).

b. Vertical acceleration of the gravimeter. This method was proposed by Brein (1962), realized by Valliant (1973), later by Van Ruymbeke (1989) and Richter (1990). These authors used an oscillating platform and reached a relative accuracy of 0.25 % (VanRuymbeke, 1989).

c. Artificially induced gravity changes can be generated on different ways. Earlier it was common practice to calibrate gravimeters by the tilt of the instruments. In this way high quality and realistic calibration values cannot be achieved in principle because the instrument's system is in a deformed state during this operation. The other possibility of the generation of gravity changes is the vertical displacement of the gravimeters. In this way, however, only very small ($\sim$ 10 μGal = 100 nms^2) gravity changes can be generated (Bonatz, 1971), the vertical gradient is very sensitive to the local mass disturbances and cannot be measured directly. An other possibility of calibration experiments of this type is: exposing the gravimeter to the influence of a big and well defined mass (see for e.g. Groten (1970) or Goodkind (1991)). In this way gravity variations (Δg) of the order of 100 μGal can be generated. This change in gravity is sufficient for an acceptable calibration accuracy, if no deformation occurs during the calibration process, and if both the geometry and the masses participating in the experiment are known with very high accuracy.

A calibration device of latter type was proposed and designed by Varga (1989) and it was installed in the Geodynamical Observatory Budapest in 1989–1990.

The principle of the equipment is simple: a suspended cylindrical ring with an inner diameter somewhat bigger than the width of the instrument to be calibrated is raised and lowered vertically and moved over the gravimeter equipped by a distant reading device and installed on a column of suitable height.

The advantages of this calibration procedure are as follows:

- the homogeneity of the generated gravity field at the extrema is very high;
- the raised and lowered ring does not load the ground around the instrument;
- the gravimeter remains stationary during the procedure what is a necessary condition for a small instrumental drift;
- the experiment is symmetrical with respect to the gravimeter and owing to technical reasons the gravity change brought about by the ring is greater than that caused by another geometrically regular body.

The disadvantages of the method are:

- this solution is immobile, it can be used only at the place where the device has been installed;
- the device in his recent form is rather sensitive to seismic noise.

All technical problems and the results of calibrations are described in Varga et al. (1991) and in Varga et al. (1995).

It is worth to mention that this device allows absolute calibration with an accuracy of 0.1–0.2 % and it can be used to solve different problems of gravimetry:

- to study the non-linearity of the gravimeters (Götze & Meurers, 1983; Becker 1984) and to detect small instrumental imperfectnesses (Meurers, 1996);
- a calibration of tidal gravimeters is necessary with an accuracy of 0.1 %. This condition is important to prove the latitude dependence of earth tidal parameters and to discover mantle heterogeneities on the basis of gravimetric tidal records;
- to study the dependence of the gravitational constant G on the scale of the masses used for the determination of this fundamental constant of the nature.

The calibration device installed in the Geodynamical Observatory Budapest to generate gravity variations has a heavy stainless ring (density 8.0056 ± 0.0060 gcm^{-3}) the total mass of which is $3.2 \cdot 10^6 \pm 21$ g and generates a gravity change of $\pm$ 56 μGal. The first calibration of LCR gravimeter was carried out by this device in August 1991 with an accuracy 0.2 %. Calibrations carried out later on in 1993 support this error value, and the average of the runs carried out with two LCR instruments of the Eötvös Loránd Geophysical Institute of Hungary gave 0.1 % uncertainty.

A device similar to ours to calibrate superconducting gravimeters was completed at ENEA Laboratories near Lago Brasimone (Italy) (Achilli et al., 1995). Because of the very high sensitivity of the cryogenic gravimeters (of the order of 0.001 μGal) for a calibration precision approaching 0.3 % a ring with a mass of 273 kg was needed only. The generated artifical gravity variation was 6.7 μGal.

To perform high quality calibrations numerous error forces must be investigated. These are described in detail in Varga et al., 1995. They are among others the gravimetric effect

of air pressure variation (here the attraction and loading effect of the atmosphere as well as the buoyancy of the ring must be considered), the accurate position determination of the ring (in our case it was 0.1 mm and 1 arcsec), the magnetic effect (in the case of experiments carried out in Budapest the maximum magnetic variation of the ring was 14 μT what does not influence the LCR devices remarkably), the temporal variation of the digital voltmeter constant used to record the gravimeter output (1 % variation of this value leads to a fictive gravity variation of the order of 0.1 μGal).

The gravity field exerted by the cylindrical ring can be exactly calculated along the axis of symmetry ($z = 0, y = 0$) at any point $P(\xi)$ with

$$\begin{aligned} g(\xi) \quad &= 2\pi G\rho\Big[\sqrt{R_2^2 + (z_2 - \xi)^2} - \sqrt{R_2^2 + (z_1 - \xi)^2} - \\ &- \sqrt{R_1^2 + (z_2 - \xi)^2} + \sqrt{R_1^2 + (z_1 - \xi)^2}\Big] \end{aligned} \tag{1}$$

(here ρ is the constant density of the annular mass, G is the gravitational constant, R_1 and R_2 are the inner and external radii, z_2 and z_1 denote the top and bottom of the calibration mass.) To calculate the gravity field of the cylindrical ring outside of the axis is also of importance: the gravity effects caused by deviations from axial symmetry must be calculated. This can be done by the theorem of potential theory: if a body has an axial symmetry the gravity field caused by it along this axis determines the distribution of the gravity along any perpendicular to its directions (e.g. along x and y) expressed with the series of Legendre polynomials.

According the experience accumulated during the operation with the calibration device developed by us it was concluded that the most serious error sources are the instrumental drift together with the earth tidal effect and the microseismic noise.

a.) *Removal of the tidal effect and the instrumental drift.*

For the Geodynamical Observatory Budapest on the basis of earth tidal observations carried out there in 1988–92 the earth tidal parameters (amplitude ratio δ and phase difference κ) are known with high accuracy. A comparison campaign with the Askania recording gravimeter of the Technical University Prague proved that the reliability of δ factors of the Observatory for main tidal constituents is 0.1–0.2 % (Table 1).

The influence of Earth tides was removed with the use of the Cartwright–Taylor–Edden development and with the δ and κ values determined from gravity records carried out in the Geodynamical Observatory Budapest. Of course this procedure has problems at the 10^{-1} μGal level needed for 0.1 per cent calibration accuracy, because the tidal parameters are known with sufficient accuracy only for the few biggest tidal waves. The residual of the lunisolar effect can be excluded from the observation data together with the instrumental drift.

The accurate removal of the instrumental drift is one of the most important problems in the laboratory calibration procedures. For this purpose a hypothesis was used: the gravity effect of the ring on the gravimeter is the same at a given position of the ring and the measured Δg at this point is the drift. The tidal and atmospheric effects must be removed already before the determination of the drift curve. By repeated up and down movements of the ring an accurate drift curve can be obtained which allows to exclude this effect with the reliability of 0.1 μGal or even better.

Table 1. Gravity earth tide parameters determined for the Geodynamical Observatory Budapest (A) and results obtained with the gravimeter of the Technical University Prague (B)

	A		B	
Epoch	1988–1992		1988–1989	
	δ	κ	δ	κ
Diurnal Waves				
O_1	1.1515	+0.1°	1.1496	+0.1°
K_1	1.1378	−0.1°	1.1362	0.0°
Semidurnal Waves				
M_2	1.1813	−0.6°	1.1823	−0.8°
S_2	1.1764	−0.5°	1.1855	−0.5°

b.) *The microseismic noise*

Microseisms or seismic noise originate because of external influences first of all from the atmosphere and the sea. These waves always exsist on seismic records but with varying intensity (Bath, 1979; Bullen, 1979; Bernard, 1990). The nature of the microseismic waves is not quite clear. Recent observations allow the following classification:

- short period microseisms ($T < 2$ s) depend on near disturbances and they decrease significantly with distance
- $T \sim 6$ s generated by cyclons of some hundred (up to 1000) km distance
- $T = 9 - 10$ s microseisms are produced by large low–pressure areas at greater distances
- $T = 17 - 20$ s microseisms are observed more seldom (few times per year). They can be escribed to coastal effects.

The microseismic noise at the Geodynamical Observatory Budapest was recorded with an Askania type gravimeter. It can be concluded that at this place the microseismic activity has a seasonal amplitude variation of 5–30 μGal at period between 5 and 10 s. What is very important for high quality laboratory gravimetric measurements: the observed microseisms undergo systematic beating with periods from 1 to 4 min. This last phenomenon is the most remarkable error source of the calibration procedure described in this paper. The corresponding gravity variations range from 1–2 μGal to 10–30 μGal. (This gravity amplitude values can be used only qualitatively because the linearity of the used Askania gravimeter was not proved at this periods.) The influence of microseisms can be significantly reduced by increasing the number of the observations. In this way the microseismic noise can be reduced to 0.2 % even in the case of a single calibration procedure (Table 2). Of course calibrations should be performed at times of low microseismic noise level.

under the surface of the Earth. This underground calibration line consists of 14 stations with a range of 1400 ± 1 μGal. Gravity differences, separation and the elevation difference between neighbouring stations are 100 μGal, 2–5 m and less than 2 cm, respectively. Because the line is horizontal it was possible to measure the differences with a computer controlled Eötvös torsion balance. The instrumental constant of the torsion balance is obtained by the measurement of the sensor masses, the lenght of the arm of the balance and the torsion of the wire. This means: the gravity values of the underground calibration line were determinded without the use of gravimeters. The difference of the calibration factors obtained for the same gravimeter along the calibration line (i.e. by means of gravitational effect of big geological masses) and by the cylindrical ring is of the order of 10^{-3} what means that the difference between the G_∞ obtained from large-scale Airy-type experiments and the laboratory type G_0 is at most 10^{-3}.

An other problem connected to the gravitational constant G is its temporal variation as supposed by many authors. This follows from Dirac's expanding Universe model proposed in 1937 what leads to a decreasing constant of gravitation and to the geophysical theory of the expanding Earth. On the basis of Dirac's theory Jordan concluded (1966) that the Earth radius a increases with a speed $da/dt = 0.5\ mm \cdot y^{-1}$. Similar expansion value was obtained by Egyed (1957) $da/dt = 0.7mm \cdot y^{-1}$ who supposed that originally the surface of our planet was as big as the areas of all recent continents together. The most recent and complete description of these theories can be found in the book of Carey (1988).

The critical review of da/dt ad consequently of dG/dt can be carried out on the basis of the study of the influence of earth tides on the long-term variations of the angular speed. Studies of this type are usually based on the principle of conversation of angular momentum and it is supposed that the Earth–Moon system is isolated. For the sake of simplicity it can be supposed that the Moon revolves around the Earth on a circular orbit in the plane of the terrestrial equator. The law of conversation of the angular momentum can be written as

$$\frac{\partial(Jw)}{\partial t} = \frac{1}{3}\frac{MM_m}{M+M_m}R_m^2\frac{\partial n_m}{\partial t} \tag{4}$$

In (4) M, J, w is the mass, the inertia tensor and the angular speed of the Earth, respectively. M_m, R_m, n_m stands for the mass of the Moon, for the Earth–Moon distance and for the Moons orbital speed. Kepler's law can be written as

$$n_m^2 R_m^3 = G(M + M_m) \tag{5}$$

Its time derivative is

$$2n_m R_m^3\frac{\partial n_m}{\partial t} + 3n_m^2 R_m^2\frac{\partial R_m}{\partial t} = \frac{\partial G}{\partial t}(M + M_m) + G\frac{\partial(M + M_m)}{\partial t} \tag{6}$$

In r.h.s. of (6) it can be evidently supposed that the time derivative of the gravitational constant is not a time dependent value ($\partial G/\partial t = C$) while the second term is equal to zero. Therefore

$$\frac{\partial n_m}{\partial t} = -\frac{3}{2}\frac{n_m}{R_m}\frac{\partial R_m}{\partial t} + \frac{\partial G}{\partial t}\frac{M + M_m}{2n_m R_m^3} = -\frac{3}{2}\frac{n_m}{R_m}\frac{\partial R_m}{\partial t} + C^* \tag{7}$$

In r.h.s. of (7) C^* is of course a constant value. Introducing $\partial n_m/\partial t$ into the basic equation (4):

$$\frac{\partial(Jw)}{\partial t} = -\frac{1}{2}\frac{MM_m}{M+M_m} n_m R_m \frac{\partial R_m}{\partial t} + \frac{1}{6}\frac{MM_m}{n_m R_m}\frac{\partial G}{\partial t} = L_m + \frac{1}{3}\frac{MM_m}{M+M_m} R_m^2 C^* \qquad (8)$$

(L is the tidal torque)

From astronomical data (see e.g. Zharkov et al., 1996):

$$\frac{d(Jw)}{dt} \approx -4.1 \cdot 10^{16} N \cdot m$$

The total tidal torque is composed by the atmospheric (L_{AT}), the earth (L_{ET}) and the oceanic (L_{OT}) tidal torques

$$L_m = L_{AT} + L_{ET} + L_{OT}$$

With numerical values

$L_{AT} = +0.5 \cdot 10^{16} N \cdot m$

$L_{ET} = -0.5 \cdot 10^{16} N \cdot m$

$L_{OT} = -5.0 \cdot 10^{16} N \cdot m$

consequently in (8) it is $\frac{\partial G}{\partial t} \geq 0$ what is in contradiction with Dirac's theory on the expanding Universe as well as with the theory of the expanding Earth, because an increasing gravitational constant requires a compressing Earth.

4. THE GRAVITATIONAL CONSTANT, ITS NUMERICAL VALUE AND ACCURACY

The value of the gravitational constant is known with less accuracy than other fundamental constants of physics. Authors of the best G value determinations claim to their experimental results an accuracy of 10^{-4}. Table 3 shows that the disagreement between the individual results is of the order of 10^{-3}.

More over it can be concluded that G is the least well known constant of fundamental physics (Table 4). There are several explanations why G is known with such a low accuracy. First of all there is a "psychological problem": at this time there are no big research problems in the science which would urgently need a more accurate value for the gravitational constant. The second problem is connected with the weakness of gravitational attraction in scales used in laboratories. For example: a force interaction of two masses of 1 g at the distance of 1 cm is 10^{-12} Newton while the pressure of the light of the sun is 10^{-10} Newton or the acting of forces between a proton and a neutron is 10^{-8} Newton. Additionally there is a metrological difficulty: G is defined by the fundamental quantities, time, length and mass to be determined in absolute scale. This circumstance leads of course also to experimental difficulties. The scatter of the data listed in Table

Table 3. Gravity constant values published after 1969 (Chen & Cook, 1993)

Authors	Year	$G \times 10^{-11} Nm^2 kg^{-2}$
Rose et al.	1969	6.6699±0.0014
Facy & Poinkis	1970, 1971	6.6714±0.0006
Renner	1974	6.668±0.002
Sagitov et al.	1978	6.6745±0.0008
Luther&Towler	1982	6.6726±0.0005
De Boer	1987	6.6670±0.0007
		6.6706±0.0028

Table 4. Relative errors of basic physics constants
(A selection based on Brockhaus's lexicon Naturwissenschaften und Technik, 1989)

Avogadros constant	$5.2 \cdot 10^{-10}$
Boltzman's constant	$1.2 \cdot 10^{-4}$
Elementary charge	$2.8 \cdot 10^{-6}$
Faraday constant	$2.8 \cdot 10^{-6}$
Gravitational constant*	$8.5 \cdot 10^{-4}$
Mass of the neutron	$5.1 \cdot 10^{-6}$
Planck's constant	$5.5 \cdot 10^{-6}$
Rydberg's constant	$8.3 \cdot 10^{-6}$
Speed of the light	$4.0 \cdot 10^{-6}$

* The error value of the gravitational constant is the value given with the current CODATA value (Cohen & Taylor, 1986)

3 suggests that there can be a systematic error in the gravitational constant determined by different scientists. In fact the basic idea of the measurement of G is the same in all experiments. The hearth of them is the torsion balance which was used in the beginning in static way and later on, after the successful attempt of Eötvös at the very end of the last century, dynamically. It was discovered however by Kuroda in 1995 that the torsion force is dependent on the frequency with which the torsion bar is oscillating. The variability of the elastic constants is particularly significant at low frequencies of oscillating torsion balances used in laboratory experiments. According to Maddox (1995) the frequency dependence of the elastic parameters of the materials used in the torsion balances is the main source of the systematic and big differences between the different laboratory G determinations.

In spite of the recent lack of interest to the G and the considerable experimental difficulties it is important to try to increase the accuracy of the gravitational constant. It seems that one way can be in this direction the use of the laboratory calibration device developed by us. This experimental tool has a clear geometry and the used quantities (mass of the ring, the position of it etc.) are already or can be obtained with an accuracy

necessary to determine G with relative error of 1 part in 10^4 (or even a few times 10^5). To reach this level in our knowledge about the value of the gravitational constant needs some development of the calibration device.

The influence of microseismic noise must be reduced significantly. As it was mentioned above the systematic beating with a period of some minutes caused by the microseisms characterised with periods between 5 and 10 s produces gravity variation of $\sim$ 10 μGal. This influence must be reduced either with an appropriate antiseismic isolation or with a special feed–back system.

If the construction of new superconducting gravimeters allows an effective way to increase the gravity effect the reduction of the inner diameter of the ring used in the calibration device can be possible. If the inner diameter of the ring is reduced from 30 cm to 20 or to 15 cm, the corresponding gravity effect generated by the cylindrical ring of the mass of 3200 kg will be $\pm$89 or $\pm$118 μGal instead of $\pm$56 μGal.

The accurate removal of the instrumental drift (together with possible residuals of the lunisolar and meteorological effects) are of first order importance. To carry out more accurate drift determinations beside the more sophisticated measuring technics new statistical data processing methods – like the robust estimates – are also needed.

Of course to get uncertainties of 10^{-4} or even better the spring gravimeters – used earlier – must be replaced by transportable superconducting gravimeters with reduced diameter. Such "thin" instruments were demonstrated by the GWR company during the XXIst Assembly of the International Union of Geodesy and Geophysics (July 1995, Boulder, Colorado, USA). An important feature of these instruments is that their sensor has an axial symmetry.

The superconducting gravimeters must be calibrated first along the gravity lines measured with absolute gravimeters. The accuracy of these calibration lines is 10^{-5} (Atzbacher & Gerstenecker, 1992). Afterwards with this gravimeters the gravity effect generated by a ring moved up and down must be measured. The gravity effect caused by the ring is known with an accuracy of $\sim 10^{-5}$. If the value of G is suitable the measured and generated-calculated gravity values must coincide. With other words by the comparison of these two gravity values the gravity constant can be obtained.

5. CONCLUSIONS

a.) The methods of modern laboratory gravimetry – among them the device with a heavy cylindrical ring – allows calibration accuracy of 0.1 %.

b.) At this time there is no basis to conclude that the gravitational constant determined in a laboratory are different from those obtained with the use of gravity effect of big geological masses.

c.) Similarly at present there is no ground to speak about temporal variation of G.

d.) There is a possibility to improve our knowledge on the numerical value of the gravitational constant with the use of the calibration device equipped with an annular mass.

6. REFERENCES

ACHILLI V, BALDI P, CASULA G, ERRANI M, FOCARI S, GUERZONI M, PALMONARI F, RAGUNI G, 1995: A calibration system for superconducting gravimeters. *Bulletin Geodesique, 69, 73–80*

ATZBACHER K, GERSTENECKER C, 1993: Secular gravity variations: recent crustal movements or scale factor changes? *J. Geodynamics*, 18, 1–4, 107–121.

BATH M, 1979: Introduction to seismology. *Birkhäuser Verlag*

BECKER M, 1984: Analyse von hochpräzisen Schweremessungen. *Deut. Geod. Komm.* C, 294, München, 1-99.

BERNHARD P, 1990: Historical sketch of microseisms from past to future. *Physics of the Earth and Planetery Interiors* 63, 145–150

BONATZ M, 1971: Zur Frage der Startbeschleunigungen bei der Eichung von Registriergravimetern auf einer vertikalen Labor – Eichbasis. *Bull. d'Inf. Marrées Terrestres* 67, 3066–3069.

BREIN R, 1962: Gezeitenregistrierung mit Hilfe der elektromagnetischen Feder und ihre Eichung. *Bull .d'Inf. Marrèes Terrestres,* 28, 648-652

BROCKHAUS NATURWISSENSCHAFTEN UND TECHNIK, 1989: *F.A. Brockhaus*, Mannheim

BULLEN K E, 1979: An introduction to the theory of seismology. *Cambridge University Press*

CAREY S W, 1988: Theories of the Earth and Universe *Standford University Press*, Standford, California

CHEN Y T & COOK A, 1993: Gravitational experiments in the laboratory. *Cambridge University Press*

COHEN E H, TAYLOR B N, 1986: Adjustment of the fundamental physical constants. *Codata Bulletin*, 62

EGYED L, 1957: A new dynamic conception of the internal constitution of the Earth *Geologische Rundschau* 46, 101–121

GOODKIND J M, 1991: The superconductive gravimeters: principle of operation, current performance and future prospects. Procedings of the Workshop Non Tidal Gravity Changes. *Walferdange, Luxemburg Cahiers du Centre Européen de Géodynamique et de Séismologie*, 3, 81–90.

GÖTZE H J & MEURERS B, 1983: Some results of calibration factor determination of LaCoste–Romberg gravity meters (Model D.) *J. Geophys.*, 52, 136–139.

GROTEN E, 1970: Calibration of a gravimeter by using a heavy mass. *Symp. Int. Marées Terrestres, Strasbourg. Obs. Royal Belg. Comm. A. 9. Ser.Geophys.*, 96, 210 –212.

HINDERER J, FLORSCH C N, MÄKINEN J, LEGROS H, FALLER J E, 1991: On the calibration of a superconducting gravimeter using absolute gravity measurements. *Geophys. J. Int.* 106, 491-497.

JORDAN P, 1966: Die Expansion der Erde. *Verlag Viehweg & Sohn,* Braunschweig

MADDOS J, 1995: Systematic errors in "Big G"? *Nature*, 377, 573.

MEURERS B, 1996: Comparison of feedback calibration methods – results from LCR D–9. (this volume)

RICHTER B, 1987: Das supraleitende Gravimeter. *Deutsche Geodätische Komission*, Reihe C, 329.

SOMOGYI J, ZÁVOTI J, 1993: Robust estimation with interactively reweighted least–squares method. *Acta Geod. Geoph. Mont. Hung.*, 28, (2–4), 465–490.

STACEY F D, TUCK G J, MOORE G I, HOLDING S C, GOODWIN B D, ZHOU R K, 1987: Geophysics and the law of gravity. *Rev. of Modern Physics*, 59, No. 1, 157–174.

STUBBS, 1989: Fifth force remains elusive. *Nature*, 338, 301–302.

VALLIANT H D, 1973: A technique for the precise calibration of continously recording gravimeters. *Phil. Trans. R. Soc. Lond.* 274, 227-230.

VAN RUYMBEKE M, 1989: A calibration system for gravimeters using a sinusoidal acceleration resulting from a vertical periodic movement. *Bull. Géod.*, 63, 223–235.

VARGA P, HEGYMEGI L, 1985: Multichannel recording of different earth tide components at Budapest station. *Bull. d'Inf. Marées Terrestres*, 96, 5848–5859.

VARGA P, 1989: Laboratory calibration of gravimeters. *Österreichische Beiträge zur Meteorologie und Geophysik.* 2, 111–121.

VARGA P, CSAPÓ G, BECKER M, GROTEN E, 1991: Laboratory calibration of LCR type gravimeters. XX^{th} General Assembly IUGG, Vienna.

VARGA P, HAJÓSY A, CSAPÓ G, 1995: Laboratory calibration of LaCoste–Romberg type gravimeters by using a heavy cylindrical ring. *Geophys. J. Int.* 120, 745–752.

ZHARKOV N Z, MOLODENSKY S M, BRZEZINSKY A, GROTEN E, VARGA P, 1996: The earth and its rotation. *Wichmann.*

THE AUSTRIAN ABSOLUTE GRAVITY PROJECTS

D. Ruess

Federal Office of Metrology and Surveying (BEV)

The figure of the earth is defined by the contribution of the mass and its movement, by its attraction and its inertia. All the geodetic positioning observations are performed in the gravity field and influenced through it. Observations of geodynamic phenomena therefore have to consider the gravity field and its changes.

In Austria 1986 the ballistic absolute gravimeter JILAG-6 was purchased by seven scientific institutes. Several projects in determining the absolute gravity were initiated since 1987 in cooperation with the BEV.

Objective of absolute projects

The most important purposes are

- datum of the Austrian gravity base net (ÖSGN)
- measurements in geodynamic sensitive zones
- regarding the repeatability of measurements

In addition cooperations in bilateral and international absolute gravity projects were started.

Absolute gravity projects in Austria (Fig. 1)

- Base stations
  The first 4 absolute base stations of the Austrian gravity base network (ÖSGN) were established in 1980 and measured by the absolute gravity meter IMGC-Italy (Marson and Steinhauser, 1981). They were remeasured 1987/88. Further 3 base stations were founded in Innsbruck, Klagenfurt and Vienna to stabilise the ÖSGN.
- Obergurgl / Tyrol
  1987 the station Obergurgl in the Central Alps was established. Measurements have been repeated twice a year in spring and in autumn (Ruess, 1995). On one hand the aim was to detect seasonal gravity effects due to precipitations (rainfall in summer, snowfall in winter), on the other hand the repeatability of gravity measurements could be checked. The time serie is shown in Figure 2.
- Hochkar Calibration Line (HCL) Göstling - Hochkar
  The HCL was established in 1982 to check the LaCoste&Romberg gravimeters in Austria (Meurers and Ruess, 1985). The endpoints of this line were fixed 1988 by absolute measurements. Remeasurements were realized in 1995, also the 2 intermediate points were decided.
- Leoben - Präbichl calibration line
  3 stations of the local gravimeter calibration line were determined 1989/90 (Posch, Tengg, Walach, 1989).
- Rhine Valley
  3 absolute stations were established in a project of the Institute of Geophysics at the Montanistic University in Leoben (Posch and Walach, 1989).
- Vienna Basin
  In Mannswörth one station was observed 1987/88 at the trench of Schwechat, 6 stations

were established 1991/92 on a profile Hirtenberg - Kaisereiche across the trench of the Southern Vienna Basin to control the effects of subsettings together with levelling control measurements (Ruess et al., 1993).

- Karawanken
  4 new absolute stations are prepared in the Karawanken in the area of the periadriatic linement. First absolute measurements should start in autumn 1996. The aim is to detect geodynamic effects in combination with levelling and GPS observations. Further absolute stations will be occupied in the surrounding area in the north (Klagenfurt) and in the south (Slowenia). Also a station in a geologically stable zone (Altenburg, Bohemian Massif) will be measured as reference.

periode	stations	observations	project
1987/88	7	8	ÖSGN
1987-	1	16	Obergurgl / Tyrol
1988/95	4	6	Hochkar Calibration Line (HCL) Göstling - Hochkar
1989/90	3	4	local calibration line Leoben - Präbichl
1988	3	3	Rhine Valley
1987/88	1	2	Mannswörth
1991/92	6	10	Vienna Basin
1996-98	4	0	Karawanken (periadriatic linement)
total	29	49	

international and bilateral contributions

periode	stations	observations	country / project
1989/94	1	3	comparisons at BIPM (Sévres, France)
1990-94	6	6	Germany
1992/95	4	4	Czech Republic
1993	4	4	Slovakia
1991-95	5	5	Hungary
1994	5	5	Switzerland
1997	2	-	Slowenia
1997/98	4	-	UNIGRACE *)
total	25	27	

*) UNIGRACE (unification of gravity systems of Central and Eastern European Countries) is a project that has been derived from the former activities concerning absolute gravity measurements and sea level monitoring in the framework of CERGOP. Absolute measurements will be established in Germany, Austria, Bulgaria, Croatia, Czech Republik, Finland, Hungary, Italy, poland, Romania, Slovakia, Slovenia using the absolute gravimeters of Germany, Austria, Finland, Italy, Poland.

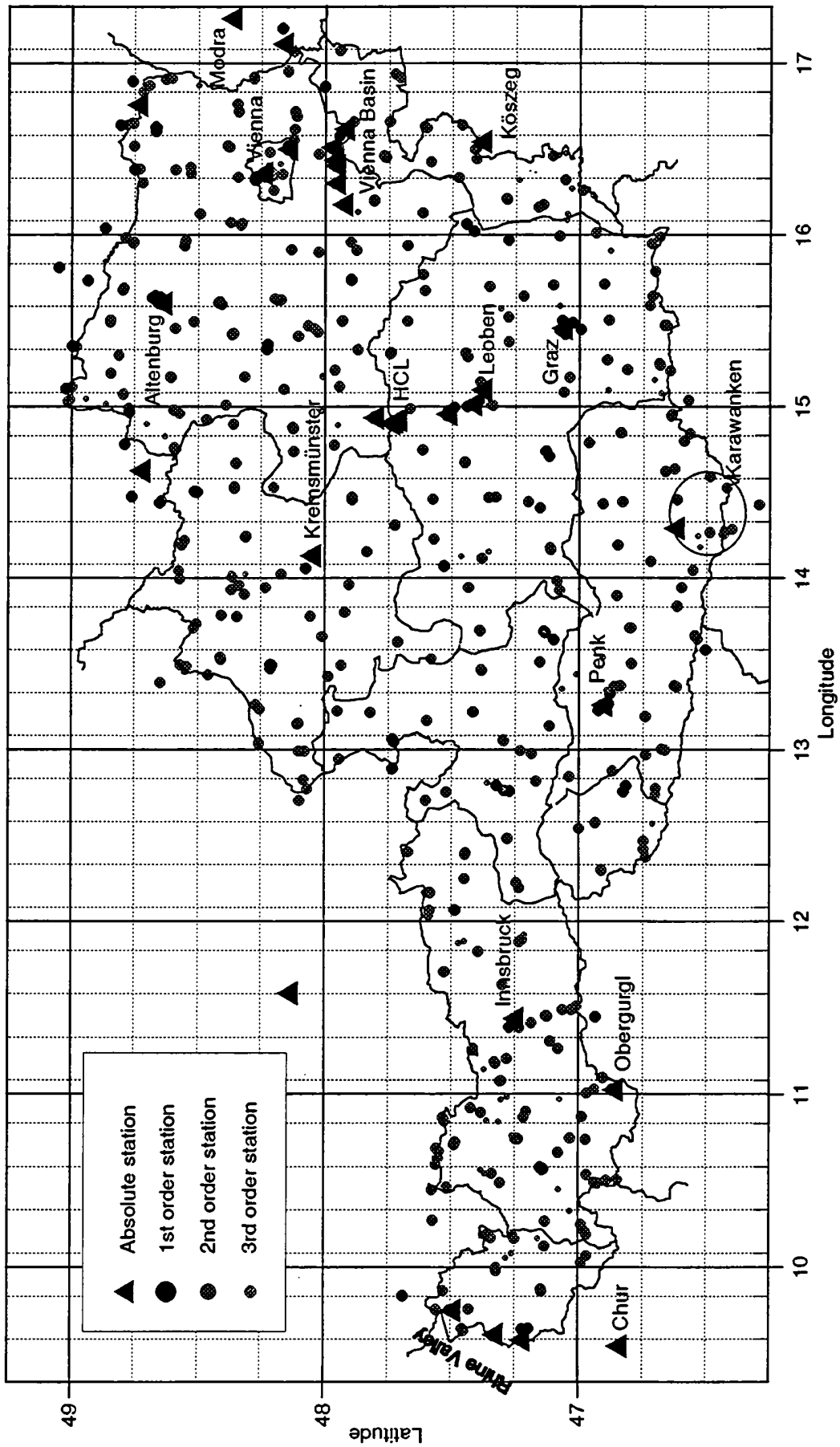

Fig. 1: Austrian gravity base net (ÖSGN) and absolute gravity stations in Austria

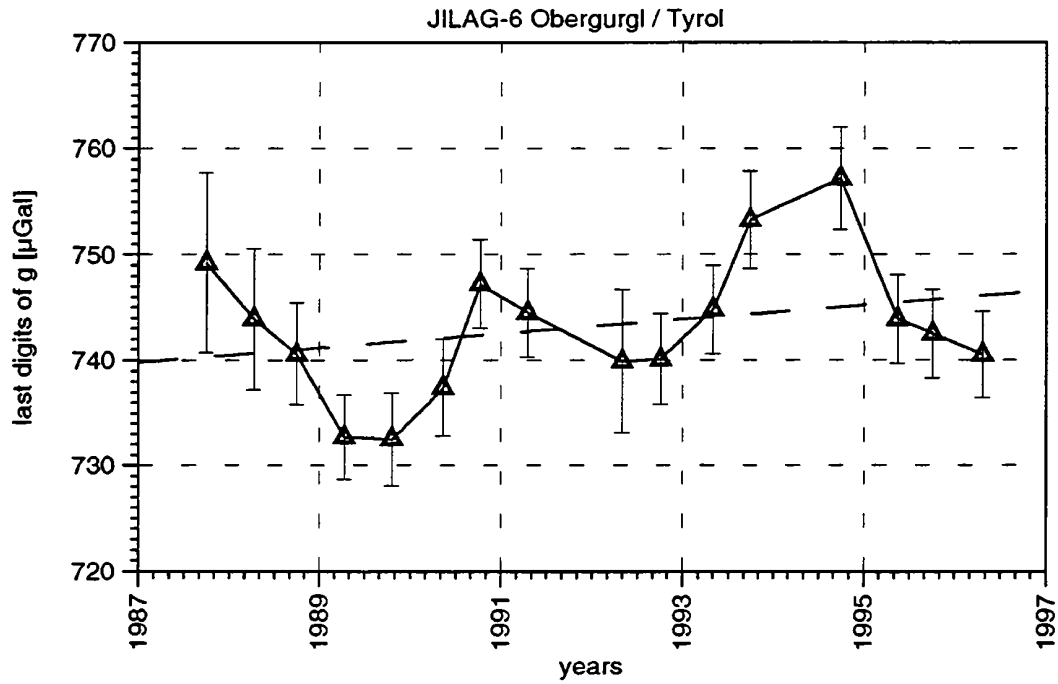

Fig. 2: Absolute gravity observed with JILA G-6 in Obergurgl, Tyrol.

References:

Marson I., Steinhauser P., 1981: Absolute Gravity Measurements in Austria. EOS, Trans. Am. Geoph. Un., 62, 258.

Meurers B., Ruess D., 1985: Errichtung einer neuen Gravimeter - Eichlinie am Hochkar. Österr. Zeitschr. f. Verm. u. Photogr., Heft 3.

Posch E., Tengg St., Walach G., 1989: Die Gravimetereichstrecke Leoben - Präbichl. Tagungsber. 5. Int. Alpengravimetrie-Kolloquium Graz 1989, Österr. Beitr. Meteorol. u. Geophysik, 2, 123-124.

Posch E., Walach G., 1989: Das Bouguerschwerefeld in Vorarlberg und im Bereich der Übergangszone zwischen West- und Ostalpen. Tagungsber. 5. Int. Alpengravimetrie-Kolloquium Graz 1989, Österr. Beitr. Meteorol. u. Geophysik, 2, 147-152.

Ruess D., Steinhauser P., Jeram G., Faller J., 1989: Neue Absolutschweremessungen in Öster-reich. Tagungsber. 5. Int. Alpengravimetrie-Kolloquium Graz 1989, Österr. Beitr. Meteorol. u. Geophysik, 2, 95-110.

Ruess D., 1993: Schwerevariationen im Alpinen Raum. Tagungsber. 6. int. Alpengravimetrie-Kolloquium Leoben 1993, Österr. Beitr. Meteorol. u. Geophysik, 8, 113-126.

Ruess D., Duma G., Nief M., 1993: Absolutschweremessungen im südlichen Wiener Becken. Tagungsber. 6. Int. Alpengravimetrie-Kolloquium Leoben 1993, Österr. Beitr. Meteorol. u. Geophysik, 8, 127-142.

Ruess D., Gold W., 1995: The Austrian Gravity Base Net 1995 stabilised by Absolute Gravity Measurements and Connected to the European Network Adjustment. Posterpresentation, XXI IUGG general meeting, Boulder, Colorado, USA.

Ruess D., 1995: Das Österreichische Schweregrundnetz. EVM Nr. 80, BEV Wien.

Ruess D., 1995: Die Absolutschwerestation Obergurgl. Institut für Hochgebirgsforschung der Leopold-Franzens-Universität Innsbruck, Jahresbericht 1995, 57-60.

Steinhauser P., 1987: Absolutschweremessungen in Österreich. Oppolzer-Gedächtnissymposium 1986, Geodät. Arbeiten Österr. f. d. Int. Erdmessung, Bd. 5.

INTERPRETATION OF LOCAL GEOID UNDULATIONS IN THE PANNONIAN BASIN

Gábor Papp and János Kalmár

Geodetic and Geophysical Research Institute
of the Hungarian Academy of Sciences
H–9401, Sopron, Pf. 5

Abstract

Due to the huge amount of geological and geophysical data concerning the structure of the lithosphere in the Pannonian basin which have been systematized and released recently in Hungary the construction of a 3-D volume element model of the crustal structure and density distribution of the basin was realized in 1993-94 (Kalmár et al., 1995). At that time the model consisted of only two main structural elements of the lithosphere: (1) the Neogene-Quaternary sediments and (2) the upper mantle. Based on this model the question of sediment compaction was investigated in the Little Hungarian Plain sub-basin (N-W Hungary) in order to interpret the unusually moderate Bouguer anomaly depression of the area contradicting to the 7 – 8 km maximum thickness of the sediments (Papp and Kalmár, 1995a). Later on the density model was supplemented by a simple model of the lower crust derived from deep seismic sounding data and gravity inversion. Based on this 3 element version a succesfull attempt was made to reconstruct short wavelength geoid undulations in the Pannonian basin (Papp and Kalmár, 1996) which were compared to the undulations of an existing local gravimetric quasi-geoid solution (Kenyeres, 1993). The first results showed decimetre agreement ($m_{\Delta N} = +0.08$ m, $\sigma_{\Delta N} = \pm 0.22$ m) and by the "tuning" of the determination method of the "lithospherical geoid" as well as by completing the 3-D model with the surface topography the agreement was improved and the standard deviation of undulation discrepancies was decreased to ± 0.10 m. Statistical comparisions proved that the reliability of the lithospheric geoid relative to other local and global geoid solutions is the same as the reliability of two different local gravimetric quasi-geoid solutions obtained from some hundred thousands of surface gravity anomalies. Such a result drew the attention to the physical interpretation of the short wavelength/local geoid undulations and spectral computations were carried out (Papp and Kalmár, 1995b) to demonstrate (1) how the gravity field of the Pannonian basin may be generated by the different structural elements of the lithosphere (Fig. 1) and (2) what their relative contribution is in different wavelength ranges (Papp, 1996).

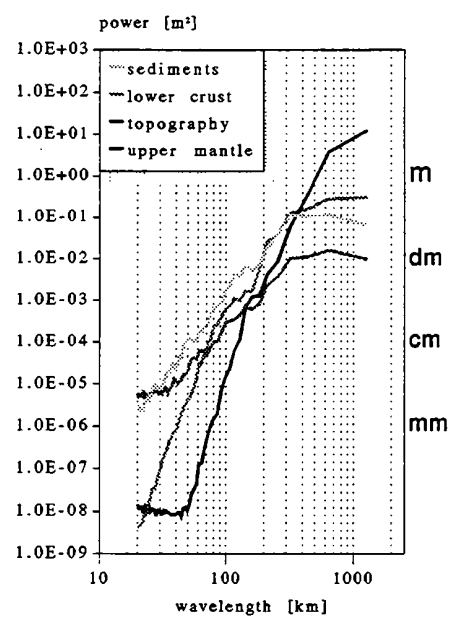

Figure 1. Radial power spectra of the undulation contributions of different structural elements of the lithosphere in the Pannonian basin, Hungary.

References

Kalmár J., Papp G., Szabó T., 1995. DTM-Based Surface and Volume Approximation. Geophysical Applications. Computers & Geosciences, Vol. 21, 245–257.

Kenyeres A., 1993. Detailed Geoid Determination Using the Combination of Truncated Global Integrals and Geopotential Models. In: Global and Local Geoid Investigations, National Scientific Research Fund Project Report, No. 5-204, Dept. of Geodesy, Technical Univ. Budapest, Budapest, p. 195.

Papp G., Kalmár J., 1995a. Investigation of Sediment Compaction in the Pannonian Basin Using 3-D Gravity Modelling. Physics of the Earth and Planetary Int., Vol. 88 No.2, 89–100.

Papp G., Kalmár J., 1995b. Construction of the Geoid from OSU91A Geopotential Model and 3-D model of the Lithosphere and its Spectral Interpretation in the Pannonian Basin, Hungary, presented at XXI General Assembly of the IUGG, IAG Session G5, Boulder, Colorado, USA

Papp G., Kalmár J., 1996. Toward the Physical Interpretation of the Geoid in the Pannonian Basin Using 3-D Model of the Lithosphere (in print), IGeS Bulettin, DIIAR-Politecnico di Milano, Milano

Papp G., 1996. Gravity Field Modelling in the Pannonian Basin for Geodetic Purposes (in Hungarian), PhD Theses, Geodetic and Geophysical Res. Inst., Sopron, Hungary

Austrian Geoid 2000

E. Erker[1], B. Hofmann-Wellenhof[2], H. Moritz[2], H. Sünkel[2]

(1) Federal Office of Metrology and Surveying,
Schiffamtsgasse 1–3, A-1025 Vienna, Austria
(2) Technical University Graz,
Steyrergasse 30, A-8010 Graz, Austria

Abstract

By the impact of the relative GPS accuracy of 1 ppm to 0.1 ppm (for longer baselines), the Austrian geoid with its present mean accuracy of about 1 ppm is no longer considered to be sufficiently consistent. For this reason, a new computation of the Austrian geoid was initiated with the objective to obtain a relative accuracy of at least 0.5 ppm throughout the country. The project is denoted as Austrian Geoid 2000 to indicate that the resulting product is intended to survive the turn of the century.

The new computation of the Austrian geoid will be performed by three approaches, (1) the conventional least squares collocation method, (2) the fast collocation method which implies gridded input data and a symmetric block Toeplitz matrix for the covariance function, and (3) the gravimetric solution by the Fast Fourier Transform based on either a planar approximation or a spherical approach for the kernel functions.

As far as Austria is concerned, the data input consists of a 50 × 50 m digital terrain model, some 30 000 gravity data, about 700 deflections of the vertical, and GPS derived points. From the neighboring countries, gravity and height information is available in different quality and density.

1 Least squares collocation today

Slightly more than a quarter of a century ago, the estimation of linear functionals of the anomalous potential based on heterogeneous and noisy gravity data, one of the key problems in physical geodesy, was not yet solved. The mathematical solution of this problem was given by Krarup (1969) and extensively elaborated by Moritz (1980) and other scientists and is known as "least squares collocation" (LSC).

The theoretical beauty of LSC has one practical drawback: the processing quickly exceeds the computational capacity of the computer because the solution time increases with the third power of the size of the data set. Therefore, numerous efforts have been made in tuning LSC to manage large data sets.

Among the various methods, the following techniques have been applied frequently and are capable of reducing the LSC computational effort:

1. The LSC patchwork method. The area under consideration is subdivided into a number of overlapping subareas. For each subarea, the LSC solution is performed. The solution for the whole area is obtained by "glueing" together (in a mathematical sense) the subarea solutions.

This paper was presented first at the XXI General Assembly of IUGG in Boulder, Colorado, July 2–14, 1995

2. LSC with finite covariance functions. The correlation of data decreases with the separation of the data points. Data with a large spatial separation are almost uncorrelated. Therefore, using a covariance function with finite support produces a band-structured covariance matrix which significantly reduces the computational effort for LSC processing of large areas.

3. Local LSC solutions. Data interpolation and differentiation are mainly affected by the local data environment; the effect of remote data is often negligible. Based on this principle, local LSC solutions with only a small data set can be obtained very efficiently by updating the inverse covariance matrix and the solution vector when the prediction point is moved over the prediction area.

4. Fast Fourier Transform (FFT) solution. For planar gridded homogeneous data sets with homogeneous noise and a covariance function depending on the planar distance, the covariance matrix is a block Toeplitz matrix consisting of symmetric Toeplitz blocks. This specific situation offers the transformation of the LSC solution into the frequency domain by means of the FFT algorithms, cf. Eren (1982). However, errors due to edge effects caused by the finite grid must be carefully considered.

5. Fast collocation. For homogeneous data with homogeneous data noise on a geographical grid and a covariance function depending on the spherical distance, the covariance matrix, due to the convergence of meridians, has no longer the block Toeplitz structure of symmetric Toeplitz blocks. The symmetric Toeplitz structure of each block is preserved, but the block Toeplitz structure is lost. This fact can be overcome as outlined below (Sect. 2.2).

2 The Austrian Geoid 2000

Due to the steadily increasing accuracy requirements, a new effort will be made to recompute the Austrian geoid. For reasons of comparison, three groups will compute independently three different methods: (1) the conventional least squares collocation, (2) the fast collocation, and (3) a gravimetric solution by using the FFT. Some brief explanations of the typical characteristics of these methods are given.

2.1 Conventional least squares collocation

The main input source for the geoid used so far in Austria are deflections of the vertical. The new solution will use heterogeneous data, i.e., gravity data and deflections of the vertical. In addition, GPS data will be used to account for the datum problem.

Details on the solution as realized in the GRAVSOFT program package are given by Tscherning et al. (1992). This program uses stepwise least squares collocation. The method requires data sets with known standard deviations and, in addition, isotropic covariance functions being specified by a set of empirical anomaly degree-variances. For the input of observations, the GRAVSOFT program package allows potential coefficients, mean or point gravity anomalies, height anomalies, deflections of the vertical, gravity gradients, and density contrasts.

2.2 Fast collocation

Among the previously described methods, the favorite candidate is fast collocation because it is both extremely efficient and provides at the same time an exact solution on the sphere (in contrast to the planar FFT approach).

The idea of fast collocation is simple: for a small area on the sphere, a planar grid may be used as a good approximation for a geographical grid. As a consequence, the block Toeplitz structure of the covariance matrix for the planar case may be used as a good approximation for the non-block Toeplitz structure of the covariance matrix for the geographical case.

Following Bottoni and Barzaghi (1993), the covariance matrix C may be split into

$$C = \tilde{C} + \delta C \tag{1}$$

where $\tilde{C}$ represents the block Toeplitz matrix of symmetric Toeplitz blocks, and the matrix δC accounts for the deviation of the spherical from the planar case. The diagonal elements of each block correspond to the covariances between data on the same meridian. Therefore, δC has zeroes on each block diagonal. The size of the off-diagonal elements in each block depends on the grid size and can reach about 10% of the diagonal elements of C for solutions such as the one considered here.

This small deviation suggests the application of an iterative solution with $\tilde{C}$ as the zero-order approximation of the covariance matrix. Denoting the data vector by y and the solution vector by x, the iterative solution is accomplished by

$$\tilde{C}\, x_{n+1} = y - \delta C\, x_n\,. \tag{2}$$

It is important to note that the product $\delta C\, x_n$ can be computed very rapidly if advantage of the structure of δC is taken: by properly arranging the elements of δC in a vector, the product $\delta C\, x_n$ can be transformed into a circulant convolution of two vectors which can be computed very efficiently by the Fast Hartley Transform (FHT) by taking into account the convolution theorem.

The convergence rate of Eq. (2) can be improved dramatically by a skillful preconditioning. Two conflicting requirements must be fulfilled by a preconditioner: first, it should be as simple as possible, and, second, it should be as close as possible to the inverse of the operator. The second requirement is certainly achieved by $\tilde{C}^{-1}$ as preconditioner. Therefore, the proposed collocation solution for the Austrian geoid project will focus on a preconditioned conjugate gradient method with incorporated FHT.

The proposed LSC solution will be supplemented by the usual data reduction due to residual terrain and a high resolution geopotential model. Gridded residual gravity data for Austria and all neighboring countries, at least 100 km beyond the Austrian border, will be used.

According to feasibility studies which have been conducted recently, a relative geoid accuracy of about 0.2 – 0.3 ppm may be expected for the entire country.

2.3 Gravimetric geoid by FFT techniques

The classical formula to determine the geoid from gravity data is the Stokes formula

$$N = \frac{R}{4\pi\gamma} \iint_{\sigma} \Delta g\, S(\psi)\, d\sigma \tag{3}$$

where N denotes the geoidal undulation, R is the radius of a sphere, γ is a mean value of gravity, σ indicates the unit sphere, Δg are the gravity anomalies, and $S(\psi)$ is the Stokes function. The gravity anomalies Δg refer to the geoid. Thus, measured surface gravity data must be reduced to the geoid by a terrain reduction using height data (digital terrain model) and further reduced by the global geopotential model. The reduced data is used to generate the residual part of the geoid by means of (3). The final geoidal undulation results from the residual part, the reference undulation computed by the geopotential model, and the indirect effect (which may be derived from the height data).

The solution of the gravimetric method may be carried out conventionally (e.g., by numerical integration) or by the FFT technique. Several approaches for the FFT were developed: the

planar approximation, see Sideris and Schwarz (1985), the spherical approach, see Strang van Hees (1990), and other methods.

The principle of the planar approximation is expressed by the following equation

$$N(x_p, y_p) = \frac{1}{2\gamma} \int\int_E \frac{\Delta g(x,y)}{\sqrt{(x_p - x)^2 + (y_p - y)^2}} \, dx \, dy \tag{4}$$

where the geoidal height at x_p, y_p is computed from Δg in an area E. This approximation is now a two-dimensional convolution integral. The application of a two-dimensional FFT is straightforward. The error inherent in the planar approximation will grow with the integration area.

The drawback of the planar approximation may be circumvented by the spherical approach where the Stokes integral is transformed to a two-dimensional convolution integral by a modification of the Stokes function. The evaluation is performed on the sphere which causes the superiority compared to the planar approximation. However, Strang van Hees (1990) introduces also an approximation by using a mean latitude for each grid mesh. The geoid undulations for all grid points can simultaneously be computed by applying a two-dimensional FFT accordingly.

The Stokes function may also be expressed as a convolution in east-west direction (along a parallel), because the Stokes function is constant for all computation points on one parallel, cf. Li (1993). Applying a one-dimensional FFT, the simultaneous computation of geoid undulations on a parallel is possible without approximation as far as the Stokes function is concerned. This approach was proposed by Haagmans et al. (1993).

Detailed formulas of these and other approaches may be found e.g. in Li (1993) and in She (1993).

2.4 Available data sets

Gravity data

For Austria, some 32 400 gravity data is available at the Section of Physical Geodesy of the Technical University Graz. This data was provided from several institutions: Institute of Meteorology and Geophysics of the University Vienna, Institute of Geophysics of the University Leoben, Austrian Petroleum Industry, Institute of Geophysics of the Technical University Clausthal, and the Federal Office of Metrology and Surveying. The data refer to the Austrian gravity network which is compatible with the international system IGSN71. The position parameters referring to the gravity data are related to the datum of the former Military Geographical Institute (MGI), i.e., a local datum associated with the Bessel ellipsoid. Using a grid with a mesh size of 2×2 km, the gravity data set may be reduced to 14 255 data for Austria.

Deflections of the vertical

At 683 homogeneously distributed points in Austria, deflections of the vertical are available. The data refers to the same local datum as the gravity data (datum of MGI associated with the Bessel ellipsoid). This data was the primary source of the previously computed Austrian astro-geodetic geoids, cf. Erker (1983), Grasegger and Wotruba (1983), Sünkel (1983), Sünkel (1987).

GPS data

From several campaigns, GPS data is ready to be used all over Austria. The main purpose of the introduction of GPS data is the possibility of an accurate datum relation. The GPS data refers to a geocentric system, e.g., the World Geodetic System 1984 (WGS-84). The most important Austrian campaigns since 1990 are the "Austrian Geodynamic Reference" campaigns AGREF90, AGREF92, and AGREF94. Some 75 GPS points established by these campaigns are located on Austrian territory.

Digital terrain model
The Federal Office of Metrology and Surveying provides a high resolution 50×50 m digital terrain model for Austria. The positions of the grid points are expressed in geographical coordinates φ, λ. The heights refer to the official Austrian height system consisting of normalorthometric heights associated with the datum point Molo Sartorio in Trieste, Italy.

Surface density model
The two-dimensional surface density model, cf. Walach (1987), was derived from a geological map of Austria comprising 40 regions and twelve different densities between 2000 and 2850 kg/m^3.

Global earth model
For the low to medium frequency part of the gravity field of the earth, a global geopotential model (e.g., OSU81 or the model being currently developed by DMA) will be used.

Data of neighboring countries
Gravity and DTM data of all neighboring countries, i.e., Germany (Bavaria and Baden-Württemberg), Czech Republic, Slovakia, Hungary, Slovenia, Italy, Switzerland, are available. The gridding of the data is different. However, all data will be transformed to mean values in a $3' \times 3'$ grid. The densification of data is performed by prediction and interpolation, thinning is achieved by averaging data.

3 Conclusion

The three approaches, (1) the conventional least squares collocation method, (2) the fast collocation method, and (3) the gravimetric solution by the FFT will be computed independently from three different groups. After a comparison of the results, the Austrian geoid 2000 will be established. It is almost unnecessary to say that the fast collocation method will yield this Austrian geoid 2000. The reasons are the computational efficiency compared to the conventional least squares collocation method and the superiority with respect to input data compared to the purely gravimetric solution.

Acknowledgment

The authors express their sincere thanks to Konrad Rautz (Graz), Herbert Lichtenegger (Graz), Josef Graf (Vienna), and Volker Sturm (Vienna) for valuable support.

References

Bottoni GP, Barzaghi R (1993): Fast collocation. Bulletin Géodésique, 67(2): 119–126.

Eren K (1982): Toeplitz matrices and frequency domain collocation. Manuscripta geodaetica, 7: 85–116.

Erker E (1983): Das Geoid in Österreich; Berechnungen des Bundesamtes für Eich- und Vermessungswesen. In: Österreichische Kommission für die Internationale Erdmessung (ed): Das Geoid in Österreich. Geodätische Arbeiten Österreichs für die Internationale Erdmessung, Neue Folge, vol III: 89–115.

Grasegger J, Wotruba M (1983): Geoidbestimmung; Berechnungen an der TU Graz, 1. Teil. In: Österreichische Kommission für die Internationale Erdmessung (ed): Das Geoid in Österreich. Geodätische Arbeiten Österreichs für die Internationale Erdmessung, Neue Folge, vol III: 117–124.

Haagmans R, de Min E, van Gelderen M (1993): Fast evaluation of convolution integrals on the sphere using 1D FFT, and a comparison with existing methods for Stokes' integral. Manuscripta geodaetica, 18: 227–241.

Krarup T (1969): A contribution to the mathematical foundation of physical geodesy. Danish Geodetic Institute, Copenhagen, vol 44.

Li YC (1993): Optimized spectral geoid determination. Reports of the Department of Geomatics Engineering of the University of Calgary, vol 20050.

Moritz H (1980): Advanced physical geodesy. Wichmann, Karlsruhe.

She BB (1993): A PC-based unified geoid for Canada. Reports of the Department of Geomatics Engineering of the University of Calgary, vol 20051.

Sideris MG, Schwarz KP (1985): Computation of geoidal undulations and deflections of the vertical for Alberta. Alberta Bureau of Surveying and Mapping Contract Report No 84004, Edmonton, Alberta, Canada.

Strang van Hees G (1990): Stokes formula using fast Fourier techniques. Manuscripta geodaetica, 15: 235–239.

Sünkel H (1983): Geoidbestimmung; Berechnungen an der TU Graz, 2. Teil. In: Österreichische Kommission für die Internationale Erdmessung (ed): Das Geoid in Österreich. Geodätische Arbeiten Österreichs für die Internationale Erdmessung, Neue Folge, vol III: 125–143.

Sünkel H, Bartelme N, Fuchs H, Hanafy M, Schuh W-D, Wieser M (1987): The gravity field in Austria. In: Austrian Geodetic Commission (ed): The gravity field in Austria. Geodätische Arbeiten Österreichs für die Internationale Erdmessung, Neue Folge, vol IV: 47–75.

Tscherning CC, Forsberg R, Knudsen P (1992): The GRAVSOFT package for geoid determination. In: Holota P, Vermeer M (eds): Proceedings of the First Continental Workshop on the Geoid in Europe, Prague, Czech Republic, May 11–14, 327–334.

Walach G (1987): A digital model of surface rock densities of Austria and the Alpine realm. In: Austrian Geodetic Commission (ed): The gravity field in Austria. Geodätische Arbeiten Österreichs für die Internationale Erdmessung, Neue Folge, vol IV: 3–9.

GRAVIMETRIC GEOID OF AUSTRIA

Norbert Kühtreiber and Konrad Rautz
Institute of Theoretical Geodesy, Section of Physical Geodesy
Technical University Graz

Abstract:

The lastest version of the Austrian geoid was computed in 1987. This geoid determination was based on astrogeodetic measurements using least squares collocation. Gravity anomalies were only used to determine the covariance function of the disturbing potential but were not included as measurements in the collocation process. In the following a new pure gravimetric geoid using Stokes' formula is presented. After a summary of the theoretical background and formulas, the solution using the so-called RTM-method in connection with collocation is shown. Finally the new geoid is compared to the astrogeodetic solution and GPS reference points.

1. Introduction

Gravimetric geoid computation by Stokes' formula requires information about gravity data all over the world. This problem is solved by the combination of local gravity data, a local high resolution topographic model and a global potential model. We distinguish three main parts of the computation.
The first part consists of the reduction of the gravity anomalies. At the beginning the anomalies are reduced by a global potential model which eliminates the long wavelength part. This step makes it possible to apply Stokes' formula to a local set of gravity anomalies. Further the effect of topography which is responsible for the short wavelength part of the gravity, is substracted. After this the data should be smooth enough to avoid numerical instabilities during computation. An additional advantage of this reduction process is the possibility of applying appropiate interpolation methods to the reduced gravity anomalies.
In the second step the reduced anomalies are entered to Stokes' formula leading to reduced geoid heights.
Finally we add the influence of the global potential model, the influence of the topographic model and the well known indirect effect to the reduced geoid heights.
This commonly used technique for geoid computation is called a remove-restore process. In the following we mention two different computation methods which differ in the way the effect of topography is treated (Mainville et al., 1994).

2. Theory

2.1 Helmert Condensation

We start with the definition of the reduced free-air anomalies

$$\Delta g_{\text{FA-red}} = g - \gamma + \delta g_{\text{atm}} - \delta g_{\text{OSU}} \,, \tag{1}$$

with g as the measured gravity value at ground level, γ the normal gravity at normal height, δg_{atm} the atmospheric correction (Moritz, 1992), and δg_{OSU} the effect of the global potential model.
Helmert's classical approach of computing the geoid by Stokes' equation requires gravity anomalies referring to the geoid. In addition, all masses outside the geoid have to be removed. Helmert's approach, see Heiskanen and Moritz (1967), consists of three steps: reducing gravity data from the effect of topography, condensing the masses of topography to the geoid and restoring the indirect effect to the geoid heights due to the effect of the condensed masses. In this case the gravity anomalies used for the evaluation of Stokes' equation will be reduced Faye-

anomalies $\Delta g_{FAYE\text{-}red}$ defined by

$$\Delta g_{FAYE\text{-}red} = \Delta g_{FA\text{-}red} + A_t \quad . \tag{2}$$

A_t is the classical terrain correction. In order to get reduced Faye-anomalies at sea-level terms due to the difference between the normal and the true gravity gradient and part of the effect of condensation have to be added. Martinec et al. (1993) show that these terms cancel each other when it is assumed that gravity anomalies are linearly dependent on the elevation of topography and planar approximation is used. Therefore the reduced Faye-anomalies in equation (2) can directly be used as input to Helmert's approach.
Possible methods for the solution of Stokes' equation are least squares collocation (LSC) and FFT-techniques. As a result we get reduced geoid heights N_{red}. After restoring the geoid height obtained from the geopotential model N_{OSU} and the indirect effect we get

$$N = N_{red} + N_{OSU} + N_{ind1} + N_{ind2} \tag{3}$$

with

$$N_{ind1} = \frac{-\pi G \rho H^2}{\gamma} \quad , \tag{4}$$

the first order term of the indirect effect, and

$$N_{ind2} = \frac{-G\rho}{6\gamma} \int\int \frac{h^3 - h_P^3}{l^3} dx\, dy \quad , \tag{5}$$

the second order term.

2.2 RTM Method

RTM as the abbreviation for residual terrain model means that the gravity anomalies for the evaluation of Stokes' equation are defined by

$$\Delta g_{RTM\text{-}red} = \Delta g_{FA\text{-}red} + A_{t\text{-}RTM} \quad . \tag{6}$$

$A_{t\text{-}RTM}$ is computed with some approximations using

$$A_{t\text{-}RTM} = -0.1119\,(H - H_{ref}) + A_t \quad . \tag{7}$$

A_t is the classical terrain correction, H is the height of the measured point. The RTM-reduced gravity anomalies $\Delta g_{RTM\text{-}red}$ are referred to a mean reference height model H_{ref}. This mean height model is obtained by low-pass filtering the detailed topographic model by a moving-average operator (Forsberg, 1984). The problem of this method is to find a smooth and appropiate reference model. If the moving average operator does not eliminate the whole short wavelength part of the topographic model, this wavelength part still remains in the RTM-reduced data. On the other hand if the smoothing is too great, wavelength parts which have already been removed by the global potential model are removed twice (Lehmann, 1994).
After the reduction of the gravity anomalies by equation (6) these smooth gravity anomalies are used for the solution of Stokes' equation by least squares collocation or FFT-techniques. As a result, RTM method in principle provides height anomalies. After restoring the influence of the global potential model N_{OSU} and the effect of the RTM-reduction ζ_{RTM} to $\zeta_{RTM\text{-}red}$, the solution of Stokes' equation, the final height anomalies are obtained as follows

$$\zeta = \zeta_{RTM\text{-}red} + N_{OSU} + \zeta_{RTM} \quad . \tag{8}$$

Terms with no impact on practical results of ζ were neglected. For details on RTM reduction refer to Mainville et al. (1994), Sideris and Forsberg (1991), Forsberg (1984). In order to get

geoid heights, the following approximate formula (Wang, 1993)

$$N = \varsigma + H\,\delta g_{Bouguer}/\gamma \qquad (9)$$

is used.

3. Software

The gravimetric geoid computation consists of many steps. Often the different tasks are solved with the help of heterogeneous programs which seldom are organized in one single program-system. In principle, there are two main topics: data management and manipulation as well as gravity field modelling.
The first step, data manipulation, starts with collecting the data. Even nowadays collecting data is a non-trivial problem, as rights of the owner of data collections at home and abroad have to be considered. The software which solves the different problems of data preparation was written at the section of physical geodesy. There exist separate programs for the following tasks:

- management of gravity data
- management of grid data (heights)
- quality tests
- coordinate transformations
- interpolation of grid values.

All this data management and preparation is very time-consuming and is one of the main parts of the realization of the project. One should keep in mind that this work forms the basis for the quality of the solution.

Gravity modelling as the second main part can be divided into the following sections:

- reduction of measurements (topography)
- influence of the global potential model
- determination of empirical covariance functions
- fitting of analytical covariance functions
- collocation.

For all these tasks we used the programsystem GRAVSOFT, which was developed at the University of Copenhagen (Tscherning et al., 1991). The programsystem is freely distributed for scientific applications. In 1988 the package was developed by combining existing programs for regional and local geoid computations. The data exchange between the different programs is standardized. One of the advantages of GRAVSOFT is the possibility of executing the program on different platforms (pc, unix). One problem with GRAVSOFT is that because of the lack of an users-interface, professional knowledge is highly recommended. The package has already been used for various geoid computation in various countries: Forsberg (1990), Duquenne et al. (1994), Yun (1994).

4. Data sets

Two different data sets are used for the following computations. One set covers the area of Austria. The institutions providing these data were: Institute of Meteorology and Geophysics, University of Vienna; Institute of Geophysics, Montanistic University of Leoben and the Federal Bureau of Surveying and Mapping. Figure 1 shows the data distribution which approximately forms a "grid" of 6 x 6 km. After performing quality tests for the 2200 gravity measurements the reductions according to equation 6 and 7 were computed. All anomalies refer to GRS80. Table 1 lists the main statistical properties.

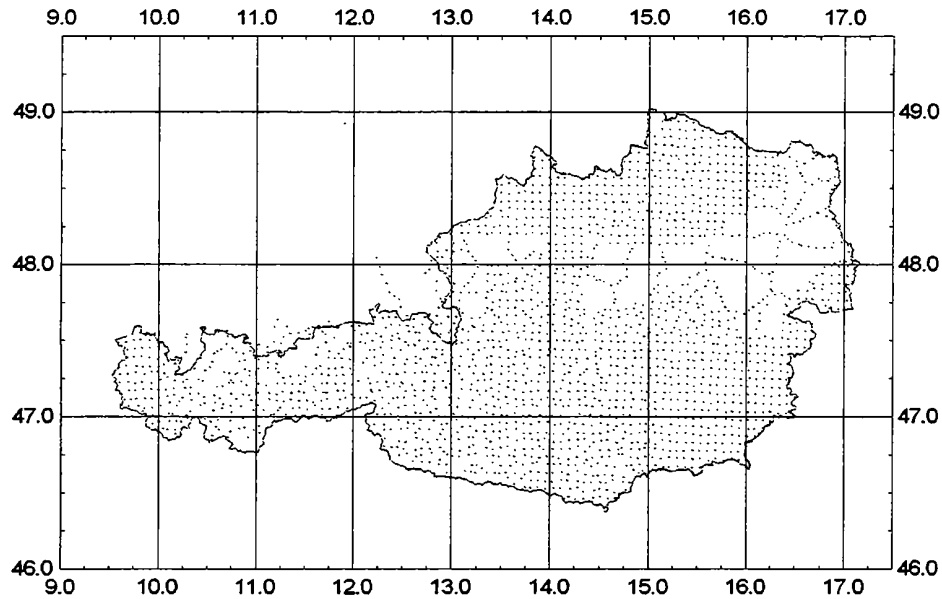

Figure 1: Distribution of gravity measurements used

Gravity anomaly (mgal)	Min	Max	Mean	Std.dev.
Δg_{FA}	-110.8	168.5	9.0	46.3
$\Delta g_{FA\text{-}red}$	-192.5	122.7	-23.8	45.8
$\Delta g_{RTM\text{-}red}$	-59.9	40.4	-4.5	18.0

Table 1: Statistic of gravity anomalies of data set Austria

The reduced free-air anomalies in Table 1 were calculated with the global potential model OSU91A. This reduction changes mainly the mean value, while the standard deviation hardly changes. As a result of the RTM-reduction we get smooth values, which is indicated by the decreasing of the standard deviation by 60%. Figure 2 shows the contour plot of $\Delta g_{RTM\text{-}red}$.

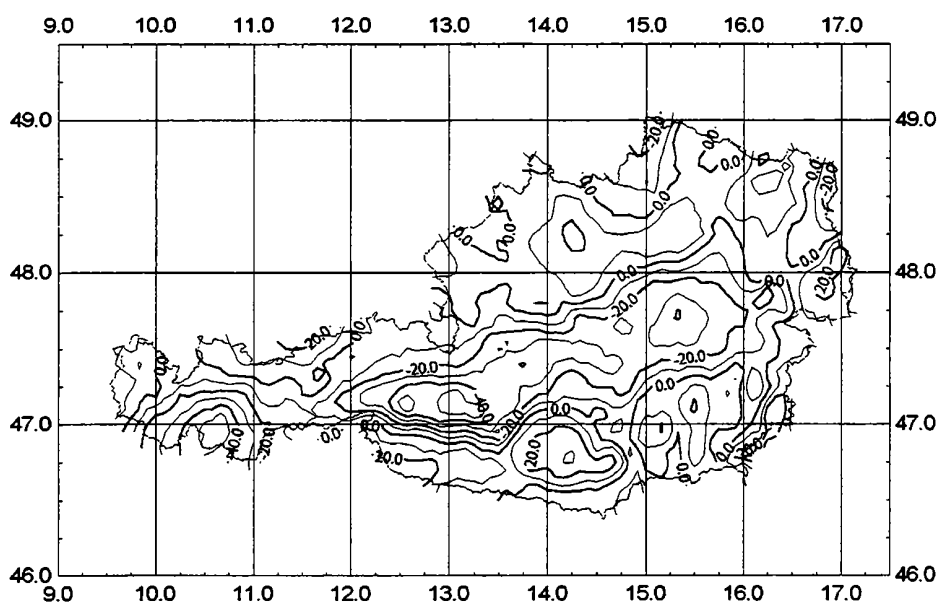

Figure 2: Gravity anomalies $\Delta g_{RTM\text{-}red}$ (contour interval 10 mgal)

The second data set for the area outside of Austria was provided by the Bureau Gravimetrique International (BGI). These data cover a region of 45.5 < φ < 49.9 degrees and 8.0 < λ < 18.5 degrees and include approximately 12000 point data values in a 3' x 3' grid. The steps of gravity reduction are the same as for the Austrian data set. The disadvantage for the computation of the terrain corrections was that for the area outside Austria only a 1.5' x 2.5' height model existed. The resolution of this model is not good enough to eliminate the high frequence part of the reduced free-air anomalies $\Delta g_{FA\text{-}red}$, which is responsible for high standard deviation of $\Delta g_{RTM\text{-}red}$ (Table 2).

Gravity anomaly (mgal)	Min	Max	Mean	Std.dev.
Δg_{FA}	-161.4	192.9	1.7	36.4
$\Delta g_{FA\text{-}red}$	-220.7	139.8	-17.1	39.4
$\Delta g_{RTM\text{-}red}$	-276.1	89.0	-14.8	41.0

Table 2: Statistic of gravity anomalies of data set BGI

Due to this fact and due to the lack of a high resolution height model, the BGI data set has not been used in the following solution. It is clear that thereby long wavelength errors are introduced and edge effects will occur in the final result.

5. Solution by Least Squares Collocation

The programsystem GEOCOL was used to compute the gravitational geoid of Austria by least squares collocation method. The data set of 2200 RTM-reduced gravity anomalies $\Delta g_{RTM\text{-}red}$ served as input to GEOCOL. As a result a regular grid (3' x 5') of reduced height anomalies ζ_{LSC} was obtained.

Height anomaly (m)	Min	Max	Mean	Std.dev.
N_{OSU}	43.86	51.69	47.64	1.57
ζ_{RTM}	-0.72	2.73	0.39	0.71
ζ_{LSC}	-0.63	4.43	0.80	0.86

Table 3: Statistic of restoring process

In order to get the final height anomaly the effect of the global potential model N_{OSU} and the effect of the RTM-reduction ζ_{RTM} were added for all grid points.Table 3 shows the statistic of 2401 grid points covering the area of Austria. Finally the height anomalies ζ were transformed

(m)	Min	Max	Mean	Std.dev.
ζ	43.30	55.93	48.82	2.64
$N - \zeta$	-0.56	0.00	-0.10	0.11
N	43.29	55.45	48.72	2.55

Table 4: Height anomaly vs. geoid height

to geoid heights N by equation 9 with the help of Bouguer anomalies which were predicted for all

grid points. The maximum difference between geoid height and height anomaly is 0.56 m, see Table 4. Due to long wavelength effects (no outer zone, global potential model) this geoid is shifted and distorted. In order to get an estimation for the precision of the predicted geoid, GPS points with orthometric height information are necessary. The Federal Bureau of Surveying provided 46 points with height information. These points are used as reference points.
Figure 3 shows the difference between N_{PRE} (geoid heights by LSC-solution) and N_{GPS} (geoid heights by GPS) both referred to GRS80. In the eastern part of Austria we recognize a nearly linear trend. The western part shows an additional distortion which may be caused by the lack of gravity data outside Austria. This long-wavelength effect was modelled by using 5 GPS

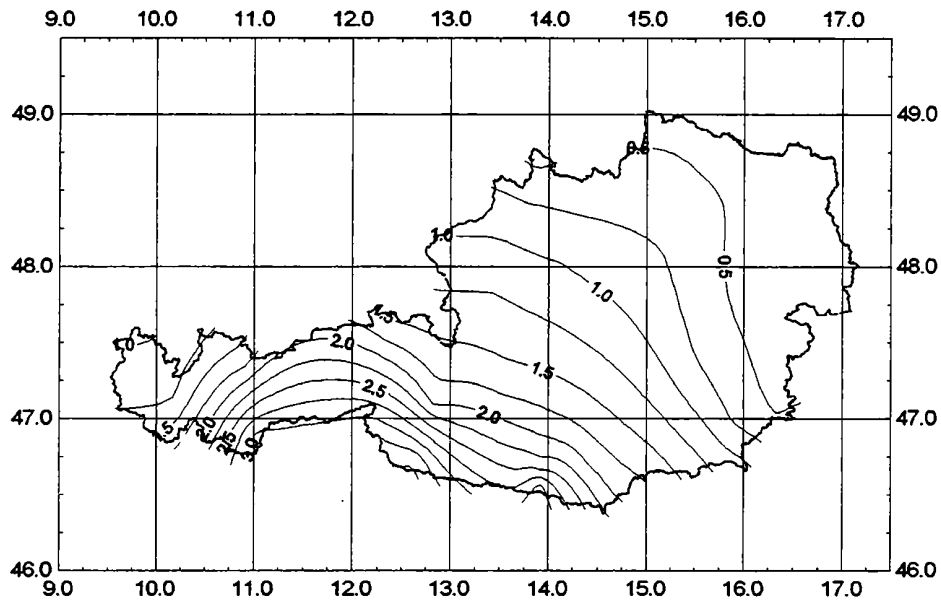

Figure 3: Difference N_{PRE} - N_{GPS} (contour interval 0.25 m)

reference points in the eastern part and all the provided 9 GPS reference points in the western part of Austria. As a result we get the final new geoid solution of Austria merely based on gravimetric data. Figure 4 shows the geoid referred to GRS80 with a contour interval of 20 cm.

6. Accuracy

In order to get an estimation for the accuracy, the OSU91A model, Sünkel's geoid solution of 1987 and the new geoid are compared to all GPS points which were not used for the modelling of the long-wavelength effect. This means the comparison is restricted to 23 well distributed

(m)	Min	Max	Mean	Std.dev.
N_{OSU} - N_{GPS}	-0.87	0.98	0.35	0.38
N_{1987} - N_{GPS}	1.45	2.18	1.84	0.23
N_{PRE} - N_{GPS}	1.30	1.94	0.90	0.49
N_{1996} - N_{GPS}	-0.11	0.19	0.03	0.07

Table 5: Comparison of different geoid heights (23 points)

points east of 13° longitude. Table 5 compares geoid heights derived by the global potential model OSU91A (N_{OSU}), geoid heights of Sünkel's solution in 1987(N_{1987}), geoid heights of the new solution before long-wavelength correction (N_{PRE}) and geoid heights of the long-wavelength corrected solution(N_{1996}) with the geoid height derived from GPS points (N_{GPS}).

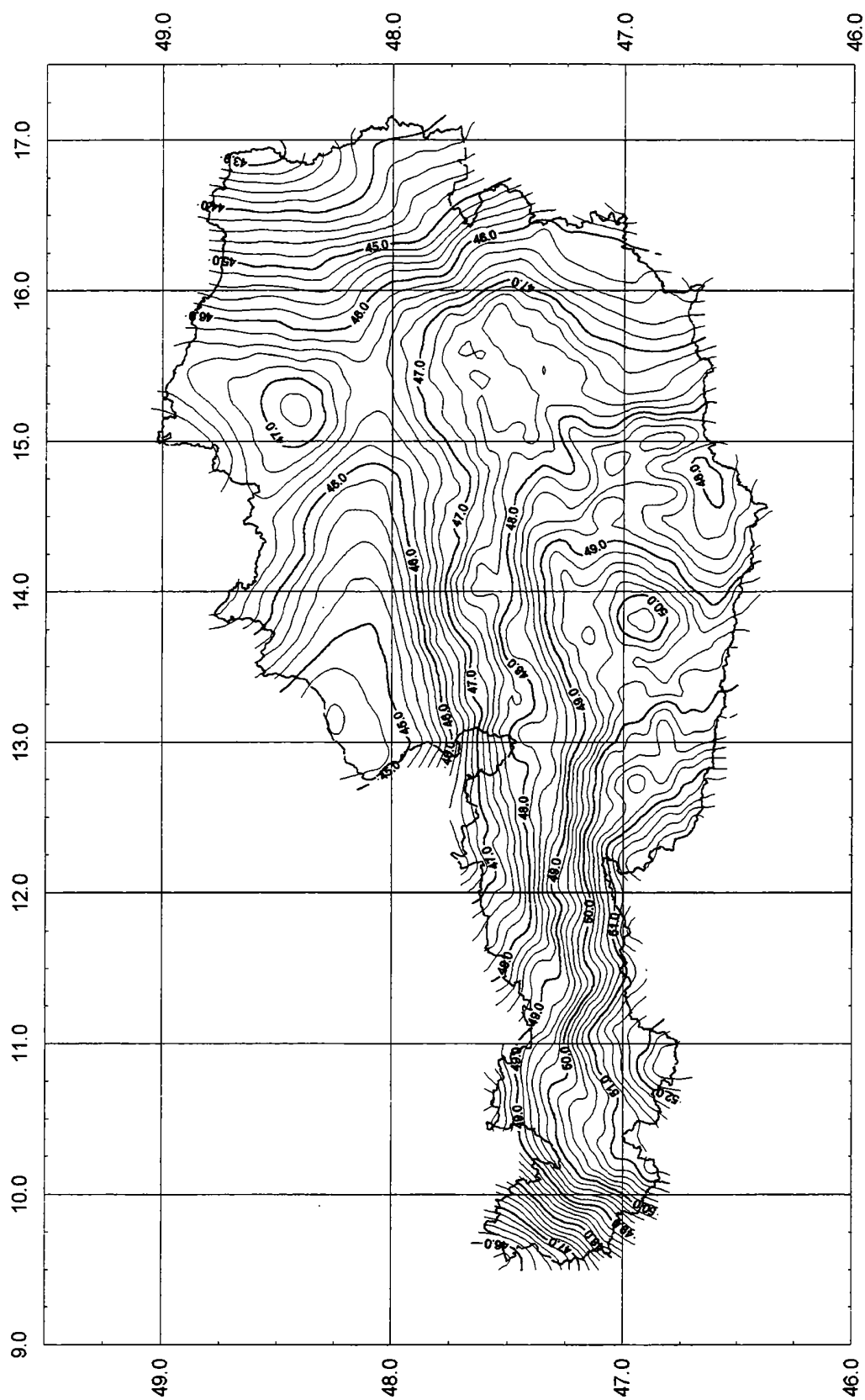

Figure 4: Gravimetric Geoid (contour interval 20 cm)

The agreement of the OSU91A model for the eastern part of Austria is good. The minimum and maximum values are below one meter, while the mean value is 0.35 m. Additionally Figure 5 shows the difference as a contour map which is based on all 46 GPS reference points. One should keep in mind that the map only shows a regional behaviour. Figure 5 confirms the good correspondence of the global model too. Nearly 60% of the region show an accuracy better than 0.5 m!

The geoid solution by Sünkel in 1987 has a poor absolute precision. All differences are positive and the mean value is approximately 1.8 m. One possible reason for this big "shift" is the

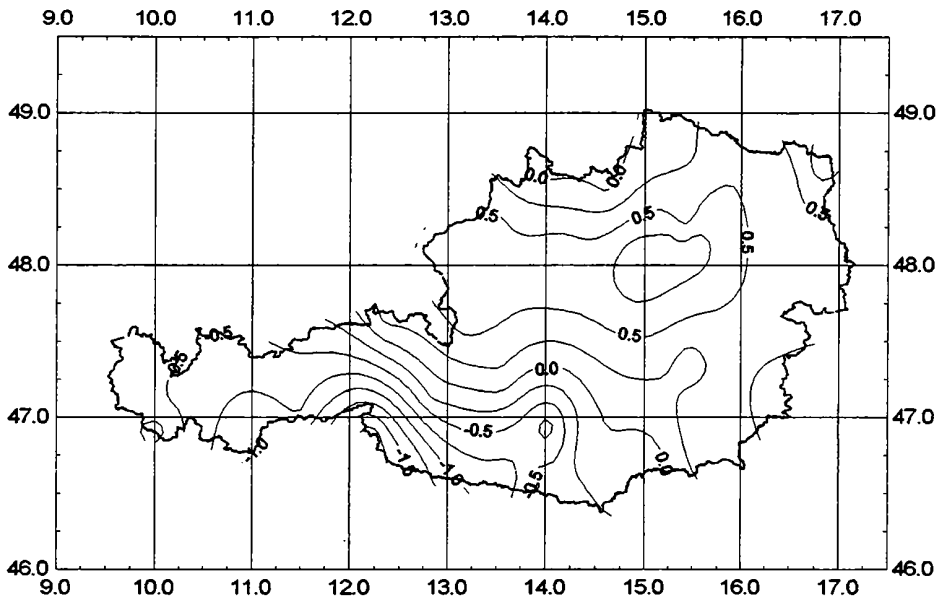

Figure 5: Difference N_{OSU} - N_{GPS} (contour interval 0.25 m)

unprecise transformation of this geoid solution to the global system by Doppler observations (Sünkel, 1987). Figure 6 shows the nature of the difference of N_{1987} minus N_{GPS}. Obviously the difference corresponds to a nonlinear trend which makes it impossible to handle it with a simple 3D-transform.

The difference of N_{PRE} minus N_{GPS} is shown in Figure 3. As mentioned earlier it shows long-wavelength effects. The new geoid solution N_{1996} shows a large improvement in absolute precision. Table 5 shows that the maximum difference is less than 20 cm, while the standard deviation is ± 7 cm. Additionally the accuracy of the GPS reference points in the order of ± 1cm

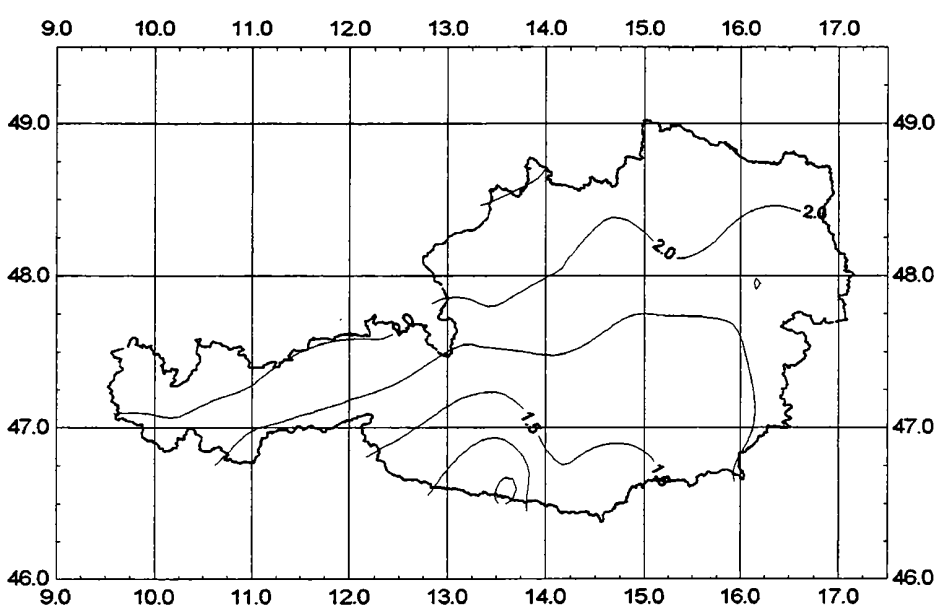

Figure 6: Difference N_{1987} - N_{GPS} (contour interval 0.25 m)

should be mentioned. This result can be seen as a major step on the way to GEOID 2000 which should reach an accuracy of a few centimeter for the geoid itself.

7. Conclusions

This new geoid solution based on 2200 gravity anomalies has a very good accuracy. It points out the way to GEOID 2000. Based on a more detailed topographic model with a resolution of 50 m the short wavelength part of the data can be modelled to a higher degree. Additionally the use of outer zones is essential while the global potential model seems to be accurate enough. Last but not least more input data in addition to a combination of gravity anomalies with deflection of the vertical should contribute to the the improvement of the geoid.

References:

Duquenne, H., Jiang, Z., Lemarié, C.: Geoid determination and levelling by GPS: Some experi ments on a test network. Gravity and Geoid, IAG Symposium No. 113, Graz 1994, pp. 559-568, Springer-Verlag, Berlin 1994.

Forsberg, R.: A Study of Terrain Reductions, Density Anomalies and Geophysical Inversion Methods in Gravity Field Modelling, Dep.of Geod.Sci. Rep. 355, Ohio State University, Columbus 1984.

Forsberg, R.: NKG Nordic Standard Geoid 1989. Proc. 11th General Meeting Nordic Geodetic Commission, Copenhagen May 1990, pp. 472-493, Kort-og Matrikelstyrelsen, Copenhagen 1990.

Heiskanen, W.A. and Moritz, H.: Physical Geodesy, W.H.Freeman and Co., San Francisco 1967.

Lehmann, R.: Zur Bestimmung des Erdschwerefeldes unter Verwendung des Maximum- Entropie-Prinzipes, Deutsche Geodätische Kommission, Reihe C, Heft Nr. 425, München 1994.

Mainville, A., Véronneau, M., Forsberg, R., Sideris, M.G.: A Comparison of geoid and quasigeoid modeling methods in rough topography. Gravity and Geoid, IAG Symposium No. 113, Graz 1994, pp. 491-500, Springer-Verlag, Berlin 1994.

Martinec, Z., Matyska, C., Grafarend, E.W. and Vaníček, P.: On Helmert's 2nd Condensation Method, Manuscripta Geodaetica 18, pp. 417-421, Springer-Verlag, New York 1993.

Moritz, H.: Geodetic Reference System of 1980. Geodesist's Handbook, Bulletin geodésique, Springer-Verlag, New York 1992.

Sünkel, H.: The Gravity Field in Austria, Geodätische Arbeiten Österreichs für die Internationale Erdmessung, Neue Folge, Band IV, Graz 1987.

Sideris, M.G., Forsberg, R.: Review of Geoid Prediction Methods in Mountainous Regions, Proceedings of the IAG Symposia on the Determination of the Geoid - Present and Future, Springer-Verlag, New York 1991.

Tscherning, C.C., Knudsen, P., Forsberg, R.: Description of the GRAVSOFT package. Geophysical Institute, University of Copenhagen, Technical Report, 1991, 2. Ed. 1992, 3. Ed. 1993, 4. Ed. 1994.

Wang, Y.M.: Comments on Proper Use of the Terrain Correction for the Computation of Height Anomalies, Manuscripta Geodaetica 18, pp. 53-57, Springer-Verlag, New York 1993.

Yun, H.S.: Determination of a Gravimetric Geoid Solution of South Korea. Gravity and Geoid, IAG Symposium No. 113, Graz 1994, pp. 550-558, Springer-Verlag, Berlin 1994.

GRAVITY CALCULATIONS ON THE ORTHOMETRIC HEIGHT SYSTEM IN AUSTRIA

Diethard Ruess

Federal Office of Metrology and Surveying (BEV), Vienna

Abstract

In Austria it is decided to introduce the orthometric height system. Therefore gravity data are necessary for each levelling point at the surface and at the plumbline. The gravity calculations are made using the best available digital terrain model of Austria, therefore the influence of gravity errors may be not remarkable in elevations below 1000 m. Levelling data and gravity data are merged into a common data base. The state of gravity calculations for the orthometric height system is shown in a graph.

Introduction

The present Austrian height system in use at the BEV has been established since 1873 (Military Geodetic Institute - MGI) by precise levelling observations (Zeger, 1986). Knowing the dependence of gravity in 1893 pendulum measurements were started in the area of the K.u.K. monarchy. At least after development of spring gravity meters it was possible to take enough gravity measurements to fulfill the theory of the height systems in practice.

Gravity measurements were started 1949 systematically in Austria along the precise levelling lines. Hence it was possible to calculate geopotential differences. Since that time gravity observations are located in the BEV, department of fundamental measurements and joined to the precise levelling.

After the decision in the 80^s to introduce the orthometric height system in Austria the logical consequence was to merge gravity and levelling data into one data base.

Fundamentals

The most important component in the new height system is the geopotential unit:

$$C = \int g \cdot dh \cong \sum g_i \cdot \Delta h_i$$

C	geopotential unit
g	gravity value of dh
dh	differential height
Δh_i	height difference between two benchmarks
g_i	average gravity of Δhi

The closed loop condition is valid: $\oint g \cdot dh = 0$

The Austrian levelling loops of the first order precise levelling network are connected to the main European lines. The European geopotential differences ΔC are adjusted by the Unified European Levelling Network (UELN) - at present state without including the levelling networks of the so-called former eastern states. The datum is given by the gauge of Amsterdam.

Height systems

The potential value C [m^2/s^2] has to be divided by the dimension of a gravity value to get a height, i.e. the distance [m] between the benchmark and the reference level. According to the kind of used gravity values we obtain the height in a certain system.

dynamic heights: $H_{dyn} = \frac{C}{\gamma_\varphi}$ γ_φ normal gravity of latitude φ e.g.: $\varphi = 45°$

$\Rightarrow$ not pure heights, actually potential values in dimension [m].

normal heights:

$$H_N = \frac{C}{\bar{\gamma}_Q}$$ $\bar{\gamma}_Q$ average normal gravity between telluroid and ellipsoid

$\Rightarrow$ height above the quasigeoid

normalorthometric heights = "Gebrauchshöhen":

$$H_{orth} = \frac{C}{\bar{\gamma}_S}$$

$\bar{\gamma}_S$ average gravity between benchmark and geoid according to the level - spheroid (GRS 30)

orthometric heights:

$$H_{orth} = \frac{C}{g_L}$$

g_L average gravity of the plumbline between benchmark and geoid (GRS 80)

$\Rightarrow$ height above the geoid

The levelling & gravity data base ("Nivellement-Schwere-Daten-Bank" = NSDB)

In the NSDB of the BEV there are included all data necessary to obtain the elevations in the orthometric height system. Implicitly the height values of the different height systems can be calculated with these data.

groups of data fields in the NSDB:

description of points:	number, stabilizing, identities, former numbering, notes
position:	geographical coordinates, cadastral community, number of the Austrian map 1:50.000
elevation data:	"Gebrauchshöhe", geopotential unit, average error, year of observation, geoid-undulation
gravity data:	gravity at benchmark, year of observation, mean gravity of plumbline, topographic mass effect, Bouguer anomaly, vertical gradient

Estimation of accuracy due to levelling observations

These errors due to levelling measurements are influenced by the horizontal part of the observations and by the vertical part of the height differences.

The network adjustment of the 1st order precise levelling network (1966 - 1985) shows a mean error of ± 0,57 mm / km observation length (Höggerl 1986).

Detailed error checking were made at the levelling line Villach - Dobratsch in Carinthia. The elevation difference there is 1600 m. The error of the rod scale is 15 µm/m and the influence of refraction gives 6 µm/m (Höggerl et al., 1987). Therefore a vertical error of ± 12 µm/m can be given in the existent levelling network.

Estimation of accuracy due to the gravity field

Modern gravity measurements at the benchmarks are normally better than ± 25 µGal ($\sigma < \pm$ 250·nm/s²). Economic considerations causes that gravity is not observed at each benchmark. The missing gravity values are interpolated using the Bouguer field. The density of measured gravity stations in Austria enables an accuracy of 1-2 mGal (10 - 20 µm/s²) in predictions.

Practically gravity at the levelling points is measured each 1 km at least along the lines - that corresponds each 2nd - 3rd benchmark. At steep sections or in areas with strong gravity anomalies the space of measured points is shortened.

Assuming an interpolation error of 1.5 mGal, the influence on the elevation error due to the surface gravity in ΔC gives:

$f(H) \leq 0{,}4$ mm by $\Delta H = 100$ m
$f(H) \leq 1{,}2$ mm by $\Delta H = 1000$ m
$f(H) \leq 1{,}7$ mm by $\Delta H = 2000$ m
$f(H)$ ... error of elevation

In flat areas with very small height differences this error is also very small. Only one effect should be noticed: in hilly areas, where the line goes often up and down, the error-parts have all the same sign, caused by the Gaussian error budget law.

$$f(\Delta C)_g = \sqrt{\sum \left[\Delta H_i \cdot f(g_i)\right]^2} \qquad (1)$$

$f(\Delta C)_g$ ... error of geopotential units due to the station gravity
$f(g_i)$ ... error of the station gravity

The total error budget of the orthometric height due to the error of the gravity values can be written:

$$f(H_{orth})_g \approx \frac{H}{g_L} \cdot \sqrt{f(g_L)^2 + f(g)^2} \qquad (2)$$

$f(g_L)$ ... error of plumbline-gravity

the gravity at the plumbline is given by:

$$g_L = g + \frac{H}{2} \cdot VG - \left(T_S + T_0\right) \qquad (3)$$

VG ... vertical gradient
T_S, T_0 ... topographic mass effect at surface-point, at foot point (0 m)

list of error-parts:

$$f(g_L)^2 = f(g)^2 + \left(\frac{H}{2}\cdot f(VG)\right)^2 + \left(\frac{VG}{2} f(H)\right)^2 + f(T_O)^2 + f(T_U)^2 \qquad (4)$$

f(g)	$\leq 0{,}1$	measured
	≈ 1	interpolated
VG	= 0,3086 [mGal/m]	vertical-gradient (free air)
f(VG)	$\leq 2\cdot10^{-4}$ [mGal/m]	error of gradient
f(H)	$\approx 2.5\cdot10^{-4}\cdot H$	absolute error of height
$f(T_S)$	$\approx 2\cdot10^{-3}\cdot H$	error by the topographic effect at the surface i.e. ~15% of the total contribution
$f(T_O)$	$\approx 2.5\cdot10^{-4}\cdot H$	error by the topographic effect at the footpoint (geoid)
		units: g [mGal], H [m]

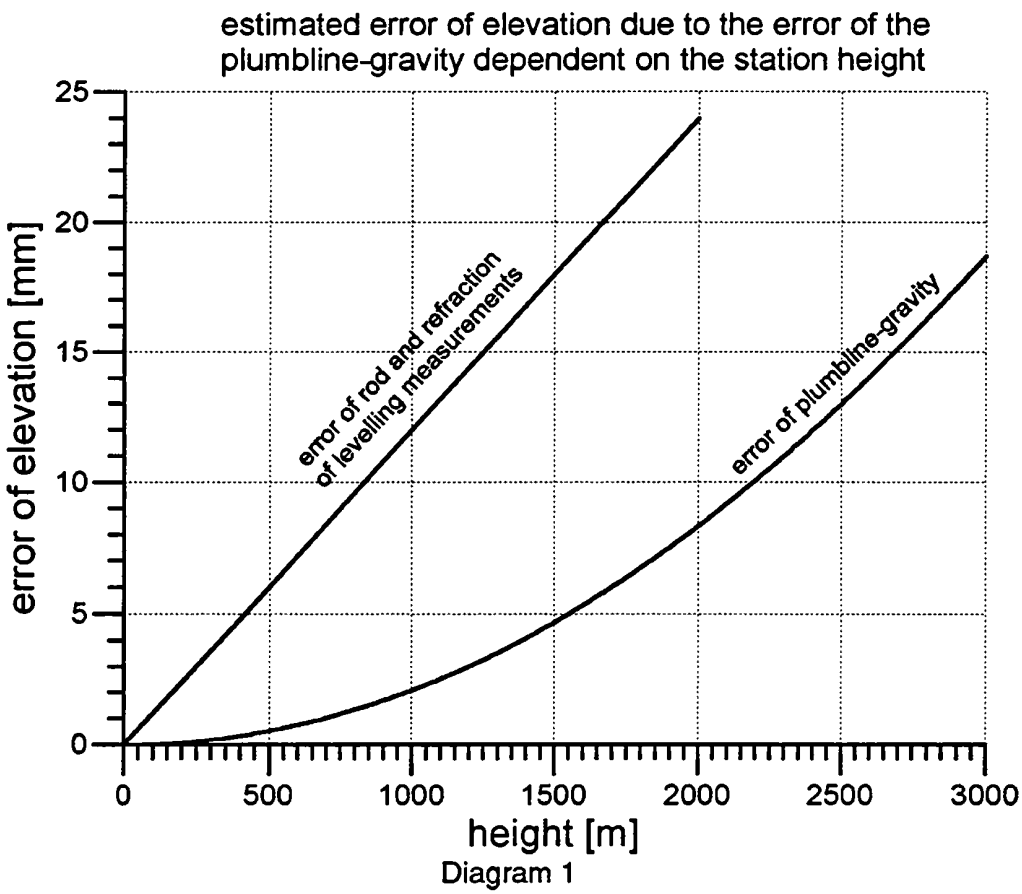

Diagram 1

Diagram 1 shows the error parts of the orthometric height due to the errors of levelling observations and due to the errors of the plumbline-gravity.

Diagram 2 shows the estimated error of the average plumbline gravity versus the point elevation. Assuming that an elevation error of 2 mm is kept, the error of the plumbline gravity must have a limit. The point of intersection of these 2 curves gives that elevation, where the influence of the error of the plumbline-gravity reaches this assumption.

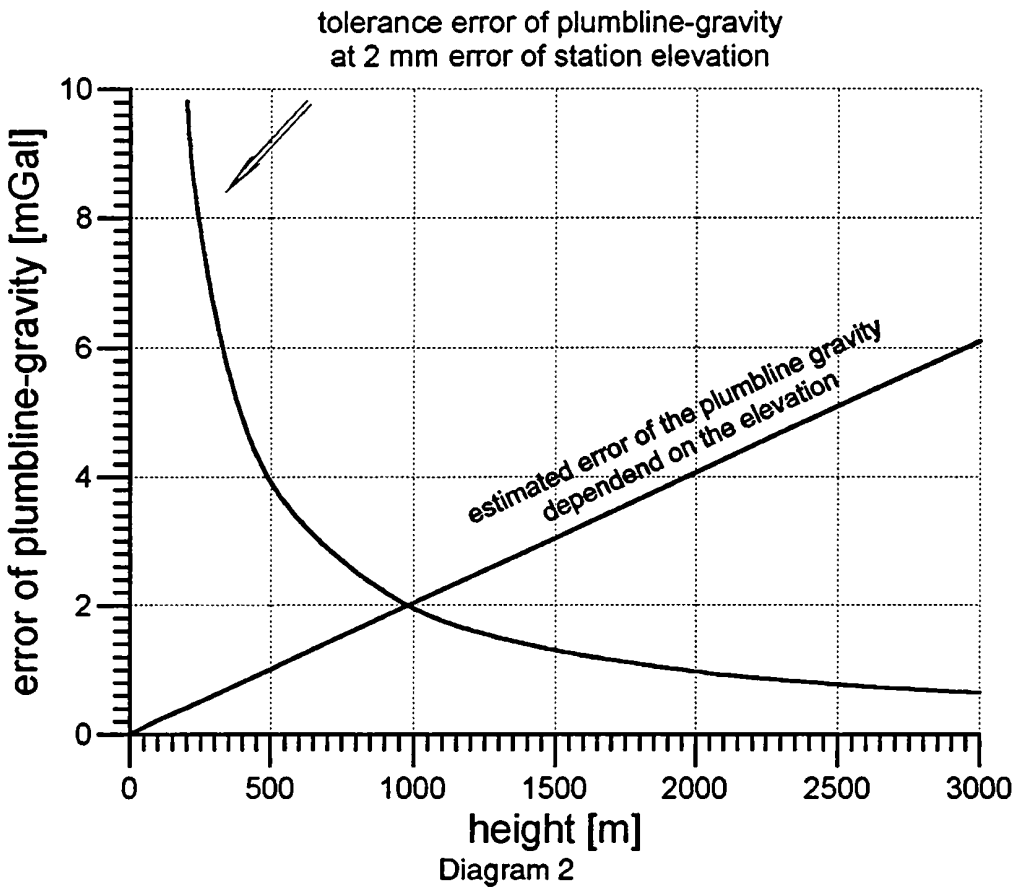

Diagram 2

Coordinates and digital terrain model

It is very important to know the coordinates of the levelling points in accordance to the digital terrain model. The benchmarks are all drafted in the Austrian Map 1:50 000. Practically all coordinates were digitized out of these maps. Generalizations, new editions of the maps and also original drafting cause inexact coordinates. Only a few part of benchmarks have coordinates which were directly obtained by geodetic methods. Therefore inaccuracies of 100 - 300 m were detected.

The digital terrain model is bases on the photogrammetric evaluation of aerial surveying (Graf, 1996). A grid of about 50×50 m is used to calculate the terrain effect surrounding each station up to 1×1 km. The surrounding area up to 167 km is considered using mean heights in different grids (Ruess, 1983). These mean heights are actualized using the 50×50 m DTM.

In rough areas position errors of 100 - 300 m may cause 1 - 2 mGal errors in the terrain correction. On one hand there is a direct influence on the plumbline gravity, which is calculated by using the mass correction, on the other hand the prediction to the non gravity-measured points is not correct.

At present status all coordinates are going to be checked to obtain best conditions for orthometric heights.

Influence of different rock densities

The way of calculating the average gravity along the plumbline between the levelling benchmark and the foot point on the geoid is similar to the procedure of Prey. Instead of using the Bouguer-plate the digital terrain model is used to calculate the mass effects (eq. 3). Actual the mass effect is calculated with the unified density 2.67 g/cm³. In Austria the rock densities are in a range of 2.00 to 2.85 g/cm³ (Granser et al., 1983, Walach 1987). Large regions like the Northern Calcareous Alps and the Bohemian Massive have a density of about 2.70 g/cm³ which is close to the average density of the earth crust (2.67 g/cm³). The Central Alps or the Southern Alps include rock formations with a density between 2.65 and 2.85 g/cm³. The Vienna Basin, the Molasse Zone and the larger basins of the tertiary formation have densities of 2.00 - 2.50 g/cm³.

Determining the plumbline-gravity means that the mass effect may be calculated wrong about 7% - 25%. But similar regions with big density discrepancies are in lower areas by elevations below 400 m, therefore the influence on the height calculation is rather small.

Estimating these effects on the orthometric height, mass reductions were calculated on two stations respective, using the local density for the total terrain or the standard density (2.67 g/cm³).

site	C [gpu]	$\bar{g}_{2.67}$ [m/s²]	$\bar{g}_{2.00}$ [m/s²]	$\Delta\bar{g}$ [mGal]	$H_{2.67}$ [m]	$H_{2.00}$ [m]	ΔH [mm]
Vienna	163.74042	9.8086432	9.8086765	3.32	166.9348	-166.9343	-0.5
Mistelbach	276.77280	9.8085850	9.8086371	5.22	282.1740	282.1725	-1.5
difference					115.2392	115.2382	-1.0
Enns valley	1090.22406	9.8050544	9.8049637	-9.07	1111.9001	-1111.9103	+10.2
Tauern reef	1705.42571	9.8042506	9.8041187	-13.19	1739.4758	1739.4993	+23.5
difference					627.5757	627.5890	+13.3

Table 1: reduction density and orthometric height

Introducing a digital density model into the reductions the different density areas will be considered in a better way. So the differences in orthometric heights will be smaller than in the table shown above.

The present state of the levelling & gravity data base at the BEV is given in table 2 and shown in figures 1 and 2.

Kind of points	number	g-observed since 1949	g-interpolated
precise levelling	46528	23241 (50%)	11134 (24%)
2nd ord. levelling	29479	345 (1.2%)	779 (2.6%)
triangulation	3476	132 (3.8%)	1569 (45%)
others	5266	3117 (59%)	641 (12%)
total	84749	26835 (32%)	14123 (17%)

Table 2: present state of levelling and gravity data base (BEV) in April 1996

Conclusion

The quality of the orthometric height system established in Austria is influenced by the possibility in obtaining gravity values on the surface and at the plumbline in a sufficient accuracy. In layers below 1000 m there is no problem to fulfill the conditions. In higher areas the desired accuracy can be acquired, if the position of the benchmarks is known better than about 25 m regarding to the used digital terrain model. Introducing a detailed rock density model will increase the accuracy of orthometric heights. Errors due to the gravity field than should amount only view millimeters also in greater elevations.

References

Bretterbauer K., 1986. Das Höhenproblem in der Geodäsie. Österr. Zeitschr. f. Verm. u. Photogr., 74, 4, 205-215.

Graf J., 1996. Das digitale Geländemodell für Geoidberechnungen und Schwerereduktionen in Österreich. This volume.

Granser H., Hösch K., Steinhauser P., Zych D., 1983. Über das Dichtemodell in Österreich. Das Geoid in Österreich, Geodätische Arbeiten Österreichs für die intern. Erdmessung, Neue Folge, Band III, 159 - 182, ÖKIE Graz.

Höggerl N., 1986. Die Ausgleichung des österreichischen Präzisionsnivellementnetzes. Österr. Zeitschr. f. Verm. u. Photogr., 74, 4, 216-249.

Höggerl N., Kahmen N., Schwarz J., Stangl G., Sünkel H., Zeger J., 1987. Die WM101 GPS-Kampagne 1987 in Österreich. Österr. Zeitschr. f. Verm. u. Photogr., 75, 4.

Höggerl N., 1989. Rezente Höhenänderungen in Österreich abgeleitet aus Präzisionsnivellement - Messungen. Tagungsber. 5. Int. Alpengrav. Kolloquium Graz 1989. Österr. Beiträge zu Meteorologie und Geophysik, Heft 2, Wien.

Ruess D., 1983. Über das digitale Geländemodell in Österreich. Das Geoid in Österreich, Geodätische Arbeiten Österreichs für die intern. Erdmessung, Neue Folge, Band III, 153 - 158, ÖKIE Graz 1983.

Ruess D., 1993. Schwere und Höhe im alpinen Bereich. Fachvorträge d. 7. Geodätischen Woche in Obergurgl 1993; Univ. Innsbruck, Inst. f. Geodäsie, Institutsmitteilungen Heft 15, Innsbruck.

Torge W., 1989. Gravimetry. De Gruyter Berlin New. York.

Walach G., 1987. A Digital Model of Surface Rock Densities of Austria and the Alpine Realm. The Gravity Field in Austria. Geodätische Arbeiten Österreichs f. d. Int. Erdmessung, Neue Folge, Band IV, 3 - 9, ÖKIE Graz.

Zeger J., 1986. Historische Entwicklung des Präzisionsnivellements in Österreich. Österr. Zeitschr. f. Verm. u. Photogr., 74, 4, 250-263.

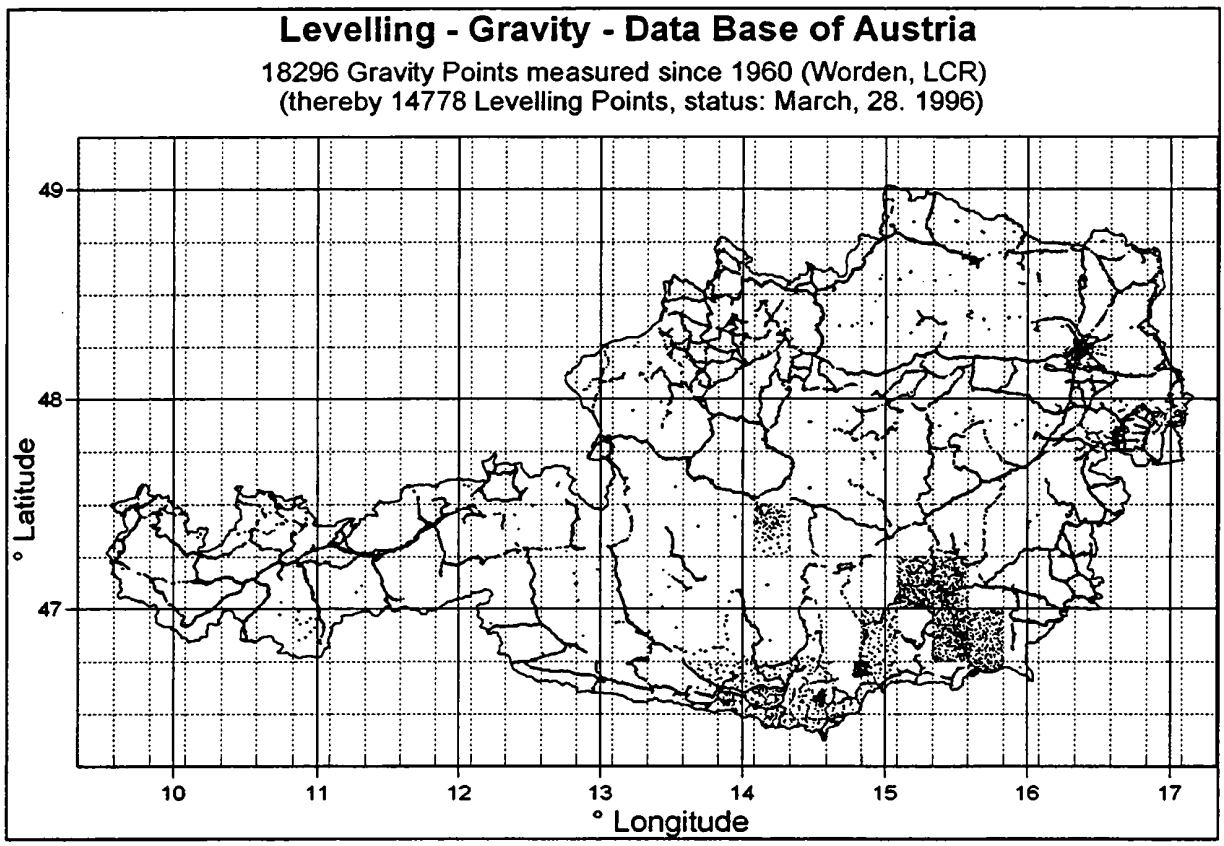

Figure 1

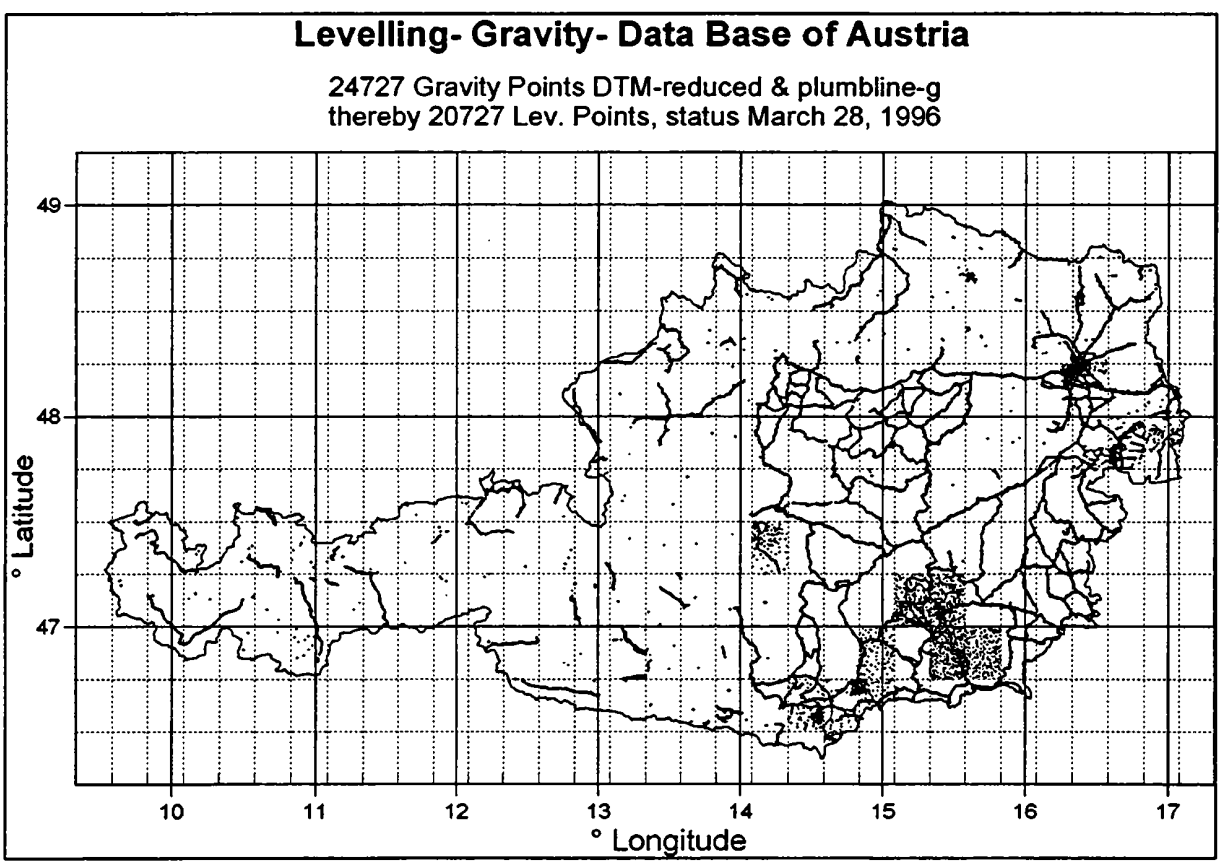

Figure 2

DAS DIGITALE GELÄNDEMODELL FÜR GEOIDBERECHNUNGEN UND SCHWEREREDUKTIONEN IN ÖSTERREICH

Josef Graf

Federal Office of Metrology and Surveying (BEV), Vienna

Abstract

The goal of this work was to provide a digital elevation model in a homogeneous grid and coordinate-system compiled from varied data sources. The data should be used for reduction of gravity in the Federal Office of Metrology and Surveying (BEV) and for reduction of measured values (g-values, deflection of the vertical) in general in the project GEOID-2000 (Erker, 1995). The area was defined in this project by 45°-50° in latitude and 8°-19° in longitude and with a grid distance of 1°/2560 in latitude and 1°/1536 in longitude.

Main objectives were the determination of parameters required for transforming all coordinates into the Austrian system, calculation of point-heights in areas where only mean elevations were available and interpolation of the defined grid. In addition it was necessary to fill the gaps, to check for consistency and to provide the format which was required by other programs. The data was supplied by Austria (BEV), by neighbouring countries and by a model covering the whole European area (Row, 1995).

Due to the lack of information - and almost no influence - some simplification was made. The difference between height-systems (orthometric, normal,..) was also neglected as well as the fact that data-sets were not referring the same point (topography, surface of vegetation ; sea surface or bottom in case of lakes). In most cases it was possible to obtain parameters for a transformation of coordinates into the Austrian system.

The accuracy of the heights was estimated by calculating the heights of known positions or by comparing data-sets in overlapping areas. All data manipulation was done on a PC with the operating systems DOS/WINDOWS95 where the source code of all used programs is available (FORTRAN77). The data is stored in 900 direct-access files using about 450 MB of the mass-storage system, each of them defining an area of 15' × 15'.

Zusammenfassung

Das Ziel in dieser Arbeit war es, in einem einheitlichen Raster und Koordinatensystem Punkthöhen bereitzustellen, die im Bundesamt für Eich- und Vermessungswesen (BEV) für Schwereredukti onen und im Projekt GEOID-2000 (Erker, 1995) für Reduktionen von Meßgrößen verwendet werden. Neben der Transformation der Koordinaten auf das österreichische System mußte im gesamten Gebiet auf Punkthöhen in einem einheitlichen Gitter umgerechnet werden. Dieses in geographischen Koordinaten definierte Gebiet war durch das Projekt GEOID-2000 mit einer Ausdehnung von 45°-50° Nord und 8°-19° Ost vorgegeben und lückenlos mit Daten aufzufüllen. Die Daten kommen dabei aus Österreich selbst, aus den Nachbarstaaten, sowie aus einem Europa-Modell.

1.) Vorgaben

• Raster- und Gebietsdefinition

Die aus dem Inland und Ausland bereitgestellten Höhen sollen für das Projekt GEOID-2000 ein Gebiet abdecken, welches mindestens 100 Kilometer über die Grenzen Österreichs hinausreicht. Aus programmtechnischen Gründen und wegen einer schematisierten, einfacheren Verarbeitung ist dieses Gebiet definiert durch

45° bis 50° in der Breite und
8° bis 19° in der Länge.

Die im ganzen Gebiet konstanten Rasterweiten waren vorgegeben mit

1°/2560 ≈ 45 Meter in der Breite und
1°/1536 ≈ 50 Meter in der Länge.

- **Höhenart**

Es sollten einheitlich im gesamten Bereich Punkthöhen gegeben sein und keine mittleren Höhen vorkommen. In jedem Gitterpunkt soll der dort angegebene Wert die Höhe der Geländeoberfläche an eben dieser Stelle wiedergeben.

- **Bezugssystem**

Bezugssystem für alle Daten sollte das österreichische Gebrauchsnetz mit Bessel-Ellipsoid und dem Datum des Militärgeographischen Institutes (MGI) sein. Dies hatte eine Umrechnung aller ausländischen Daten zur Folge.

- **Verwendung**

Die Ergebnisse werden einerseits im Bundesamt für Eich- und Vermessungswesen (BEV) für Schwereredukti̇onen verwendet, andererseits werden sie für die Reduktion von Meßwerten generell im Projekt GEOID-2000 eingesetzt (restore-remove Technik).

2.) Aufgaben

- **Datensammlung**

Alle Daten mußten auf ein Format gebracht werden, so daß sie in einer PC-Umgebung mit FORTRAN Programmen bearbeitet werden konnten. Dies machte eine Speicherung auf ein einheitliches Medium notwendig, wobei einige Umformatierungen auf UNIX-Workstations erfolgten. Es mußten teilweise Programme erstellt werden, die zuerst eine Komprimierung der Daten durchführten, damit sie dann von den eigentlichen Programmen zur Interpolation oder Kontinuisierung verwendet werden konnten.

- **Bestimmung der Transformationsparameter**

Die Bestimmung der Transformationsparameter für die Umrechnung der ausländischen Datensätze in das österreichische Koordinatensystem erfolgte nicht einheitlich. Dabei wurden teilweise 7-Parameter Helmert-Transformationen eingesetzt, teilweise aber auch nur konstante Zuschläge zu Breite und Länge ($\Delta\varphi$, $\Delta\lambda$) verwendet. Diese Parameter konnten zumeist dadurch bestimmt werden, daß zum ausländischen Datensatz die Werte für einen Übergang auf das System WGS84 erhalten wurden, und bei bekanntem Übergang von MGI zu WGS84, daraus Transformationswerte gerechnet werden konnten. Siehe auch Lageverschiebungen.

In wenigen Fällen konnten keine Parameter ermittelt werden, was aber keine gravierenden Folgen hatte, weil dort die Ausgangsdaten nur in einem sehr groben Raster gegeben waren und Verschiebungen in der Lage nur geringe Auswirkungen auf die Höhe der interpolierten Punkte haben.

- **Datenlücken ermitteln und füllen**

Vor allem an Übergängen bei Staatsgrenzen, aber auch sonst im gesamten Bereich, war der Datensatz auf Vollständigkeit zu prüfen. Im Falle von Lücken wurde mit dem jeweiligen besten Datensatz ergänzt und aufgefüllt, wobei eine Entscheidung für einen Datensatz nur auf Grund der Gitterweiten erfolgte. Es wurde kein Ausgleich im Übergangsbereich gerechnet.

Durch ein grobes 5' × 5' Datenmodell des NOAA (Row, 1995) über ganz Europa, wurden alle restlichen Lücken geschlossen, die trotz der Daten aus dem Ausland vorhanden waren.

- **Umrechnung von mittleren Höhen auf Punkthöhen**

Weil im Ergebnis Punkthöhen gefordert waren, in vielen Fällen aber nur mittlere Höhen gegeben waren, mußte in diesen Fällen auf Punkthöhen umgerechnet werden. Diese Berechnung, die nicht als reine Interpolation behandelt werden kann, erfolgte unter Verwendung einer Programmbibliothek der Universität Wien.

- **Interpolation von Punkthöhen auf das Raster**

In allen Fällen wo Punkthöhen geliefert wurden, mußte auf das geforderte Raster interpoliert werden. Dies geschah mit Hilfe von Programmodulen aus dem Paket 'GSPP' (Sünkel, 1979).

- **Prüfen des Datensatzes**

Die Ergebnisse waren auf Vollständigkeit und Konsistenz zu überprüfen. Grobe Fehler konnten ermittelt werden und die fehlerbehafteten Daten durch Verwendung der übrigen Datensätze ersetzt werden.

- **Ausgabe im gewünschten Format**

Damit die Nachfolgeprogramme die Daten verwenden können, mußte bei der Ausgabe ein bestimmtes Format eingehalten werden. Dies betrifft vor allem auch die Dateiorganisation. Erst durch Unterteilung in überschaubare Einheiten und Gebiete von 15' × 15' waren Berechnungen und Kontrollen leichter möglich.

3.) Datenherkunft

- **Inland**

Innerhalb von Österreich stammen die Daten zum Großteil aus dem digitalen Geländemodell (DGM) des BEV. Dieses Modell entstand aus photogrammetrischen Auswertungen, die, je nach Topographie, in einem Raster von 30 × 30 bis 160 × 160 Meter durchgeführt wurden. Aus diesen Daten wurde ein über das ganze Bundesgebiet konstantes Raster von 50 × 50 Meter abgeleitet. Erst in diesem Raster erfolgte die Interpolation für die endgültigen Höhenwerte.

Neben dem DGM gibt es schon seit längerer Zeit die bekannten "mittleren Höhen von Österreich" (Ruess, 1986), die aus Kartenwerken erhoben wurden. Diese Höhen liegen in 7 verschiedenen Rastern vor, welche jeweils lückenlos ineinander übergeführt werden können und im größten Raster bis mindestens 167 Kilometer über Österreich hinausgehen.

- **Ausland**

Die Daten aus dem Ausland liegen in den unterschiedlichsten Rastern und Formen vor. Neben photogrammetrisch erhobenen Daten gibt es aus Karten erhobene oder aus einem anderen Raster abgeleitete Daten. Auch die Rasterweiten sind sehr unterschiedlich.

Vervollständigt werden alle diese Daten durch ein 5' x 5' Europa-Modell, das aus den USA stammt und das ganze Gebiet lückenlos überdeckt (Row, 1995).

Herkunft Land	Art der Höhe	Gitterweite Hoch x Rechts	Gitterweite [m] Hoch x Rechts
Österreich	Punkt-	1°/2560 x 1°/1536	44 x 49 ca
	mittlere	11,25" x 18,75"	350 x 390 ca
	mittlere	1,5' x 2,5'	2780 x 3100 ca
Tschechien	mittlere	5,0' x 7,5'	9300 x 9300 ca
Ungarn	mittlere	1,5' x 2,5'	2780 x 3100 ca
Kroatien/Slow.	mittlere	5,0' x 5,0'	9300 x 6500 ca
Italien	mittlere	7,5" x 10,0"	250 x 250 ca
Schweiz	Punkt-		250 x 250
Baden-Württemberg	Punkt-		50 x 50
Europa Modell	mittlere	5.0' x 5.0'	9300 x 6500 ca
Bayern	Punkt-		100 x 100

Tabelle 1 : allgemeine Übersicht über die Datenherkunft

4.) Umrechnungen

- **Höhenbezug**

Die in den Daten angegebenen Höhen haben nicht immer den gleichen Bezugspunkt. Im allgemeinen ist zwar die Oberfläche des Geländes, der Topographie, definiert, doch in einzelnen Ausgangsdaten wird die Vegetationsoberfläche durch die Höhen bestimmt. Im Falle von Gewässern ist teilweise die Oberfläche angegeben, teilweise aber der Gewässergrund. Im Ergebnis gibt es dabei auf Grund von fehlenden Informationen keine Differenzierung.

- **Höhenart**

In den Ausgangsdaten kommen die beiden Höhenarten 'Punkthöhe' und 'mittlere Höhe' vor. Da im Ergebnis nur Punkthöhen gefragt waren, mußten mittlere Höhen in diese umgerechnet werden. Dabei genügen nicht Interpolationen, sondern es werden Algorithmen angewendet, die bei einer Rückrechnung auf mittlere Höhen wieder das gleiche Volumen in einem Element ergeben als dies durch die (mittlere) Ausgangshöhe gegeben war.

- **Höhensysteme**

Die in den einzelnen Datensätzen unterschiedlichen Höhensysteme wie Gebrauchshöhen, Normalhöhen oder orthometrische Höhen, wurden als ident angenommen. Im Ergebnis wurden also die Unterschiede wegen ihrer geringen Auswirkung vernachlässigt.

- **Höhenverschiebungen**

Die einzelnen Höhenverschiebungen auf Grund der unterschiedlichen Systeme oder Bezugshöhen (Pegel) erreichen zwischen Österreich und den Nachbarländern nirgends den

Betrag eines Meters (Höggerl, 1995). Sie sind daher zu klein um sich im Ergebnis auszuwirken. Vor allem auch deshalb, weil in den Ausgangswerten fast überall nur der Meter angegeben war. Diese Verschiebungen wurden daher auch vernachlässigt.

• Lageverschiebungen

Als Bezugssystem für alle Berechnungen wurde das österreichische Koordinatensystem mit dem Bessel-Ellipsoid und mit dem Datum des MGI gewählt.

Die in den einzelnen Datensätzen verwendeten Koordinatensysteme benutzen weder das gleiche Ellipsoid, noch beziehen sie sich auf das gleiche Datum. Für die Übergänge auf das österreichische System konnten teilweise 7-Parameter Helmert-Transformationen gerechnet werden, teilweise konnten nur Zuschläge zu den geographischen Koordinaten angegeben werden und teilweise waren keine Informationen für die Bestimmung von Transformationen vorhanden.

Die Angaben für Transformationen, die von den Nachbarstaaten erhalten wurden, bezogen sich zumeist auf den Übergang des jeweiligen Datensatzes zum System WGS84. Damit wurde dann folgender Vorgang gewählt :

- Umrechnung der geographischen Koordinaten des MGI auf 3-D
- Transformation von MGI nach WGS84 , 7-Parameter
- Transformation von WGS84 in das ausländische System , 7-Parameter
- Umrechnung von 3-D auf X,Y oder φ, λ im ausländischen System
- Berechnung der Höhe für diese Koordinaten im Datensatz des Auslandes.

Teilweise war für den Übergang von WGS84 in das jeweilige System nur eine konstante Verschiebung in $\Delta\varphi$, $\Delta\lambda$ bekannt.

Da die Abweichungen in den Verschiebungen innerhalb einer Berechnungseinheit - Gebiet von 15' $\times$ 15' - nur sehr gering sind, wurde je Einheit nur eine konstante, mittlere Verschiebung angenommen.

5.) Genauigkeit

Es gibt nur für einen Datensatz Angaben über die Genauigkeit. Eine Abschätzung konnte aber durch Vergleiche von Daten gewonnen werden. Dies war dort möglich, wo mehrfache Überdeckungen gegeben waren und die Rasterweiten ähnlich groß waren.

• Österreich

Die Genauigkeit der Höhen aus dem DGM wurde durch Vergleiche der Modell-Höhe mit der bekannten Höhe in einigen tausend Festpunkten abgeschätzt. Daraus ergaben sich im Schnitt Abweichungen von 2 bis 5 Meter, in extremer Topographie können aber Werte über 10, 20 Meter vorkommen.

Die Genauigkeit der mittleren Höhen von Österreich ist bekannt und entspricht der Kartengenauigkeit.

• Ausland

Eine Abschätzung ist nur für einzelne Bereiche möglich, wo ähnliche Rasterweiten gegeben sind und mehrfache Überdeckungen vorliegen.

In nachfolgender Tabelle sind einzelne Ergebnisse gesammelt. Es wurden dabei Datensätze aus dem gleichen Gebiet verglichen, nachdem sie auf das einheitliche Gitter umgerechnet wurden. Im Falle von Ergebnissen, die durch '*' gekennzeichnet sind, wurde kein einheitliches Koordinatensystem verwendet.

Die Bedeutung:

Land1 , 2 :	Ursprungsland von Datensatz-1 bzw. Datensatz-2 Ba-Wü = Baden-Württemberg
OEK :	Name = Berechnungseinheit in Gebieten von je 15' × 15'
Mittelwert :	Summe der Abweichungen durch Anzahl verglichener Punkte
Abweichung :	Summe der Absolutwerte der Abweichungen durch Anzahl verglichener Punkte
Min :	minimaler Wert , Datensatz-1 - Datensatz-2
Max :	maximaler Wert , Datensatz-1 - Datensatz-2
Verglichene Punkte :	Anzahl der vergleichbaren Gitterpunkte
Einheit :	Meter

Land1 = H1	Land1 = H2	OEK	Mittelwert Σ(H1-H2)/N	Abweichung Σ[H1-H2]/N	Min H1-H2	Max H1-H2	verglichene Punkte (N)
Bayern	Ba-Wü	N12	0.0	0.7	-15.0	18.0	229032
Bayern	Ba-Wü	K12	4.0	5.1	-78.0	58.0	23945
Schweiz	Ba-Wü	L05	0.1	6.7	-80.0	114.0	236152
* Schweiz	* Ba-Wü	L05	-0.1	7.9	-98.0	116	236175
Schweiz	Ba-Wü	L06	-0.4	7.1	-75.0	100.0	243886
* Schweiz	* Ba-Wü	L06	-0.8	9.1	-91.0	120.0	243806
Schweiz	A / DGM	141	-5.2	19.4	-471.0	262.0	162211
* Schweiz	A / DGM	141	-11.1	39.5	-493.0	445.0	163911
Schweiz	A / DGM	170	-4.5	20.8	-239.0	197	119793
* Schweiz	A / DGM	170	-6.0	38.8	-305.0	246.0	119793
A / DGM	Italien	174	2.4	19.9	-130.0	230.0	46241
A / DGM	Italien	177	-0.4	20.6	-390.0	188.0	59911
A / DGM	Italien	198	-3.5	18.0	-162.0	157.0	53216
A / R1	Ba-Wü	082	4.5	6.7	-55.0	53	159462
A / R1	Ba-Wü	083	-0.1	8.0	-121.0	218.0	137256
A /R1	Bayern	084	-1.6	9.8	-182.0	195	218715
A /R1	Bayern	093	-1.8	23.8	-651.0	552.0	198564
A /DGM	Bayern	093	-0.9	13.8	-195.0	178.0	8355

Tabelle 2 : Vergleiche von Datensätzen

6.) EDV-Umgebung

Sämtliche Daten wurden auf PC-Basis unter den Betriebssystemen DOS und WINDOWS95 bearbeitet. Für alle Berechnungen, Transformationen oder Visualisierungen wurden Programme verwendet, die in der Programmiersprache FORTRAN77 im Source-Code vorhanden sind.

Die verwendeten Programme oder Programmteile sind zum Großteil Eigenentwicklungen, die im Laufe des Projektes entstanden. Für die Interpolation von Höhen wurden vorhandene Unterprogramme eingesetzt, die aus dem Programmpaket 'GSPP' entnommen wurden. Für die Kontinuisierung wurden Module verwendet, die aus einer Programmbibliothek der Universität-Wien stammen.

Allein in jenen Fällen wo ein Transportmedium am Entwicklungsrechner nicht lesbar war, mußte auf andere Rechnersysteme (UNIX-Workstation's) ausgewichen werden, wo die Daten dann auf ein PC-Format umgespeichert wurden.

7.) Format und Struktur der Daten

• **Dateistruktur**

Um überschaubare Einheiten zu erhalten, sind alle berechneten Daten im Blattschnitt der österreichischen Karte 1:50 000 (OEK-50) von jeweils einem Gebiet von 15' × 15' unterteilt. Die Namengebung der dadurch entstehenden Dateien ist einerseits durch die Definition des Gebietes vorgegeben, andererseits durch die Bezeichnung der OEK-50. Überall dort, wo es eine OEK-50 gibt, wird ihr Name (Nummer) mitverwendet

Alle Dateinamen bestehen grundsätzlich aus 10 Zeichen (Character), wobei die ersten 3 Zeichen sowie die Extension konstant bleiben. Den eigentlichen Namen bestimmen Zeichen 4 bis 6, Zeichen-4 definiert die Breite auf welche sich die Daten beziehen, die Zeichen 5 und 6 bestimmen die Länge.

Alle Gebiete oder Blätter in denen eine OEK-50 definiert ist, enthalten im Namen die Nummer dieser OEK-50, die in 3 Zeichen angegeben werden muß (001,043,213,etc.). So wird zum Beispiel der Name 'Q31' ersetzt durch '001' oder 'J22' durch '123' .

Schematische Verteilung der Dateien - Vergabe der Dateinamen
Koordinatenangaben beziehen sich auf die Süd-West Ecke einer Einheit = einer OEK-50

φ / λ	25° 00'	25° 15'	..	..	36° 30'	36° 45'
49° 45'	T01	T02	..	..	T47	T48
49° 30'	S01	S02	..	..	S47	S48
..	..	..	..	..	..	..
..	..	..	..	..	..	..
45° 15'	B01	B02	..	..	B47	B48
45° 00'	A01	A02	..	..	A47	A48

Tabelle 3 : Dateinamen

Im Anhang findet man eine komplette Übersicht mit allen Dateinamen.

• <u>Dateiformat</u>

Alle Dateien sind in der Programmiersprache FORTRAN mit nachfolgenden Merkmalen angelegt :

Datei-Format ..... DIRECT-ACCESS
Recordlänge in Byte's..... 770
Records je Datei..... 641
Format einer Variablen..... 2 byte Integer
Dimension..... Meter
Dateigröße..... 0,5 MB ca

8.) Mengenangaben

• Ausgangsdaten
Die Ausgangsdaten der 10 verschiedenen Datensätze lagen in extrem unterschiedlicher Form und Dichte vor. Es waren dazu neben Punkthöhen noch mittlere Höhen vorhanden und die Rasterweite reichte von 5' × 7,5' bis zu 50 × 50 Meter.

Land / Staat	Dateigröße	Werte	Anmerkung
Tschechien	30 KB	899	ASCII
Ungarn	1 MB	13089	ASCII
Slowenien/Kroatien	15 KB	1296	ASCII
Italien	20 MB	3114601	ASCII
Schweiz	6 MB	1148070	ASCII , RIMINI
Baden-Württemberg	380 MB	ca 15000000	ASCII
Bayern	170 MB	ca 4000000	ASCII , WINPUT
Österreich	0,5 MB / OEK	246785	Binär , je OEK
	110 MB	ca 40000000	Binär , insgesamt
Österreich	10 MB		ASCII , mittlere Höhen

Tabelle 4 : Mengenangaben - Übersicht

• Ergebnisse
Die endgültigen Daten liegen nun in einheitlicher Form und Rasterweite als Punkthöhen in 900 Dateien vor. Sie benötigen ungefähr 450 MB Plattenplatz und stellen etwa 220 000 000 Höhenangaben dar.

An Rechenzeit auf einem Pentium/75Mhz Rechner beanspruchte je Berechnungseinheit eine Interpolation etwa 2-3 Minuten, eine Umrechnung der mittleren Höhen etwa 8-9 Minuten. Insgesamt war damit eine Rechenzeit von 120 Stunden oder 5 Tagen gegeben.

Nicht inbegriffen in diesen Angaben sind alle Rechenschritte zur Bestimmung des DGM's von Österreich. Nicht eingeschlossen sind dabei auch alle Ergänzungen der Datenlücken, die Erstellung von Übergabeformen, Testrechnungen und sämtliche Programmentwicklungen oder Kontrollrechnungen.

9.) Abbildungen

• Allgemeines
Um das Ergebnis zumindest optisch kontrollieren zu können waren Programme notwendig, welche die Daten selbst oder Differenzen davon auf einem Bildschirm darstellen. Diese Darstellung erfolgte grundsätzlich nur auf einem VGA-Schirm und in den Dateneinheiten, wobei durch die Software bedingt, nur 16 Farben zur Verfügung standen.

Bestimmten Höhenklassen werden dabei bestimmte Farben zugeordnet und die Lage der Einheiten ist so gewählt, das am Bildschirm rechts nach Norden weist, die Einheit oder das OEK-Blatt liegend dargestellt ist. Es ist damit jeweils ein Gebiet von ca 28 × 18 Kilometer gegeben.

• **Abbildung 1**
Blatt '050' - Großglockner. Die Daten kommen hier ausschließlich aus dem DGM des BEV.

• **Abbildung 2**
Blatt '212' - Vellach ist aus Daten von 3 verschiedenen Sätzen gebildet. Nördlich der Grenze, also im rechten Teil, scheinen Daten aus dem DGM auf. Der Mittelteil wurde durch Daten aus den mittleren Höhen (Raster-1) ergänzt und im Südteil wurde mit Daten aus den mittleren Höhen (Raster-4) aufgefüllt; alle Daten stammen aus Österreich.

• **Abbildung 3 + 4**
Blatt '174' - Timmels Joch. Differenz aus den Daten des DGM von Österreich und aus den Daten von Italien, soweit eine doppelte Überdeckung gegeben war. Abbildung 4 zeigt dabei die Verteilung der Höhenabweichungen.

• **Abbildung 5 + 6**
Blatt 'L05' - Ausland. Differenz aus den Daten von Baden-Württemberg und der Schweiz, soweit eine doppelte Überdeckung gegeben war. Abbildung 6 zeigt dabei die Verteilung der Höhenabweichungen.

• **Abbildung 7**
Übersicht über die Datei-Namen. Die Dateien auf DOS-Ebene haben Namen der Form "OEKxxx.GEO" , wobei an Stelle von 'xxx' 3 stellige Namen eingesetzt werden. Innerhalb von Österreich ersetzen die OEK-Nummern (001 bis 213) diese Namen.

• **Abbildung 8**
Verteilung der Daten der Nachbarländer. Die Gitterweiten sind kein Maß für die Rasterweite in den gelieferten Daten.

• **Abbildung 9**
Ergebnis einer Kontinuisierung -Umrechnung von mittleren Höhen in Punkthöhen- entlang eines Profiles. Vergleichshöhen sind dabei die Ergebnisse des DGM von Österreich. Die Profillänge ist 384 Rasterelemente lang, das entspricht etwa 18 Kilometer.

• **Figures**
To control data or differences of data-sets some programs were written, enabling a representation on a VGA-screen. Limited by software 16 colors are assigned to different range of heights and the data is represented in areas of 15' × 15' or 28 × 18 kilometers. The units are turned 90° clockwise, pointing towards north at the right side of the screen.

• **Fig. 1**
Unit '050' , data only from DGM , Austria.

• **Fig. 2**
Unit '212' , in the north (right site) data from DGM , Austria. In the middle and south data from Austria (mean heights) in 2 different grids were used.

• **Figs 3+4**
Unit '174' , difference between data from DGM (Austria) and Italy in overlapping areas.

• **Figs 5 + 6**
Unit 'L05' , difference between data from Baden-Württemberg (Germany) and Suisse in overlapping areas.

- **Fig. 7**

Summary of (file-) names. Under DOS file-names are formed as "OEKxxx.GEO" , 'xxx' is replaced by the name of an individual area or unit. Within Austria the name is replaced by the official number of the corresponding map (1:50 000).

- **Fig. 8**

Distribution of data provided by neighbouring countries. The grid distance is not proportional to the density of data.

- **Fig. 9**

Calculation of point-heights from mean elevations. Comparison with heights from DGM (Austria) along a west-east profil. The profil length is 384 elements or 18 km.

Literatur

Adam, J., Denker, H., Sarhidai, A., Szabo, Z., 1995: The Hungarian Contribution to the Determination of a Precise European Reference Geoid. In: proceedings of the IAG Symposium 113 on 'Gravity and Geoid' , Springer.

Erker, E., Hofmann-Wellenhof, B., Moritz, H., Sünkel, H., 1995: Austrian Geoid 2000. paper presented at XXI General Assembly of IUGG in Boulder, Colorado, July 2-14.

Höggerl, N., 1995:Contribution of Austria to the UELN95, Veröffentlichungen der Bayerischen Kommission für die internationale Erdmessung der Bayerischen Akademie der Wissenschaften, Astronomisch-Geodätische Arbeiten, Heft Nr. 56.

Hubeny, K., Reithofer A., 1977: Isotherme Koordinatensystem und konforme Abbildungen des Rotationsellipsoides - Koeffiziententafeln und Rechenprogramme, Mitteilungen der geod. Institute der TU-Graz, Folge 27.

Moritz, H., Heiskannen, W.A., 1993: Physical Geodesy , Reprint, Institute of Physical Geodesy Technical University, Graz.

RIMINI : Das digitale Höhenmodell der Schweiz mit einer Maschenweite von 250 Meter, Produktinformation, Bundesamt für Landestopographie, CH-3084Wabern, Schweiz.

Row, L.W., Hastings, D.A., Dunbar, P.K.: TerrainBase , Worldwide Digital Terrain Data , Documentation Manual, CD-Rom Release 1.0, April 1995, NOAA - US Department of Commerce, USA.

Ruess, D., 1988: Stand des Österr. Schweregrundnetzes und des digitalen Geländemodelles. Tagungsbericht über das 4. Int. Alpengravimetrie - Kolloquium, Wien 1986. Berichte über den Tiefbau der Ostalpen, 159-164, Wien.

Sünkel, H.: GSPP-FORTRAN Program Library, OSU , February 1979; Institute of Physical Geodesy, Technical University Graz / Department of Geodetic Science, The Ohia State University

Abb.1 : OEK50 , Blatt-100 , Großglockner

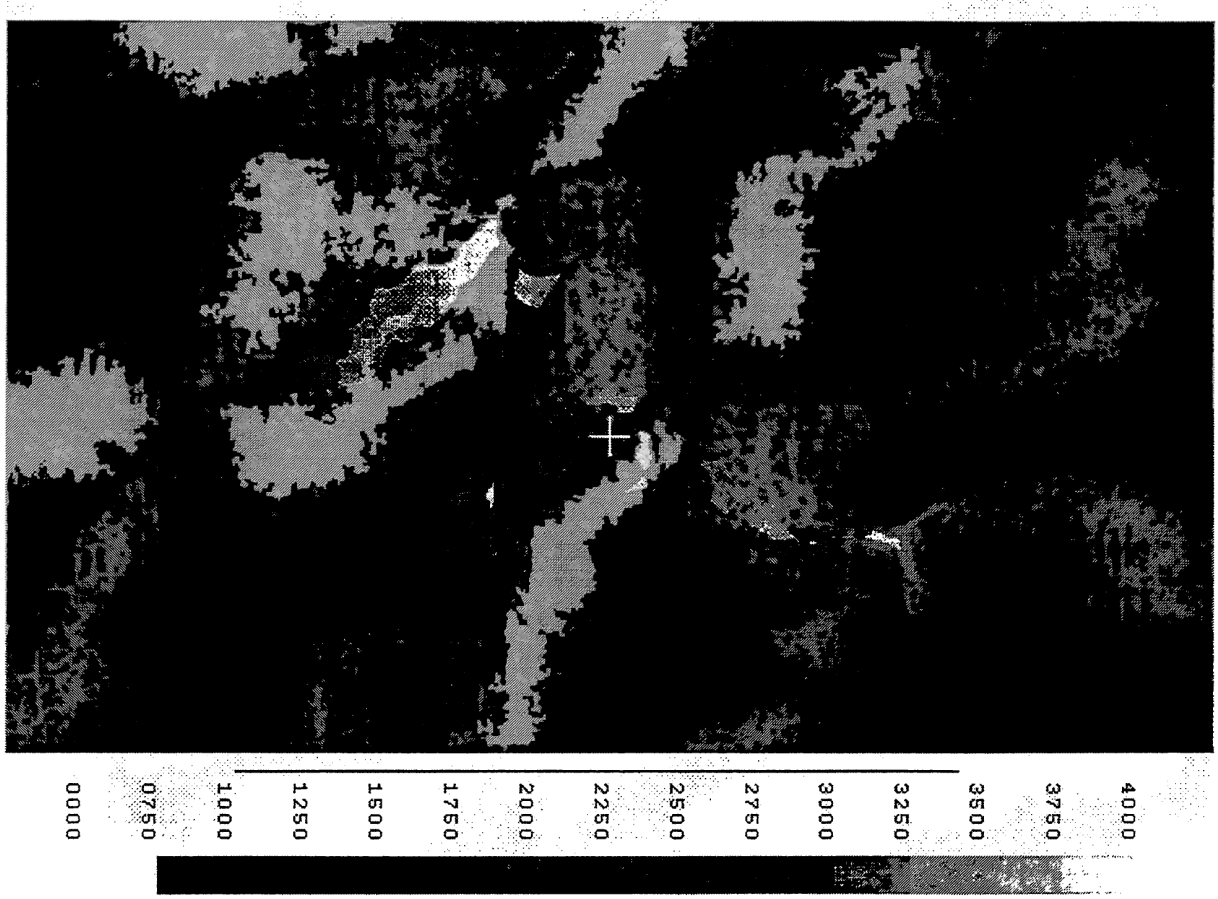

Abb. 2 : OEK50 , Blatt-212 , Vellach

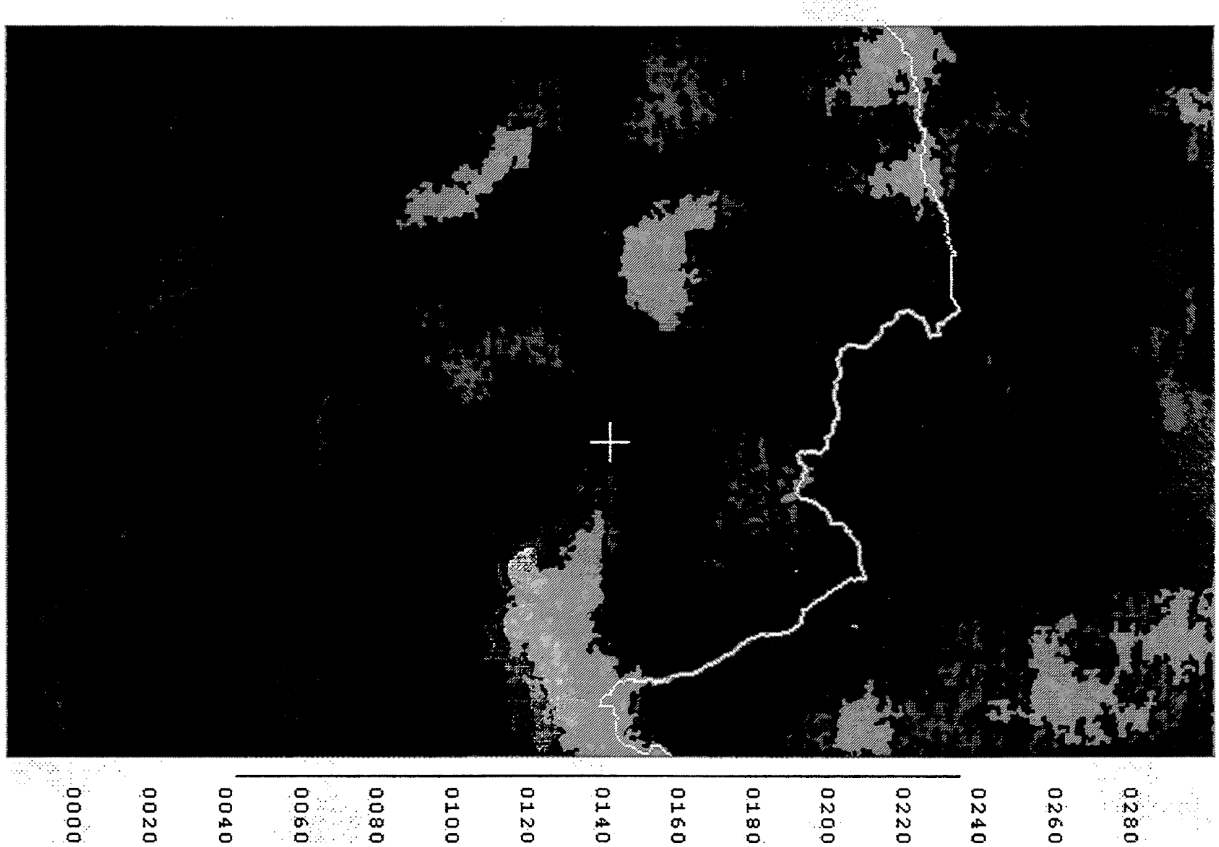

Abb. 3 : OEK50 , Blatt-174 , Timmels Joch

Abb. 4 :

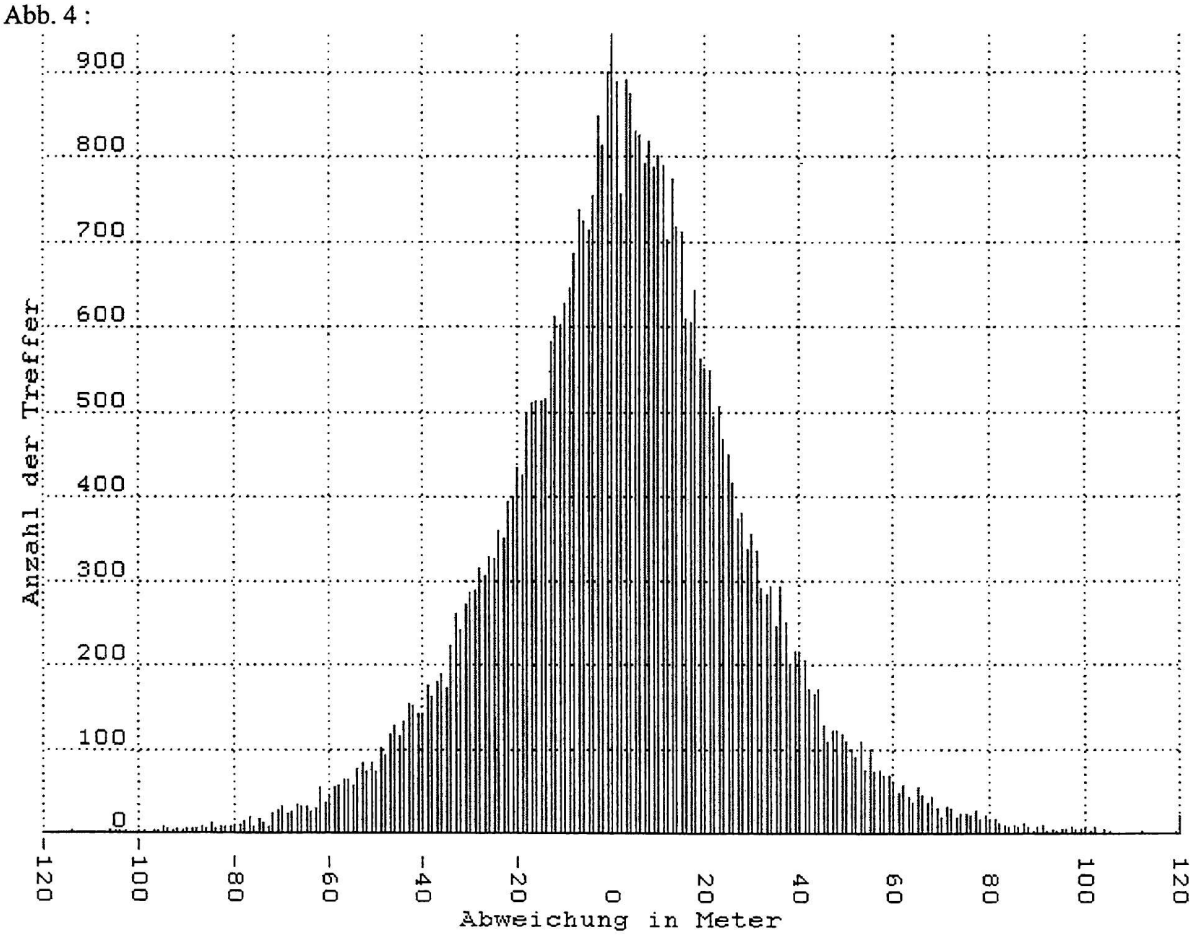

Abb. 5 : OEK50 , Blatt-L05 , Ausland

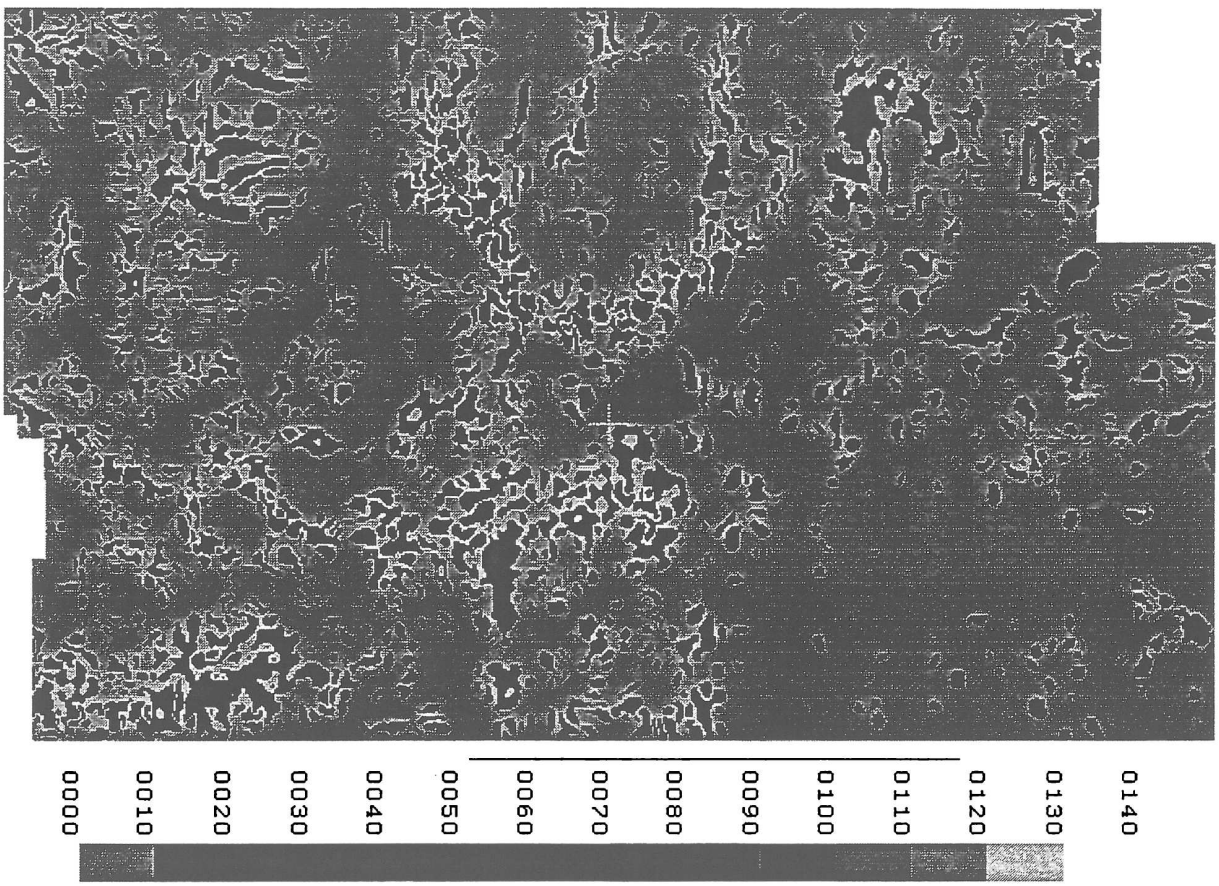

Abb. 6 :

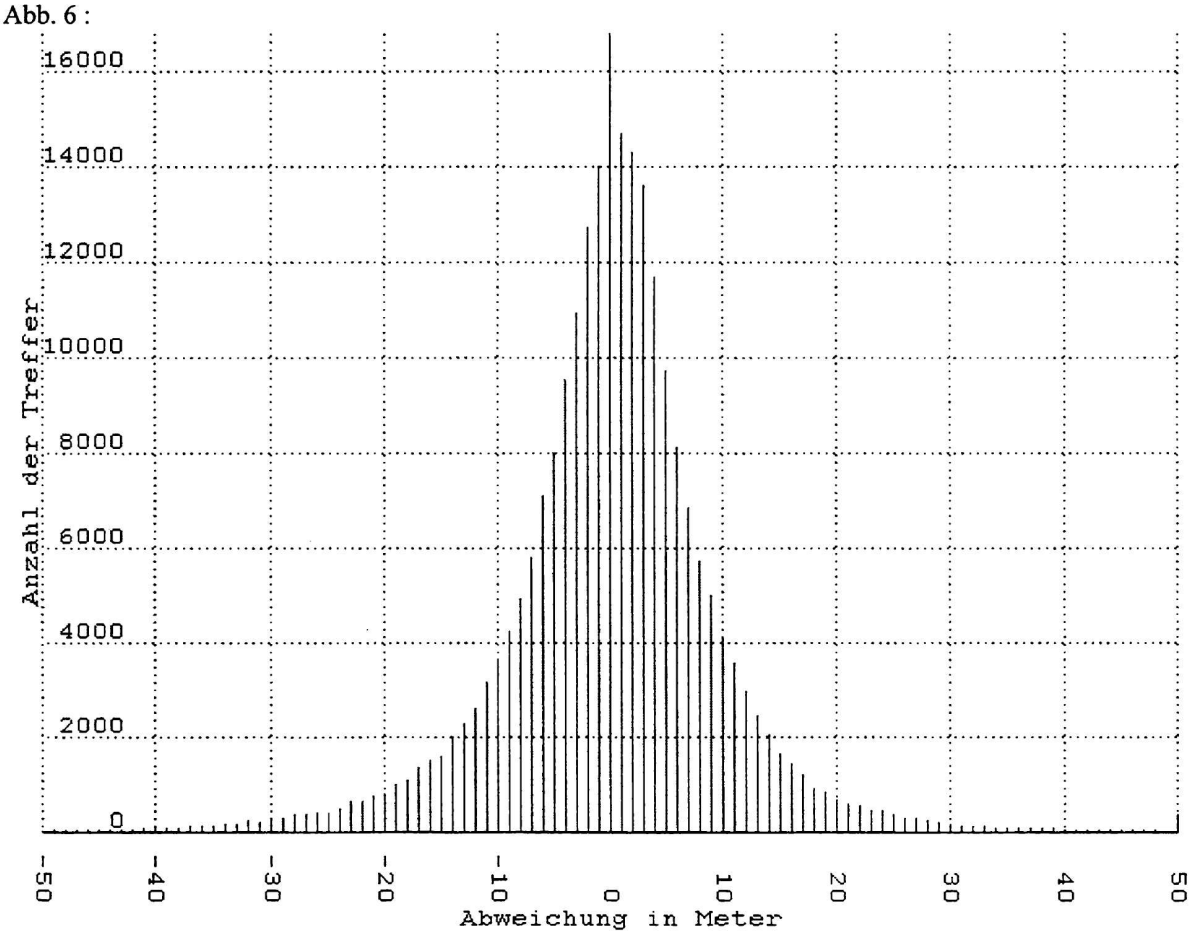

Abb. 7 :

Dateinamen - Übersicht

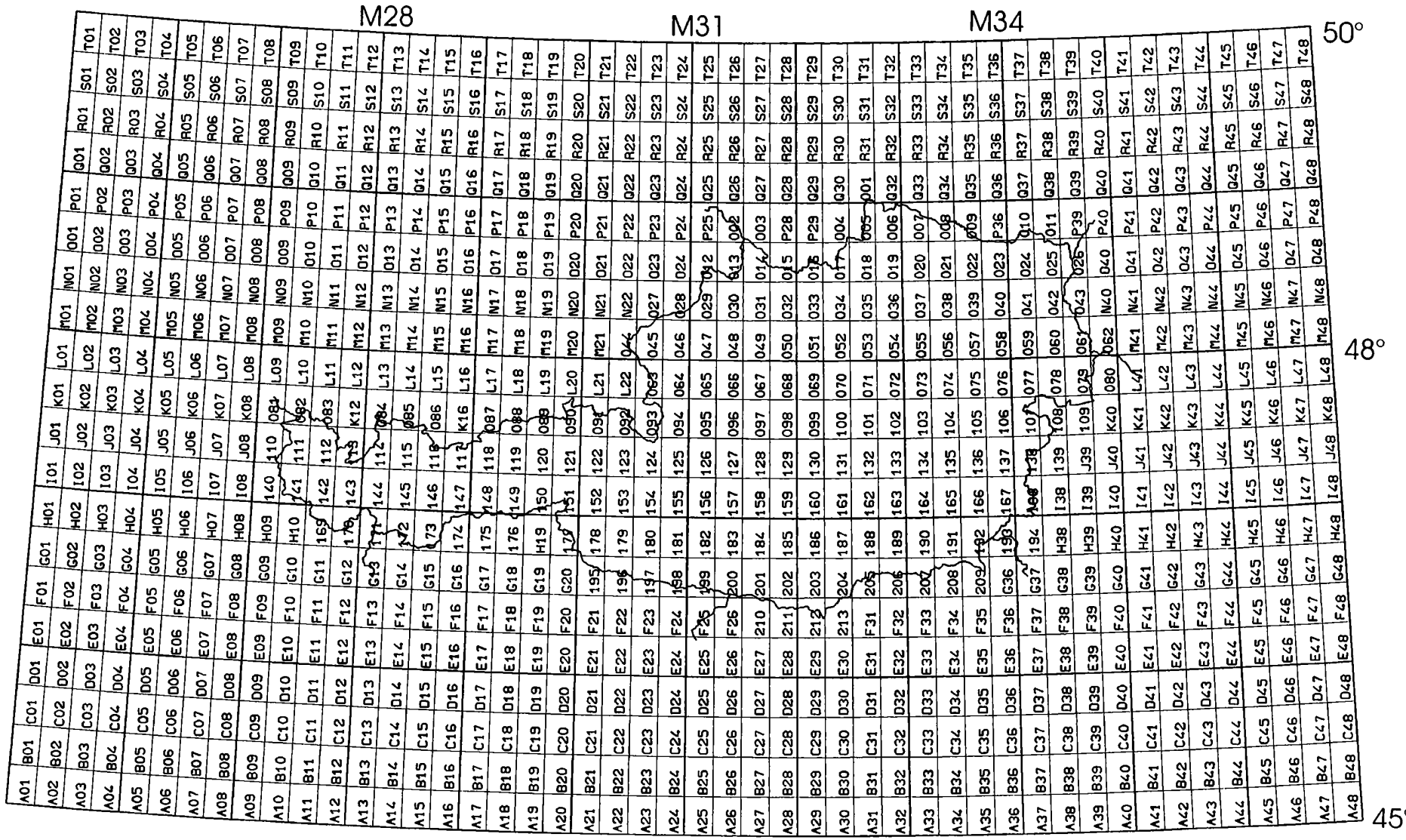

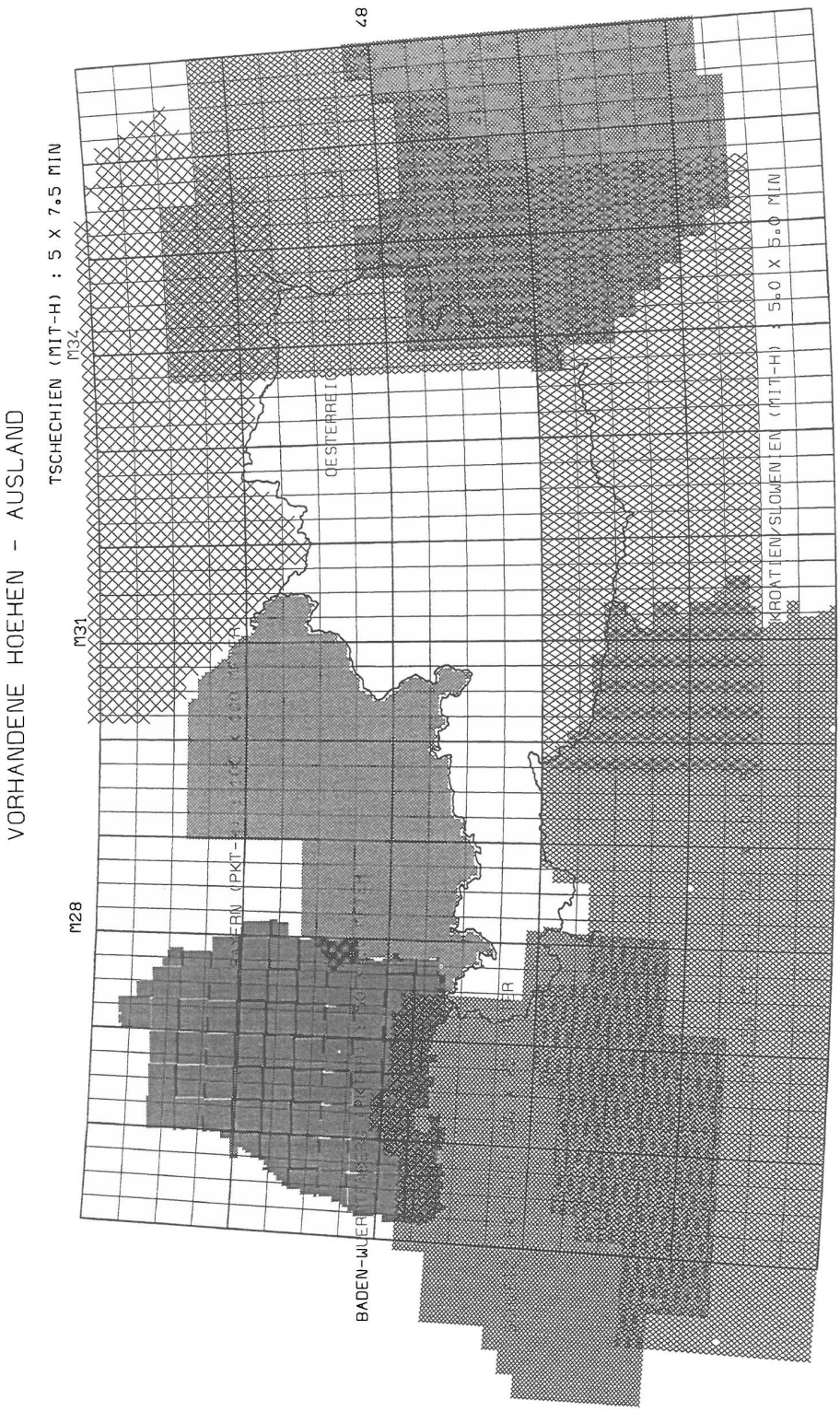
VORHANDENE HOEHEN - AUSLAND
TSCHECHIEN (MIT-H) : 5 X 7.5 MIN
M34
M31
M28
87
48
KROATIEN/SLOWENIEN (MIT-H) : 5.0 X 5.0 MIN
BADEN-WUER

Abb. 9 :

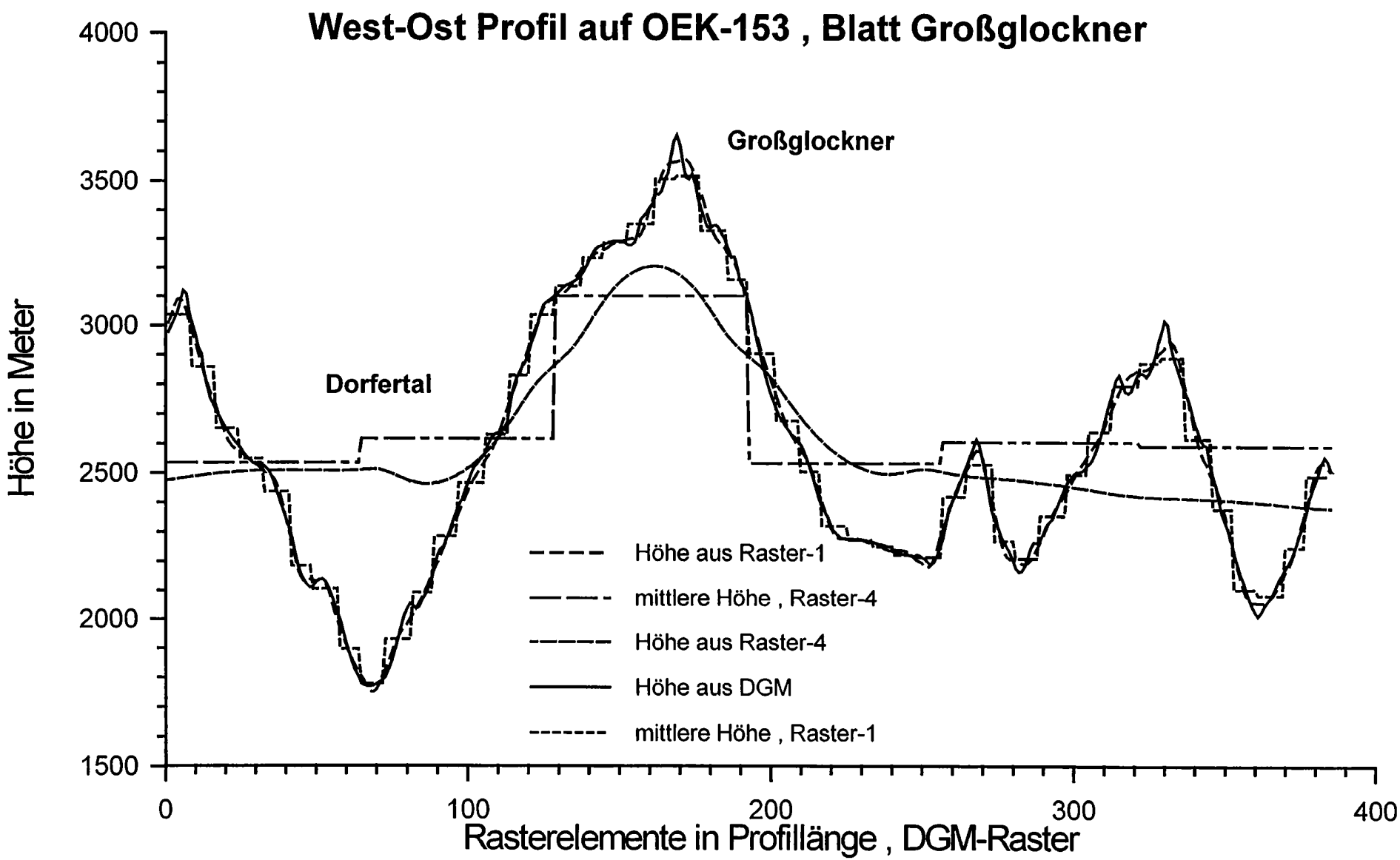
West-Ost Profil auf OEK-153 , Blatt Großglockner
Großglockner
Dorfertal
Höhe in Meter
4000
3500
3000
2500
2000
1500
0
100
200
300
400
Rasterelemente in Profillänge , DGM-Raster
Höhe aus Raster-1
mittlere Höhe , Raster-4
Höhe aus Raster-4
Höhe aus DGM
mittlere Höhe , Raster-1

3D MODELLING OF GEOID AND GRAVITY USING GIS-FUNCTIONS

Sabine Schmidt

Institut für Geologie, Geophysik und Geoinformatik, FU Berlin,
Haus N, Malteserstraße 74-100, D-12249 Berlin, Germany;
Email: sschmidt@zedat.fu-berlin.de

Abstract

Three-dimensional (3-D) interactive modelling permits integrated processing and interpretation of potential data, yielding an improved geologic interpretation. Generally 3-D models are constructed by polyhedra of suitable geometry and constant density and/or induced and remanent susceptibility.

In general it is to be assumed, that the interpretation of gravity or magnetic anomalies is based on determining plausible shapes, positions, and physical parameters for the geologic structures which cause that field. This problem of data inversion in its broadest sense requires conversion of the information which has been obtained by measurements into geologic models. Basically, an indirect modelling process is the calculation of the effect of elementary bodies which approximate the geological situation in the investigated area, followed by matching the model curve with the observed curve by trial and error or graphic-interactive tools.

Rather than the actual mathematical formula of a polyhedron's gravity and magnetic field, the organization of the data structure behind the program, the interactive control of model matching and the integration of constraining additional data are major parts of the software.

1 Introduction

This paper describes the application of computer graphics to geophysical interpretation problems in connection with three-dimensional modelling of potential field data. Interactive modification of model parameters, e.g. geometry, density and susceptibility, access to the numerical modelling process and direct visualization of both, calculated and measured fields of gravity and magnetics. This enables the interpreter to design the model as realistic as possible. 'Trial and error' methods became more and more important because of the fast development of computer hardware. In this context, a 'realistic' model means, that inconsistencies of existing information have been restricted to a minimum. A basic requirement for modelling is the existence of ideas and hypothesis on the investigated area, i.e. the availability of quantitative or qualitative boundary conditions (constraints). Towards this end, geophysical modelling aims in the combination and compilation of (all) existing information. The lack of information, which always exist, has to be filled by inter- or extrapolation, and contradictions of different data sources have to be clearly identified, e.g. by means of statistical methods.

The outlined procedure applied to complex interpretation tools requires a synoptical visualization of the necessary boundary conditions, which have to be selected and activated by the user. Modern GeoInformationSystems (GIS) handle this task. Today these systems are based frequently on relational data banks, and will be replaced by object orientated systems (OOS) in the near future. The advantage of OOS is an increasing effectivity, because of direct access to data and information by the definition of 'geo-objects'.

2 Definition of boundary conditions (constraints)

The problem of forward and backward modelling methods, which deal with quantitative modelling of measured geophysical fields, is the integration of additional information into the modelling process, even if it exists in a digital format. This information - data in a geophysical sense - is different in nature and origin in most cases: The data are inhomogeneous and arbitrarily distributed, in many cases uncertain, especially if they describe human knowledge. The following incomplete list contains some examples of information, which are of specific interest for gravity and magnetic modelling:

Geological data
- Outcrops of formations, geological maps,
- Location and course of fault zones, activeness and
- Density determinations of rock samples and cores.

Log data of boreholes
- Location, angle of layer boundaries,
- Density logs

Results from other geophysics
- Velocity-density relations,
- Velocity models of refraction seismics, raytracing models,
- Reflexion seismics, line drawings,
- Electrical conductivity, deduced from geoelectrics and magnetotellurics,
- Location of hypocenters, fault plane solutions and
- Stress maps.

Hypothesis, theories, models and ideas
- Qualitative ideas of structures, parameter relations, processes.

Most of this information is used in interpretation processes with different impact, but their importance is difficult to estimate: Parts of knowledge cannot be quantified, but their influence on a successful modelling process as an inportant constraint is crucial. Therefore, interactive modelling methods require a permanent availablity of infomation, in order to enable interpreters permanently to control the coincidence of model and constraints. This task is not trivial because of the inhomogeneity of data and information. Knowledge based systems have been proposed in the past (e.g. Kölling, 1991), however, the experience shows that even simple interpretation problems may turn to be too complicated for automated processing.

The main task of this paper is to describe how we can use the 'knowledge base' of the geoscientist. He will be supported by selection-, handling- and visualization functions for the required data and information. He communicates with the computer program by the graphical interface, whithout taking care of the numerical routines. This is exactly the philosophy, which stands behind the development of the 'WINDOWS' system for PC users.

A crucial point among others is the integration of different 'geotypical' information. How can we describe the type of data involved in potential field interpretation? Four groups can be distinguished:

a) Fixed boundary conditions without variability

This group contains data which have exact specification of coordinates (x, y, z), for example the depths of drilled formations. The interpretation procedure is limited to

relating the samples to a special formation, to a verbal description (e.g. Lower Cretaceous) and to one or more physical parameters. The reduction of real world structures to geometry and special physical parameters is typical for geophysical methods. Once completed this classification, their coordinates may be used as fixed points within the model.

b) Fixed boundary conditions with variable interpretation

In many cases the location of fault systems is known near the surface from geological observations, however, their continuation to depth usually is subject of estimation, as well as their effect on the physical parameters to be modelled. Sometimes these data are connected to hypothesis about their continuation to the depth, e.g. a listric fault. These data are exact (fixed) at the surface, but they continue uncertain as fuzzy information to greater depths. Gravimetric modelling should not contradict the superficial data, but in greater depth the modelling is more flexible. The physical $1/r^2$ dependency of the gravimetric field causes this effect, which has been visualized by Tsuboi (1983).

These fixed, but uncomplete data have to be handled partly as fixed constraints, and partly as more vague information, which might be subject of interactive modifications.

c) Fuzzy boundary conditions with variable interpretation

In this case areas are to be modelled, which cannot easily be defined in terms of density and susceptibility. Typical examples are models of other geophysical methods, whose parameters cannot be correlated with density and susceptibility, as e.g. anomalous electrical conductivity: Its physical relation with density and susceptibility is not known, but obviously a correlation exists in some areas. This correlation provides important hints concerning the interpretation of recent structures and physical behavior of crustal segments.

Generally, all preexisting model results within the investigated area is information, which should always be in mind, however only in some cases these models can be regarded as fixed information: Gravity models have to be adjusted to seismic models (and vice versa!), older gravity models within the same area have to be modified according to the updated knowledge of the region, because the content of information changes continuously. All these examples belong to fuzzy information, which should be visualized. They do not have a direct numerical effect on modelling.

d) Qualitative, descriptive information

3D density models appear to be rather abstract and seem to be hard for geoscientists not familiar with gravity interpretation. They become more realistic (and increases "phantasy"), if certain information is added: Geographical information (cities, coast lines, river systems etc.), topographic information and much more data can facilitate orientation in the context of the modeled area. The modelling system should provide an environment, in which even non geophysicists feel comfortable. Standardized colors and symbols (Götze and Williams, 1993, proposed to use the 'Tectonic map of the world') may contribute to an increased interdisziplinary understanding. Finally, part of this group of 'boundary conditions' is all information, which derives from hypothesises or ideas not to be quantified: They may be included as sketches.

3 System IGMAS

IGMAS is an interactive, graphical computer system for interpretation of potential fields (gravity and magnetics) by means of numerical simulation (Götze, 1978; Götze, 1984; Götze and Lahmeyer, 1988). The method is based on 'trial and error' methods, and intensive interaction between user and program system requires numerous functions. The algorithm used for potential field calculation bases on triangulated polyhedrons (Götze, 1978), and has been revised and extended recently. At the moment a parallel modelling of the following field components is possible:

- Gravity fields (x, y and z components),
- Gravity gradients (x, y and z components),
- Gravity potential,
- Geoid undulation,
- Magnetic fields (x, y and z components) and
- Magnetic total field incl. remanent magnetization.

The data structure, which is required for the description of threedimensional model geometry has to be simple and flexible enough to cover the wide field of gravity or magnetics modelling: It should facilitate representations of geological information, such as vertical or horizontal cross sections, surface and depth contour maps, as well as volume and mass calculations.

These requirements lead to the following basic elements of the input data (ref. Figure 1): The structures (geological bodies) to be modelled are bounded by triangle facets (**layer boundaries**). They represent the shape of different bodies with **constant density and/or susceptibility**. The definition of these triangulated surfaces is given by the user by defining **polygons (lines)** along vertical, parallel **planes**. The triangulation between the vertical planes is done automatically. The data input is two-dimensional, whereas the construction of the final threedimensional model structures is performed by the program and does not require any knowledge of topology of the model or triangulation techniques.

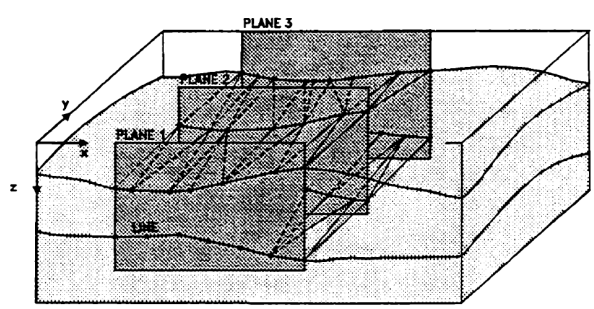

Fig. 1 IGMAS Geometry with vertical planes, lines and triangulated layer boundaries.

3.1 Graphical integration of constraints

Here, additional information, which may constrain the modelled structures, does not cause the density/susceptibility model. Constraints are visualized on the screen to inform the user on existing data sets. They are shown as overlays at the display, and may be activated or deactivated interactively to avoid too complex screen displays.

Visualization functions used by IGMAS (e.g. arbitrarily located cross sections and maps) require either a projection of the constraining data on the actual cross section, or cut of their geometry along the selected plane:

One-dimensional information (points), e.g. hypo- or epicenters, volcanoes, borehole measurements: They require two (x, y) or three (x, y, z) coordinates and sometimes additional attributes like

magnitude, age etc. If the z-coordinate is not given, points are projected on top of the model. The projection strip may be defined by the user, points with greater distance from the projection plane are ignored.

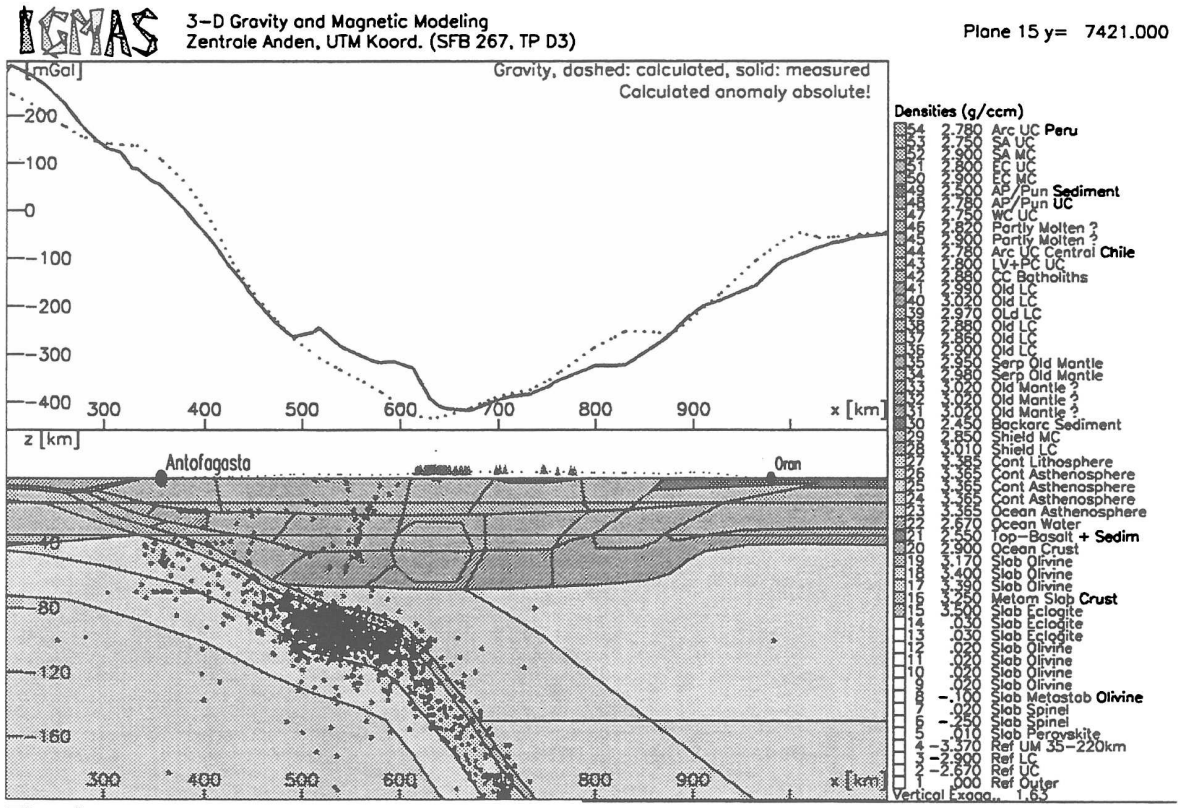

Fig. 2 West-East Cross section, Central Andes.
Shades of grey indicate density values (originally colored). Black points: Hypocenters; grey triangles: Volcanoes.

An example is shown in figure 2: It shows a vertical west-east cross section cutting through a density model of the Central Andean lithosphere (MIGRA project, discussed by Götze and Kirchner in this issue). The figure shows, besides cities for geographical orientation, the location of volcanoes along this cross section, and the projection of all hypocenters within a strip of 50 km width. The density structure, represented by grey shades, is a cross section which cuts the triangulated layer boundaries using exact world-coordinates (UTM).

Two-dimensional information (lines and profiles), e.g. geological sections or mappings, seismic models:

These data require two (x, y) or three (x, y, z) coordinates as it was shown for points. If z-coordinates are not given (e.g. for political border lines), they are projected on top of the model. This information requires special numerical handling, because the cut of a straight 3D line with a plane usually results in a single point. In this case the profiles are transformed into 'pseudo-threedimensional' strips using triangulation with constant values perpendicular to the profile direction. The width of this strip may be defined by the user.

Figure 3 shows another example of the MIGRA project: The result of a two-dimensional raytracing interpretation of the seismic research group is compared with the three-dimensional density model derived independently from gravity data (Götze and Kirchner; 1996, this issue). This overlay of two independent models enables the user to shed new light on the modelling process and to facilitate the adjustment of his model structures to the seismic features.

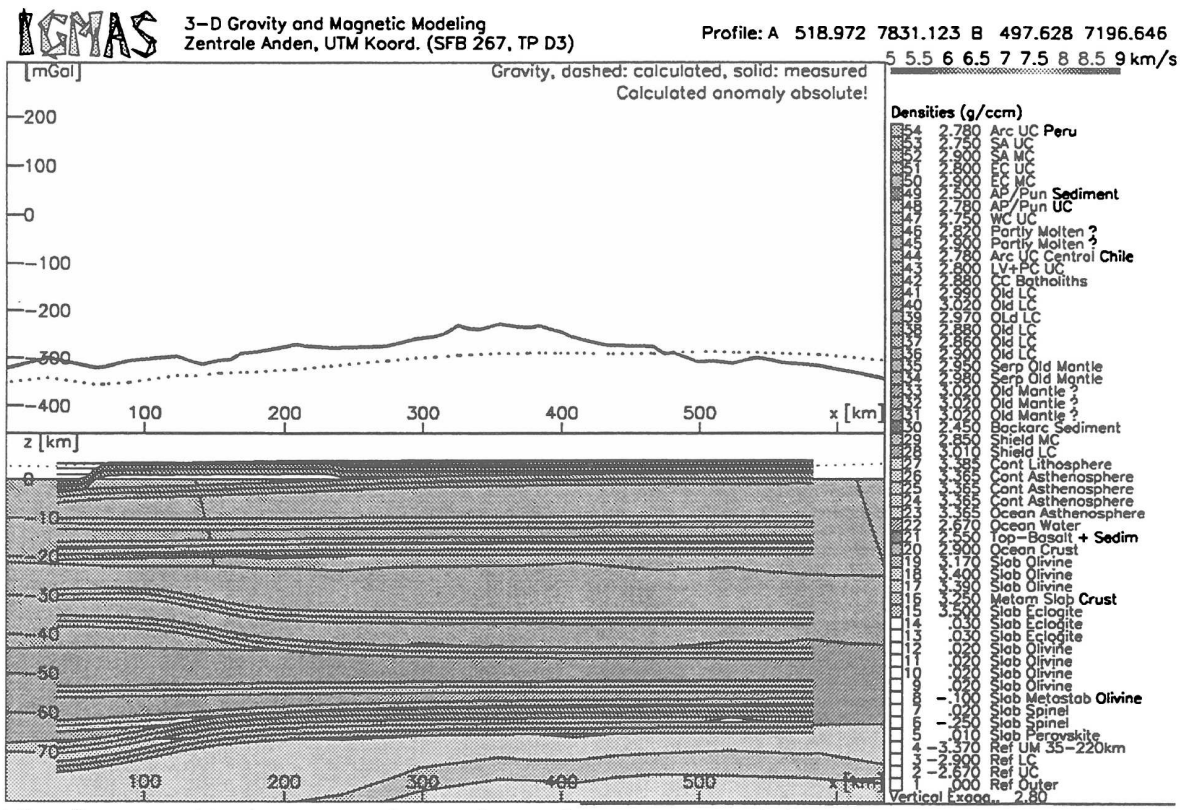

Fig. 3 Vertical North-South Cross Section, Central Andes. Overlay: 2D Raytracing Model, originally colored. Velocity scale: Upper right corner.

Three-dimensional information (gridded surfaces, triangulated models), e.g. isostatic models, 3D crustal balancing, 3D seismic surveys:

They require three (x, y, z) coordinates and a special topology. These 3D surfaces do not require any projection, they will be cut exactly by vertical or horizontal cross sections and visualized by polygon lines.

3.2 Numerical integration of constraints

Visualization of constraints in gravity models is already an important improvement of interactive modelling techniques. The visualization is performed by the program automatically, but the user still has the possibility to ignore this information. Several data, however, cannot be ignored: Exact borehole measurements of the depth of layer boundaries, outcropping faults or geological maps of layer boundaries are fixed information, as well as density constraints, which should be treated strictly 'unchangeable' by the program.

Additionally, any inversion algorithm will result in more stable and reliable data, if fixed or fuzzy constraints limit its freedom. Both, constraints for the physical parameters (e.g.: "ρ_i must always be larger than ρ_j"), as well as geometrical constraints, and even fuzzy geometrical constraints ("fault$_k$ should have an inclination of 15-30° to the east") have a stabilizing effect on inversion algorithms.

On demand, program functions can estimate the actual misfit between constraints and model and summarize this information.

3.3 Definition of Geo-Objects

The definition of constraints used so far does not describe, **how** to define them on the base of the existing data. Some of them require a 're-definition' to build a geo-object. This task has to be accomplished by the user before starting the modelling procedure, and is a crucial part of complex interpretation combining all existing geoscientific data. Some examples will illustrate this:

Definition of important boundaries
Each realistic density model is composed by several layer boundaries, which represent density contrasts between the volumes modelled. A complex object (a typical example is the Moho) consists of many of these layer boundaries with different density contrasts. In figure 2 for example, the Moho can be identified by the pronounced density contrast between crust and mantle material. However, crust as well as mantle are represented by several different densities. The density contrast between crust and mantle is not constant. The seismic method, however, defines the Moho to be a zone of strong velocity gradient, whereas absolute velocities may vary depending on the particular area. These different definitions require a new classification in order to be able to link them numerically:

Example geo-object "Moho Central Andes"
a) Gravimetric model definition:
Boundary between body 'continental asthenosphere' and body 'old mantle', and boundary between body 'continental asthenosphere' and body 'brasilian shield', and top of continental lithosphere,
or
increase of densities from < 3 to > 3 g/ccm.
b) Isostatic model definition:
Theoretical surface of isostatic equilibrium based on known topography.
c) Seismic model definition:
Increase of velocities to > 8 km/sec.

Generalization of geo-information
Borehole data often show extreme high resolution, so that their integration into a geophysical modelling process often causes severe problems, because geophysical methods usually require simplification and generalization. Therefore generalization is needed as part of a complex interpretation in the modelling process.

An examle of the geo-object "sedimentary cover"
It can be described by:
a) Stratigraphy:
Soil,
Sandy clay (quaternary),
Clay, humid (quaternary),
Sand, dry (quaternary).
b) Gravity modelling:
Body "1" (Sediments, density < 2.0 g/ccm) and
body "2" (Sediments, density 2.0-2.2 g/ccm).
c) Seismic modelling:
Velocities < 3 km/sec

The implementation of this 'object orientated' strategy of geo-objects, which can be addressed by user defined 'names', is not yet finished by now. In particular, the possibility of combining

certain physical parameters (densities, velocities) and geometries (layer boundaries and bodies) to construct complex geo-objects seems to be useful. The experience gathered in recent modelling projects of the research group shows, that any interdisciplinary interpretation requires possibilities of identifying specific 'geo-objects' during the process of modelling. Most of these 'objects' are not concerned with gravity and/or seismics but with requirements of a general geoscientific environment e.g.:

"Show the contour map of the *Moho*",
"What about the mean density of the *crust*?"
"How many *basin sediments* do we have in the *north*?"

These requirements appear to be simple, however they require more than schematic geophysically idealized representations of cubes or spheres. Todays 3D modelling frequently based on a whealth of rather inhomogeneous data bases and demand complex tools which are linked to special techniques, methods and knowledge to solve problems and questions in the geosciences.

4 Acknowledgements

This work is financially supported by the Deutsche Forschungsgemeinschaft (Az: Schm 844/4-1), which is thankfully acknowledged. Special thanks to the Gravity Research Group at FU Berlin, particularly to H.-J. Götze and A. Kirchner for numerous intensive discussions on gravity interpretation and 'Beta-Testing' new IGMAS functions. Thanks also to G. Goltz, who developed the user interface, and to all colleagues who were involved in the ongoing 'Beta-Test'.

5 References

Götze, H.-J., 1978, Ein numerisches Verfahren zur Berechnung der gravimetrischen Feldgrößen drei-dimensionaler Modellkörper. Arch. Met. Geoph. Biokl., Ser. A, 25, 195-215.

Götze, H.-J. and A. Kirchner, 1996, Gravity Field and Geoid at the South American Active Margin (20° to 29° S), this issue.

Götze, H.-J. and B. Lahmeyer, 1988, Application of three-dimensional interactive modeling in gravity and magnetics, Geophysics Vol. 53, No. 8, 1096 - 1108.

Götze, H.-J. and R.T. Williams, 1993, Digitization of maps and associated geoscience data. Special Paper, American Geophysical Union and Inter-Union on the Lithosphere, Washington, Publ. No. 205, pp.87.

Kölling, A., 1991, Ein Systemansatz zur wissensbasierten kombinierten Interpretation geophysikalischer Messungen am Beispiel der Ortung oberflächennaher bergbaubedingter Hohlräume. Dissertation, Fachbereich Geowissenschaften, FU Berlin, 257 p.

Tsuboi, Ch., 1983, Gravity. Verlag George Allen & Unwin, London.

ON THE APPLICATION OF PHYSICAL FILTERING IN 3-D FORWARD GRAVITY FIELD MODELLING

Gábor Papp

Geodetic and Geophysical Research Institute
of the Hungarian Academy of Sciences
H–9401, Sopron, Pf. 5

Abstract

Possessing a detailed 3-D volume element model of the density distribution of the lithosphere in the Pannonian basin, Hungary a successful attempt was made to reproduce short wavelength (local) geoid undulations generated by the model and to combine those with undulations provided by high resolution global geopotential models like OSU89B and OSU91A. The variants of the obtained "lithospheric geoid" agree with local gravimetric quasi-geoid solutions of Hungary very well ($m_{\Delta N} = 10 - 40$ cm, $\sigma_{\Delta N} = \pm 10 - 20$ cm). In the process of combination of local and global contributions a subsequent application of physical and mathematical (digital) filtering was introduced.

On one hand physical filtering removes properly the undesired trends from the local undulations and at the same time it improves efficiently the characteristics (zero mean, periodicity) of the residual part of the generated potential. Thus the residuals become suitable for further mathematical processing. On the other hand digital filtering provides the exact separation of local and global contributions in the frequency domain but it gives satisfactory results only if the signal processed satisfies rigorous conditions. Methodological and practical questions of forward computations of the potential are discussed in the paper and the differences between the two filtering techniques are demonstrated by an example from the modelling of the gravity field in the Pannonian basin.

Introduction

For the first glance the results obtained from a regional model of some density inhomogeneity by 3-D forward gravity modelling are sometimes disappointing. Displaying the isolines of the computed quantity (e.g. undulation contribution) one may think that there is something wrong with the computations. The expected details, short wavelength features which are certainly inherent in the density model cannot be observed only a relatively smooth "bulge" or "hump" is seen. Obviously, the computations are correct but what is seen is not what is expected based on observations of the gravity field. Usually the main purpose of the forward modelling is to produce quantities from a model of the real world which can be compared to the observations afterwards. But only the same kind of data having the same meaning can be compared to each other.

In the situation of gravity field modelling performed from observations differential quantities (gravity anomaly, disturbing potential, geoid undulation) representing very small deviations (magnitude of $\approx 10^{-4} \ldots 10^{-5}$) of the real gravity field from its simple physical-mathematical model are considered. In this sense the rotational ellipsoid and its analytically described gravity field is a very suitable model of the real Earth. This model, however, does not involve any useful information about the internal density distribution (in fact the model is independent from its generating sources) therefore its gravity field fits only to the external observations. In the case of local/regional density models, in spite of the fact that usually density contrasts ($\Delta\varrho$) are

used in the computations instead of real densities having $\overline{\varrho}$ global mean value, the magnitude of relativeness $(\Delta\varrho/\overline{\varrho})$ is only $10^{-1}\ldots10^{-2}$. From this ratio one can see that the potential (V_{DM}) generated by the density model (1) has not the same information content than what is derived from gravity field observations referenced to a global model. Therefore the comparison and combination of these two kinds of contributions need preparations which make their information content consistent.

$$V_{DM}(x',y',z') = G\int_x\int_y\int_z \frac{\Delta\varrho(x,y,z)}{r(x-x',y-y',z-z')}dxdydz\,. \tag{1}$$

The concept of physical filtering

The concept of physical filtering is based on the principles of physical geodesy where instead of the total potential of the Earth (W) rather the disturbing potential (T) is considered and used to represent the irregular features of the Earth's gravity potential (2). This way of processing of geodetic data has theoretical and also practical advantages,

$$T = W - U \tag{2}$$

(Sansò, 1994; Torge, 1980; Heiskanen and Moritz, 1967) and it removes (filters out) the systematic and long wavelength effects from W. It is obviously possible because the reference potential U is derived by physical-mathematical considerations from the observations of the linear functionals of W e.g.

$$\mathbf{g} = \mathrm{grad}W\,. \tag{3}$$

The geodetic reference model satisfies several physical and geometrical conditions (4) and therefore its application in (2) is equivalent with physical (high-pass) filtering.

$$\begin{aligned} a_{ref} &= a_{real} \\ e_{ref} &= e_{real} \\ M_{ref} &= M_{real} \\ \omega_{ref} &= \omega_{real} \\ CoM_{ref} &= CoM_{real} \end{aligned} \tag{4}$$

where subscripts ref and $real$ represent the reference and the Earth's real parameters, respectively (a is the semimajor axis, e is the first excentricity, M is the mass, ω is the angular velocity and CoM is the Center of Mass).

This scheme may be followed step-by-step in forward gravity field computations where the observables are the volume density values implied in the model. In order to get a reference model of the local density distribution (*1*) a suitable geometrical formation which represents the dimensions of the real model sufficiently and (*2*) an average density which produces the same mass for the reference model have to be found. Since in the practice generally thin, layer-like models are used (the horizontal extension of the models is much bigger than the vertical dimension) therefore it is expedient to keep the usually irregular horizontal shape of the density distribution model (Fig. 1). It helps to reduce those artificial effects (edge effects) which are caused by the lack of data around the model generating large horizontal gradients at the border between the empty $(\varrho \equiv 0)$ and the model $(\varrho \not\equiv 0)$ spaces (Kalmár et al., 1995). To obtain the vertical extension (D_r) of the reference model for a local density model built up from rectangular prisms both (5) and (6) should be satisfied simultaneously.

$$M_r = A_r D_r \overline{\varrho}_r = \sum_{i=1}^{N} \varrho_i V_i = \sum_{i=1}^{N} \varrho_i \Delta x_i \Delta y_i \Delta z_i = \sum_{i=1}^{N} m_i \tag{5}$$

$$A_r = \sum_{i=1}^{K} \Delta x_i \Delta y_i \ , \tag{6}$$

where the mass of the reference model is M_r, the mass of a single prism of the density model is m_i, $\Delta x_i, \Delta y_i$, and Δz_i are the horizontal and vertical dimensions of a single prism, respectively, the density of a single prism is ϱ_i, the homogeneous density of the reference model is $\overline{\varrho}_r$, the volume of a single prism is V_i, A_r is the area of the planar projection of the bounding surface of the reference model which is equal to the areal sum of those prism sides being in horizontal position and having a number of K which cover A_r in the horizontal plane uniquely ($K \leq N$).

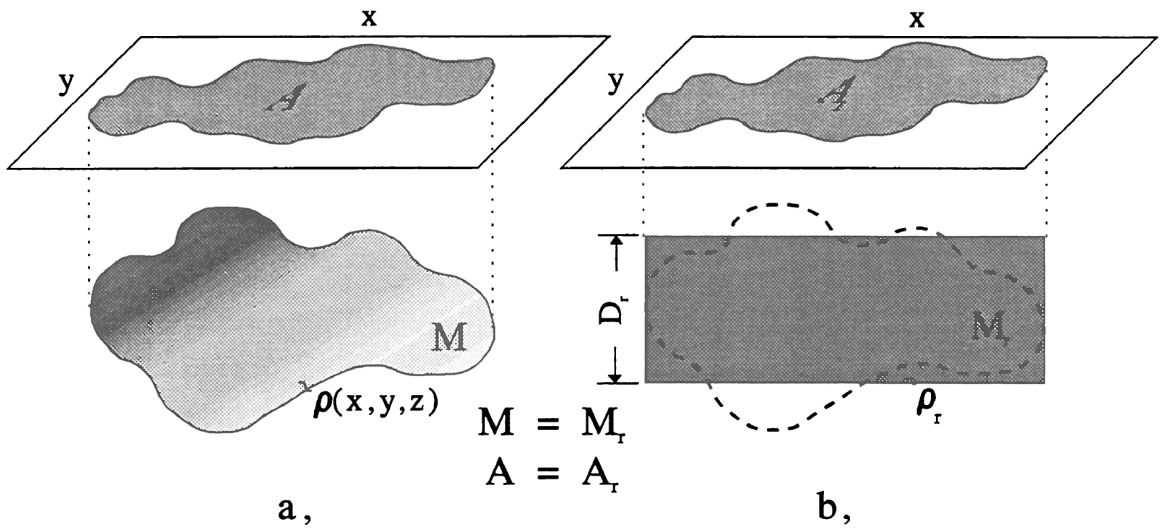

Figure 1. (a) A local density model with a density distribution $\varrho(x, y, z)$ and (b) its simplified reference model with homogeneous density $\overline{\varrho}_r$.

Applying the above constraints a horizontal slab having a constant thickness D_r, an irregular horizontal outline and a constant density is obtained. Computing the gravitational effect (e.g. potential) of both the detailed density model (V_{DM}) and its simplified reference model (V_{RDM}) one can compute local disturbing potential (T_L) by

$$T_L = V_{DM} - V_{RDM} \ . \tag{7}$$

Concerning the 3-D prism model of the upper mantle beneath Central Europe (Fig. 2) derived from different maps of the Mohorovičić discontinuity (Lillie et al., 1994; Horváth, 1993; Posgay et al., 1991) the computation of its simplified reference density model follows. The horizontal extension of the model is 950 × 750 km in E-W and N-S directions, respectively (Papp and Kalmár, 1996) consisting of 1821 rectangular prisms. The model possesses homogeneous density distribution (e.g. $\Delta\varrho = +200$ kg/m^3). The thickness D_r of the reference density model is computed by (8), where the total mass of the model is M and $M = M_r$. Based on (8) the reference density model of the upper mantle is a horizontal plate of 950 × 750 × 19.92 km with homogeneous density of +200 kg/m^3.

$$D_r = \frac{M}{\Delta\varrho \cdot 950 \cdot 750} \cdot 10^{-6} \ [m] \ . \tag{8}$$

Comparison of physical and digital filtering

In order to investigate the differences between the two kinds of filtering considered, first of all the undulation contribution of the upper mantle model was computed (Fig. 3/a) on a 10 × 10 km grid at 256 × 256 grid-nodes. The characteristic "bulging" of the total potential

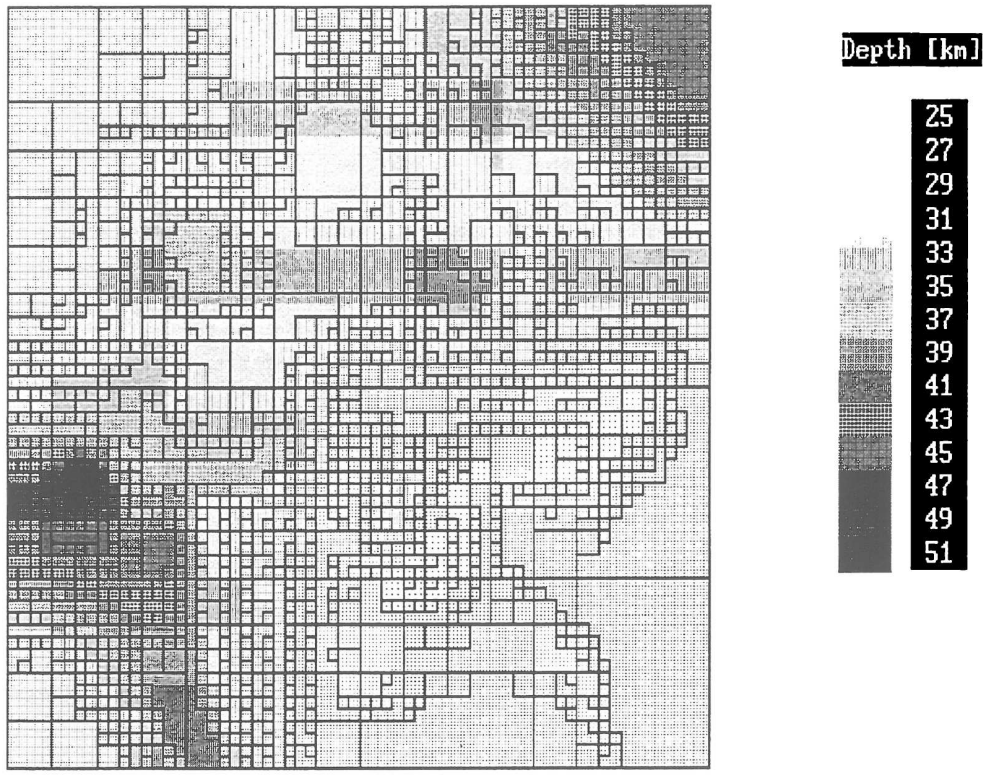

Figure 2. Horizontal arrangement of the prism system of the model of the upper mantle in Central Europe. Depth values refer to the upper side of the prisms.

field mentioned previously is clearly visible but all the other details are hidden. Computing the undulation contribution of the reference density model determined by (8) its contour line map can be seen in Fig 3/b. Both computations resulted in very smooth fields having very similar topology however subtracting them in the sense of (7) the medium and short wavelength undulations representing the variation of the local disturbing potential are recovered (Fig. 4/b). Comparing the contour lines to the gray-shaded map of the Mohorovičić discontinuity (Fig. 4/a) the large scale correlation between them is obvious. E.g. the highest undulation ($\approx +6$ m) is observed on the area of the Pannonian basin where the upper mantle is in an extremely elevated position (26–27 km) relative to the average Moho depth (33 km) of the surrounding Alpine-Carpathian orogenic belt (Papp, 1996). Moreover on the area of investigation the magnitude of the undulations (10–13 m peak-to-peak amplitude) recovered by physical filtering are comparable to the differences of undulations (max. 20 m in NE-SW direction) computed from OSU91A global geopotential model (Fig. 5) whereas the +80 m undulation maximum obtained from the total contribution cannot be correlated to any details of the OSU geoid easily.

If a digital high-pass filter provided by GMT program package (Wessel and Smith, 1991) ($\lambda_{pass} = 200$ km, $\lambda_{cutoff} = 300$ km) is applied on the total undulation contribution (Fig. 3/a) in order to "amplify" the short wavelength components ($\lambda \leq 300$ km) Fig. 6/a may be obtained. Figure 6/a shows several artificial characteristics of the high frequency undulations. First of all, as an undesired phenomenon the shape of the model area (a rectangle) is clearly indicated by the strong horizontal gradients of the undulations at the edges of the model. Along and near the edges spurious oscillations are present, however those are not connected to the structure of the density model at all. Even inside the model area the correlation factor computed from the simplest linear regression of the depth-undulation data is only 0.19.

Concerning the structure of undulations (Fig. 6/b) obtained by the subsequent application of physical and digital filtering, where the same transfer characteristics ($\lambda_{pass} = 200$ km, $\lambda_{cutoff} = 300$ km) were applied the deficiencies mentioned above are missing. At the edges the horizontal

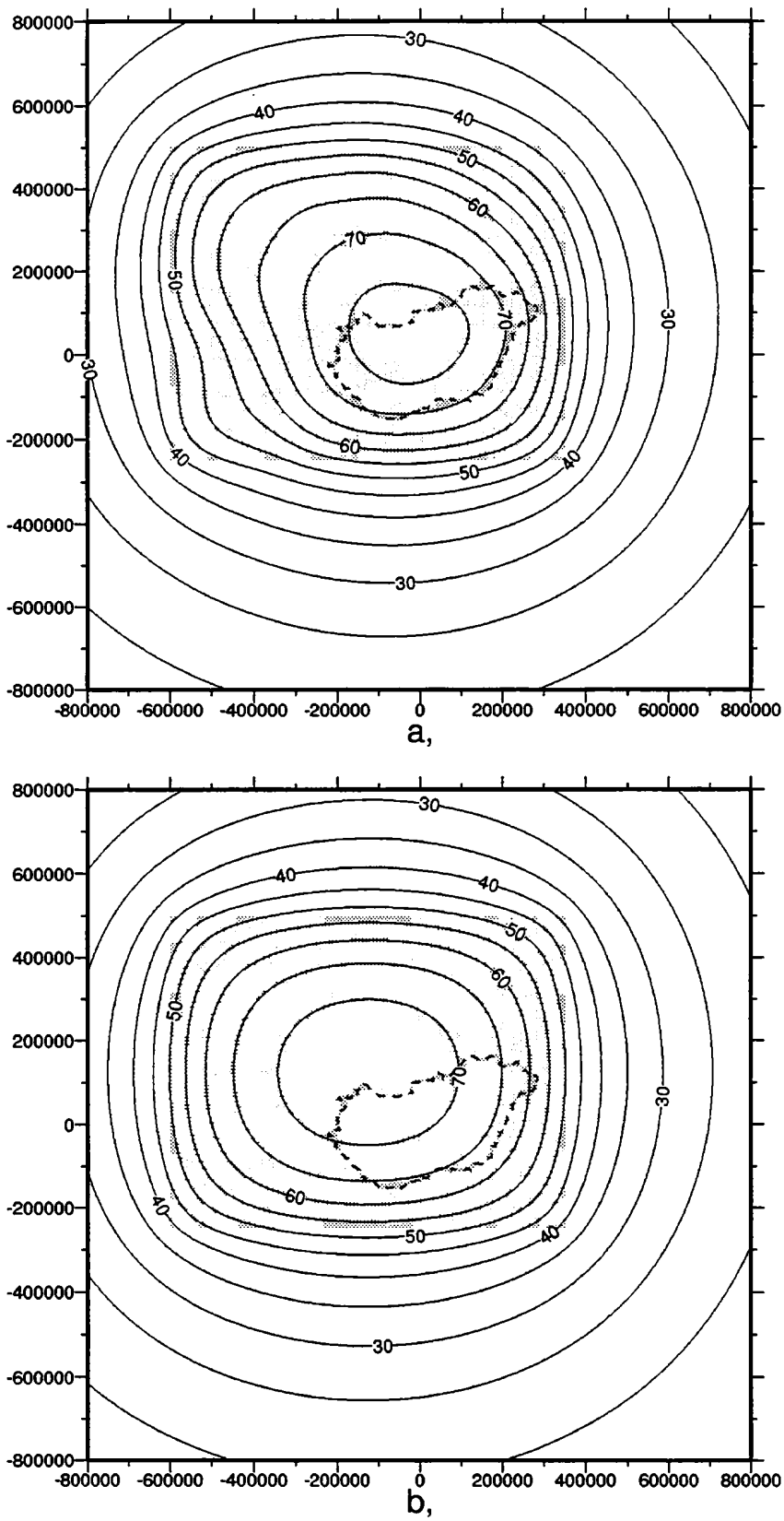

Figure 3. (a) Total undulation contribution generated by the density model of the upper mantle. (b) Undulation contribution of its reference density model. Contour interval is 5 m, plane coordinates are given in meters. Shaded rectangle shows the location and extension of the density model whereas dashed line represents the state border of Hungary (Pannonian basin).

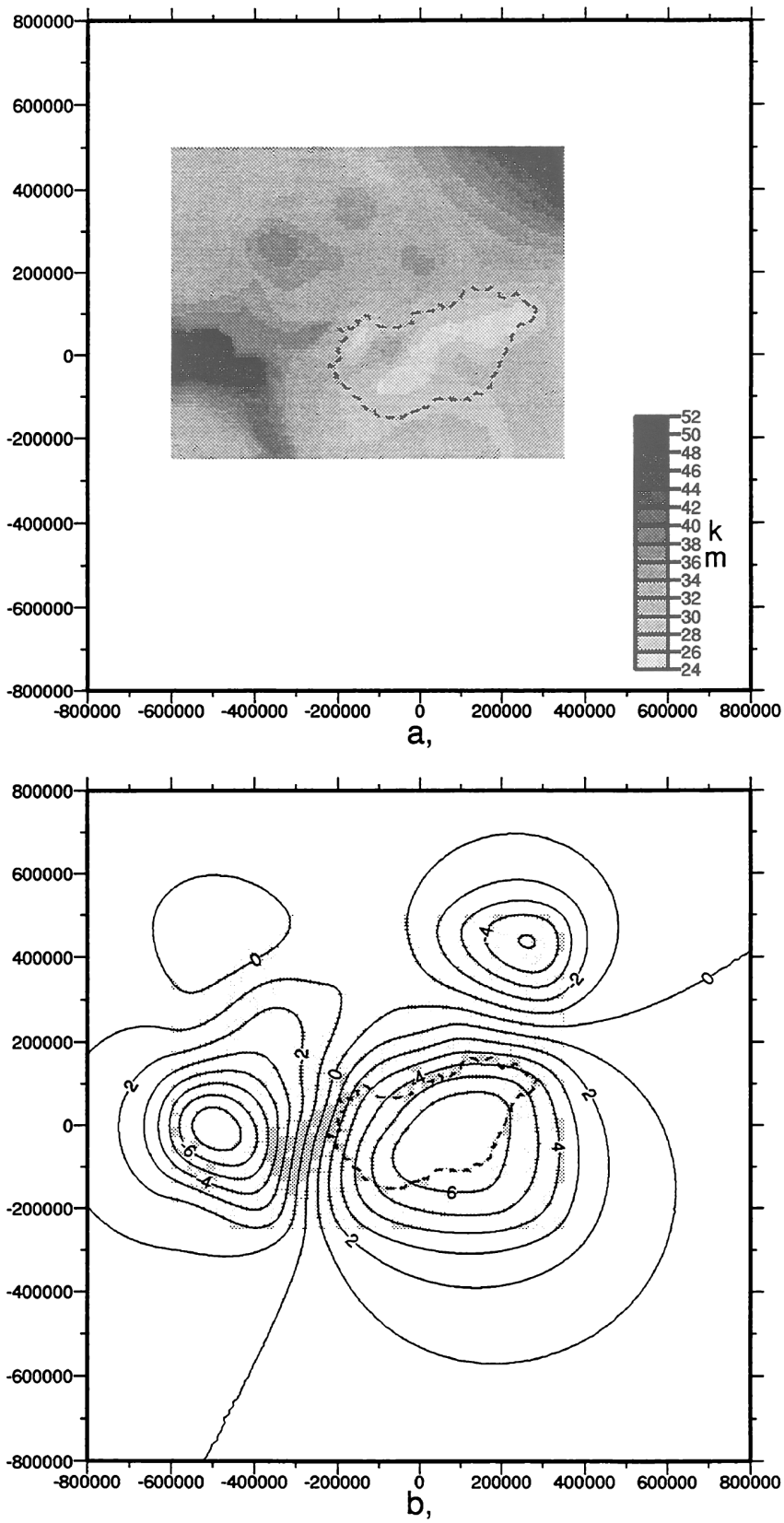

Figure 4. (a) Gray-shaded map of the depth of Mohorovičić discontinuity beneath Central Europe. (b) Undulation contribution of the density model of the upper mantle after physical filtering. Contour interval is 1 m, plane coordinates are given in meters. Shaded rectangle shows the location and extension of the density model whereas dashed line represents the state border of Hungary (Pannonian basin).

gradients are small and there are no artificial oscillations neither there nor inside the area. The correlation factor is 0.41; it indicates a somewhat higher but statistically not yet significant correlation between the undulations and the topography of the Moho.

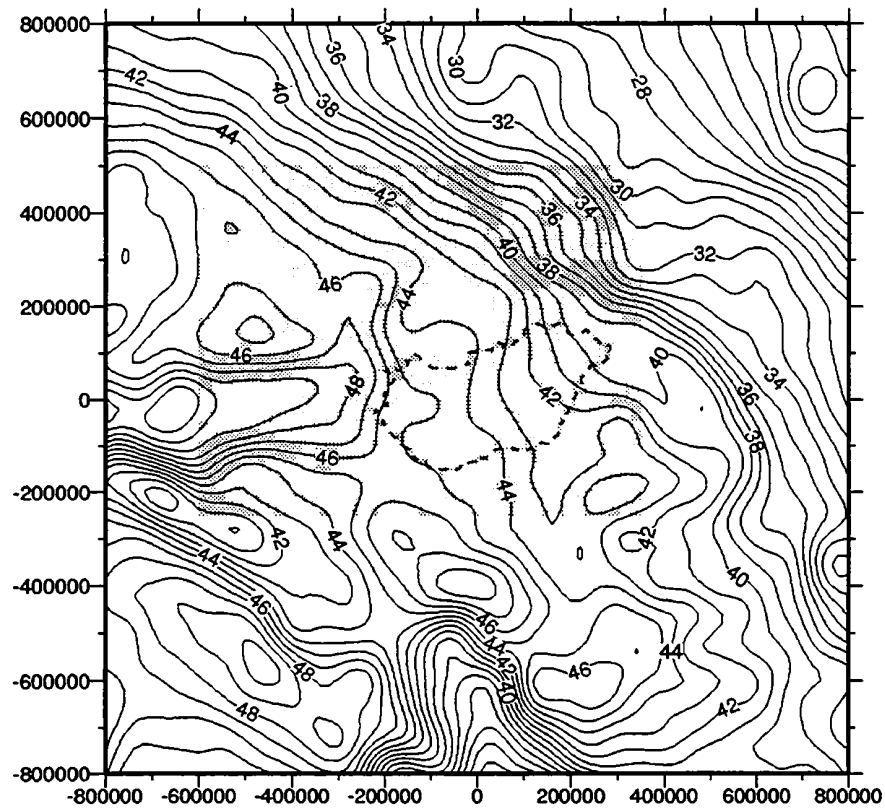

Figure 5. Contour line map of the OSU91A geoid in Central Europe (N=360). Contour interval is 1 m, plane coordinates are given in meters. Shaded rectangle shows the location and extension of the density model whereas dashed line represents the state border of Hungary (Pannonian basin).

Discussion of the results

The significant differences between physical+digital and purely digital filtering demonstrated in the previous section are caused by the properties of digital Fourier-transform (DFT) which is the basic tool in digital filtering. The "recipe" of digital filtering is very simple (e.g. Meskó, 1984). Take the DFT-s of both the signal to be filtered and of the filter itself and multiply them. Then perform inverse Fourier-transform of the product to get the filtered signal. Whereas usually the design of the filter does not make problems the proper spectral modelling of the signal, what is the undulation contribution generated by the density model is crucial. This kind of signal is obviously neither periodic nor has - in the practice - infinite horizontal extension in X and Y directions. Therefore in the whole frequency range from 0 to the Nyquist frequency the so called spectral leakage distorts the spectrum resulting in false periodicity of the spectrum itself. Furthermore the high frequencies are influenced by the "aliasing" or "folding" effect the magnitude of which depends on how sufficiently the sampling rate is able to represent the high frequency information content of the signal (Brigham, 1974). Serious problems occur if long wavelength information which may be considered as trend compared to the extension of the area of investigation is also present in the signal. Unfortunately the potential fields generated

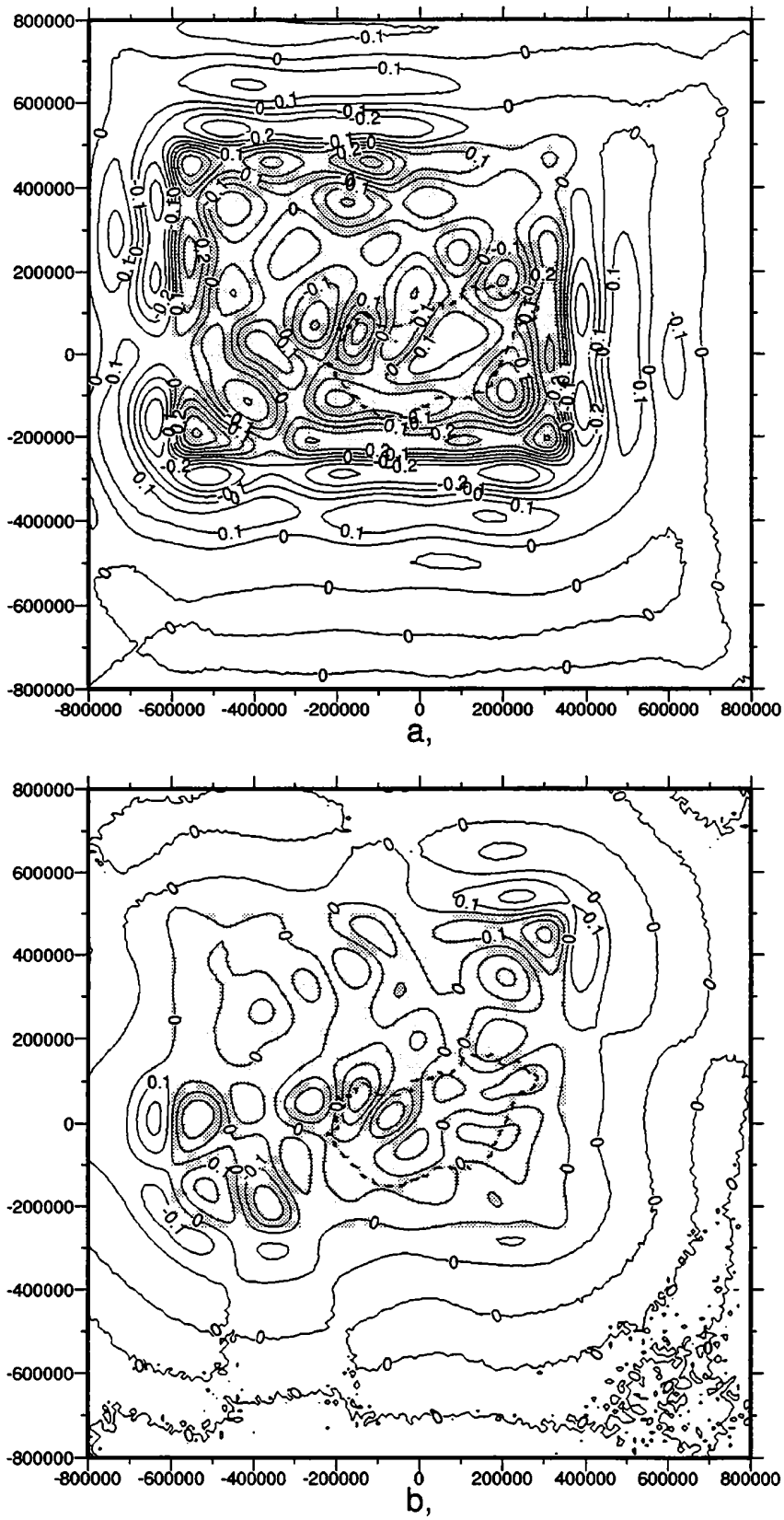

Figure 6. (a) Short wavelength undulation contribution of the upper mantle obtained by digital high-pass filtering (λ_{cutoff} = 300 km, λ_{pass} = 200 km). (b) Short wavelength undulation contribution of the upper mantle obtained by a subsequent application of physical and digital filtering (λ_{cutoff} = 300 km, λ_{pass} = 200 km). Contour interval is 0.1 m, plane coordinates are given in meters. Shaded rectangle shows the location and extension of the density model whereas dashed line represents the state border of Hungary (Pannonian basin).

by local density models contain all these undesired properties influencing the results of DFT disadvantageously. Obviously DFT models the signal self-consistently, but it is not sure at all that the DFT spectrum in local case is consistent with the global spectrum of potential related quantities because of the different information content of the signals.

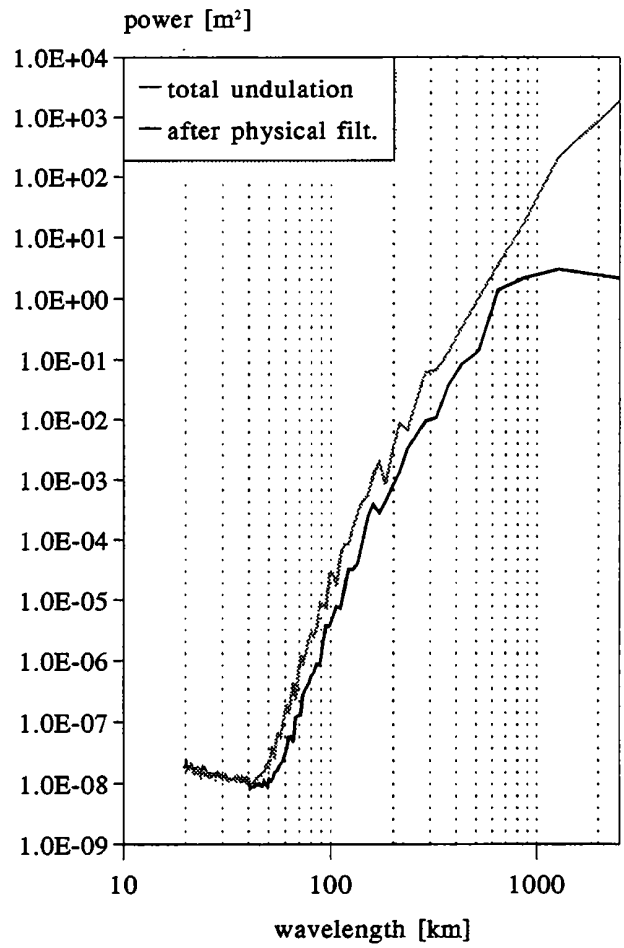

Figure 7. Radial power spectra of (gray) the total undulation contribution of the upper mantle and (black) of the residual undulations after physical filtering.

Concerning Fig. 7, one can see that there is not a simple relation between the total undulation contributions and the residuals obtained by physical filtering even in the range of high frequencies. Physical filtering affects the whole frequency range drastically decreasing the power at long wavelengths ($\lambda > 600$ km). Therefore the same result cannot be obtained by usual digital filtering what is basically a linear operation and loosly speaking it leaves the power of passed frequencies "untouched" whereas it makes the power "zero" in the cut-off band. Fig. 8 shows that an ideal transfer function should have a step-function shape providing constant transfer (0 attenuation) for the passed wavelengths whereas the observed transfer function produces gradual attenuation toward the forbidden long wavelength geoid undulations indicating strong linear trend in the logarithmic scale. Moreover in certain wavelength ranges the attenuation differs abruptly from its general trend (see e.g. the range between 105–110 km) resulting in narrow "spikes" in the transfer function. The reason of this is not known but such characteristics cannot be easily provided by a common digital filter. Therefore concerning that the application of physical filtering prior to digital filtering improves the interpretability of the processed data it is recommended to be used in 3-D forward gravity field modelling.

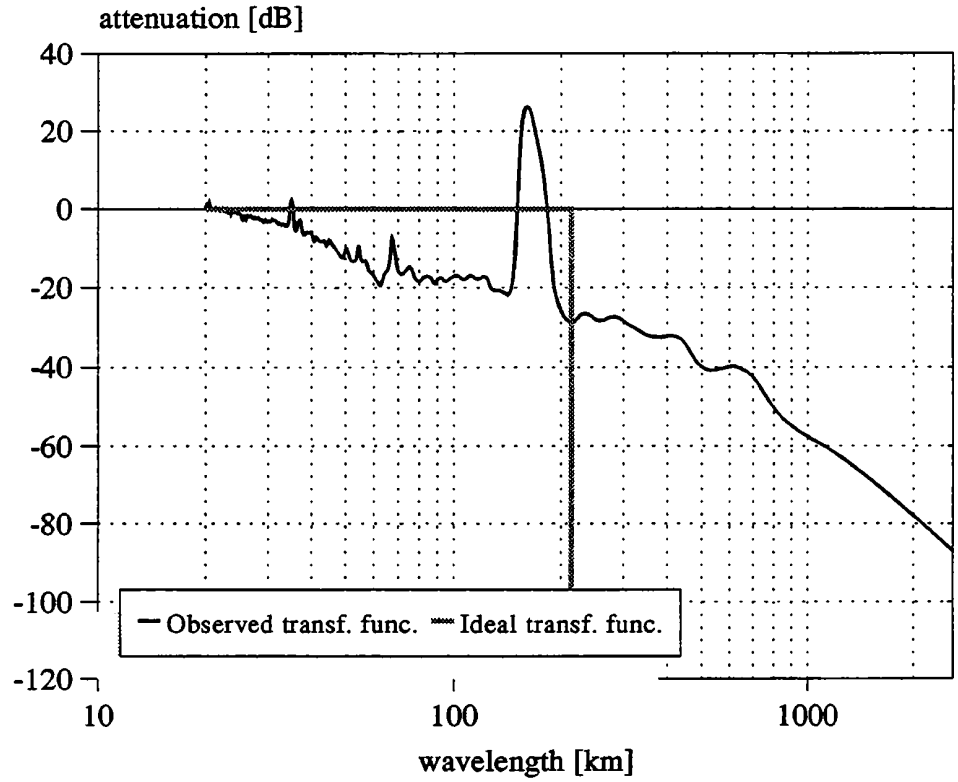

Figure 8. Spectral transfer functions of (gray) an ideal high-pass filter and of (black) the "physical filter" obtained by deconvolution.

References

Albertella A., Sansò F., 1994. A compendium of physical geodesy. In: Lecture Notes of the "International School for the Determination and Use of the Geoid", International Geoid Service, DIIAR-Politecnico di Milano, Milano

Brigham E. Oran, 1974. The Fast Fourier Transform. Prentice-Hall, Inc., Englewood Cliffs, N.J., p. 251.

Heiskanen W. A., Moritz H., 1967. Physical Geodesy. W.H. Freeman, San Francisco

Horváth F., 1993. Towards a mechanical model for the formation of the Pannonian basin. Tectonophysics, 226, 333–357.

Kalmár J., Papp G., Szabó T., 1995. DTM-based surface and volume approximation. Geophysical Applications. Computers & Geosciences, 21, 245–257.

Lillie R. J., Bielik M., Babuška V., Plomerová J., 1994. Gravity models of the lithosphere in the Eastern Alpine-Western Carpathian-Pannonian Region. Tectonophysics, 231, 215–235.

Meskó A., 1984. Digital filtering. Applications in Geophysical Exploration for Oil. Akadémiai Kiadó, Budapest, p. 636.

Papp G., 1996. Gravity field modelling in the Pannonian basin for geodetic purposes. PhD. Theses (in Hungarian) (in print)

Papp G., Kalmár J., 1996. Toward the physical interpretation of the geoid in the Pannonian basin using 3-D model of the lithosphere. IGeS Bulletin, DIIAR-Politecnico di Milano, Milano (in print)

Posgay K., Albu I., Mayerová M., Nakládalová Z., Ibrmajer I., Bližkovský M., Arič K., Gutdeutsch R., 1991. Contour map of the Mohorovičić discontinuity beneath Central Europe. Geophys. Transactions, 36, 7–13.

Torge W., 1980. Geodesy, an introduction. Walter de Gruyter, Belin, New York

Wessel P., Smith W. H. F., 1991. Free software helps map and display data. EOS Trans. AGU, 72, 441, 445–446.

INVESTIGATION OF METHODS PROVIDING FIELD CONTINUATION BETWEEN ARBITRARY SURFACES

Roland Pail and Bruno Meurers

Institute of Meteorology and Geophysics, University of Vienna

Abstract

In regions of rugged topographic relief field continuation from an arbitrary to a plane surface is required to diminish reduction anomalies due to anomalous vertical gradients. Several methods based on different concepts are investigated and compared by means of synthetic and field data. Besides two approaches to reduce edge effects are proposed, i.e. the separate continuation of a trend and residual field and the application of an appropriate field extension.

1. Introduction

Generally gravimetric or magnetic data are measured on a rugged topographic surface. The gravity data obtained by "classical" Bouguer reduction do not refer to the reduction level, but still to the height-correlated station locations. Free-air reduction only considers the standard gravity gradient and neglects the a priori unknown anomalous vertical gradient between the station and the reduction level which is caused by all disturbing masses located below the topographic surface. Therefore Tsuboi (1965) distinguishes the "station Bouguer anomaly" (SBA) on the observation surface from the "real Bouguer anomaly" (RBA) on the reduction level.

Many processing techniques, e.g. field transformations or the calculation of the anomalous mass, assume gridded data on a plane surface. Neglecting the anomalous vertical gradient results in reduction anomalies, especially in regions with high anomalous gradients and altitudes. Therefore both interpolation and field continuation from a rugged to a plane surface are necessary.

The problem of field continuation between arbitrary surfaces can be solved by a variety of methods developed during the latest decades. Tab. 1 shows a selection without claim of completeness. In this investigation some continuation methods of different conceptions are analyzed, compared and tested by means of synthetic and field examples.

2. Characteristics of the methods applied

(1) Cordell (1992)

This continuation method is based on the "generalized equivalent source" conception. The Bouguer anomaly measured on the topographic relief is approximated by the gravity effect of point sources located exactly below the station locations and at a depth proportional to the distance to the nearest neighbor. The user defines the value of this proportionality factor and therefore implicitly the frequency characteristics of the approximated field, too. The equivalent source distribution is calculated iteratively. The gravity field determined by the previous iteration step is compared with the observed one. The next point source is then fitted at the position of maximum deviation. The method solves simultaneously the tasks of continuation and interpolation of data, because a regular station distribution is not required.

equivalent source		
point mass distribution		
	Dampney (1969)	horizontal point mass distribution (MI)
	Xia and Sprowl (1991)	horizontal point mass distribution (MI)
1	Cordell (1992)	point source distribution at different depths
density or dipole layer		
	Bhattacharyya & Chan (1977)	density layer located on topography (FIE)
	Hansen & Miyazaki (1984)	dipole layer located on topography (FIE)
	Pilkington & Urquhart (1990)	dipole layer located on mirror image of topography (FIE)
2	Graber-Brunner et al. (1991)	density layer located below topography (MI)
3	Ivan (1994)	continuous dipole layer on topography approximated by a polyhedral surface (FIE)
horizontal density layer		
4	Xia et al. (1993)	iterative solution applying upward continuation (DFT)
chessboard technique		
5	Cordell (1985)	continuation to different levels (DFT) and linear interpolation
finite series expansion		
	Henderson & Cordell (1971)	finite trigonometric series expansion (MI)
	Granser (1982)	finite trigonometric series expansion (MI)
6	Grauch (1984)	Taylor series expansion (DFT)
iterative approach		
	Grant & West (1965)	anomalous vertical gradient (DFT)
7	Lahmeyer (1989)	chessboard technique and iterative downward continuation of residual gravity (DFT)
8	Meurers (1992)	anomalous vertical gradient (DFT) improved iteratively
least squares collocation		
	Lahmeyer (1988)	

FIE: solution of Fredholm integral equation, DFT: discrete Fourier transform involved, MI: matrix inversion

Tab. 1: methods providing field continuation between arbitrary surfaces

(2) Graber-Brunner, Klingelè and Marson (1991)

This equivalent source method uses vertical prisms of square section and with constant height and density. The source distribution is placed at a constant depth from the supporting surface approximating the rugged topographic relief. The problem is solved by inverting a square matrix, where the number of columns and rows each is the total number of grid points. In case of large fields a symmetrical square operator has to be used to reduce computing time. The error made by applying operators increases in principle with continuation distance, because the vertical gravity component of regions beyond the operator's area gains in power.

(3) Ivan (1994)

In this method a continuous dipole layer is located on a polyhedral surface that consists of arbitrary triangular faces and approximates the topographic relief. Suppose R to be the observation point with position vector $\mathbf{r}$ on this polyhedral surface T defined by position vectors $\mathbf{r}'$. The magnitude μ of the dipole moment is then obtained from the following modified Fredholm integral equation of the 2nd kind:

$$\mu(\mathbf{r}) = \frac{1}{2\Pi(R)}\left[\Phi(\mathbf{r}) - \iint_{T^*} \mu(\mathbf{r}')\,\mathbf{n}(\mathbf{r}')\,\frac{\mathbf{r}-\mathbf{r}'}{|\mathbf{r}-\mathbf{r}'|^3}\,dS(\mathbf{r}')\right]$$

T^* is the surface excluding the observation point R where the potential $\Phi(\mathbf{r})$ is known, and $\mathbf{n}(\mathbf{r}')$ means the upward pointing normal unit vector of each face. $\Pi(R)$ is the bisection of the solid angle under which the base triangle defined by the neighbor points is viewed from the observation point R:

$$\Pi(R) = \begin{cases} 2\pi - A_{123} \\ \pi \\ A_{123} \end{cases} \quad \text{if observation point R} \begin{cases} \text{below base triangle} \\ \text{within the plane defined by the base triangle} \\ \text{above base triangle} \end{cases}$$

A_{123} represents a sum of arc tangent functions of arguments depending on geometric parameters.

(4) Xia, Sprowl and Adkins-Heljeson (1993)

The equivalent source consists of a continuous density layer defined on a plane surface that must be placed below the minimum station altitude. The density distribution $\sigma(\mathbf{r})$ is determined iteratively. At the m-th iteration step the density distribution has to be modified according to the following equation (Bott 1960):

$$\sigma(\mathbf{r})^{(m+1)} = \sigma(\mathbf{r})^{(m)} + \left[s(\mathbf{r}) - g(\mathbf{r})^{(m)}\right] / 2\pi G$$

where G means the gravitational constant. s is the observed and g the calculated gravity on the observation surface $z(\mathbf{r}) = z_0 + h(\mathbf{r})$. z_0 is the mean distance between equivalent source and topography. The gravity anomaly is then obtained by inverse FFT:

$$g(\mathbf{r}) = 2\pi G \sum_{n=0}^{\infty} \frac{h^n(\mathbf{r})}{n!}\, \mathcal{F}^{-1}\left[(-|\mathbf{k}|)^n \sigma(\mathbf{k})\, e^{-|\mathbf{k}|z_0}\right]$$

(5) Taylor series expansion (Grauch 1984)

This algorithm is based on expanding the gravity field measured on the rugged topography by Taylor series up to 2nd order with respect to the reference level z_0. During the computation of the gravity and its derivatives a FFT-low pass filter has to be applied which leads to a loss of high-frequency information.

(6) "chessboard"-method (Cordell 1985)

In the first step a supporting surface is defined by the mirror image of the observation surface. Besides, the gravity data are assumed to be located on a plane surface. The continuation from this level to the supporting surface is then performed by means of the „chessboard"-technique: The initial gravity field is continued to various levels. The gravity value at a certain altitude can then be evaluated by linear or spline interpolation in vertical direction.

(7) Lahmeyer (1989)

This iterative algorithm also applies the "chessboard"-technique. In this case, however, only a residual field representing the difference between the observed gravity field on the rugged topography and the solution of the current iteration step is continued from an optimum supporting level to the target level. The altitude of the optimum supporting level depends on the cut off wavelength of the low pass filter and is therefore crucial for convergence. The method developed by Xia et al. (1993) is a special case and moreover the optimization of Lahmeyer's algorithm. In this case the target level coincides with the supporting level, which is located below the minimum station altitude. Then the downward continuation of the residual field and consequently the filtering procedure are not necessary anymore. The calculated field in this level coincides, apart from the factor $2\pi G$, with Xia's density distribution. Therefore in this study Lahmeyer's method has been excluded from further consideration.

(8) Meurers (1992)

This method represents a modification of an algorithm published by Grant and West (1965). The RBA is approximated by iterative calculation of the free-air correction term according to the first mean value theorem for integrals. In this way the anomalous vertical gradient as well as its vertical derivative is considered. The calculation of the gravity gradient distribution requires FFT-low pass filtering, which results in a loss of high-frequency information in the correction term, but not in the original gravity data.

3. Synthetic studies

In this paragraph the continuation methods mentioned above are investigated by means of synthetic test examples. Topography data have been obtained by interpolating mean altitudes of a high-alpine relief (518 - 3494 m) in Tyrol on a 101 × 101 grid with 1 km spacing (Fig. 1). The gravity field on this topography (Fig. 2) is generated by a sample of 23 point masses in various depths between 3 km and 80 km below the zero level (case study A). It varies between 10.83 mGal and 98.32 mGal. The object is to continue this Bouguer anomaly (SBA) by means of the various methods to a level of 3000 m (or 3500 m in case of Ivan's algorithm) and to compare the results with the exact field of the source sample.

The chosen source distribution allows to locate the continuation level below the maximum station altitude, because in this synthetic case the Laplace equation is valid within the whole range of topographic heights. On the contrary in Ivan's method the equivalent dipole layer coincides always with the topographic surface. Therefore the continuation level has to be located above the maximum station altitude. This is only an apparent disadvantage, however, because only this and similar equivalent source methods (e.g. Bhattacharyya and Chan 1977, Hansen and Miyazaki 1984) are capable to continue potential fields generated by very shallow sources, e.g. density variations within the range of topography.

The numeric results of this investigation are summarized in Tab. 2 showing the statistics of the differences between calculated and exact fields. These would be distorted by method-dependent edge effects varying in magnitude. Thus only the inner part excluding a marginal zone of 10 km is analyzed statistically. Besides, the SBA field has been considered as an approximation of RBA - as it is done with the "classical" Bouguer reduction - and has been continued from an assumed reduction level of 518 m (minimum station altitude) to 3000 m respectively 3500 m. The difference between this result and the exact field on the respective level represents the continued reduction anomaly.

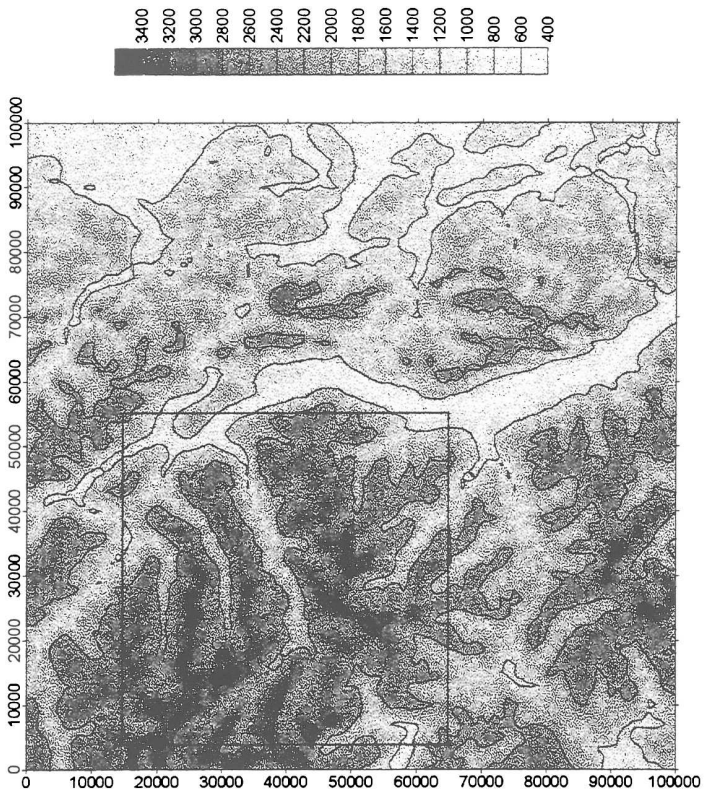

Fig. 1: Topographic relief of the synthetic case study. Colour interval: 200 m.

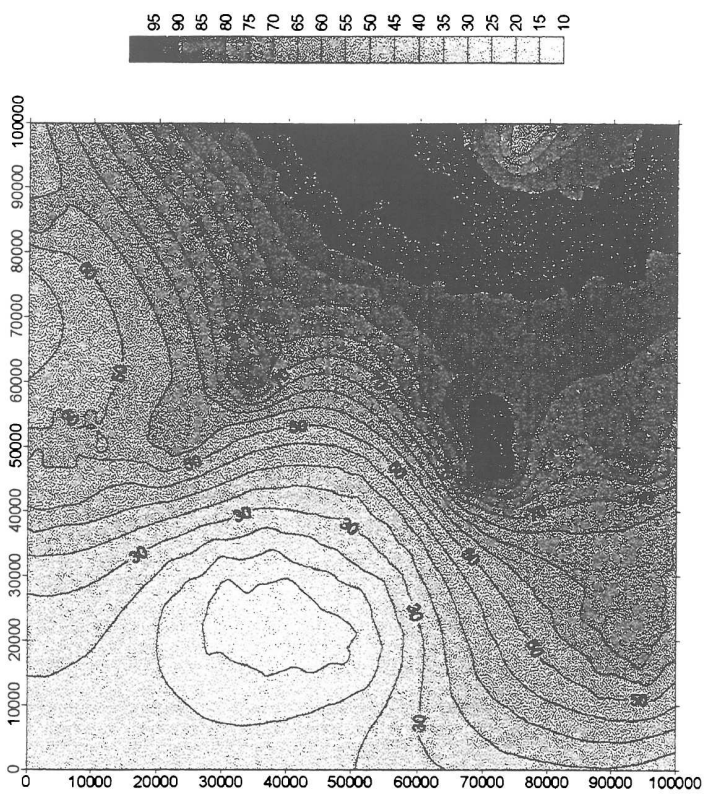

Fig. 2: Synthetic gravity field (A) on topography (SBA). Colour interval: 5 mGal.

method	Fig.	mean	min. dev.	max. dev.	RMS
Cordell	3	0.72	- 1.81	2.01	0.38
Cordell (sep.)	4	0.77	- 0.34	1.74	0.31
Xia	9	0.66	- 0.24	1.35	0.25
Taylor series expansion	10	0.68	- 0.14	1.40	0.30
"chessboard"	11	0.75	- 0.18	2.08	0.34
Meurers	12	0.64	0.06	1.36	0.25
reduction anomaly	---	1.11	1.98	5.44	1.42

Tab. 2: synthetic field (81 x 81-grid): errors on continuation plane 3000 m

(1) Cordell

Fig. 3 shows the difference between the continued field obtained by means of Cordell's method and the exact one on the plane 3000 m after 1000 iterations. The proportionality factor between the depth of the fitted point source below the station point and the grid spacing is 1.4. The result demonstrates one of the weak points of this algorithm which is based on the methodical approach: An equivalent point source distribution causes non-real high-frequency components which prefer to appear in regions with rugged topographic relief. The edge effects caused by using a finite measurement area increase with continuation distance, because no equivalent sources exist beyond that area. Applying various types of field extension does not introduce any additional information and therefore can improve the results only stochastically. Thus a new method has been developed, which separately performs the continuation of a trend field and of the remaining residual field in order to improve the representation of long wavelength components (Pail 1995).

The separation procedure is carried out by applying a low pass filter (cut off wavelength of 100 km) to the SBA field that has been previously extended by 50 km on each side. Only such field extension enables to choose a cut off wavelength similar to the original field dimension.

In the first step a source distribution is fitted to the trend field by Cordell's routine (840 iterations). As the depth of a point source corresponds approximately to a third of the anomaly's wavelength, the proportionality factor 40 has been chosen. Based on the resulting source distribution, the gravity field can be calculated both on the topographic surface and on the continuation level. In this way the long wavelength component is continued to 3000 m. The residual field, representing the difference between the SBA and the long wavelength component on the topographic surface, now is continued by a second application of Cordell's method (proportionality factor = 1.4, 1000 iterations) and added to the long wavelength component on the continuation level.

It should be mentioned that the residual field contains not only the high frequency component of the SBA field, but also the differences between the trend field and the one calculated on the topographic surface using the fitted sources, i.e. the errors of the first Cordell's computation. Besides, the error resulting from wavelength filtering, which theoretically is allowed only for potential fields referring to a plane, is not included in the final result. In principle Cordell's deep sources could be replaced by any other equivalent source that reproduces the long wavelength component of the gravity field on the topography fairly well. The trend field represented by this distribution is always continued exactly. Instead of wavelength filtering other methods of separation, e.g. higher order polynomials, can be used too.

Fig. 4 demonstrates the improvement of this method compared with Cordell's original algorithm (Fig. 3). Not only the edge effects, but also the high-frequency errors in the interior could be diminished.

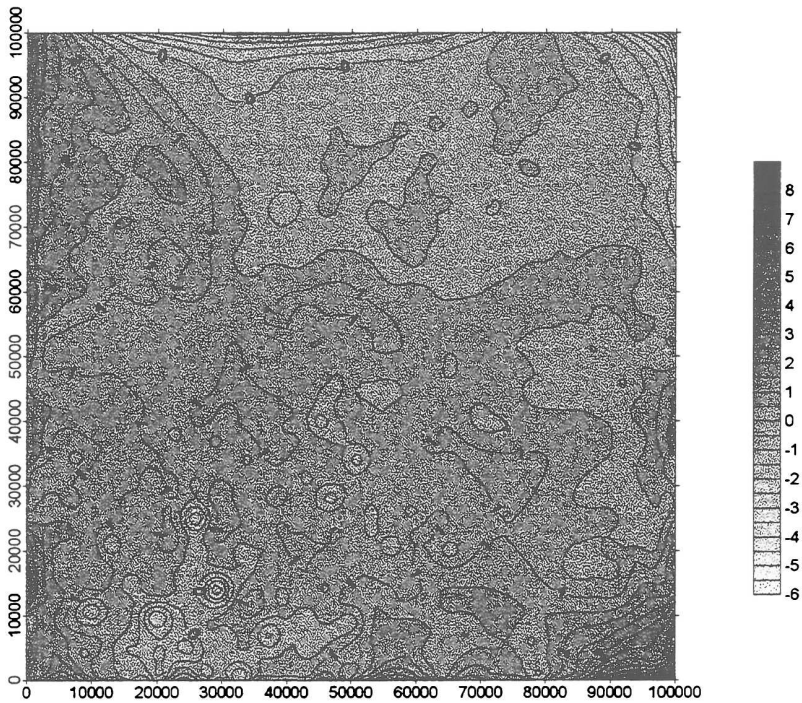

Fig. 3: Errors of Cordell's (1992) method. Contour interval: 0.5 mGal.

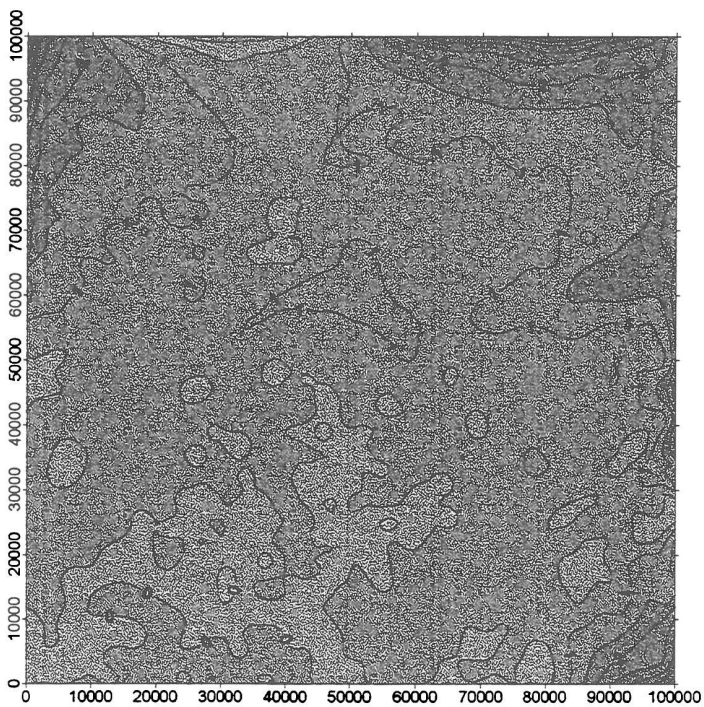

Fig. 4: Errors of Cordell's (1992) modified (trend separation) method. Contour interval: 0.5 mGal.

(2) Graber-Brunner et al.

This continuation method requires an inversion of big matrices. Because of limited computer capacity and computation time increasing with field dimensions an application of operators is indispensable. However the deviations and RMS errors resulting from the use of 15 x 15

or 21 x 21 operators are of a similar magnitude as the continued reduction anomaly itself. In the case of this synthetic study the method fails to improve the original problem.

Graber-Brunner et al. (1991) proposed to apply intermediate continuation levels. This stepwise procedure, however, often does not improve the accuracy of the method significantly. On the other hand subtracting the mean from the initial data results in a better conditioning of the matrix and a prominent improvement of the continuation problem. The continued field in the plane 3500 m included in Tab. 3 has been obtained by removing the mean value and applying a 21 $\times$ 21 operator. The height of the equivalent source prisms has been 1000 m, the constant depth below the topography 1.5 times the grid spacing (1.5 km).

(3) Ivan

Fig. 5 shows the errors in 3500 m achieved by Ivan's algorithm after 7 iterations. Prominent edge effects due to truncation extend farther to the interior of the field compared with the other methods. This phenomenon can be explained as follows. All methods using an equivalent source distribution below the topographic surface strengthen the source magnitudes at the grid boundary in order to compensate the missing gravity effect of the exterior while fitting the gravity field on the relief. In case of Ivan's method the dipole layer coincides with the topographic surface. Therefore the dipole magnitude is not increased that much in the boundary area. In the course of the continuation however the gravity effect of the exterior is entirely missing, because it is not at least partially compensated by strong magnitudes in the boundary regions. This phenomenon increases with continuation distance because of increasing influence of distant masses on the gravity effect. In addition to this height dependency the magnitude of the truncation effect depends also on the amplitudes of the gravity field in the edge regions.

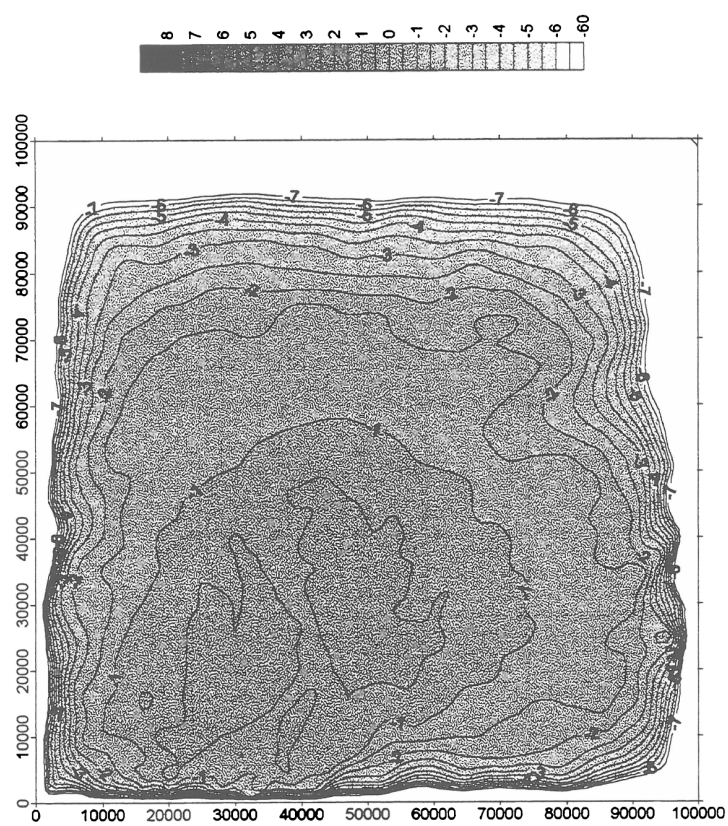

Fig. 5: Errors of Ivan's (1994) method. Contour interval: 0.5 mGal.

Therefore every method diminishing the gravity amplitudes at the boundaries is appropriate to reduce the truncation problem. In the following two approaches are developed (Pail 1995):

a) *separation of a long wavelength trend and separated continuation by means of Cordell's routine*
This method has been described in paragraph (1). No theoretical objections exist to such a combined procedure, because the application of two different types of sources (Cordell: point sources, Ivan: dipole layer) corresponds with the equivalent source principle in potential theory. Besides only the long wavelength component based on deep disturbing masses are continued by means of Cordell's method. Therefore the greatest advantage of Ivan's algorithm, i.e. the adequate continuation of masses being located within the range of topography, remains unaffected.

b) *appropriate field extension*
The developed field extension method serves the following criteria: The gravity field is expanded by linear interpolation between the gravity value of the given point at the original boundary and zero at the extended field's edge. A similar procedure is applied concerning the topography data. The only difference is that they do not tend to zero, but to the mean value of the topographic altitude.

Tab. 3 demonstrates the improvement applying these methods compared with the result based on the original SBA field.

Method	Fig.	mean value [mGal]	min. dev. [mGal]	max. dev. [mGal]	RMS [mGal]
Graber-Brunner et al. (21x21)	---	0.73	- 2.31	3.70	1.46
Ivan - original	5	- 1.58	- 8.58	- 0.01	1.23
Ivan - separation of trend field	---	0.36	- 1.17	2.41	0.63
Ivan - field extension (20 points)	---	- 0.84	- 3.65	0.00	0.59
Xia	---	0.96	0.23	1.76	0.24
Reduction anomaly (continued)	---	1.50	- 1.40	5.51	1.32

Tab. 3: Synthetic field (81 x 81 grid): errors on the level 3500 m

Ivan's method is the only one discussed in this paper that is able to represent adequately those sources located within the range of topographic altitudes, while all the other methods fail in that case because Laplace equation is violated. Therefore a second case study (B) has been performed to investigate the behavior of Ivan's algorithm in such case of high-frequency gravity fields.

The observation surface is a smaller part of the previously used topography and is marked in Fig. 1 by a frame. The space between the topographic surface and zero level is entirely filled with material of unit density. The mass exceeds the boundaries of the observation area by 5 km. Its gravity effect has been calculated by means of polyhedral approximation according to Götze and Lahmeyer (1988). The arrangement of triangles corresponds exactly to that one in Ivan's algorithm, therefore no numerical effects can arise due to the polyhedral approximation of the topographic surface. This high-frequency field on the observation surface ranges between 21.05 mGal and 129.28 mGal. The object of this study is to examine the practical behavior of Ivan's algorithm and different methods for reduction of truncation effects.

Fig. 6 shows the deviations of the calculated field from the exact one at 3500 m. In addition to prominent edge effects there exists a significant correlation with high-alpine regions

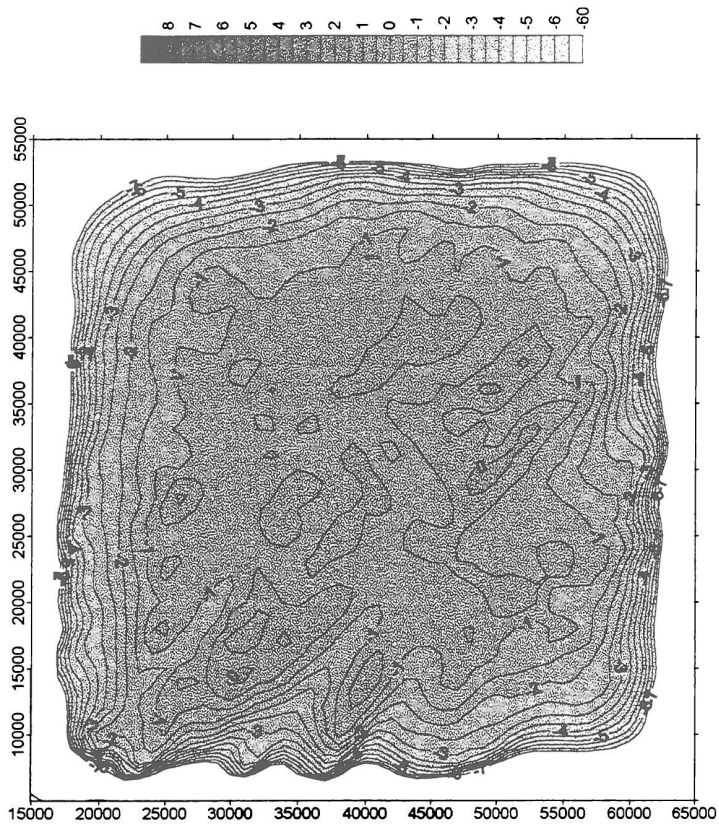

Fig. 6: Errors of Ivan's (1994) method. Case study B. Contour interval: 0.5 mGal.

which coincide also with the maximum amplitudes in the initial SBA. The method of trend field separation (Fig. 7) reduces the truncation effect slightly. On the other hand the interior shows greater errors compared with Fig. 6. This study demonstrates that the separation of a long wavelength trend does not represent a general approach to solve the truncation problem. A successful application depends highly on the structure of the initial field. In this case the separation of a trend field results in a reduction of amplitudes of the residual field neither in the interior nor in the boundary regions. Therefore minimizing the amplitudes of the initial field especially in the edge areas and reducing in that way the truncation effect fails.

On the contrary the method of appropriate field extension strongly improves the results. Fig. 8 shows the errors using a field extension of 20 km on each side. The result in the interior is similar to Fig. 6, but the truncation effect has been prominently reduced. Though it should be mentioned that a field extension means increasing dimensions, which could be of relevance considering computation time.

Tab. 4 compares the statistics of the Figs. 6 to 8 and includes the reduction anomaly continued upward analogous to Tab. 2, assuming a reduction level of 602 m (minimum station altitude).

(4) Xia

Fig. 9 shows the difference between the field continued by Xia's method after 10 iterations and the exact field at 3000 m. The density distribution has been located immediately below the minimum station altitude at a level of 500 m in order to obtain fast convergence and to

cope as far as possible with the high-frequency content. The initial field has been extended by 50 km on each side to avoid FFT edge effects.

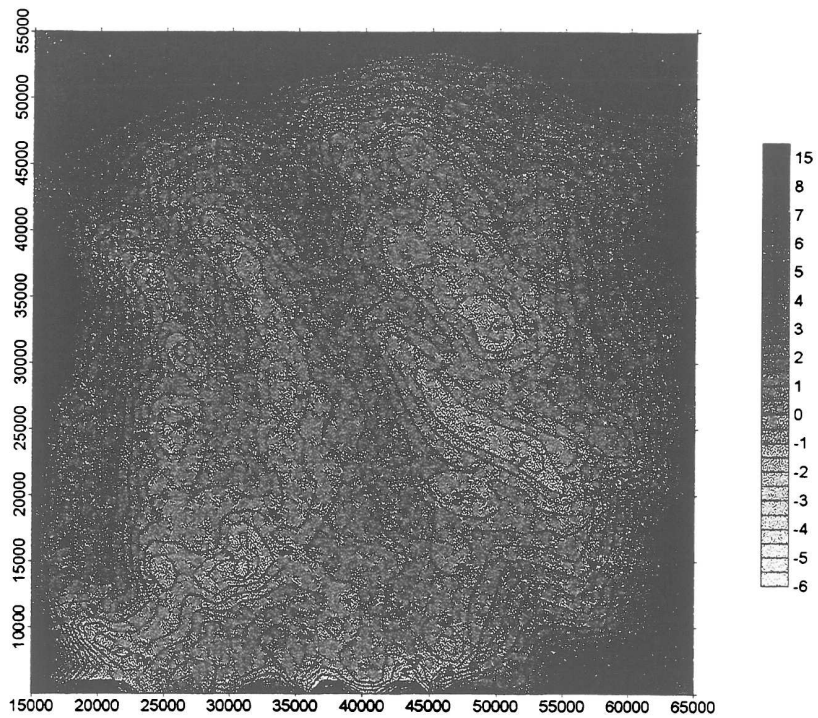

Fig. 7: Errors of Ivan's (1994) method. Case study B. Trend separation. Contour interval: 0.5 mGal.

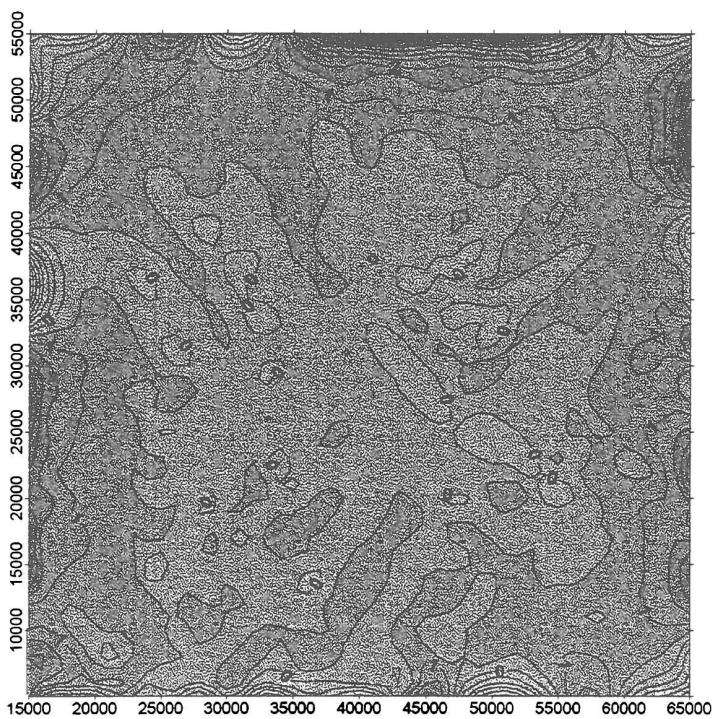

Fig. 8: Errors of Ivan's (1994) method. Case study B. Field extension. Contour interval: 0.5 mGal.

method	Fig.	mean [mGal]	min. dev. [mGal]	max. dev. [mGal]	RMS [mGal]
original	6	- 5.46	- 68.93	0.25	8.90
separation of trend	7	4.83	- 5.79	19.04	3.15
field extension 20 points	8	0.66	- 3.65	7.09	0.86
reduction anomaly (continued)	----	- 1.18	- 24.50	12.96	6.05

Tab. 4: Ivan's method - different approaches to reduce the truncation effect: errors on continuation level 3500 m

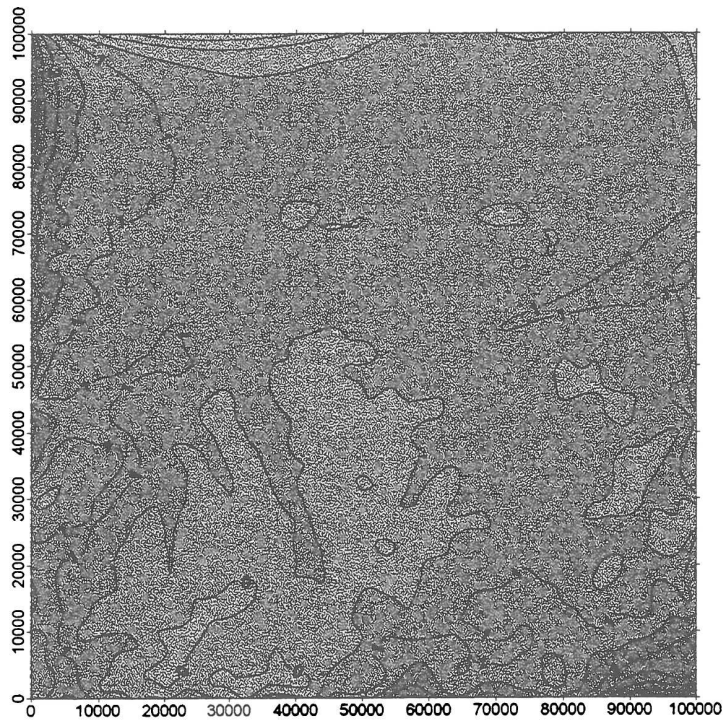

Fig. 9: Errors of Xia's (1994) method. Contour interval: 0.5 mGal.

The method proves to be very reliable and stable even in case of extremely rugged topography and high-frequency fields, as long as no sources exist between topography and the density distribution level, because such a configuration would violate the theoretical requirements of this algorithm. The most striking problem obviously is the correlation of the errors with topographic structures. The smaller the distance between the equivalent source layer and the continuation level, the stronger are the amplitudes of these high-frequency errors. On the other hand the choice of a great depth of the density layer results in the failure in fitting high-frequency components adequately. Therefore a compromise is necessary to enable a correct continuation of shallow disturbing masses and at the same time to ensure a sufficient net continuation distance. In addition all problems inherent to discrete Fourier transform occur, e.g. leakage. A reduction of edge effects can be achieved by applying the trend field separation method described in paragraph (1). In this case the long wavelength component is continued by Cordell´s procedure, the residual field by the method of Xia et al. (1993).

(5) Taylor series expansion

Fig. 10 shows the errors made by Taylor series expansion on the plane 3000 m. The initial field has been extended by 50 km on each side. Only terms up to 2nd order have been considered. The algorithm tends to become unstable, particularly in the case of high-frequency fields.

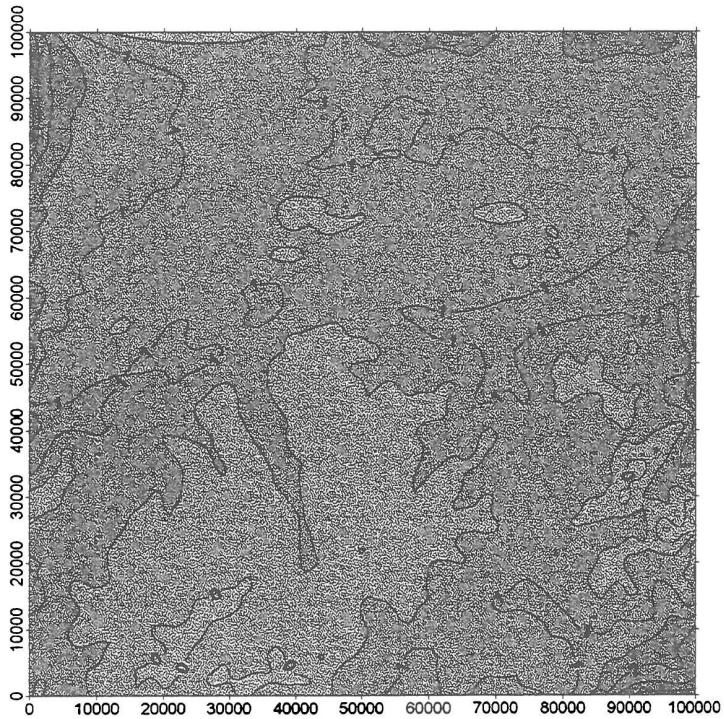

Fig. 10: Errors of Taylor series expansion method. Contour interval: 0.5 mGal.

(6) Chessboard-Method

Fig. 11 shows the errors of chessboard method on the plane 3000 m using 10 interpolation levels and field extension of 50 km on each side. The result demonstrates a significant correlation with topography due to the simplistic assumptions of this algorithm.

(8) Vertical gradient methods

In the first step the vertical gradient of the initial field has been calculated applying a low pass filter with a cut off wavelength of 10 km. So an improved Bouguer anomaly according to Grant and West (1965) is obtained. A second run of this procedure yields an improved free-air correction term (Meurers 1992), which is applied to approximate the RBA on zero level. The following level to level continuation to the plane 3000 m results - after subtraction of the exact field on the same level - in the difference field shown in Fig. 12.

It should be mentioned that the long wavelength nature of the test example is an advantage to this method. In case of high-frequency components it works incorrectly, because shallow masses are not taken into account adequately within the free-air correction term due to the indispensable low pass filtering during the calculation of the vertical gradient. Therefore short wavelength anomalies can not be continued correctly.

4. Field example

This paragraph investigates the continuation methods on the basis of real data. The topography (Fig. 13) varies between 530 m and 2530 m. The crosses mark the station locations. The gravity data have been interpolated on a 31 × 41 grid with spacing of 1 km (Fig. 14).

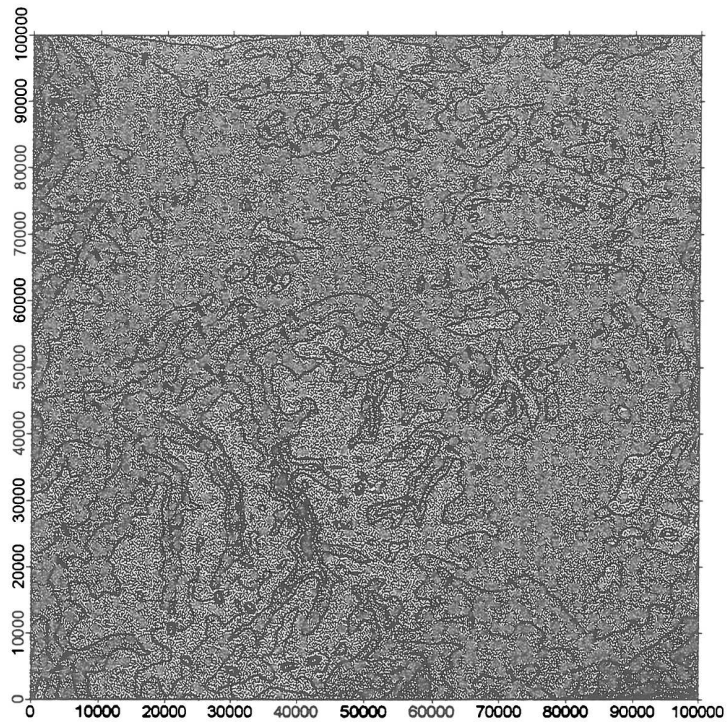

Fig. 11: Errors of chessboard method. Contour interval: 0.5 mGal.

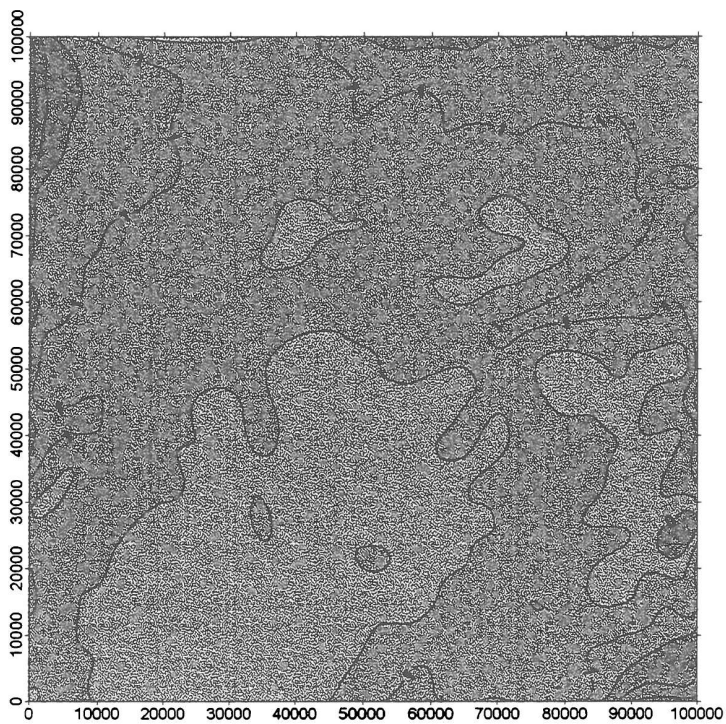

Fig. 12: Errors of vertical gradient method. Contour interval: 0.5 mGal.

In the following the continuation solution by Xia's method serves as reference field on the plane 2600 m, because this algorithm has proved to be very reliable and stable even in the case of extreme relief.

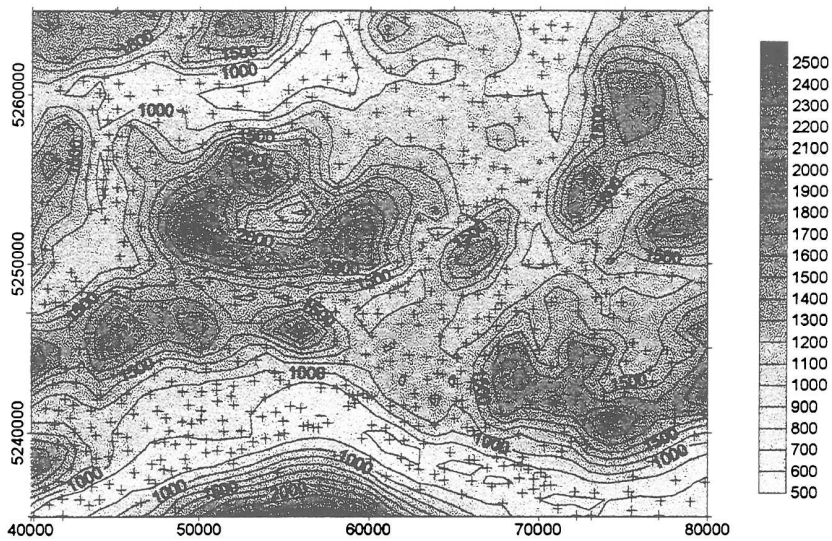

Fig. 13: Topography (real case study). Contour interval: 200 m.

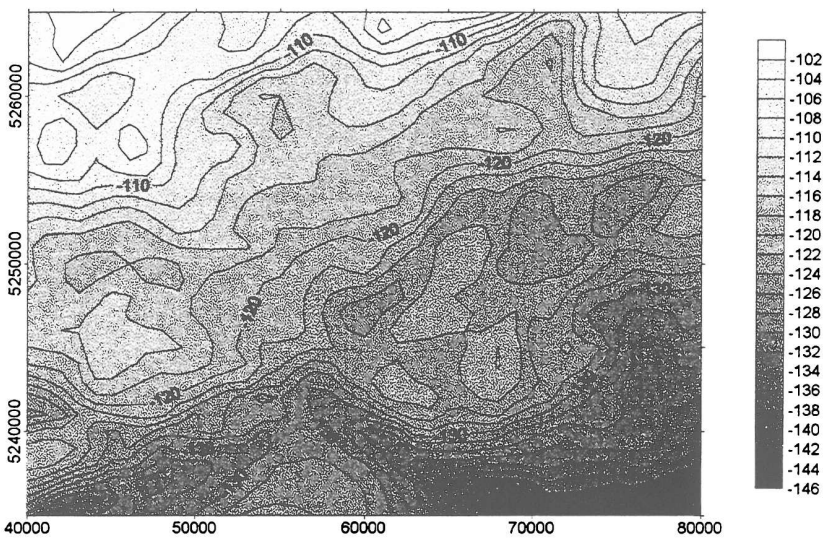

Fig. 14: Bouguer anomaly (SBA, real case study). Contour interval: 2 mGal.

(1) Fig. 15 shows the deviations of the result achieved by Cordell´s method after 1000 iterations (prop. factor = 1.4) from that one by Xia et al. The prominent edge effects in Fig. 15 can be eliminated by separate continuation (Fig. 16; prop. factor = 10.0, 840 iter.) of the trend obtained by wavelength filtering (cut off wavelength 30 km).

(2) Fig. 17 demonstrates the result of separately continuing the trend field by Cordell´s method (cut off frequency 30 km; prop. factor = 10.0, 840 iter.) and the residual field by Ivan's algorithm (field extension 20 km on each side, 6 iter.). The result differs only marginally from that one obtained by Xia's method.

(3) Fig. 18 shows the difference field concerning the chessboard technique using 10 interpolation levels. Obviously the result correlates significantly with topography.

(4) The Taylor series expansion (Fig. 19; 1 iter.) shows only small deviations from Xia's result on the plane 2600 m. Merely the valley structure stands out.

(5) One of the main disadvantages concerning the vertical gradient methods is the arbitrariness relating to the choice of a sufficient cut off wavelength during the indispensable filtering procedure. This problem can be demonstrated by comparing the different results obtained with cut off wavelength of 5 km (Fig. 20) and 10 km (Fig. 21).

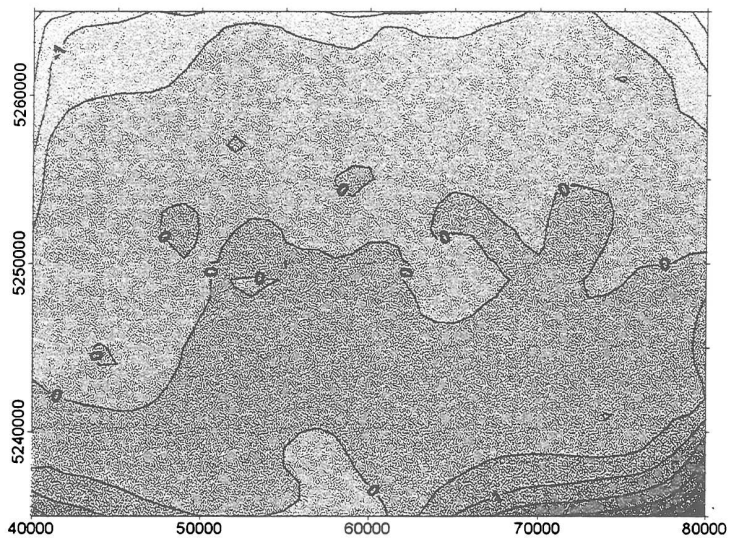

Fig. 15: Errors of Cordell's method. Contour interval: 0.5 mGal

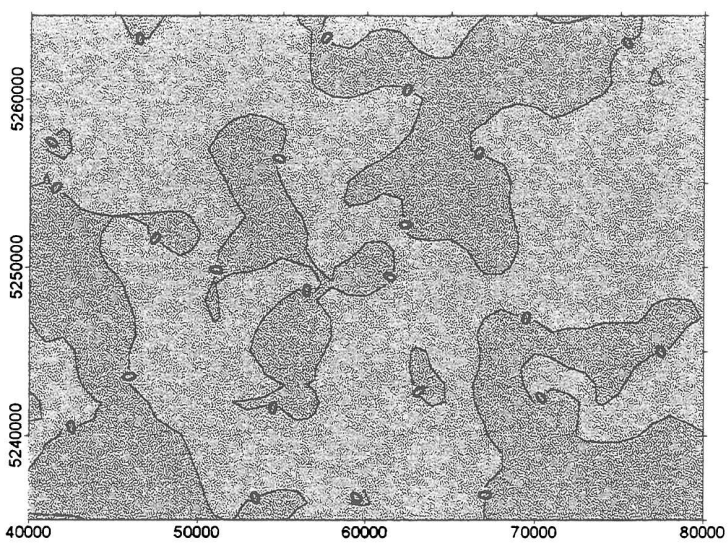

Fig. 16: Errors of Cordell's method. Trend separately continued. Contour interval: 0.5 mGal

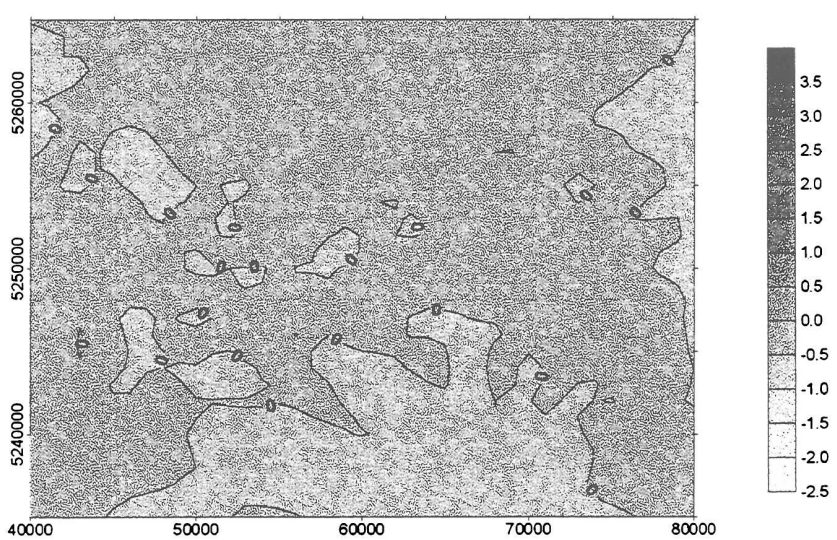

Fig. 17: Errors of Ivan's method. Trend continued separately by Cordell's procedure. Contour interval: 0.5 mGal.

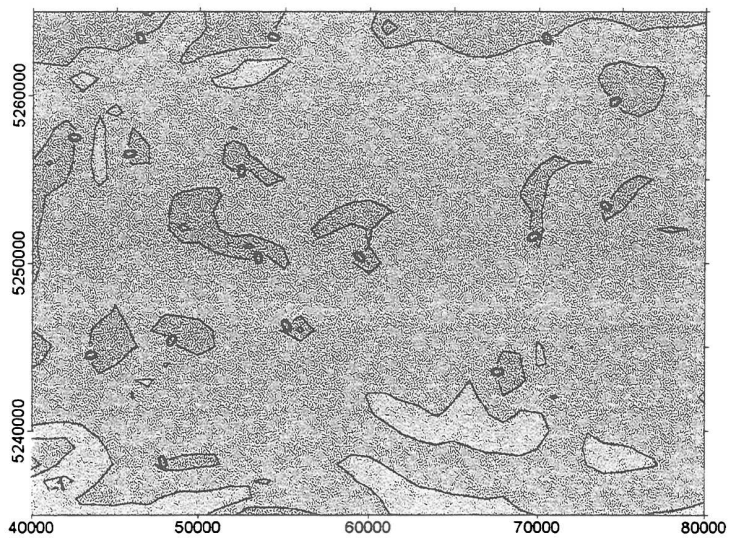

Fig. 18: Errors of chessboard method. Contour interval: 0.5 mGal.

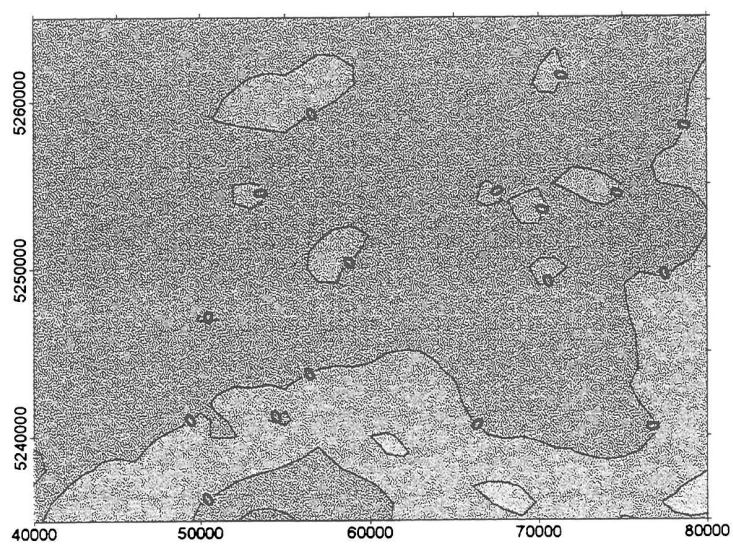

Fig. 19: Errors of Taylor series expansion. Contour interval: 0.5 mGal.

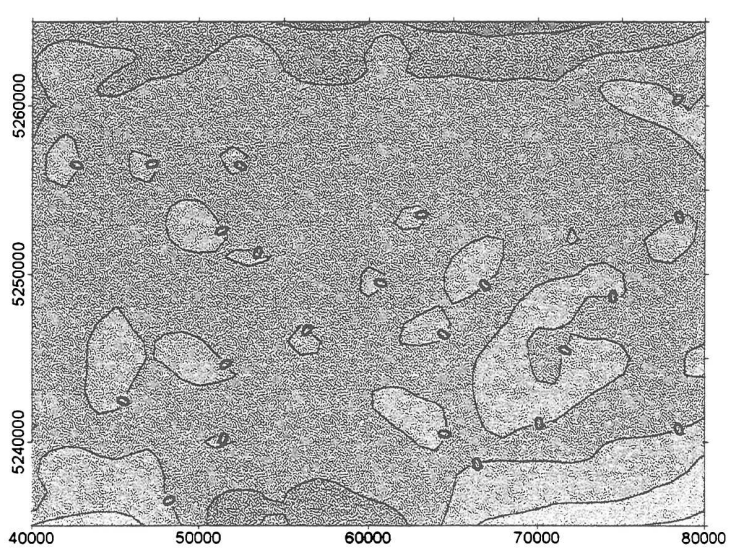

Fig. 20: Errors of vertical gradient method. Contour interval: 0.5 mGal.

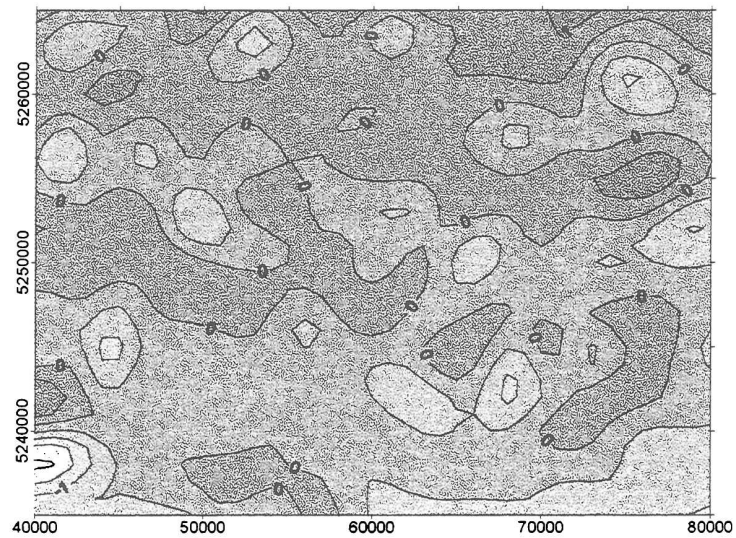

Fig. 21: Errors of vertical gradient method. Contour interval: 0.5 mGal.

Tab. 5 analyses the differences between the results of the given continuation method and the result according to Xia et al. (10 iterations) at 2600 m.

method	Fig.	mean [mGal]	min. dev. [mGal]	max. dev. [mGal]	RMS [mGal]
Cordell	15	- 0.02	- 2.25	4.00	0.53
Cordell (separation of trend)	16	- 0.01	- 0.53	0.63	0.13
Ivan - separation of trend	17	0.04	- 0.35	0.53	0.10
„chessboard"	18	- 0.20	- 1.13	0.79	0.23
Taylor series expansion	19	0.04	- 0.61	0.78	0.17
Meurers (5 km)	20	0.17	- 1.21	1.27	0.32
Meurers (10 km)	21	- 0.09	- 2.14	1.21	0.43

Tab. 5: Real field study -:differences referring to Xia et al. on the plane 2600 m

5. Conclusions

Both synthetic and field studies of this paper demonstrate the similarity of the method's results. All the algorithms except for the method of Graber-Brunner et al. (1991) are appropriate to reduce the initial reduction anomaly. However, in case of short wavelength fields on extreme topographic relief Ivan's and Xia's methods give more accurate results than the others. This has been shown by Pail (1995) and is not discussed by this paper.

Frequently Cordell´s continuation routine produces quite prominent edge effects and high frequency errors due to the use of discrete sources for fitting the SBA field. Both problems can be considerably reduced by the proposed method of trend field separation (Pail 1995). The results of the chessboard technique correlate significantly with topography, which can be explained with the simplistic basic assumptions of this algorithm. Taylor series expansion is a fast method that tends to become unstable in case of gravity fields with high frequency content. Calculating the vertical derivatives requires low pass filtering so that high frequency information is lost. The vertical gradient methods, which have originally been developed for downward continuation, are burdened with similar problems. As low pass filtering is necessary for calculating the free-air correction term the high-frequency components can not be continued correctly. Xia's FFT-method is a very fast, reliable and stable routine even in case of high-alpine relief.

From a theoretical point of view the equivalent source methods are only working correctly if the source distribution coincides with the observation surface. In that case very shallow sources can be represented, too. From all investigated methods only the one of Ivan (1994) fulfills this condition. The most striking problem of Ivan's algorithm certainly is the truncation effect that could only be partially reduced by the methods introduced in this paper. Except of the edge regions the results obtained by Ivan's and Xia's methods are of a similar quality. Therefore Xia´s routine should be preferred regarding the long computation time required by Ivan's procedure. However, once more it has to be pointed out, that Ivan's method is the only one discussed in this paper that is able to represent and to continue high-frequency components generated by sources located within the range of station altitudes. The special case study investigating the gravity field caused by topographic masses proves the excellent performance of Ivan's method even if short wavelength features are dominant. In practice, however, this advantage often is lost because of wide grid spacing. Usually station intervals are large (> 3 km) in mountainous regions and in that case high frequency signals are not well represented by the observed gravity data. This justifies to apply also methods which basically assume Laplace' equation to be valid in a specified range below topography although this is not true in most cases. Ivan's algorithm is especially suited for detailed gravity investigations in mountainous areas.

6. References

Bhattacharyya B.K., Chan K.C., 1977. Reduction of magnetic and gravity data on an arbitrary surface acquired in a region of high topographic relief. Geophysics, 42, 1411-1430.

Bott M.H.P., 1960. The use of rapid digital computing methods for direct gravity interpretation of sedimentary basins. Geophys. J., 3, 3-67.

Cordell L., Grauch V.J.S., 1982. Reconciliation of the discrete and integral Fourier transforms. Geophysics, 47, 237-243.

Cordell L., 1985. Techniques, applications and problems of analytical continuation of New Mexico aeromagnetic data between arbitrary surfaces of very high relief. Proceedings of the international meeting on potential fields in rugged topography, Institut de Géophysique Université de Lausanne, 96-101, Lausanne.

Cordell L., 1992. A scattered equivalent-source method for interpolation and gridding of potential-field data in three dimensions. Geophysics, 57, 629-636.

Dampney C.N.G., 1969. The equivalent source technique. Geophysics, 34, 39-53.

Götze H.J., Lahmeyer B., 1988. Application of three dimensional interactive modeling in gravity and magnetics. Geophysics, 53 , 1096-1108.

Graber-Brunner V., Klingelè E., Marson I., 1991. An improved solution for the problem of upward continuation of gravity field data in rugged topography. Bollettino di Geofisica Teorica ed Applicata, Vol. XXXIII. N. 130-131, p. 135-144.

Granser H., 1982. Allgemeine Feldfortsetzung und Verfahren zur Dichtebestimmung angewandt auf gravimetrische Untersuchungen im Hochgebirge. Unpublished Ph.D. Thesis, University Vienna.

Grant F.S., West G.F., 1965. Interpretation theory in applied geophysics. McGraw Hill Book Co. Inc., New York.

Grauch V.J.S., 1984. FORTRAN-Program "Taylor". In: Cordell L., Phillips J.D., Godson R.H., 1992. USGS Potential Field geophysical software, Version 2.0. USGS Open File Report 92-18.

Hansen R.O., Miyazaki Y., 1984. Continuation of potential fields between arbitrary surfaces. Geophysics, 49, 787-795.

Henderson R.G., Cordell L., 1971. Reduction of unevenly spaced potential field data to a horizontal plane by means of finite harmonic series. Geophysics, 36, 856-866.

Ivan M., 1994. Upward continuation of potential fields from a polyhedral surface. Geophysical Prospecting, 42, 391-404.

Lahmeyer B., 1988. Gravity field continuation of irregularly spaced data using least squares collocation. Geophysical Journal, 95, 123-134.

Lahmeyer B., 1989. Anwendungen der schnellen Fouriertransformation und der Quadratischen Programmierung bei der Interpretation von Schwerefeldern. Unpublished Ph.D. Thesis, FU Berlin.

Meurers B., 1992. Untersuchungen zur Bestimmung und Analyse des Schwerefeldes im Hochgebirge am Beispiel der Ostalpen. Österreichische Beiträge zu Meteorologie und Geophysik, Heft 6, Wien.

Pilkington M., Urquhart W.E.S., 1990. Reduction of potential field data to a horizontal plane. Geophysics, 55, 549-555.

Tsuboi C., 1965. Calculation of Bouguer anomalies with due regard to the anomaly in the vertical gravity gradient. Japan Acad. Proc., 41, 386-391.

Xia J., Sprowl D.R., 1991. Correction of topographic distortion in gravity data. Geophysics, 56, 537-541.

Xia J., Sprowl D.R., Adkins-Heljeson D., 1993. Correction of topographic distortions in potential-field data: A fast and accurate approach. Geophysics, 58, 515-523.

A NON-ITERATIVE 3-D INVERSION OF A GRAVITY ANOMALY IN THE VICINITY OF BAD AUSSEE (STYRIA)

Rainier Arndt, Alexander G. Römer and Wolfgang Seiberl

Institute of Meteorology and Geophysics, University of Vienna

Abstract

During the 80 'ies two geophysical campaigns had been conducted to map a negative gravity anomaly in the SW vicinity of Bad Aussee (Styria). Results derived from the data suggest a diaphir-like salt body. Three dimensional inversion methods available at this time have been restricted in their mining geological operability. Therefore, the former results have been re-interpreted by a modern Fourier-based non-iterative 3-D inversion. This non-iterative inversion algorithm, based upon a 3-D Fourier transform expression for the gravitational field of homogenous bodies, employs the spatial equivalent of frequency-domain autoregression to determine a series of coefficient from which the positions of polyhedral vertices, called depths points, are calculated. The number of these gross depths points is reduced to a final batch of vertices forming an polyhedral envelope around the proposed body. The solutions correlate well with results derived from former geophysical campaigns and are geological interpretable. The causative body associated with this gravitational anomaly has an depth extend of 100 m to 1100 m below surface.

Alpine Saline Deposits

Salt mining has a long tradition in Austria and is still done in three locations

- Bad Ischl
- Alt-Aussee
- Hallstatt.

According to ANONYMOUS (1986) in 1985 the total production reached approx. 2.2 Million m^3 of brine. The geographical position of the salt mining districts is given in Fig. 1

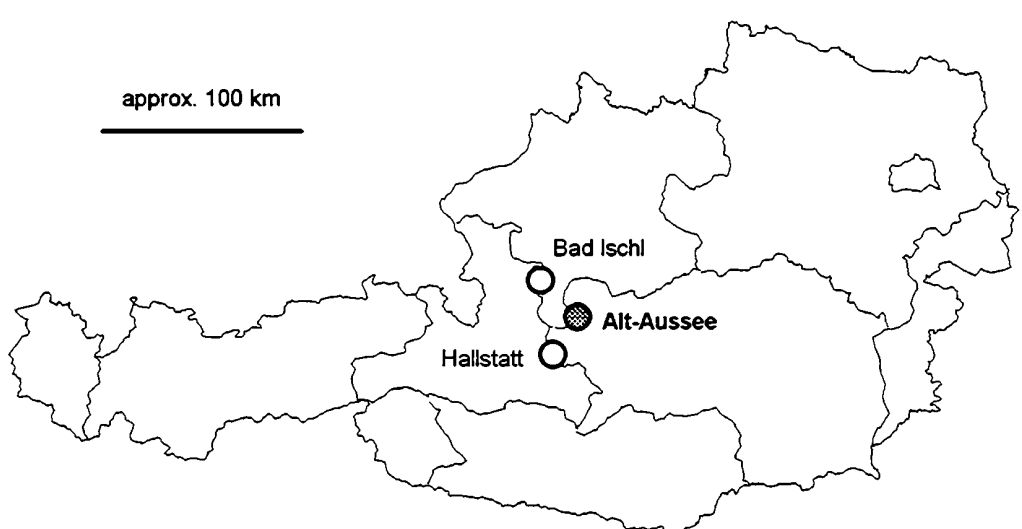

Fig. 1:
Geographical Position of Salt Mining Districts

The geological position of the mineable alpine saltdeposits are associated with the Permoskyt successions of the northern calcareous Alps. Inside this sedimentation cycle the salt beds are associated with the HALLSTÄTTER facies, thus having an age of ≈ 200 Mill years. During the Alpidic orogenesis the initial successions were overthrusted, tectonized and, finally knead with adjoining strata together. PETRASCHEK&POHL (1982) described these salt-bearing structures as sediments in a saliniferous depositional environment altered by post-tectonization processes. Salt diapirism is widely observed around the mining locations. At present, the exploitation strategy applied is lixiviation.

Mining Geophysical Campaigns

The high degree of plasticity in conjunction with adjoining positions to regional structural interfaces explain the complicated structure of salt deposits. As a result of the absence of sharp boundary surfaces between salt and the surrounding host rocks mining-geophysical campaigns remain a challenge.

Within the framework of the International Geodynamic Project and within the national reconnaissance aeromagnetic survey the anomaly in the vicinity of the village Bad Aussee was discovered and roughly outlined in 1980. Five years later STEINHAUSER *et al.* (1985) conducted a second geophysical campaign to resolve more details of this potential field peculiarity. The geophysical methods applied during the latter survey focused on refraction- and reflexion-seismics which had been combined with a high resolution gravity survey. The distribution of the gravity stations plotted onto the topographic contour lines is given in Fig. 2. This drawing, showing the dense distribution of approx. 18 gravity points per km^2, give emphasis to obstacles encountered during high-resolution gravity surveys in alpine regions.

The results of both surveys finally merged into a regional and a local gravity map. Table 1 gives the slap densities in kg m^{-3} applied to the BOUGUER correction of both gravity surveys. With the anomalous feature circumscripted by two kinds of horizontal gradients - a steep (up to 16 mgal km^{-1}) in the north and south and a gentle one (≈ 4 mgal km^{-1}) at the east and west flanks (≈ 4 mgal km^{-1}), the average trend appears as WSW-E bound. The signal strength of this salient gravitational minimum reaches - 8 mgal below the regional field. The isolines in the horizontal section, Fig. 6, also emphasis the discussed detail of the local BOUGUER map.

Rock Type	Density [in kg m^{-3}]
Crustal Rock	2670
Lime	2680
Bitter Spar	2800
Till	2400
Gypsum	2200- 2400
Saliferous Rock	2140- 2240

Table 1: Slap densities of BOUGUER corrections within in the density district SW of Bad Aussee / Styria

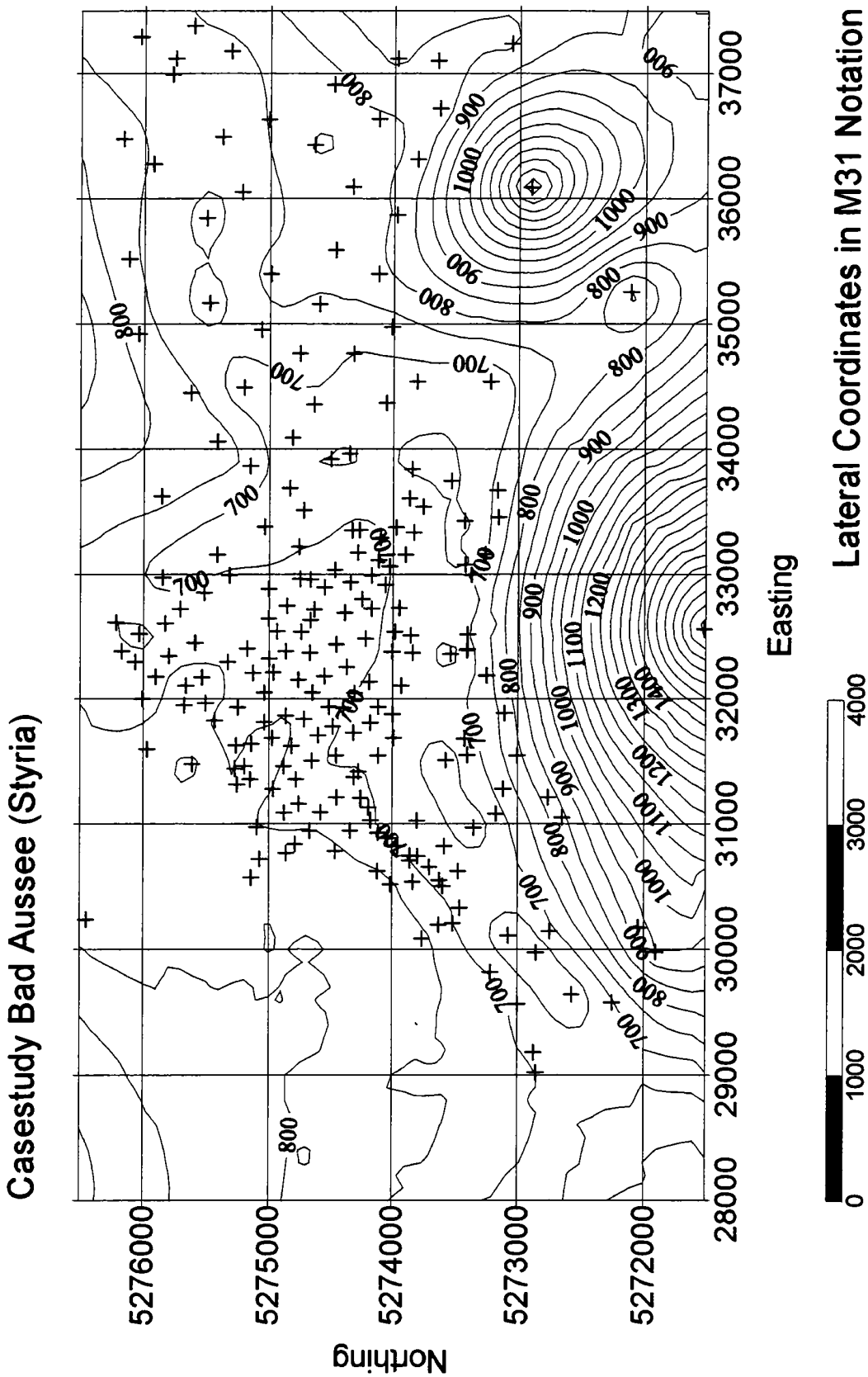

Fig. 2: Distribution of gravity stations plotted on the topographic contour lines in the vicinity of Bad Aussee, Styria.

Via a complex interpretation drawn from seismic and gravity data, an initial ambiguous geological model had been refined by combining the observation of high P-waves velocities, > 4000 m s $^{-1}$, with the mass deficiency traced to the negative anomaly. Thus STEINHAUSER *et al.*(1985) concluded, that a diaphir-like structure of salt with an estimated bulk deposit volume of approx. 3×10^{9} m^3 or an approx. size of 6×10^{12} kg is the source of the negative anomaly SW of Bad Aussee.

3-D Method

As it was pointed out by PEREYRA (1992), the 3-D modelling of deposits is seen as an important aspect of exploration geophysics. Based on the experience encountered by GÖTZE (1984), who compared results derived from 2-D and 3-D gravity inversions using a prominent gravity anomaly from the eastern alpine region, the decisission was made to re-interpret the initial findings from both Bad Aussee campaigns. The choice to apply a 3-D inversion is reinforced by LINDNER& SCHEIBE (1977), declaring the non-validity of 2-D algorithms for a complicated geology, and NABIGHIAN (1984), observing various success rates for the application of 2-D algorithm onto *real* field data. By applying a non-iterative algorithm, no initial guess for a start model is needed, hence an unbiased approach is guaranteed.

The inversion routine used in this gravity data processing is based on a forward algorithm introduced by HANSEN & WANG (1988). This forward expression, herein given as (E2) for magnetic and (E1) for gravity, calculates the contributions of the single facets of an individual homogeneous polyhedron in the time-domain of a FOURIER-transform. Fig. 3 provides the notation for the input data of (E1, E2). By summing up the various spectral components of several polyhedral bodies and performing a spatial transform on the whole spectrum, the potential field of even complicated structures is gained.

Fig. 3: Geometry of a triangular facet with vertex point P_j formed by three edges $\mathbf{m}_{j-1}$, $\mathbf{m}_{j-2}$ and $\mathbf{m}_{j-3}$.

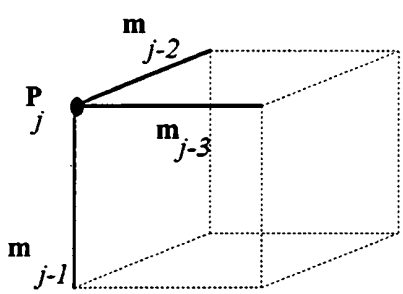

$$(E1)\quad \tilde{g}_{ej}(\mathbf{k}) = -2\pi\, G\rho \frac{1}{k} \frac{(\mathbf{e}\cdot\mathbf{K})(\mathbf{m}_{j-1}\times\mathbf{m}_{j-2})\cdot\mathbf{m}_{j-3}}{(\mathbf{m}_{j-1}\cdot\mathbf{K})(\mathbf{m}_{j-2}\cdot\mathbf{K})(\mathbf{m}_{j-3}\cdot\mathbf{K})} E_j$$

$$(E2)\quad \tilde{B}_{ej}(\mathbf{k}) = -2\pi \frac{1}{k} \frac{(\mathbf{J}\cdot\mathbf{K})(\mathbf{e}\cdot\mathbf{K})(\mathbf{m}_{j-1}\times\mathbf{m}_{j-2})\cdot\mathbf{m}_{j-3}}{(\mathbf{m}_{j-1}\cdot\mathbf{K})(\mathbf{m}_{j-2}\cdot\mathbf{K})(\mathbf{m}_{j-3}\cdot\mathbf{K})} E_j$$

with

$\tilde{g}_{ej}(\mathbf{k})$	Sum of contribution of vertex j to the total gravity field of a homogenous polyhedral body - as 2D discrete FOURIER-time domain notation for position **k** of the spectra
$\tilde{B}_{ej}(\mathbf{k})$	Sum of contribution of vertex j to the total magnetic field of a homogenous polyhedral body - as 2D discrete FOURIER-time domain notation for position **k** of the spectra
e	unit vector in direction of FOURIER-transformed spectra

E_j	Exponential factor, whereas $\exp(-ik_x x_j - iky\ y_j - k z_j)$ $= \exp(-\mathbf{K} \cdot \mathbf{r}_j)$
G	Universal gravitational constant, SI notation $(6.673 \pm .003) \cdot 10^{-11}\ m^3\ kg^{-1}\ s^{-2}$
k	$\lvert \mathbf{k} \rvert$
k	Component of wave in the (k_X, k_Y, 0) plane
J	Magnetisation vector of body
$\mathbf{m}_{ji}$	unit vector of vertex j- with edges i, whereas $i = 1, 2, 3$
ρ	Density or density contrast

The inversion method presented by WANG&HANSEN (1990) is basically a three dimensional assemblage of the classic CompuDepths algorithm introduced by O'BRIEN (1973), their forward expression, HANSEN&WANG (1988), and NABIGHIAN 's (1984) generalised HILBERT transformation. This method is used to invert the gravitational field of the Bad Aussee anomaly and providing co-ordinates of a polyhedral source body given as so called *depth points*. Seen from a strictly theoretical approach, these depth points can be described as numerical solutions of the *Poisson Equation*.

Like in CompuDepths, no initial guess or density distribution is needed, but other constraints have to be met, such as

- approximation of source body by polyhedrons,
- homogeneously distribution of density or susceptibility,
- regularly sampled data on a constant elevation;
- an even number of depths points to be calculated;

The inversion algorithm employs the spatial-equivalent of an autoregression in the frequency-domain to determine a series of coefficient. These coefficients are used as input-data for complex polynomials, which, in the subsequent, give the lateral and horizontal position of depth points. In order to reflect the degree of freedom, which is determined by the given number of depths points to be calculated, different frequencies are resolved into polyhedral co-ordinates. Then, in a final procedure, all the batches of depth points derived from the different frequency components are compiled and evaluated by statistics.

A flowchart summarising the principle steps of this inversion strategy is given in Fig. 4.

Processing Strategy

With the inversion algorithm of WANG&HANSEN (1990) implemented in the computing environment of the University of Vienna, four main steps to invert gravity data had been conducted:

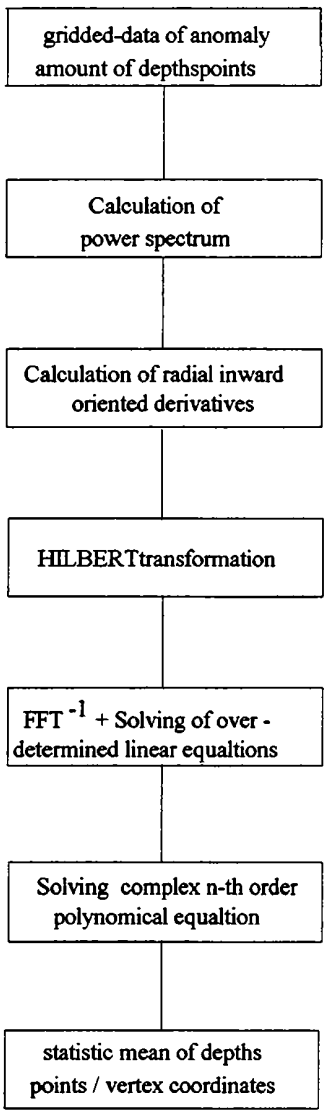

Fig. 4:
Flowchart of principle steps of the 3-D non-iterative inversion after WANG&HANSEN (1990)

- pre-processing
  within a PC environment the raw data are interpolated onto a square grid either using an algorithm proposed by BRIGGS (1974) or a geostatistical approach as introduced by MATHERON (1971). For this case-study a clipped window with 51 times 96 data points was prepared. However, depending on the FFT-subroutines used in the subsequent programme flow and the processing power available, the acceptable values of transform lengths have to be equal to the number of grid points in E and N direction.

- inversion
  The only inputs supplied to the inversion routine are the grid data and an even number of depth points to be calculated. Thus, several batches of depth points had been calculated to account for different spectral contents of the clipped data. In this casestudy batches of 12,14,..., 26 depth points for three different windows had been determined.

- post-processing
  As a primary step, all depth points calculated had been merged into one single file. By visual examination, points derived from the high-frequency part, containing an considerable amount of misinterpretable numerical noise, had been deleted. Also depth points

derived from the vicinity of the spectral DC-term, *cf.* BUTTKUS (1991), give no contribution to the final result. With the relative error margins set to $\leq$ 15 % for findings, other points had to be excluded also - derived from the widths of the standard derivation, which is calculated during the final processing step of the inversion algorithm, all depth points not meeting this quality level had been seggareted. Therefore the *n-raw* points, in this casestudy equal 324 gross depths points, are reduced to *n-net*, in this casestudy to 58 net depth points.

- visualisation
  For a better insight into the distribution pattern of the net points, a workstation-based visualisation package is used. The ability to mark and visualise arbitrary sections through the 3-D distributed point cluster and to form a single model is the actual key-operation for the final interpretation process. In a preparatory step the amount of *n-net* points is further reduced - only the points forming the outside of a volume are accepted.

- The following strategy is used for the shrouding: all possible facets spread between the *N-net* points, thus $n\text{-}net^3$ triangles, are calculated and the cross vector product is formed. By comparing the sizes and the spatial positions of all the unit vectors, marginal positions of the depth point cloud are identified and selected. In this casestudy, *n-yield* equals 22 depth points, forming an integument composed of 126 triangular facets. In a very last step these co-ordinate pairs had been fed into standard volumization & rendering routines to display a final model.

Derived Results

The presented results focused on the distribution of the *n-yield* points, but for the ease of interpretation all *n-net points* are discussed. A vertical S-N section, shown in Fig. 5, show a slight north-dipping cluster with an depth extend from 100 m to 1100 m below surface. The horizontal extend is approx. 1500 m. An E-W section is presented in Fig. 6, showing the same minimum/maximum depth distribution. To some extend a steep dip to the W is interpretable. The horizontal extend is approx. 2000 m. The top view in Fig. 7 gives the horizontal distribution of the 58 *n-net* depth points. A principle WSW-ENE trend, which correlates well with the average strike direction observed in the input-data, is demonstrated.

Discussion of Results

The second report, STEINHAUSER *et al.*(1985), proposed a model of uplifted block-like basin facies forming local sills with considerable displacements. The geometric parameter for this model, as derived from a complex geophysical interpretation, suggest a causative body stretching from 115 m to 775 m below surface. Based on this assumption, a 3-D forward model had been proposed by employing a 3-D forward algorithm published by TALWANI&EWING (1960), suggesting a WSW-ENE striking body with a depth extend from 135 m to 900 m below surface.

The *n-yield* depth point cluster derived from the applications of the WANG&HANSEN (1990) are well in accordance with the initial model published by STEINHAUSER *et al.* (1985).

Concerning the computational efficiency it is important to note, that sufficient hardware resources designed for numeric intensive computing, such as a multi-processor environment with a performance above 50 MFLOPs per chip, is compulsory. Whereas the CPU

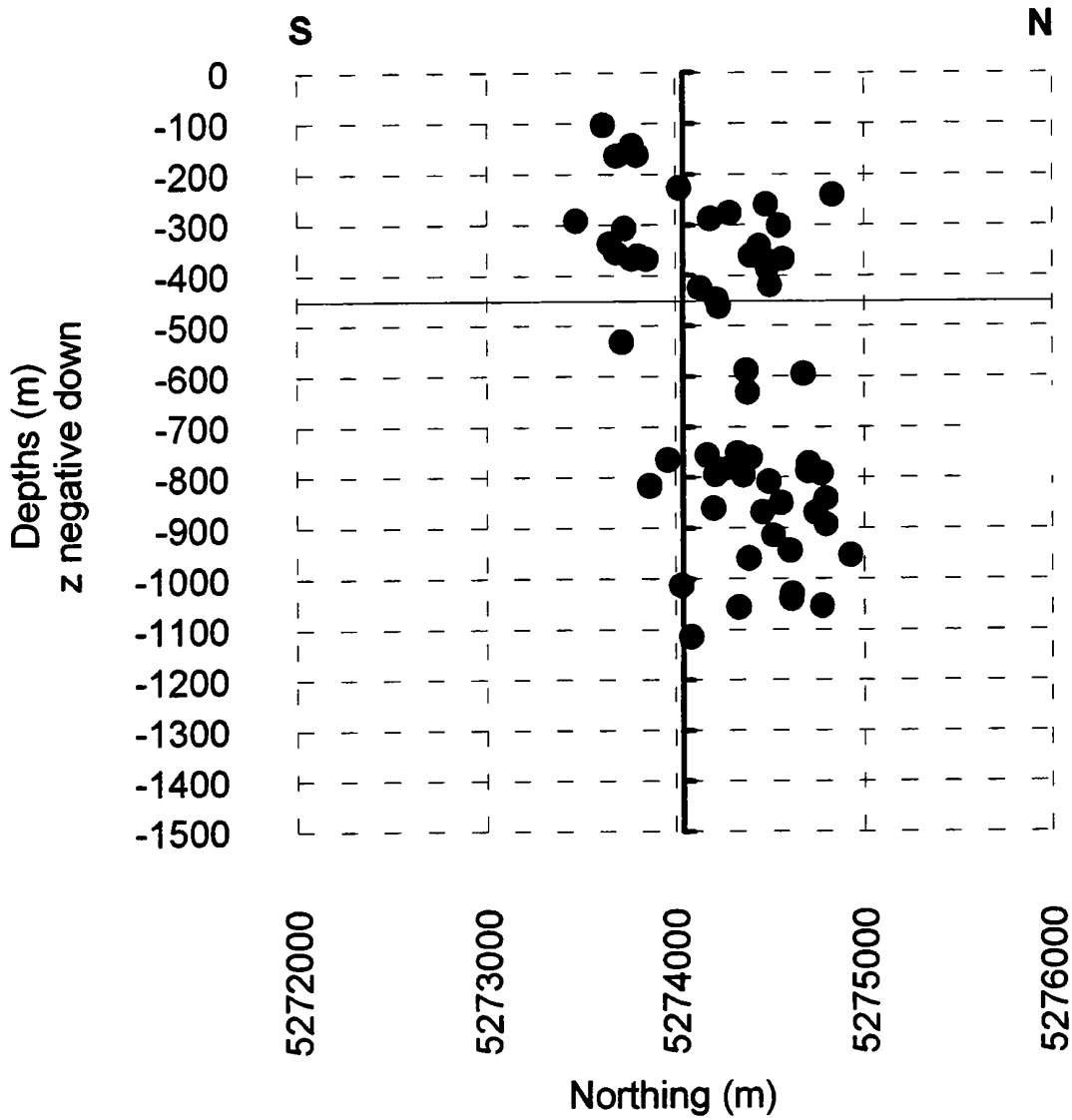

Fig. 5: Vertical S-N section of depthspoint distribution of a gravitational prospecting - casestudy Bad Aussee Anomaly. Note the vertical exaggeration of 1 to 2.7 and the M 31 system notation for the lateral coordinate.

time increases *quasi* linear with the number of depth points to be calculated, the memory requirements grows exponential - typical resource demand for a grid of 2560 data points, for the computation of batches with 14, 16, 18 .... 40 depth points, are approx. 70,000 CPU seconds and roughly 300 MB of working storage for an AlphaServer with 2100 4/275 processor. Despite the hardware necessities, this algorithm is useful for rapid examination of anomalies in large data sets and increases the efficiency of professional staff - within 8 man/hours a single casestudy can be prepared, inverted and an initial visualised model.

One typical problem, which is also adherent to the 3-D EULER deconvolution, REID *et al.* (1990), remains - the separation of valid from non-valid solutions is complex and based solely on the experience of the interpreter. However, the inversion algorithm of WANG&HANSEN (1990) is a good boundary finder and depth estimator for causative bodies, thus providing an initial model for further modelling.

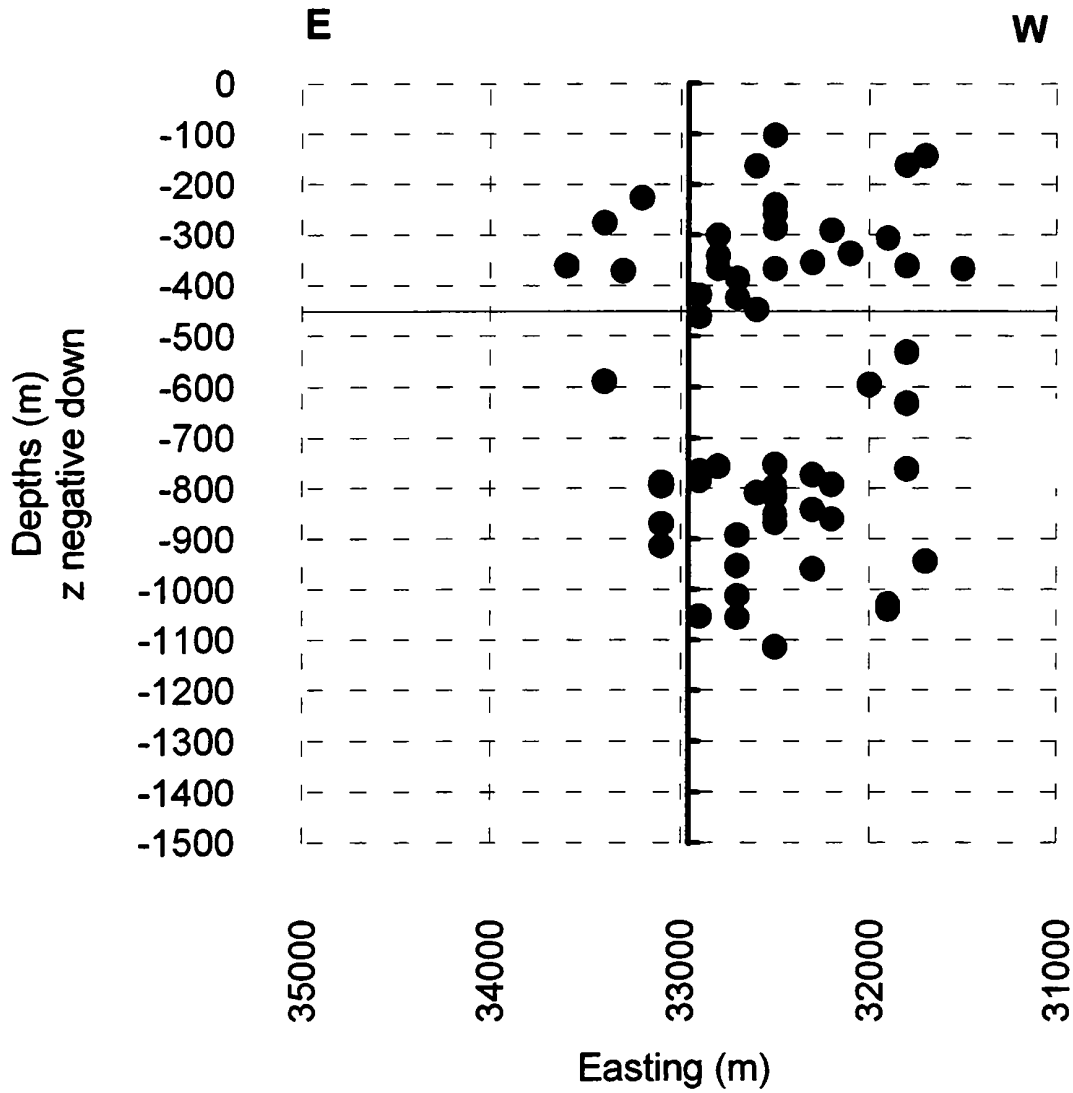

Fig. 6: Vertical E-W section of depthspoint distribution of a gravitational prospecting - casestudy Bad Aussee Anomaly. Note the vertical exaggeration of 1 to 2.7 and the M 31 system notation for the lateral coordinate.

Conclusion & Outlook

The 3-D inversion method described in this paper is best applied to real 3-D structures, because it provides realistic solutions for the geometry and the depths of the gravity source. A severe warning is necessary to be issued concerning the quality of raw data: If data are of poor quality, sources will be misinterpred or reported on a total wrong depths. Thus special care is necessary to choose the geometry and content of the initial window containing the element to be inverted. The grid has to be representative of the isolated anomaly clipped from large data sets.

The authors plan to combine results derived from the application of 3-D Euler deconvolution with depths points computed from the WANG&HANSEN (1990) algorithm to curtail the ambiguity of 3-Distributed point clusters. Further research is planned to feed validated points into forward algorithm, such as BARNETT (1976) or ROUTOISTENMÄKI (1993) aiming to provide relative density / susceptibility contrasts between causative bodies and host rocks.

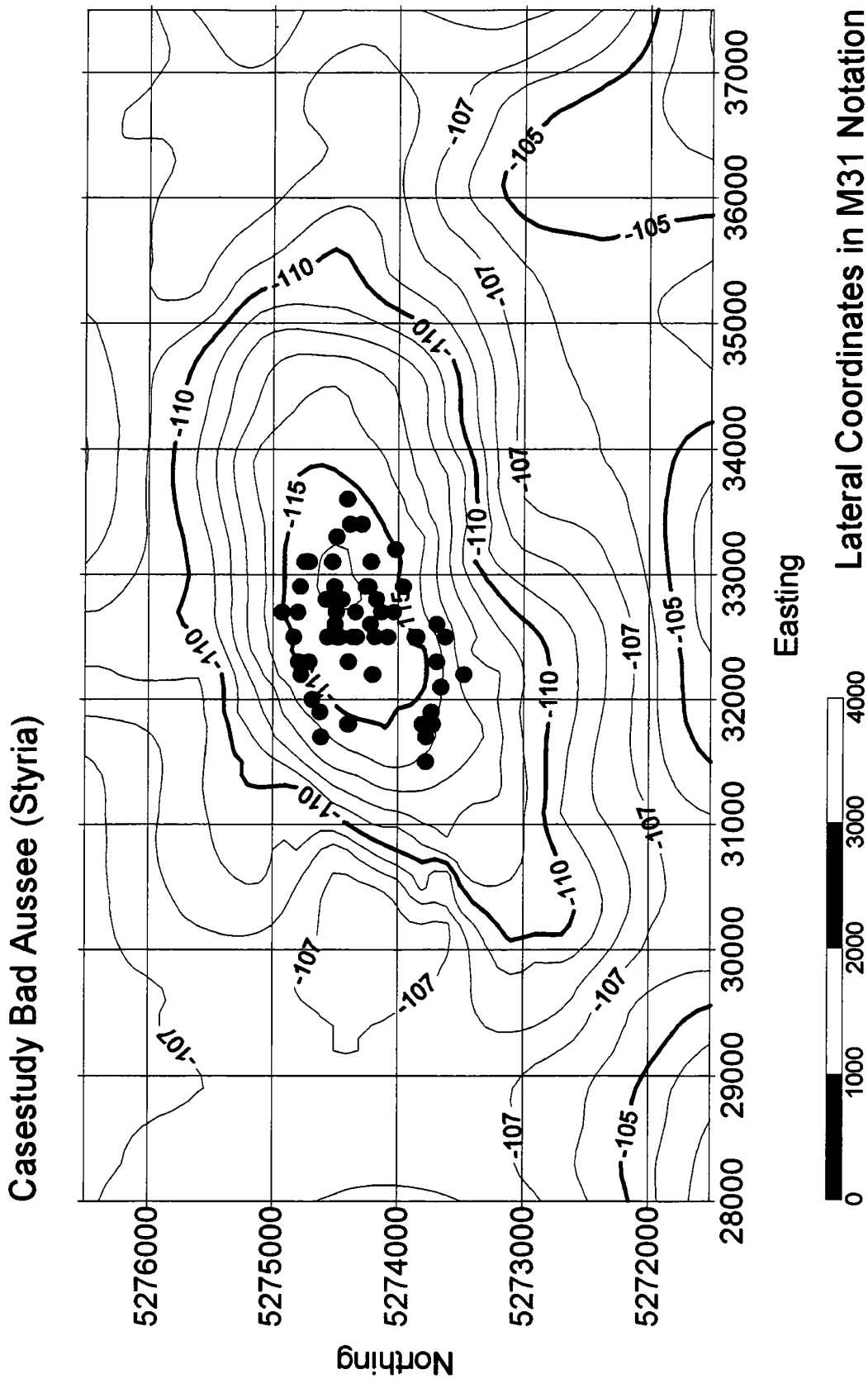

Fig. 7: Horizontal section of depthspoint distribution of a gravitational prospecting - casestudy Bad Aussee Anomaly. Note the the M 31 system notation for the lateral coordinates

Acknowledgement

The work reported in this paper was supported by DR. PETER MARKSTEINER from the computing centre at the Vienna University. The gravitational raw data have been prepared and provided by our colleague DR. BRUNO MEURERS and it is gratefully acknowledged.

Also the importance is felt to thank DR. A.S.M. WOOBAIDULLAH, Geophysicist and Associate Professor at the University of Dhaka, for many fruitful discussions during the course of preparation.

References

ANONYMOUS, 1986: Grundlagen der Rohstoffversorgung. In: Der Österreichische Bergbau. **2**, [Hrsg.] Bundesministerium für Handel, Gewerbe und Industrie, 119-145, Wien.

BARNETT, C.T., 1976: Theoretical Modelling of the Magnetic and Gravitational Fields of an Arbitrary Shaped Three-dimensional Body. Geophysics, **41**, 1353-1364.

BRIGGS, I.C., 1974: Machine Contouring Using Minimum Curvature. Geophysics, **39**, 39-48.

BUTTKUS, B., 1991: Spektralanalyse und Filtertheorie in der angewandten Geophysik. Springer, 1-650, Berlin.

GÖTZE, H.-J., 1984: Über den Einsatz interaktiver Computergraphik im Rahmen 3-dimensionaler Interpretationstechniken in Gravimetrie und Magnetik. Habilitationsschrift an der Mathematisch-Naturwissenschaftlichen Fakultät der Technischen Universität Clausthal, Clausthal Zellerfeld.

HANSEN R.O., WANG, X., 1988: Simplified Frequency-domain Expression for Potential Fields of Arbitrary Three-dimensional Bodies. Geophysics, **53**, 365-374.

LINDNER, H., SCHEIBE, R., 1977, Interpretationstechnik für gravimetrische und magnetische Felder. Freiberger Forschungshefte, **C 322**, 1-90, Leipzig.

MATHERON, G., 1971: The theory of regionalized variables and its application. Cahier **5**, Centre de Morphologie Mathématique de Fontainebleau, 211 ff.

NABIGHIAN, M.N., 1984: Toward a Three-Dimensional Automatic Interpretation of Potential Field Data via Generalized Hilbert Transforms: Fundamental Relations. Geophysics, **49**, 780-786.

O'BRIEN, D.P., 1973: CompuDepth, A New Method for depth-to Magnetic Basement Calculation. geoMetrics, 1-48, Sunnyvale.

PEREYRA, V., 1992: Two Point Ray Tracing in General 3 D Media. Geophysical Prospecting, **40**, 267-287.

PETRASCHEK, W.E., POHL, W., 1982: Lagerstättenlehre. E.Schweizerbartsche Verlagsbuchhandlung, Stuttgart.

REID A.B., ALLSOP, J.M., GRANSER, H., MILLET, A.J., SOMERTON, I.W., 1990: Magnetic interpretation in three dimensions using Euler deconvolution. Geophysics, **55**, 80-91.

ROUTOISTENMÄKI, T., 1993: The Magnetic Anomaly of 3D Sources Having Arbitrary Geometry and Magnetization. Geophysical Prospecting, **41**, 413-433, Zeist.

STEINHAUSER, P., MEURERS, B., ARIC, K., GRANSER, H., HÖSCH, K., KLINGER, G., LENHARDT, W., 1985: Geophysikalische Detailuntersuchung der Schwereanomalie von Bad Aussee. Geophysikalischer Forschungsbericht, **18**, Universität Wien, Institut für Meteorologie und Geophysik, Wien.

TALWANI, M., EWING, M., 1960: Rapid computation of gravitational attraction of three-dimensional bodies of arbitrary shape. Geophysics, **25**, 203-225.

WANG, X., HANSEN, R.O., 1990: Inversion for Magnetic Anomalies of Arbitrary Three-Dimensional Bodies. Geophysics, **55**, 1321-1326.

PROPERTIES OF THE TOTAL NORMALIZED GRADIENT OF POTENTIAL FUNCTION FOR THE DETERMINATION OF SOURCE DISTRIBUTIONS

Roman Pasteka
Institute of Geophysics, University of Vienna,
Department of Applied Geophysics, Comenius University, Bratislava

Abstract:

The basic property of the total normalized gradient operator $F = (f_x^2 + f_z^2)^{1/2}$, where f_x and f_z are the derivatives of the potential function with respect to the x and z directions) is shown for the case of 2D horizontal cylinder - the elimination of disturbing oscillations, which occur in the process of analytical continuation of a potential field (or its components) to the depths, which are close to the depth of the singularity or deeper. The maximum values of the total normalized gradient of a potential function $F^N(x,z)$ determine the position of shallower singularities for simple elementary bodies and by using empirical criteria, defined by Jelisejeva (1982) we can also make estimates about the depth of deeper sources. Results, obtained by means of this modification of the $F^N(x,z)$ method are shown for model studies and for one practical example from Gebharts region in Austria.

The method of the total normalized gradient is one of the most successful methods applied in "Russian potential school" for the determination of singular points of potential fields. This method was introduced in the middle 60's by V. M. Berezkin (Berezkin and Buketov, 1965; Berezkin, 1967) and further developed by him and many other authors (Jelisejeva 1982; Berezkin and Skotarenko, 1983; Berezkin, 1988; Jelisejeva, 1995) from the Moscow Geophysical Institute for Oil and Gas Prospecting (VNIIGeofizika). In western geophysical literature this method was published by Ciancara and Marcak (1979), Pasteka and Seiberl (1992) and also by Lindner and Scheibe (1977). The method of the total normalized gradient of potential function is very close to the method of analytical signal, introduced by Nabighian (1972), especially to it's later modification (Nabighian, 1974).

The basic property of the total normalized gradient operator $F = (f_x^2 + f_z^2)^{1/2}$, where f_x and f_z are the derivatives of the potential function with respect to the x and z directions) is the elimination of disturbing oscillations, which occur in the process of analytical continuation of a potential field (or its components) to the depths, which are close to the depth of the field singularity or deeper. From the point of view of the potential theory we cannot perform such a continuation (we cannot continue a potential field to the depths which are deeper than the position of the shallowest source), but for sampled fields it is possible to perform it formally (Jung, 1961; Berezkin, 1967). We only need to know and recognise all the distortions which result from ignoring this basic rule for the analytical continuation downwards.

For the analytical continuation we can use standard routine based on Fourier series (e.g. Jung, 1961)(we use the Sine Fourier series) which realises the analytical continuation in the wavenumber domain. For the analytical continuation of a harmonic function, given on interval <0,L>, to the level z we can write well known relation (for the 2D-problem):

$$f(x,z) = \sum_{n=1}^{N} B_n \sin\frac{\pi nx}{L}\, e^{\frac{\pi nz}{L}}, \qquad (1)$$

where $$B_n = \frac{2}{L}\int_0^L f(x,0)\sin\frac{\pi nx}{L}\,dx \cdot$$

For the derivatives with respect to the x- and z-direction we get:

$$f_x(x,z) = \frac{\pi}{L}\sum_{n=1}^{N} B_n \cos\frac{\pi nx}{L}\, e^{\frac{\pi nz}{L}} , \qquad (2)$$

$$f_z(x,z) = \frac{\pi}{L}\sum_{n=1}^{N} B_n \sin\frac{\pi nx}{L}\, e^{\frac{\pi nz}{L}} \qquad (3)$$

In Fig. 1,2 and 3 we can see such typical oscillations (we can see for deeper depth levels a dominant sinusoidal component with Nyquist wavelength) for gravity field and its first derivatives with respect to the x- and z- directions for a horizontal cylinder in the depth of 50 m. The scales of the graphs had to be adjusted, because of the strong increase of the values of the continued field (especially on levels deeper than 50 m).

In Fig. 4 we can see the total gradient (also the amplitude of the analytical signal), calculated from components f_x (x,z) and f_z (x,z) by means of relation:

$$F(x,z) = \sqrt{f_x^{\,2}(x,z) + f_z^{\,2}(x,z)} . \qquad (4)$$

As we can see, there still exists a strong increase of the continued values, but the disturbing oscillations are removed. This property of the total gradient (or amplitude of the analytical signal) was also shown by Nabighian (1974) for a function $Z^2(x)+H^2(x)$, where Z(x) and H(x) are the vertical and horizontal components of the magnetic field respectively.

For the case of the 2D horizontal cylinder we can analytically describe the behaviour of the continued field. For the Fourier spectrum of the gravity field V_z, caused by a 2D-horizontal cylinder with the centre in the depth h and length density λ (e.g. Gladkij, 1967) we can write for the level of continuation z :

$$S(\omega)_{V_z} = F\{V_z(x,z)\} = \int_{-\infty}^{+\infty} V_z(x,z)e^{-i\omega x}dx = 2\pi f\lambda e^{-\omega(h-z)} , \qquad (5)$$

where f - is the gravitational constant. Inverse Fourier transformation yields to an integral, which can be evaluated only for levels z<=h, for z>h is this integral singular. This is also the reason for the basic rule of analytical continuation: we can continue only to the depths which are shallower than the depth of the first singularity. It means that breaking this rule for functions with unlimited spectrum yields to a singular integral.

The inverse Fourier transformation of this spectrum for limited spectrum <- ω_c, ω_c> equals:

$$F^{-1}\{S(\omega)_{V_z}\} = V_{z(\omega_c)}(x,z) = \frac{1}{2\pi}\int_{-\omega_c}^{+\omega_c} S(\omega)_{V_z} e^{i\omega x}\, d\omega =$$

$$= 2f\lambda\frac{h-z}{(h-z)^2+x^2} - 2f\lambda\frac{e^{-\omega_c(h-z)}}{(h-z)^2+x^2}\left[(h-z)\cos\omega_c x - x\sin\omega_c x\right].$$

Similarly we can derive relations for the derivatives with respect to the x- and z-direction:

$$F^{-1}\{S(\omega)_{V_{xz}}\} = V_{xz(\omega_c)}(x,z) = \frac{1}{2\pi}\int_{-\omega_c}^{+\omega_c} S(\omega)_{V_{xz}} e^{i\omega x}\, d\omega =$$

$$= -4f\lambda\frac{x(h-z)}{\left[(h-z)^2+x^2\right]^2} + 2f\lambda\frac{e^{-\omega_c(h-z)}}{\left[(h-z)^2+x^2\right]^2}\left[A\cos\omega_c x + B\sin\omega_c x\right] =$$

$$= V_{xz}(x,z) + 2f\lambda \frac{e^{-\omega_c(h-z)}}{\left[(h-z)^2 + x^2\right]^2}\left[A\cos\omega_c x + B\sin\omega_c x\right], \qquad (6)$$

$$F^{-1}\left\{S(\omega)_{V_{zz}}\right\} = V_{zz(\omega_c)}(x,z) = \frac{1}{2\pi}\int_{-\omega_c}^{+\omega_c} S(\omega)_{V_{zz}} e^{i\omega x} d\omega =$$

$$= 2f\lambda \frac{(h-z)^2 - x^2}{\left[(h-z)^2 + x^2\right]^2} - 2f\lambda \frac{e^{-\omega_c(h-z)}}{\left[(h-z)^2 + x^2\right]^2}\left[B\cos\omega_c x - A\sin\omega_c x\right] =$$

$$= V_{zz}(x,z) - 2f\lambda \frac{e^{-\omega_c(h-z)}}{\left[(h-z)^2 + x^2\right]^2}\left[B\cos\omega_c x - A\sin\omega_c x\right], \qquad (7)$$

where $A = \omega_c x(h-z)^2 + \omega_c x^3 + 2x(h-z)$; $B = \omega_c(h-z)^3 + \omega_c x^2(h-z) + (h-z)^2 - x^2$.

We can see that breaking of the basic rule of analytical continuation for functions with a limited spectrum yields additive disturbing functions (containing sinusoidal and cosinusoidal components with the wavelength = ω_c) which "overlay" the correct solution for greater depths than the depth of the source.

We now create a summation of squares from these two derivatives (6), (7) and obtain:

$$V_{xz}^{\ 2}{}_{(\omega_c)}(x,z) + V_{zz}^{\ 2}{}_{(\omega_c)}(x,z) = V_{xz}^{\ 2}(x,z) + V_{zz}^{\ 2}(x,z) + 4f^2\lambda^2 \frac{e^{-2\omega_c(h-z)}}{\left[(h-z)^2 + x^2\right]^4}\left[A^2 + B^2\right] -$$

$$- 16f^2\lambda^2 \frac{x(h-z)e^{-\omega_c(h-z)}}{\left[(h-z)^2 + x^2\right]^4}\left[A\cos\omega_c x + A\sin\omega_c x\right] - 8f^2\lambda^2 \frac{\left[(h-z)^2 - x^2\right]e^{-\omega_c(h-z)}}{\left[(h-z)^2 + x^2\right]^4}\left[B\cos\omega_c x - A\sin\omega_c x\right]. \qquad (8)$$

As we can see, the obtained result consists of three components: the first is a sum of squares from "correct" derivatives of the field $V_{xz}^{\ 2}$ (x,z)+ $V_{zz}^{\ 2}$ (x,z) , the second component describes the disturbing part (without oscillations) with dominant exponential function, which increases for z>h, and the third component, which is more complicated and contains the oscillating terms, the amplitude of which decrease faster with the x-distance from the source as that in equations (6) and (7). In the Fig. 5, 6, 7 and 8 we can see the graphs of the total gradient and its three components on depth levels z = 21 m, 41 m, 61 m and 71 m (passing the singularity in the depth of 50 m). We can see that there is a compensation of the disturbing oscillations, but they are not totally removed. Sinusoidal and cosinusoidal component stay in the third component, but their amplitudes decrease very quickly in the x-direction from the source and also after passing the source (this is connected with the lower exponent of the exponential function in the third component). Berezkin (1988) and Nabighian (1974) explained the removing of sinusoidal and cosinusoidal oscillations by summing the squares of the orthogonal components (in the derivation showed it is the second component), but as we can see on results, the third component cannot be removed from the considerations connected with the behaviour of continued orthogonal components of a potential field.

After calculating the total gradient F(x,z) by means of relation (4) we can construct its normalized value by dividing it with the average value of the total gradient on every continued level z:

$$F^N(x,z) = \frac{\sqrt{f_x^{\,2}(x,z) + f_z^{\,2}(x,z)}}{\frac{1}{M}\sum_{i=1}^{M}\sqrt{f_{xi}^{\,2}(x,z) + f_{zi}^{\,2}(x,z)}}, \qquad (9)$$

where M - is the number of points on the profile <0, L> .

In Fig. 9 we can see the picture of the total normalized gradient field for the case of 2D horizontal cylinder in the depth h = 50 m. Isolines of the total normalized gradient are closed and the maximum value points approximately at the centre of the cylinder (it is about 10 % shallower). A similar result was obtained by Nabighian (1974), where he constructed a normalized function $Z'^2(x)+H'^2(x)/(Z^2(x)+H^2(x))$, where Z and H are components of the magnetic field and Z', H' are derivatives in x-direction of this components. It is important to point out the fact that in western geophysical literature were not published many applications of this modification of Nabighian's analytical signal method in the comparison to the total normalized gradient method, which was applied and further developed by many authors from the Russian geophysical school.

In the Fig. 10 we can see the field of $F^N(x,z)$ values for a thin ribbon - two local maximums point the horizontal extension of the ribbon. In the Fig. 11 we can see similar picture for a depth extended rectangular prism. The maximum values of $F^N(x,z)$ determine the position of upper corners of the prism.

For the elimination of the Gibb's effect (Berezkin, 1967), the Lanczos smoothing term $[\sin(n\pi/N)/(n\pi/N)]^2$ was added to the equations (2) and (3) which can be now written in the form:

$$f_x(x,z) = \frac{\pi}{L}\sum_{n=1}^{N} B_n \cos\frac{\pi n x}{L}\, e^{\frac{\pi n z}{L}} \left(\frac{\sin\frac{\pi n}{N}}{\frac{\pi n}{N}}\right)^2, \qquad (10)$$

$$f_z(x,z) = \frac{\pi}{L}\sum_{n=1}^{N} B_n \sin\frac{\pi n x}{L}\, e^{\frac{\pi n z}{L}} \left(\frac{\sin\frac{\pi n}{N}}{\frac{\pi n}{N}}\right)^2, \qquad (11)$$

Berezkin (1967) found out that by using the equations (10) and (11) with various N (number of Fourier terms in the summation process), causes changes of the "picture" of the $F^N(x,z)$ field, how it can be seen in Fig. 12. Maximum values of the field are "moving upwards" along the edges of the prism until they achieve approximately the upper boundary of the prism (for N = 150 = M - 1, where M is the number of profile points). Changes of the maximum are shown in Fig. 13: a) changes of the depth position of the maximum according to the increasing number of Fourier terms and b) changes of the value of this maximum in the process of the movement. We can see that the movement made a strong change of its "velocity" near the lower boundary of the prism and after this change it was slightly stable until it reached the upper boundary of the prism. The highest value of all maximum values (for every used N) fixed approximately the centre of the edge.

Jelisejeva (1982) enlarged the possibilities of the interpretation of the maximum values in such a way that she introduced the determination of so called "zones of maximum values". This semi-empirical approach is based on the recognition of these zones as micro structures of the $F^N(x,z)$ field. Zones of maximum values are obtained by connecting the positions of all local maximums, which are situated approximately beneath each other, on all depth levels. These zones have a start-point, end-point and a maximum, which can lie

between them. Maximum and also the start- and end-point can change their position and value during the process of increasing the number of Fourier terms (N). Behaviour of these zones was studied and tested on many model studies and Jelisejeva (1982) defined empirical criteria for the determination of positions of singular points. These criteria are based on changes of the position and value of the characteristic points of a zone (maximum, start- and end-point). Two basic types of zones were classified: the first is connected with subvertical and the second with subhorizontal density contacts. Subvertical zones have always the highest values from all determined zones and the axes of them cross mostly all depth levels. Subhorizontal zones have lower values and contain only few depth-levels.

Results of the interpretation by means of this two types of zones are shown in Fig. 14, where fields from a rectangular prism and a model of a fault (two prisms with opposite density and inclined contact) were interpreted. Subvertical contacts were detected by the slightly stable movement of maximums of subvertical zones (x) and by highest values of a maximum from interpreted zone for all used N (+) and subhorizontal contacts were determined by changes of the movement of end-points of subhorizontal zones (●). False subhorizontal points in the right part of the profiles are connected with the Gibb's effect (which is connected with the discontinuities of the profile curve in start- and end-points of the profile).

In Fig. 15 we can see results, obtained by means of the total normalized gradient method, applied on one profile which was extracted from the map of Bouguer anomalies from the region Gebharts (Austria). Before starting calculations a linear trend (by connecting the start- and end-points of the profile curve) was subtracted from the profile values. In the middle part of the profile (2000 - 3000 m) we can see a positive anomaly, caused by a diorite complex body. Results obtained by means of the total normalized gradient method show that the depth extension of the complex body could be about 300 m. This result stands in disproportion with results obtained by 2D and 3D modelling of the gravity field (König, 1994), where the diorite body has the lower boundary in the depth about 100 m. This disproportion can be connected with the fact that the results, obtained by means of $F^N(x,z)$ method can reflect a bigger structure, which is built by cordieritic gneiss with density contrast 0.1 $g.cm^{-3}$ according to the surrounding granites of Eisgarner and Weinsberger types.

REFERENCES:

Berezkin, V. M. and Buketov, A. P., 1965: Application of the harmonical analysis for the interpretation of gravity data, Prikladnaja geofizika 46, 161 - 166, Moscow (in Russian).

Berezkin, V. M., 1967: Application of the total vertical gradient of gravity for determination of the depth to the sources of gravity anomalies, Razvedocnaja geofizika 13, 69 - 79, Moscow (in Russian).

Berezkin, V. M., 1988: Method of the total gradient in geophysical prospecting. Nedra, Moscow (in Russian).

Berezkin, V. M. and Skotarenko, S. S., 1983: Further ways in development of the total gradient method for solving structural problems. From book: Application of gravimetry for researching of anticlinal deposits of oil and gas., 110 - 116, Neftegeofizika, Moscow (in Russian).

Ciancara, B. and Marcak. H., 1979: Geophysical anomaly interpretation of potential fields by means of singular points method and filtering, Geophysical Prospecting, 27, 251 - 260.

Gladkij, K. V., 1967: Gravimetry and magnetometry. Nedra, Moscow, (in Russian).

Jelisejeva, I. S., 1982. Methodical recommendations for the study of density inhomogenities of cross-sections based on gravimetrical research data. VNIIGeofizika, Moscow, (in Russian).

Jelisejeva, I. S., 1995. Methodical recommendations for the interpretation of gravity and magnetic data by means of the quasi-singular points method, VNIIGeofizika, Moscow, (in Russian).

Jung, K., 1961: Schwerkraftverfahren in der angewandten Geophysik, AV Geest & Portig, Leipzig.

König, Ch., 1994. Gravimetrische Untersuchung des Dioritkomplexes bei Gebharts (NO), Diplomarbeit, Institut für Meteorologie und Geophysik, Universität Wien , Wien.

Lindner, H. and Scheibe, R., 1977: Interpretationstechnik für gravimetrische und magnetische Felder. Freiberger Forschungshefte, DV für Grundstoffindustrie, Leipzig.

Nabighian, M. N. 1972. The analytic signal of two-dimensional magnetic bodies with polygonal cross-section: its properties and use for automated anomaly interpretation. Geophysics 37, 507-517.

Nabighian, M. N. 1974. Additional comments on the analytic signal of two-dimensional magnetic bodies with polygonal cross-section. Geophysics 39, 85-92.

Pasteka, R. and Seiberl, W., 1992: Die Auswertung polreduzierter Magnetfelddaten anhand des totalen Feldgradienten. LHA Geophys., 133 - 143.

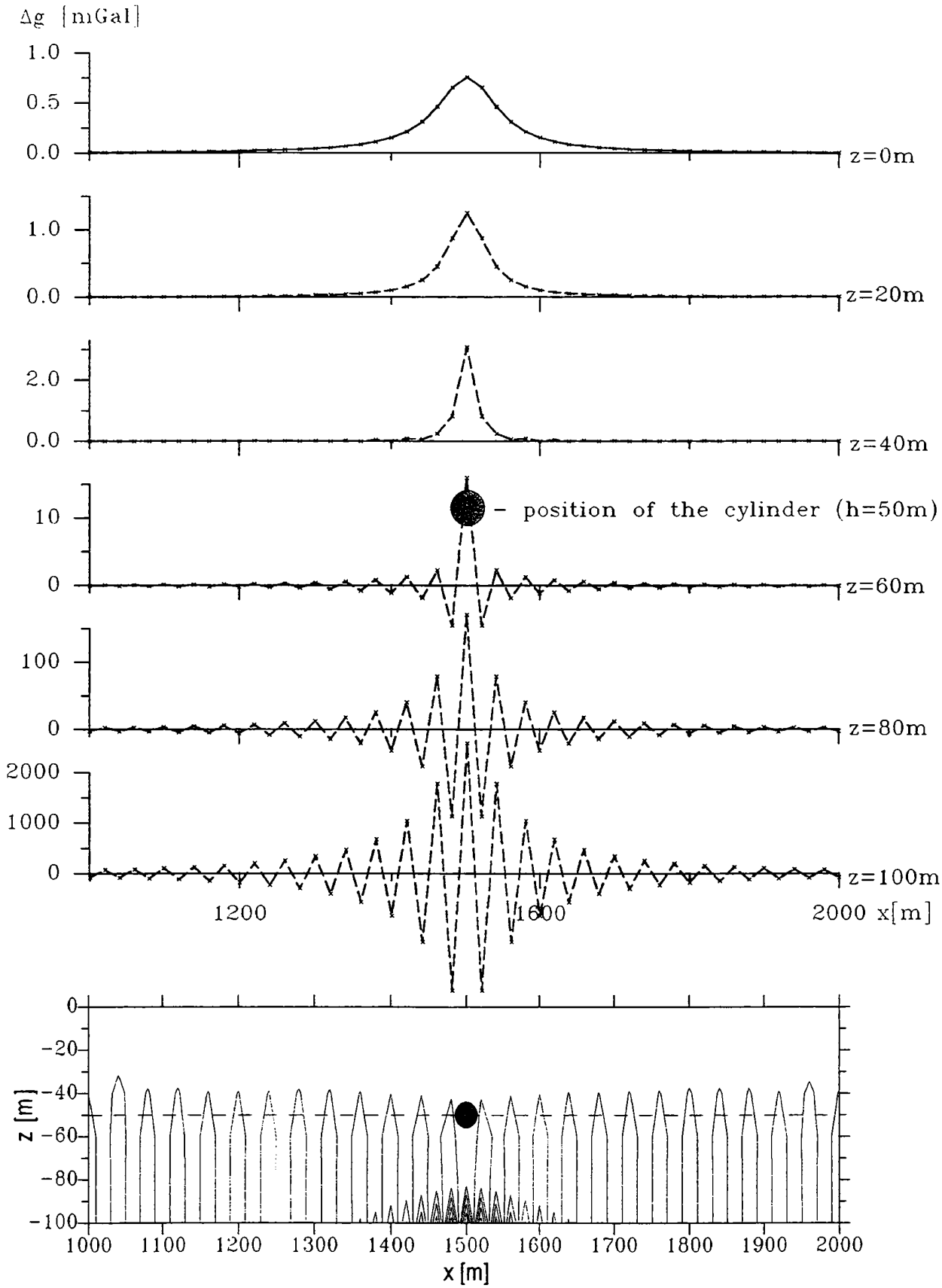

Fig. 1. Results of analytical continuation downwards,
(transformed Δg(x,0) for 2D-horizontal cylinder in the depth h = 50 m),
levels of continuation: z = 20, 40, 60, 80 and 100 m,

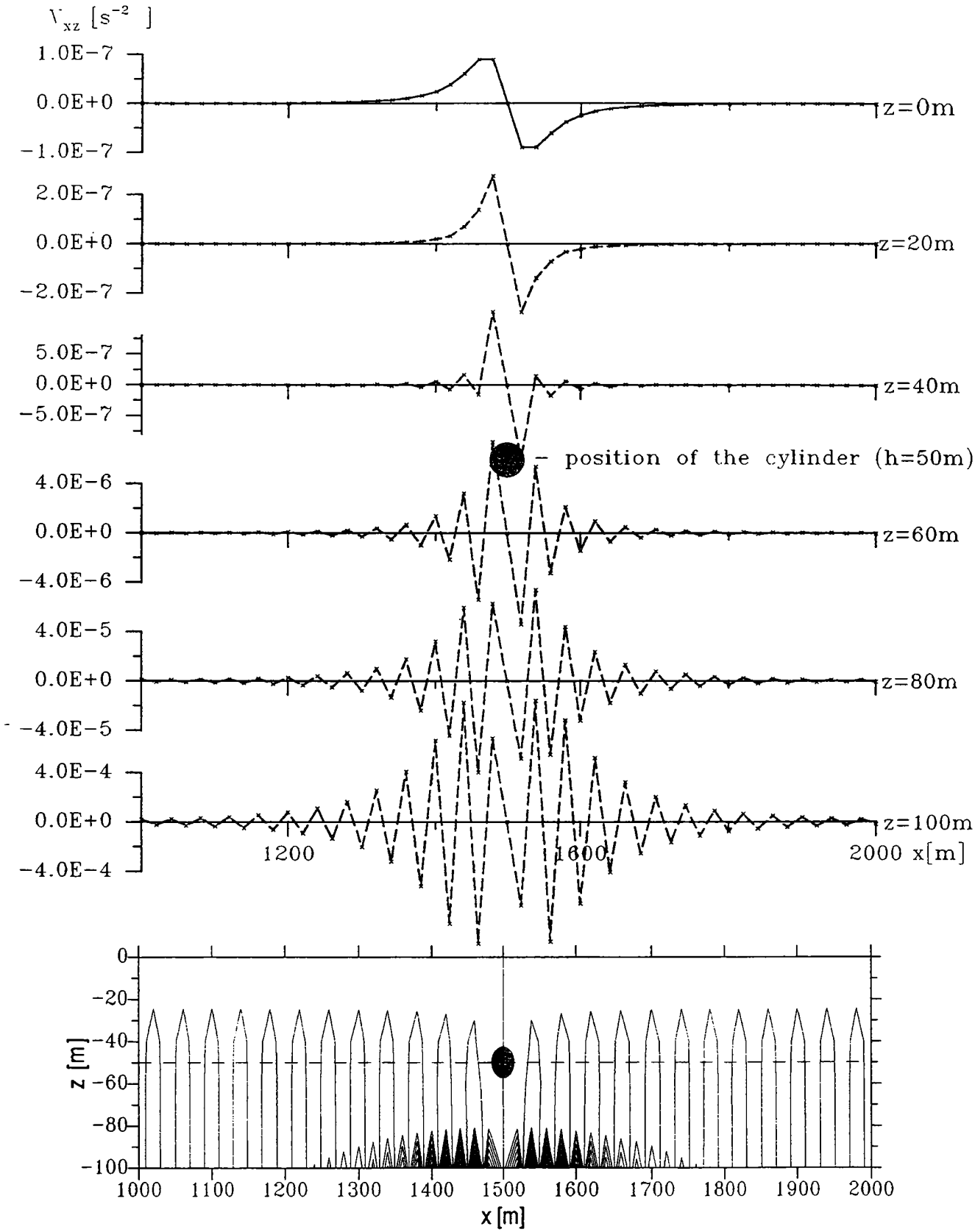

Fig. 2. Results of analytical continuation downwards,
(transformed V_{xz} (x,0) for 2D-horizontal cylinder in the depth h = 50 m),
levels of continuation: z = 20, 40, 60, 80 and 100 m,

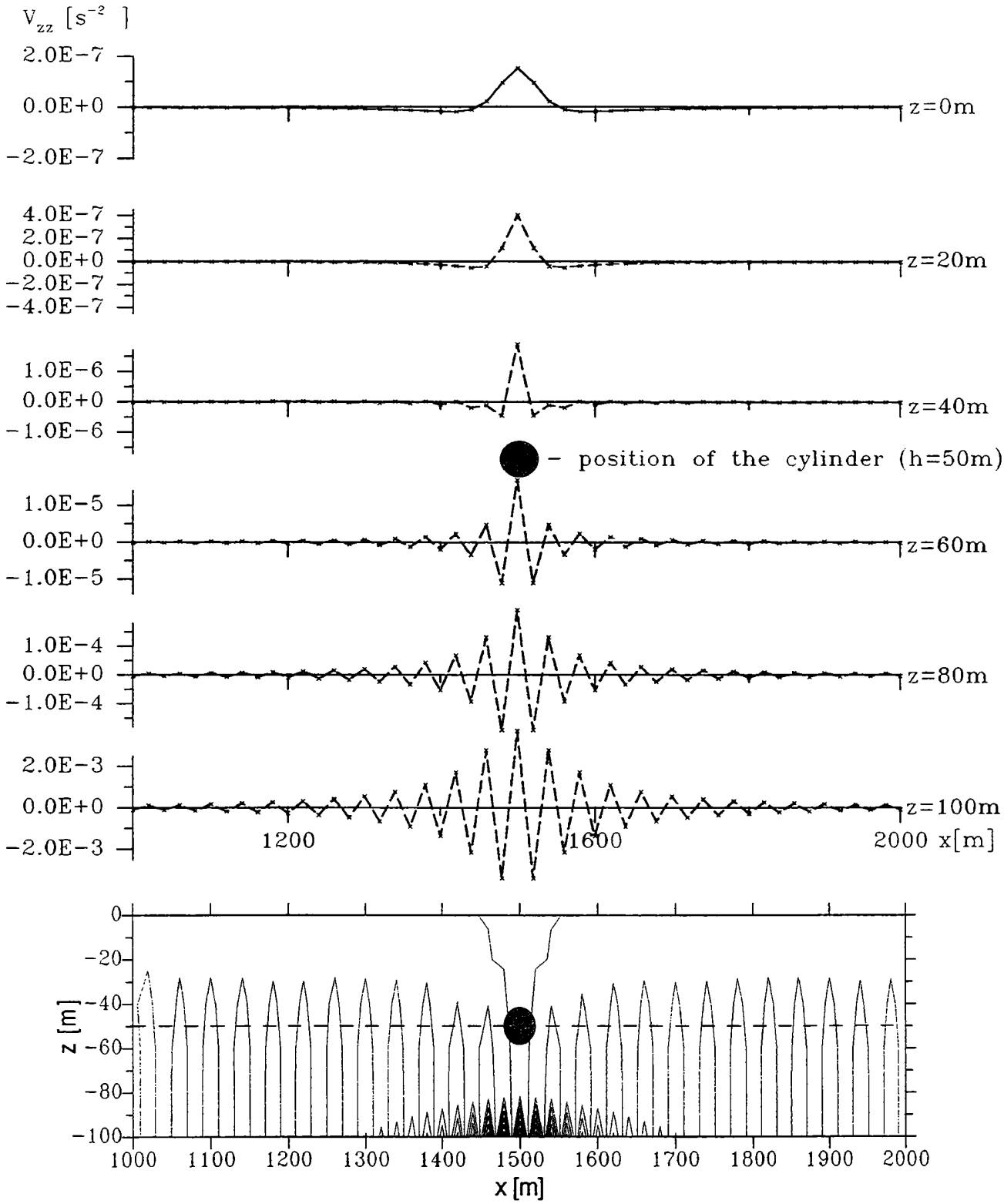

Fig. 3. Results of analytical continuation downwards,
(transformed V_{zz} (x,0) for 2D-horizontal cylinder in the depth h = 50 m),
levels of continuation: z = 20, 40, 60, 80 and 100 m,

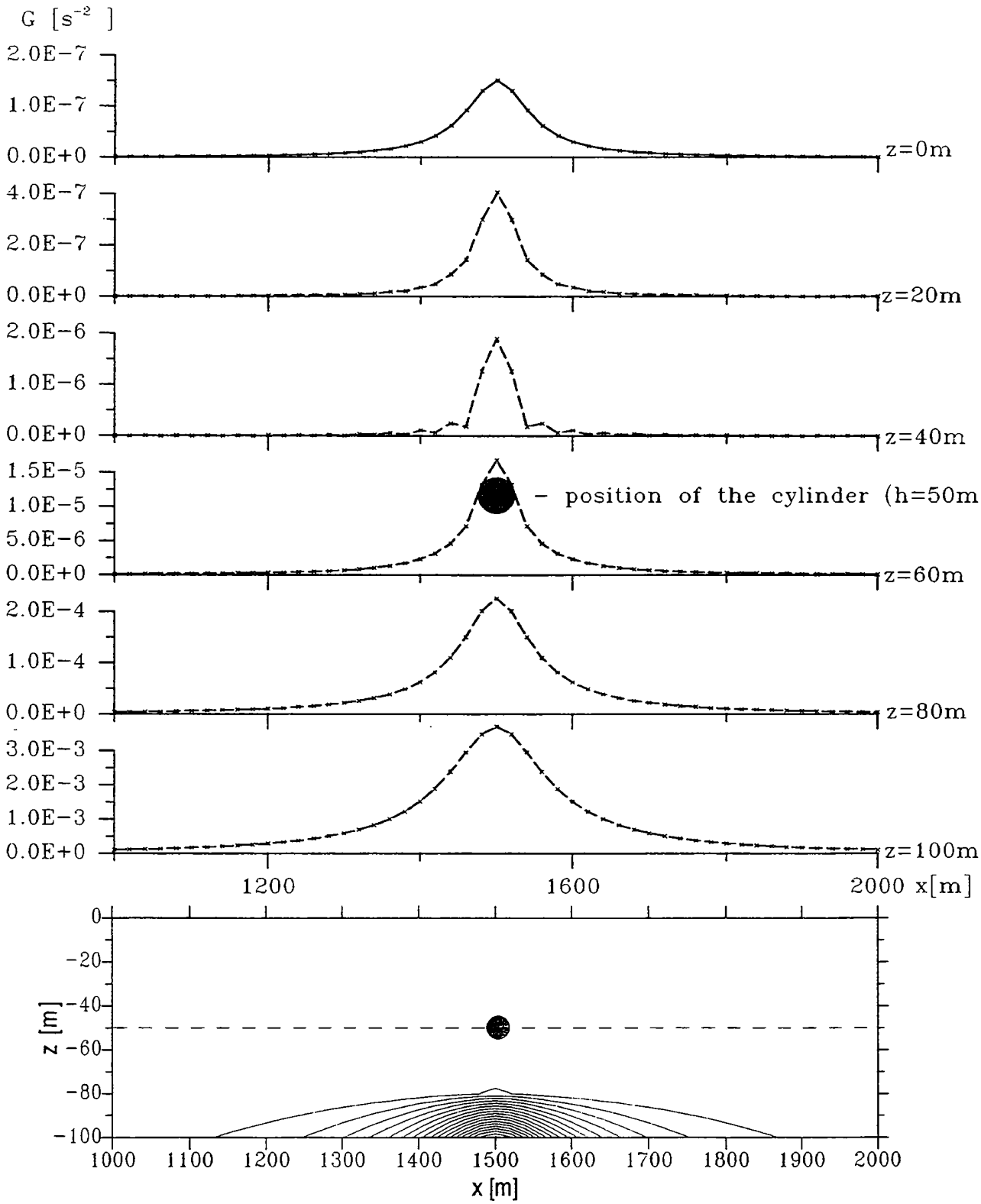

Fig. 4. Results of analytical continuation downwards,
(total gradient G(x,z) calculated from transformed V_{xz} (x,0)
and V_{zz} (x,0) for 2D-horizontal cylinder in the depth h = 50 m),
levels of continuation: z = 20, 40, 60, 80 and 100 m,

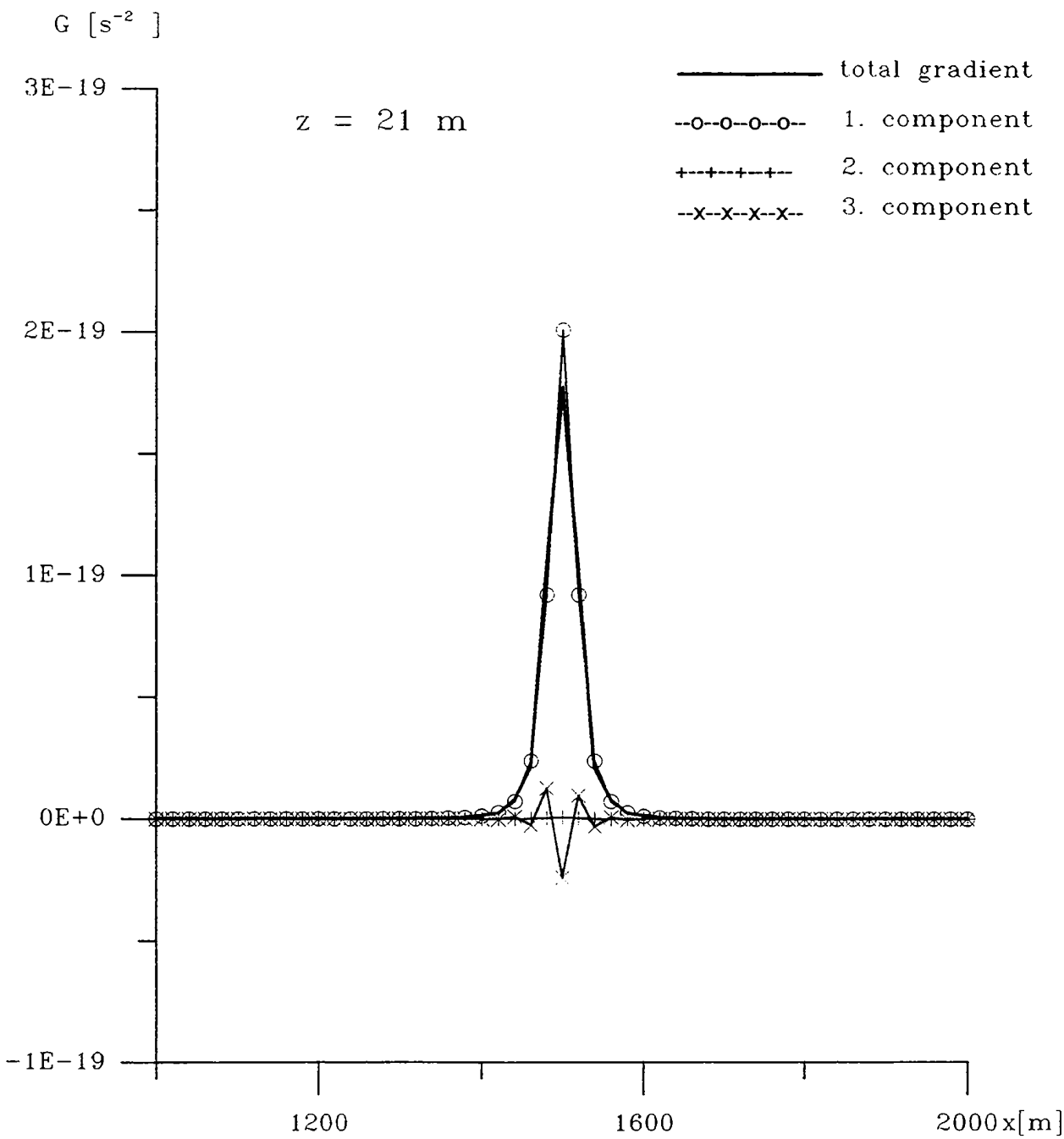

Fig. 5. Values of the total gradient and its three components for 2D-horizontal cylinder in the depth h = 50 m,
level of continuation = 21 m,

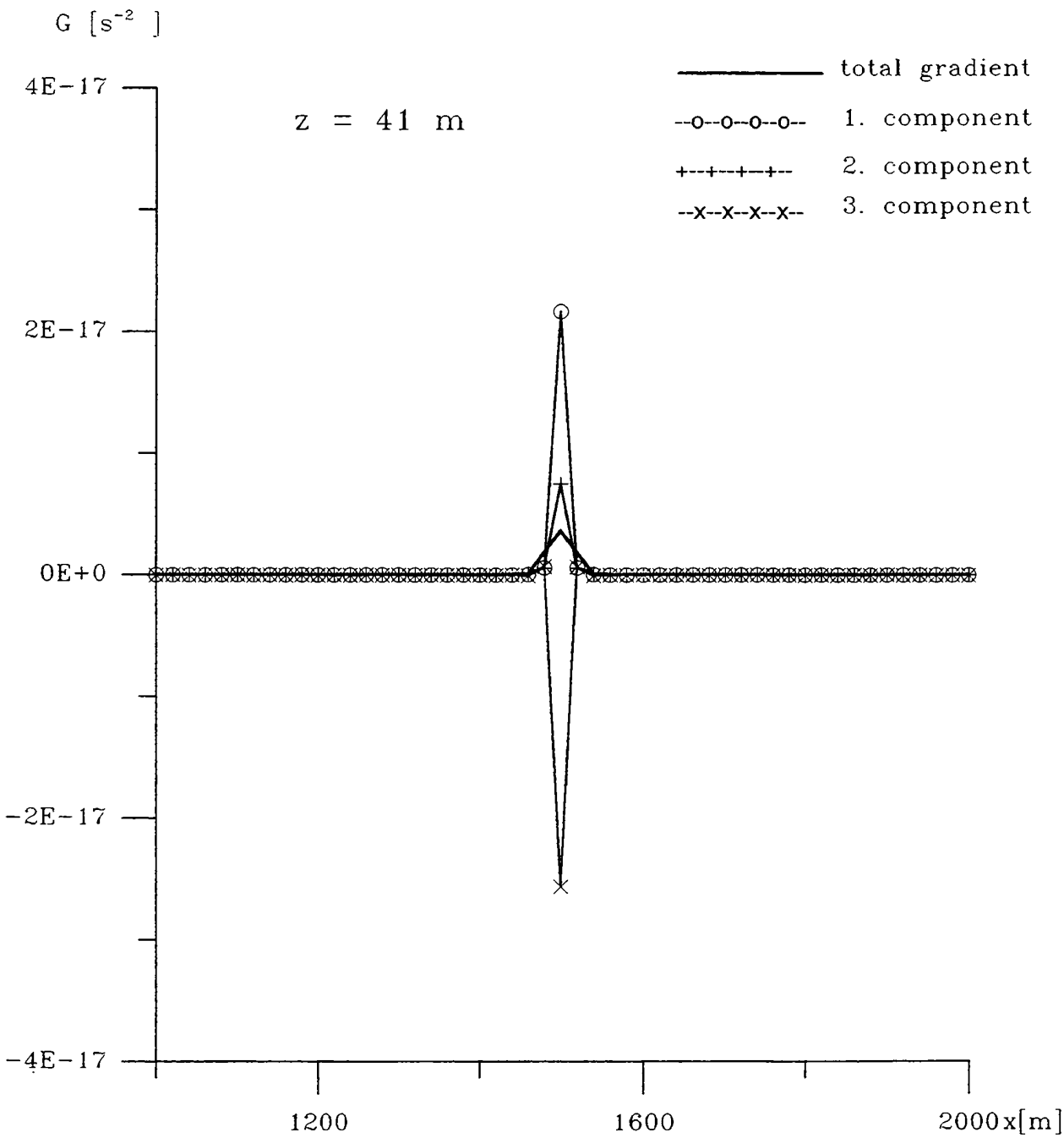

Fig. 6. Values of the total gradient and its three components for 2D-horizontal cylinder in the depth h = 50 m,
level of continuation = 41 m,

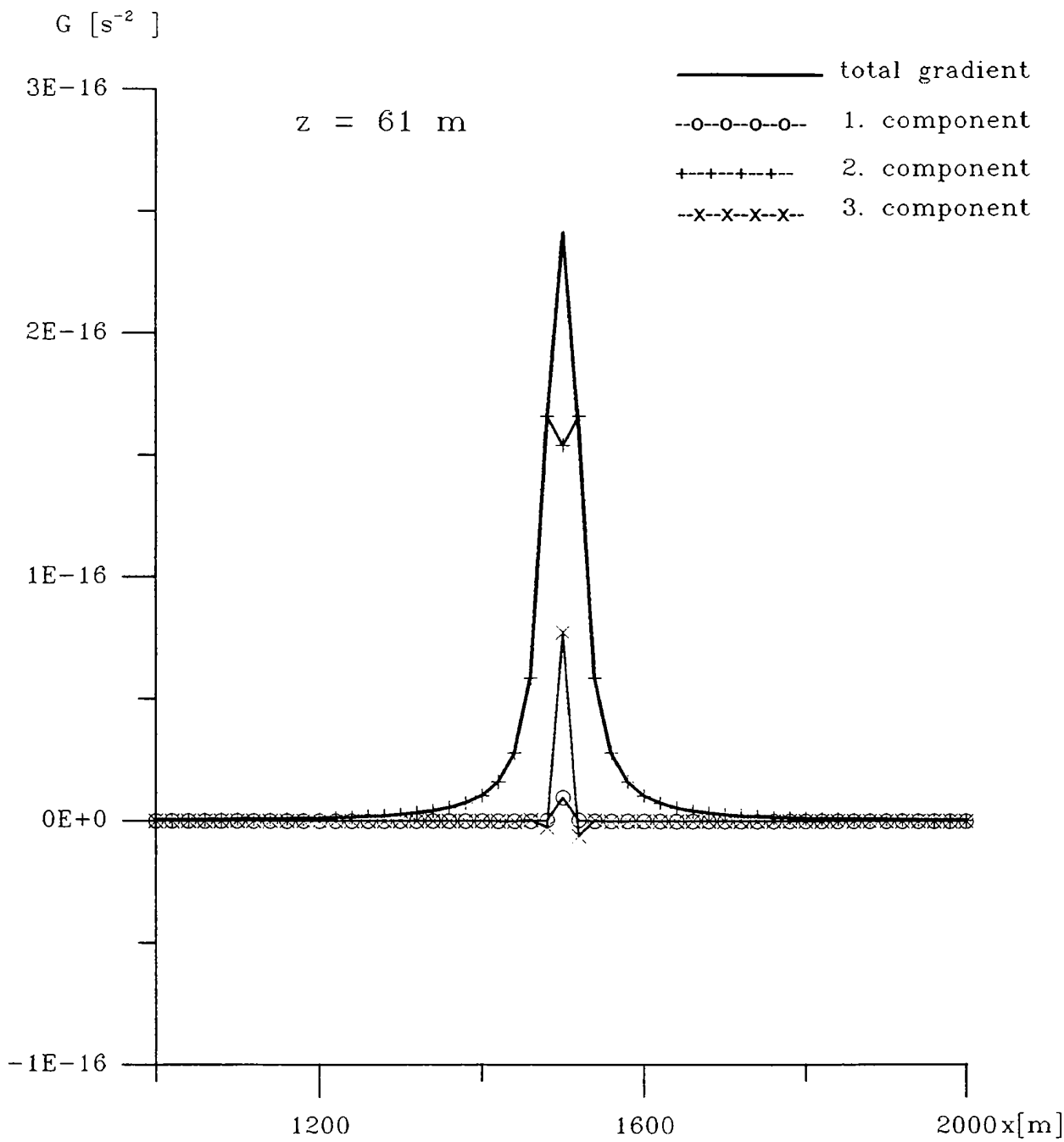

Fig. 7. Values of the total gradient and its three components for 2D-horizontal cylinder in the depth h = 50 m,
level of continuation = 61 m,

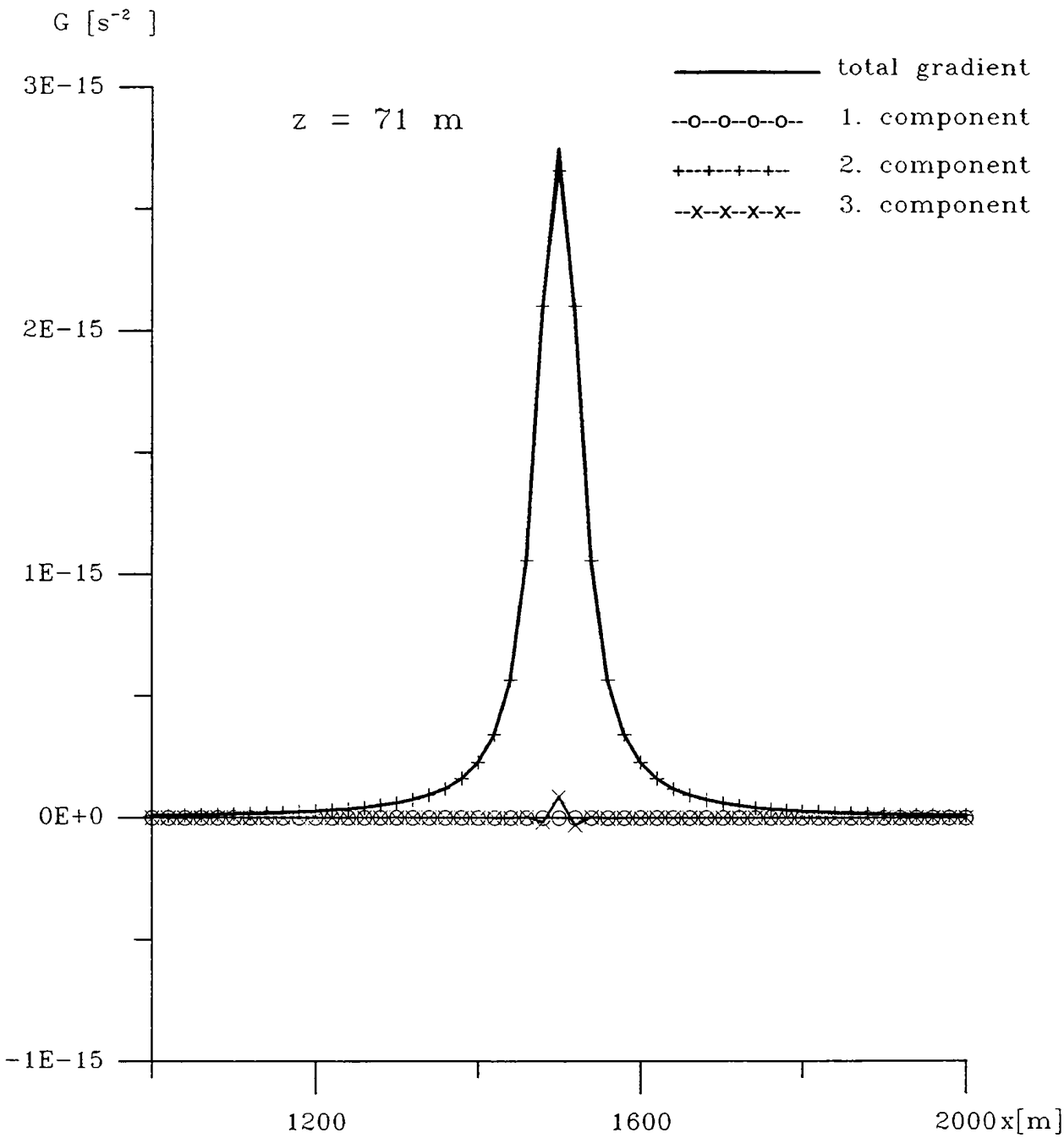

Fig. 8. Values of the total gradient and its three components for 2D-horizontal cylinder in the depth h = 50 m,
level of continuation = 71 m,

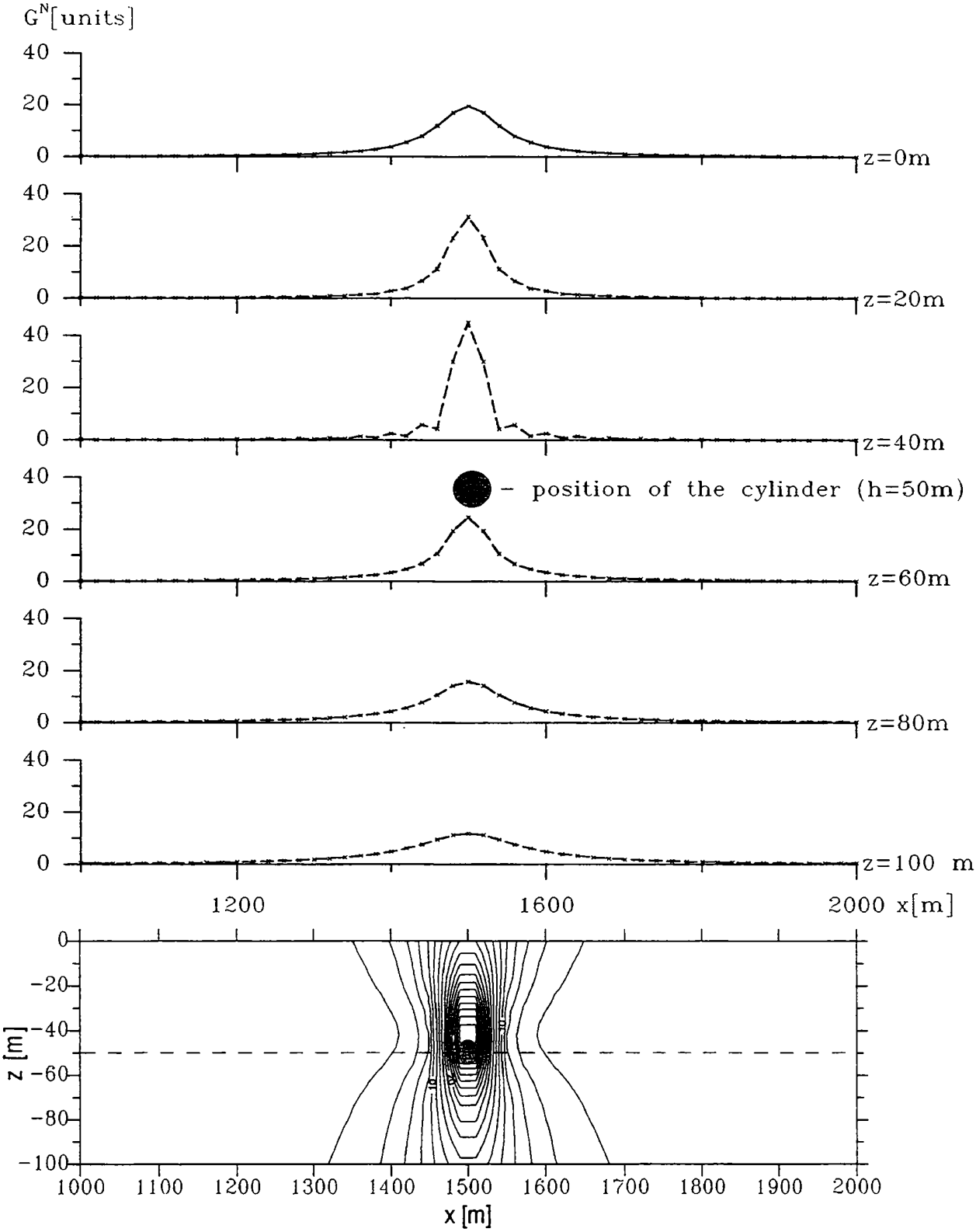

Fig. 9. Results of analytical continuation downwards,
(total normalized gradient $G^N(x,z)$ calculated from transformed
$V_{xz}(x,0)$ and $V_{zz}(x,0)$ for 2D-horizontal cylinder in the depth h = 50 m),
levels of continuation: z = 20, 40, 60, 80 and 100 m,

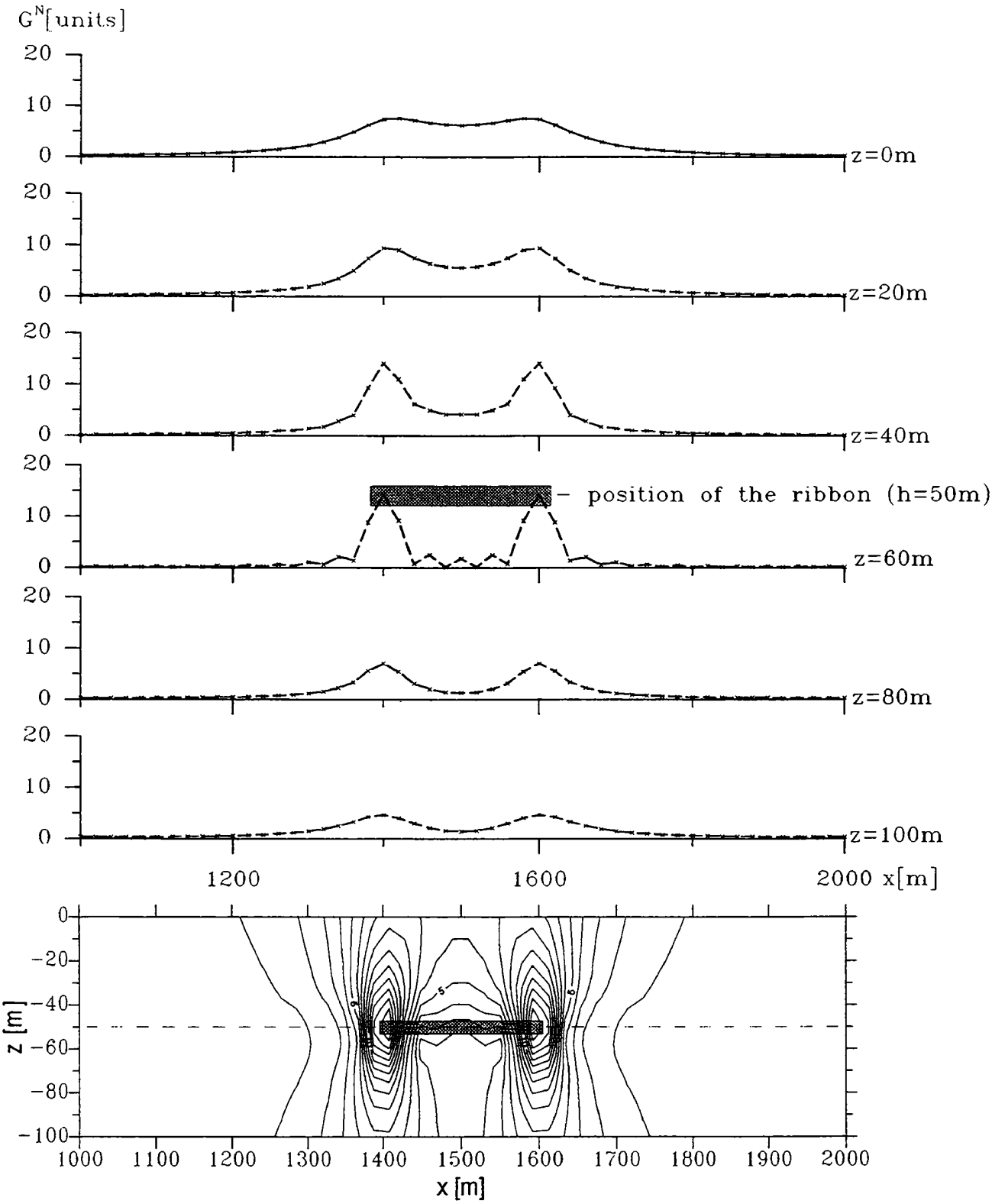

Fig. 10. Results of analytical continuation downwards,
(total normalized gradient $G^N(x,z)$ calculated from transformed
$V_{xz}(x,0)$ and $V_{zz}(x,0)$ for 2D-horizontal ribbon in the depth h = 50 m),
levels of continuation: z = 20, 40, 60, 80 and 100 m,

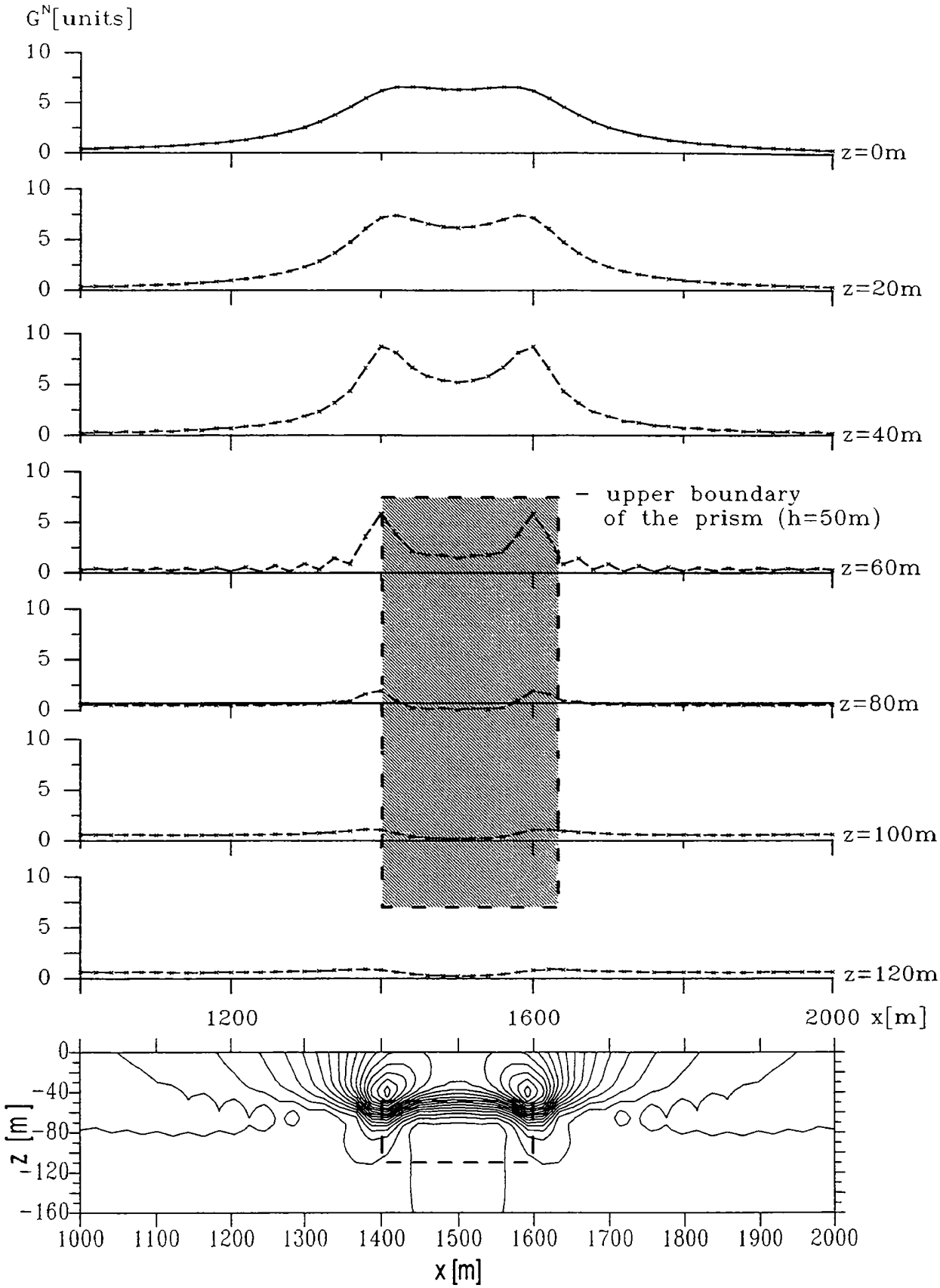

Fig. 11. Results of analytical continuation downwards,
(total normalized gradient $G^N(x,z)$ calculated from transformed
$V_{xz}(x,0)$ and $V_{zz}(x,0)$ for 2D-horizontal prism: h_1= 50 m, h_2= 110 m)

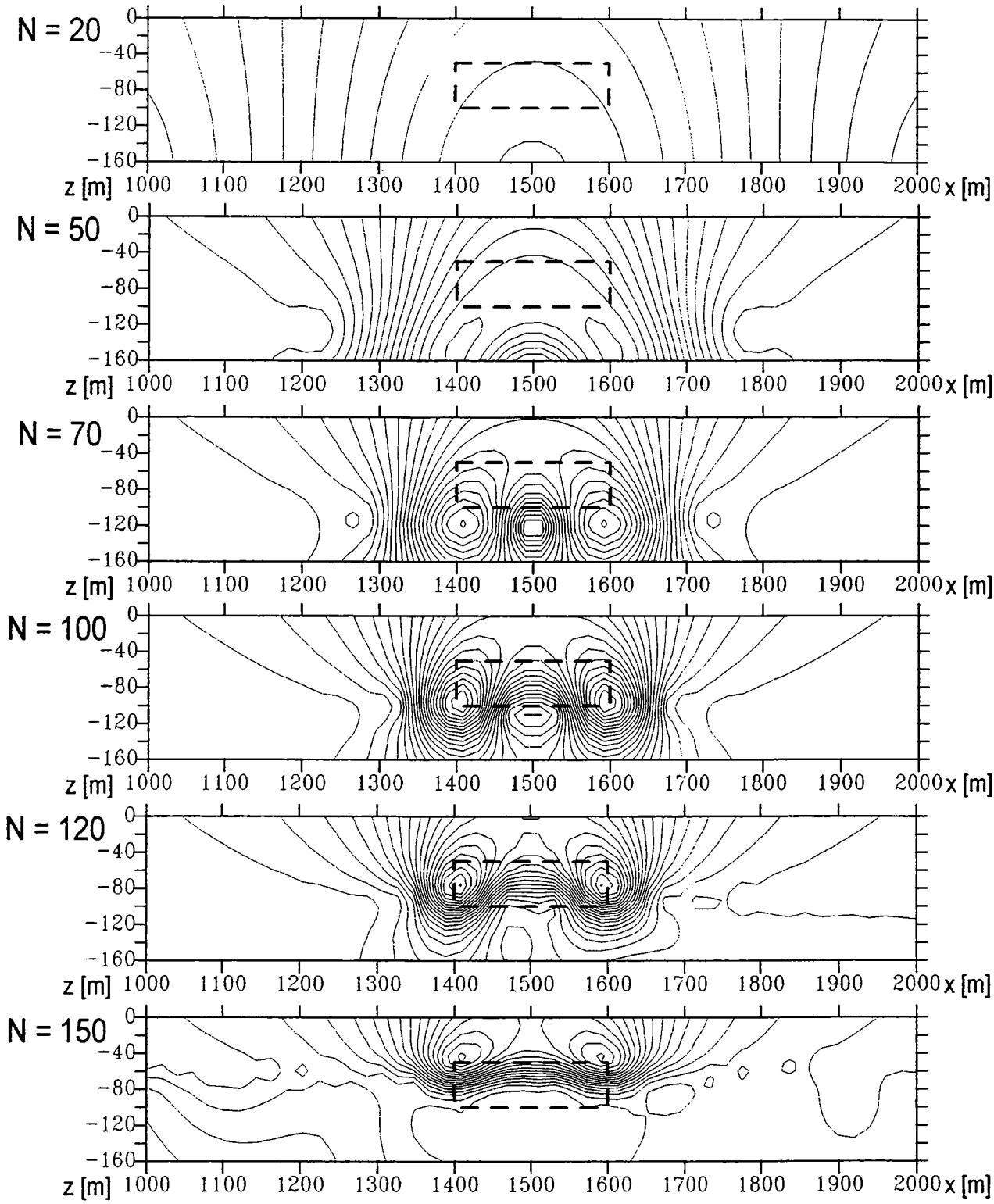

Fig. 12. Values of the total normalized gradient of gravity in the xz-plane for N = 20, 50, 70, 100, 120 and 150, step of isolines = 0.5 units, (2D- horizontal prism, density = 1 g.cm^{-3}, h_1= 50 m, h_2= 110 m number of points = 151, length of the profile = 3000m)

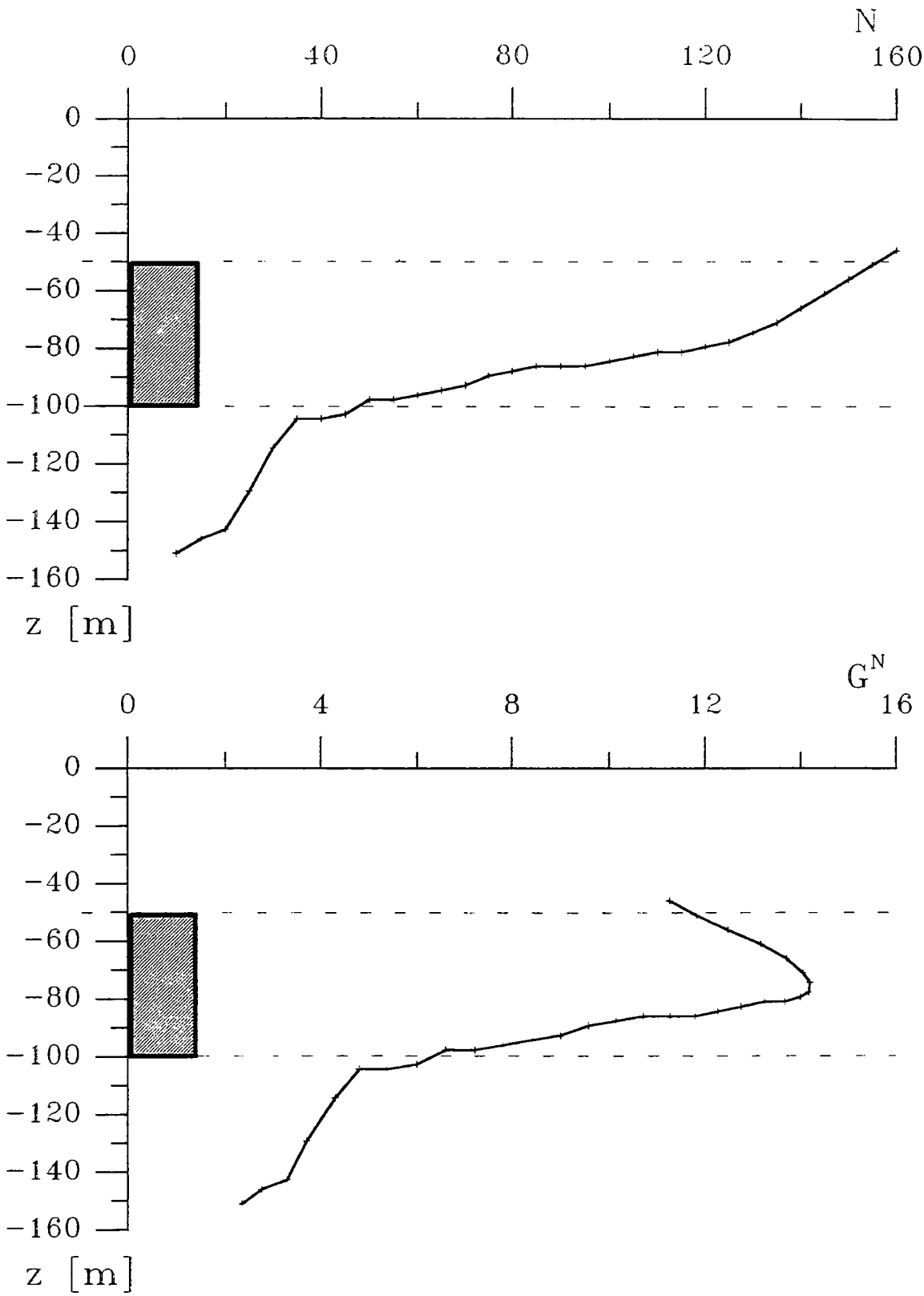

Fig. 13. Changes of the maximum value,
(2D- horizontal prism with density 1 g.cm^{-3}, h_1= 50 m, h_2= 100 m)
a) changes of the depth position of the maximum due to the increasing number of terms of Fourier series
b) changes of the value of the maximum in the process of moving upwards

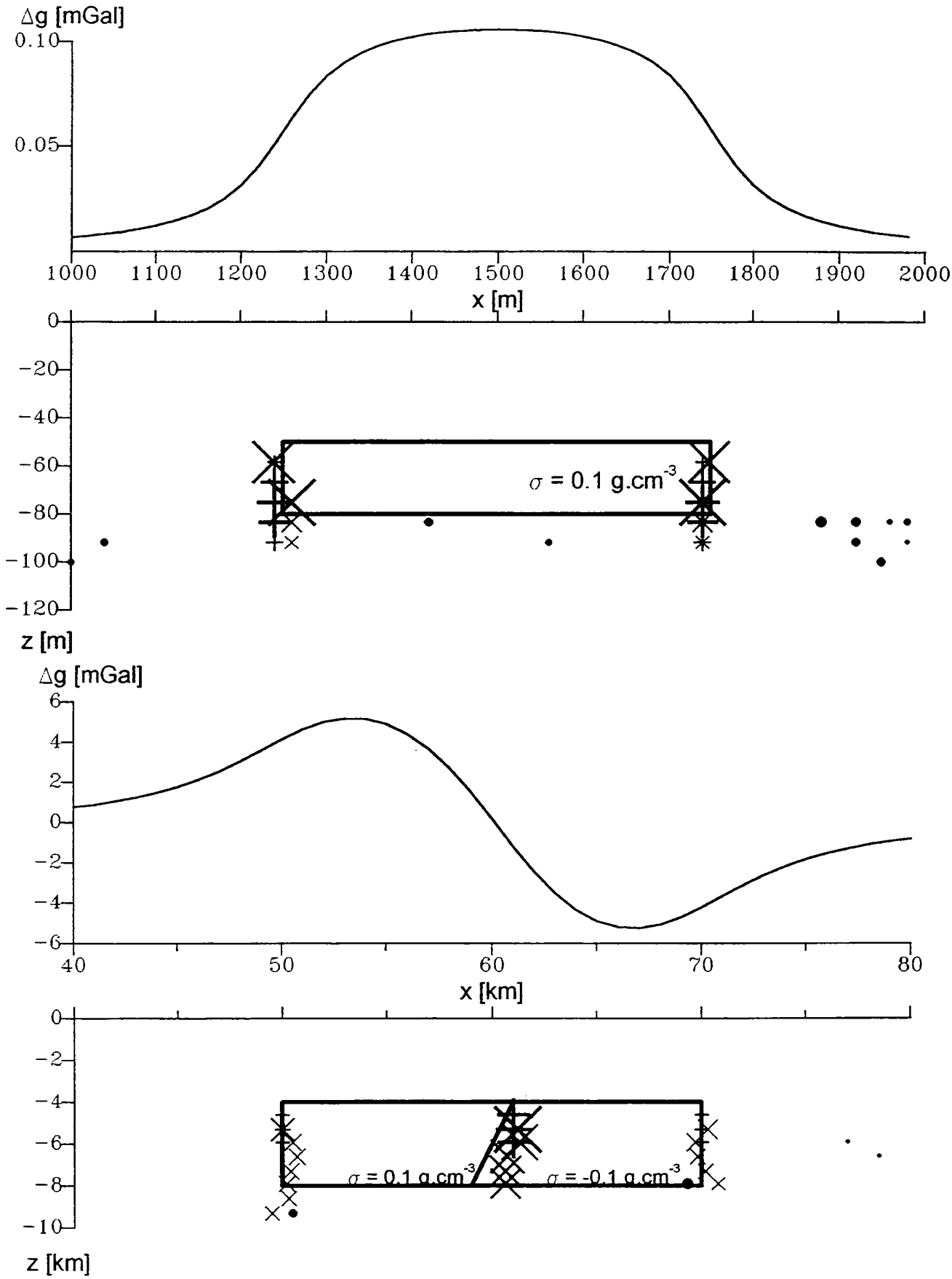

Fig. 14. Results obtained by the interpretation of changes of zones of maximum values,
x - "subvertical points", determined by means of changes of the position of the zone-maximun
+ - "subvertical points", determined by means of changes of the value of the zone-maximum,
● - "subhorizontal points", determined by means of changes of start-points and end-points of zones,

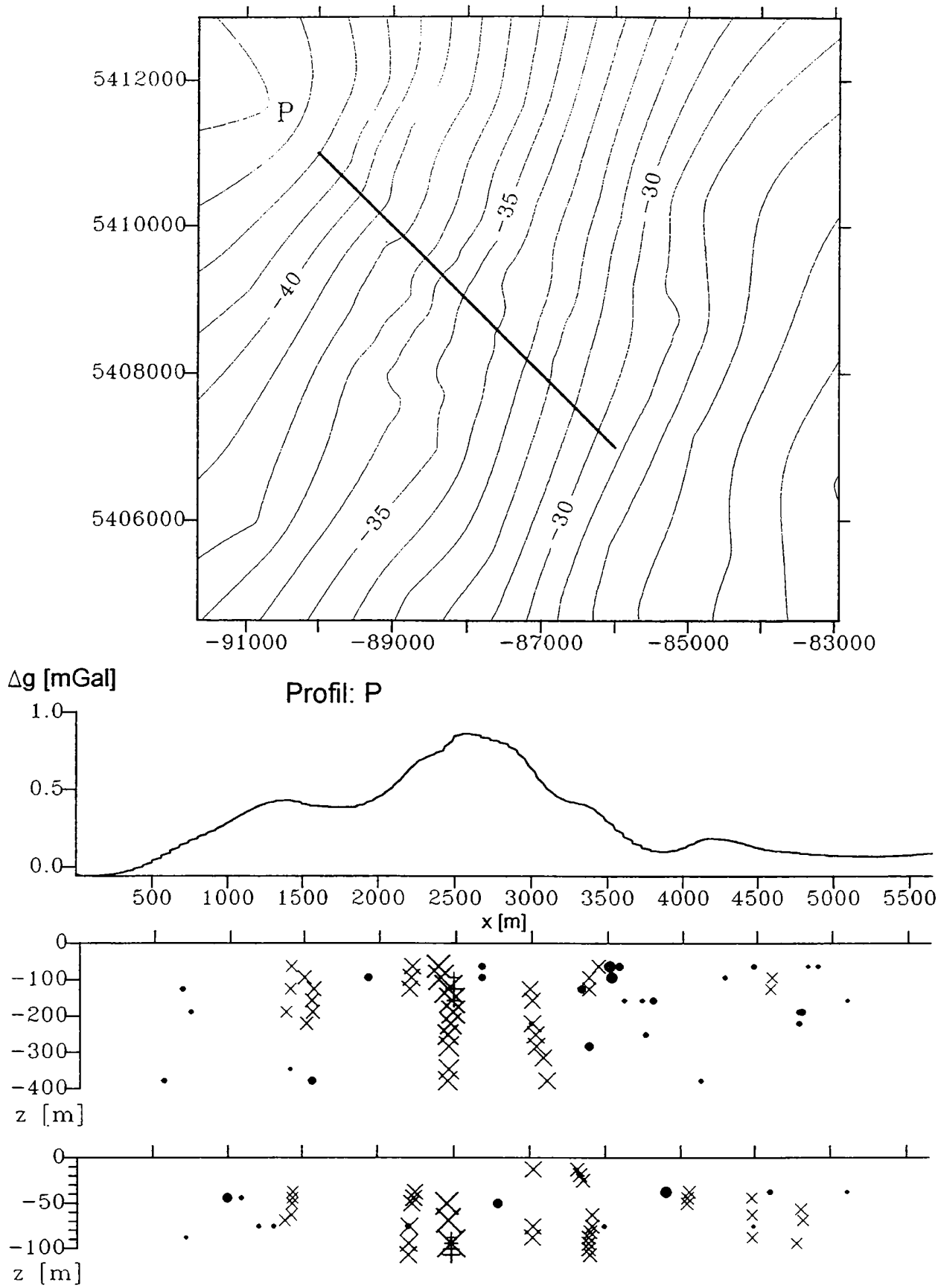

Fig. 15. Results obtained by the interpretation of changes of zones of maximum values, Profil P, interpolated from Bouguer anomaly map from Gebharts region (Austria),
x - "subvertical points", determined by means of changes of the position of the zone-maximum,
+ - "subvertical points", determined by means of changes of the value of the zone-maximum,
● - "subhorizontal points", determined by means of changes of start-points and end-points of zones,

Berechnung der topographischen Reduktion mit digitalen Geländemodellen in den zentralen Anden

Georg Goltz, Sabine Schmidt, Andreas Müller und Hans-Jürgen Götze
Institut für Geologie, Geophysik und Geoinformatik, FU Berlin

Abstract

This study provides information about availability of digital elevation models for the Central Andes which may be used for the calculation of gravimetric terrain corrections. First results of a accuracy analysis of the high resolution 30"×30" DEM published by JENSON & BLISS (1995) of USGS are presented. Finally, the paper is introducing a method for calculation of terrain corrections which is based on the approximation of the terrain by polyeders.

Einführung

Seit Beginn der Achtziger Jahre sind die zentralen Anden Südamerikas, zwischen etwa 20° und 26° südlicher Breite, Gegenstand intensiver geowissenschaftlicher Forschung der Forschergruppe "Mobilität aktiver Kontinentalränder" und des Sonderforschungsbereichs "Deformationsprozesse in den Anden". Die Schaffung eines dichten gravimetrischen Stationsnetzes ist dabei stetig vorangebracht worden, um sowohl regionale, als auch lokale Fragestellungen in Zusammenarbeit mit den Nachbardisziplinen lösen zu können. Die auf Messungen vor 1982 basierende Datenbasis war sehr lückenhaft und ausschließlich für global-regionale Untersuchungen geeignet, wie die Arbeiten von DRAGICEVIC (1970), JAMES (1971), GROW & BOWIN (1975) zeigen, in denen lediglich die Grobstruktur der Anden in gravimetrischen Modellen erfaßt wurde.

Aufgrund der schlechten Zugänglichkeit vieler Teilgebiete in den Hochanden und der sehr lückenhaften Erschließung Chiles und Argentinens mit Straßen, ist die Stationsverteilung insgesamt sehr inhomogen (GÖTZE et al., 1990, 1996); angestrebt wurde ein Stationsabstand von etwa 5 km entlang der befahrenen Wege. Eng verknüpft mit der, verglichen mit mitteleuropäischen Verhältnissen, völlig andersartigen Infrastrukur, ist die nur sehr eingeschränkte Verfügbarkeit eines Netzes von Höhenfestpunkten, Nivellements und Triangulationspunkten, deren Qualität zudem sehr unterschiedlich ist. Bei der Bestimmung der Höhen der Gravimeterstationen muß deshalb in vielen Fällen auf die barometrische Höhenbestimmung (SCHMIDT, 1986) zurückgegriffen werden, so daß die Genauigkeit der Stationshöhen im günstigsten Fall bei etwa ± 0.1 m und im ungünstigsten Fall nur bei ± 15 m liegt (GÖTZE, 1986).

Die zum Erhalt der Bougueranomalie an den Schweremeßwerten anzubringende topographische Reduktion erfordert in den Anden, wie im Hochgebirge allgemein, bei der Bestimmung einige Sorgfalt, weil die Reduktionbeträge in Einzelfällen 25 bis 40 mGal betragen können (STRUNK, 1990). Methoden, bei denen die Geländeoberfläche gut approximiert wird, sind hier besonders gut geeignet.

Digitale Höhenmodelle

Weil ein digitales Höhenmodell des Meßgebiets zu Beginn der Meßkampagnen (1982) fehlte, wurden durch Digitalisierung des vorliegenden Kartenmaterials im Maßstab 1:50 000, 1:100 000 und 1:200 000, mittlere Höhen bestimmt, um eine Grundlage für die Berechnung der topographischen Reduktion zu erhalten. Als Rastergröße dieses DEM's (Digital Elevation Model), das fast 21000 mittlere Höhen umfaßt, wurde 2.5'×2.5' gewählt. Es liegt innerhalb des Gebiets -67° bis -72° westlicher Länge und -19.3° bis -26.5° südlicher Breite vor. Für das Höhenmodell außerhalb des kontinentalen Festlands wurden die Tiefenlage des Trenchs aus der geologischen Karte Chiles im Maßtab 1:1 000 000 und Tiefen von Stationen der Seegravimetrie des BGI (Toulouse) benutzt (STRUNK, 1985). Für Teilgebiete mit extrem schroffer Topographie existieren darüberhinaus verfeinerte Raster mit der Rastergröße 0.625'×0.625' (Chile) bzw. 0.75'×0.75' (Argentinien), um den Übergang der Reduktion vom Nahbereich zum Fernbereich bei der Methode von EHRISMANN & LETTAU (1971) zu gewährleisten.

Weitgehend ersetzt wurde dieses Höhenmodells durch das digitale Geländemodell Südamerikas, das an der Cornell University im Rahmen des "Central Andes Project" entwickelt wurde (ISACKS, 1988). Basierend auf Luftfahrtkarten im Maßstab 1:1 000 000 (Operational Navigation Chart, ONC) der Defense Mapping Angency (DMA) wird etwa der Bereich zwischen -62° bis -80° westlicher Länge und -12° bis -36° südlicher Breite mit einer Rastergröße von 3'×3' erfaßt. Für einige wenige Gebiete in Bolivien und Peru dienten topographische Karten als Grundlage der Digitalisierung. Im Gegensatz zum DEM der TU Clausthal handelt es sich nicht um mittlere Höhen, sondern um digitalisierte Punkthöhen. Der Offshorebereich von der Pazifikküste bis zum Peru-Chile Trench wurde der bathymetrischen Karte von PRINCE et al. (1980), die ebenfalls im Maßstab 1:1 000 000 vorliegt, entnommen. Für die weiter westlich liegenden Gebiete dienten digitale bathymetrische Daten (Synthetic Bathymetric Profiling System, SYNBAPS) der NOAA als Grundlage, die an den Nahtstellen zwischen beiden Tiefenmodellen möglichst plausibel angepaßt wurden. Eine Angabe zur Genauigkeit dieses Höhenmodells liegt nicht vor.

Eine von der TU Graz bearbeitete Version des globalen Höhenmodell ETOPO5 ergänzte das DEM von Isacks im Pazifik, war aber wegen der geringeren Auflösung kein Ersatz für die landseitigen Höhen. Zwei hauptsächliche Quellen sind Grundlage dieses DEM, das die Rastergröße 5'×5' aufweist, nämlich zum einen ein vom US Navy Fleet Numeric Oceanographic Center (FNOC) generiertes 10'-Gitter, das eine Genauigkeit von ± 30 feet aufweist und für die Kontinente nachträglich auf ein 5'-Gitter interpoliert wurde (± 1m Auflösung). Während

Tabelle 1: *Zusammenstellung der für die topographische Reduktion in den zentralen Anden benutzten digitalen Höhenmodelle.*

Jahr	Gebiet	Rastergröße	Erstellung	Datengrundlage
ab 1982	Chile	2.5' × 2.5'	TU Clausthal	Karten 1:50 000
	Pazifik	2.5' × 2.5'	TU Clausthal	geol. Karte 1:1 000 000 BGI-Daten
	Teilgebiete (Chile)	0.625' × 0.625'	TU Clausthal	Karten 1:50 000
	Teilgebiete (Argentinien)	0.75' × 0.75'	TU Clausthal	Karten 1:50 000
ab 1986	zentrale Anden, Pazifik	3' × 3'	Cornell University	DMA 1:1 000 000
ab 1988	Südamerika, Pazifik	5' × 5'	TU Graz	ETOPO 5
ab 1996	Südamerika	30" × 30"	USGS	DMA 1:1 000 000

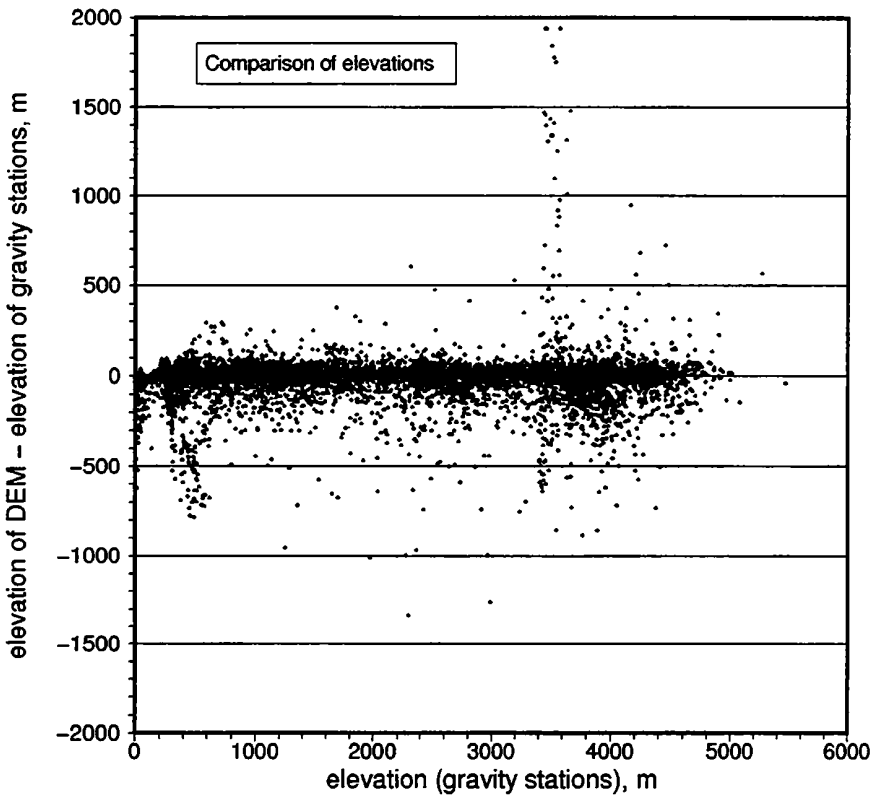

Abbildung 1: *Abweichung der Stationshöhen vom digitalen Geländemodell von* JENSON & BLISS *(1995).*

der marine Bereich aus der Digital Bathymetric Data Base 5-minutes (DBDB5) des USA Naval Oceanographic Office's abgeleitet wurde.

Eine wesentliche Verbesserung der Auflösung der bisher beschriebenen DEM bietet das von JENSON & BLISS (1995) beim USGS kompilierte Höhengitter mit der Rastergröße 30"×30", das seit Ende 1995 in einer vorläufigen Version frei verfügbar ist und im Rahmen des 'EROS Data Center (EDC) 30 arc-second DEM project' entstand. Bei der Generierung des Höhengitters wurden verschiedene Quellen verwendet, u. a. ein 3"-Raster (Defense Mapping Agency) und Karten im Maßtab 1:1 000 000 (Digital Chart of the World, DCW). Eine spezielle Bearbeitung der hypsographischen Information der DCW wurde mit der ANUDEM-Gridding-Software von HUTCHINSON (1988, 1989, 1991) durchgeführt, um ein hydrologisch realistisches DEM zu erhalten. Darüberhinaus sind diverse Techniken angewandt worden, um Diskontinuitäten an den Nahtstellen der verschiedenen Datensätze zu minimieren. Meerestiefen sind im bislang publizierten Datensatz noch nicht enthalten.

In Tabelle 1 sind die für die zentralen Anden vorhandenen Höhenmodelle ihrer zeitlichen Verfügbarkeit nach aufgelistet. Daneben existieren noch weitere DEM's aus dem militärischen Bereich, die jedoch der Öffentlichkeit nicht zur Verfügung stehen.

Da eine Angabe zur Genauigkeit des USGS-Höhengitters nicht vorliegt, wurde durch einen Vergleich der Höhen der Gravimeterstationen mit den Höhen des DEM's eine erste Abschätzung der Brauchbarkeit des Gitters versucht. Durch Projektion der Lage einer Gravimeterstation auf das zugehörige Rasterelement erhält man für jede Station die durchschnittliche Höhe in der Stationsumgebung (etwa 800 m). Grobe Fehler im DEM lassen sich dadurch schnell ermitteln, wenn man annimmt, daß die Stationshöhenbestimmung korrekt durchgeführt worden ist. Trägt

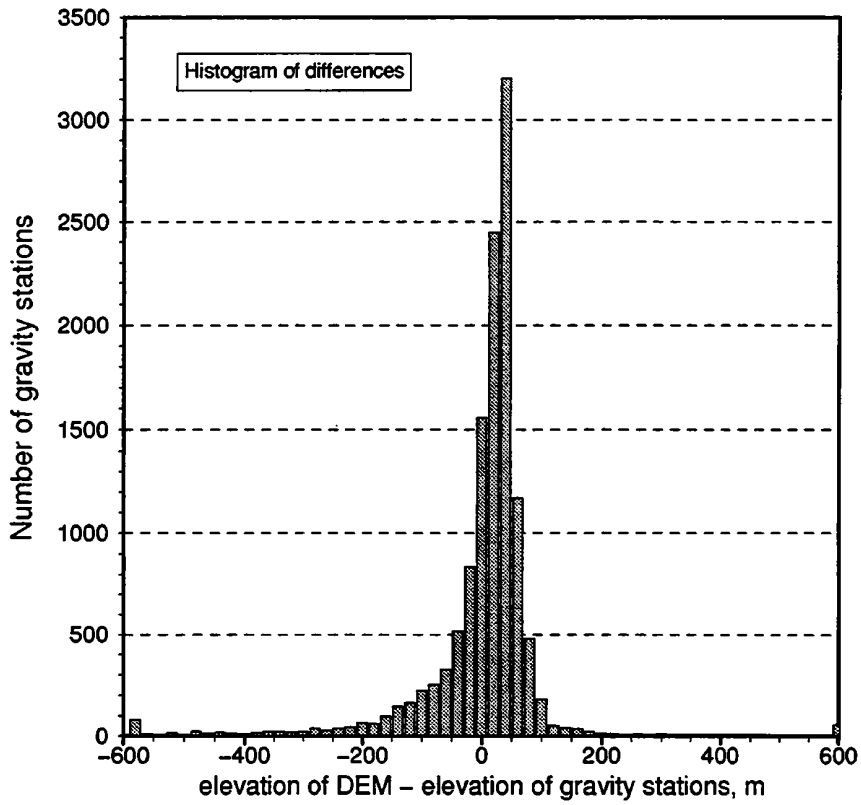

Abbildung 2: *Histogramm der Abweichungen der Stationshöhen vom digitalen Geländemodell von* JENSON & BLISS *(1995).*

man die so erhaltenen Höhendifferenzen gegen die Stationshöhen auf (Abb. 1), zeigt sich, daß für Stationshöhen um etwa 500 m und bei etwa 3400 m die Abweichungen besonders groß sind. Eine genauere Untersuchung hat ergeben, daß tatsächlich in der Puna Nordargentiniens bzw. Boliviens das DEM fehlerhaft ist. Da es sich jedoch um eine vorläufige Version de Höhenmodells handelt, werden die festgestellten Unstimmigkeiten in der endgültigen Version behoben werden. Um das Höhenmodell bis zu diesem Termin verwenden zu können, wurden die entsprechenden Bereiche von S. Mohr (FU Berlin) lagemäßig erfaßt. In einem zweiten Schritt sind dort Höhen aus dem DEM der Cornell University, nach einem Regridding auf die Rastergröße 30"×30", eingepaßt worden.

Insgesamt beträgt der Mittelwert des Betrags der Abweichung zwischen den insgesamt 12415 Schwerestationen von den Höhen des DEM's etwa 61 m; während der Mittelwert der gebildeten Differenzen -0.1 m und die Standardabweichung 167 m beträgt. Für ein Gitter mittlerer Höhen repräsentiert das neue DEM die Topographie für die Geländereduktion in ausreichender Genauigkeit (Abb. 2). Aus Übersichtsgründen sind in dieser Abbildung nur Abweichungen dargestellt, die kleiner als ± 600 m sind; in diesem Bereich liegen über 99% aller Abweichungen.

Topographische Reduktion

Die Berechnung der topographischen Reduktion wird bislang mit der Methode von EHRISMANN & LETTAU (1971) durchgeführt, die schon in der Alpengravimetrie ihre Tauglichkeit für die Verwendung im Hochgebirge bewiesen hat (MEURERS, 1992). Die Bestimmung der Geländereduktion erfolgt in drei Stufen. Zuerst wird die Nahreduktion durchgeführt, für die das Gelände topographisch bis zu einer Entfernung von 200 m auf acht Strahlen für verschiedene Entfernungszonen aufgenommen wird. Es schließt sich die Berechnung des Beitrags des Übergangsbereichs an, der die Zone zwischen dem festen Raster des Höhenmodells und der Nahaufnahme umfaßt. Die Berechnung der Fernreduktion basiert auf dem digitalen Geländemodell eines regelmäßigen Gitters. Dieses Berechnungsschema ist zwar sehr flexibel, hat aber mehr oder weniger historische Gründe. Die erzielte Genauigkeit ist hervorragend, weil zum einen die Sphärizität der Erde berücksichtigt wird, und zum anderen die Approximation des Geländes durch die verwendeten Elementarkörper sehr realistisch ist; auf eine Näherung durch artifizielle Körper wie Massenlinien wird verzichtet.

Eine Mitte der Achtziger Jahre vorgeschlagene Methode zur schnellen Berechnung der Geländereduktion, die auf die Verwendung von digitalen Geländemodellen zugeschnitten ist (SIDERIS, 1984), benutzt die Fast Fourier Transformation, erzielt aber, wie die Untersuchungen von GOLTZ (1989) zeigen, nur die Genauigkeit der sogenannten Massenlinienformel. Für größere Höhenunterschiede zwischen Schwerestation und Punkten des digitalen Höhenmodell können sich beträchtliche Unterschiede zum Ergebnis anderer Methoden ergeben. Die Nichtberücksichtigung der Erdkrümmung könnte durch Benutzung eines modifizierten FFT-Verfahren umgangen werden.

Die schon seit einiger Zeit für die dreidimensionale gravimetrische Modellierung von Untergrundmodellen eingesetzte Polyedermethode (GÖTZE & LAHMEYER, 1988), kann auch für die Berechnung der topographischen Reduktion benutzt werden, wobei drei Arbeitsschritte durchzuführen sind:

- Aufbau eines digitalen Höhenmodells,
- Vermaschung aller Höhenpunkte durch ein Dreiecksnetz,
- Berechnung der Schwerewirkung aller Polyeder für jede Schwerestation.

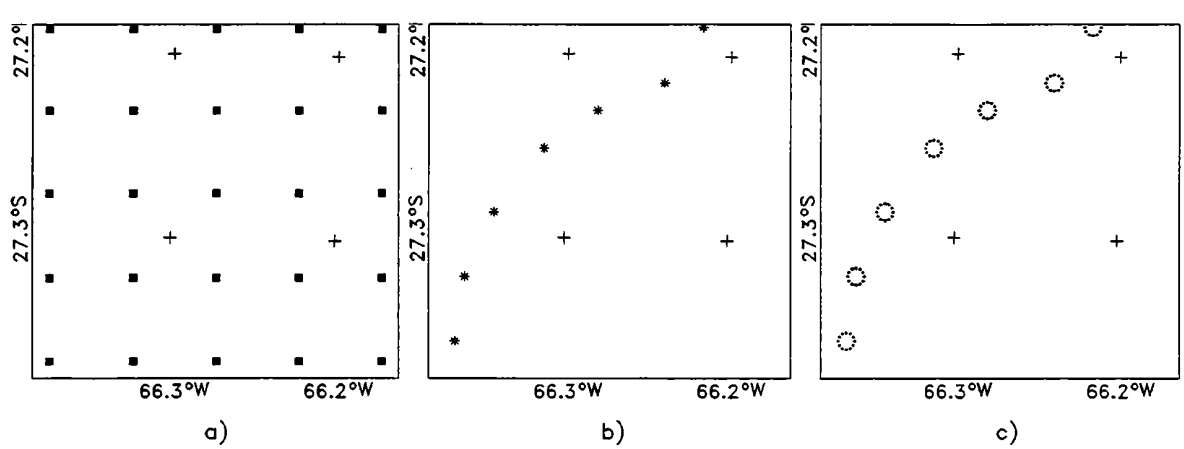

Abbildung 3: *Stützstellen der verwendeten Höheninformationenen bei der Berechnung der topographischen Reduktion mit der Polyedermethode, a) DEM, b) Stationshöhen, c) topographische Geländeaufnahme.*

Tabelle 2: *Zusammenstellung der für die topographische Reduktion benutzten Methoden.*

Jahr	Geländeapproximation durch	Berechnungsart	Entwicklung
ab 1982	Quader	sphärisch	Ehrismann, Lettau
ab 1989	Massenlinie (FFT)	eben	Sideris, Goltz
ab 1996	Polyeder	eben	Götze, Müller
geplant	Polyeder	sphärisch	

Zuerst wird ein kombiniertes Höhenmodell aufgebaut, das aus den Höhen der Gravimeterstationen (Abb. 3 a) und den auf einem regelmäßigen Gitter vorliegenden Höhen des digitalen Geländemodells (Abb. 3 b) besteht. Dazu kommen eventuell Höheninformationen aus einer topographischen Geländeaufnahme in unmittelbarer Stationsnähe (Abb. 3 c), wobei im Gegensatz zur Methode von EHRISMANN & LETTAU (1971) keine Einschränkung bezüglich der Lage der Höhenpunkte besteht.

Die sich anschließende Triangulierung aller Höhenpunkte benutzt den Algorithmus von RENKA (1984), der die Topographie durch möglichst gleichseitige Dreiecke annähert. In Stationsnähe ist die Geländeapproximation aufgrund genauerer Höheninformationen in der Regel wesentlich genauer als in den übrigen Bereichen, wo ausschließlich die Höhen des DEM's benutzt werden. Da die Generierung der Dreiecke jedoch zunächst nur dem mathematisch vorgegebenen Prinzip einer "optimalen Dreiecksbildung" genügt, ist eine nachträgliche Kontrolle notwending, um zu entscheiden, ob die Topographie dem erzeugten Modell entspricht. Durch Vorgabe von Zwangsbedingungen kann die Dreiecksbildung so gesteuert werden, daß bestimmte Punkte durch Dreiecksseiten verbunden werden müssen. An Gravimeterstationen, an denen keine topographische Geländeaufnahme vorliegt, werden im Umkreis von 200 m zusätzliche Hilfshöhenpunkte eingefügt, die auf dem gleichen Höhenniveau wie die Station selbst liegen, um ebenes Gelände in Stationsumgebung zu simulieren. Es könnten sonst Dreiecksflächen mit sehr starker Neigung entstehen, wenn eine Station in unmittelbarer Nähe eines Rasterpunktes des DEM's läge, deren Schwerewirkung die topographische Reduktion verfälschen würde. Abbildung 4 zeigt die Dreiecksbildung für ein Testgebiet im Nordwesten Argentiniens.

Die Geländereduktion für eine Station erhält man schließlich durch Summierung der Schwerewirkung aller Polyeder, deren Grundflächen aus ebenen Dreiecken im Stationsniveau und deren Deckflächen aus geneigten Flächen der Geländeapproximation bestehen. Die Berechnung der Schwere erfolgt durch eine von GÖTZE (1995) entwickelte analytische Lösung des auftretenden Volumenintegrals, die sich gegenüber anderen Lösungen durch seine Rechengeschwindigkeit auszeichnet.

Erste Testrechnungen mit dem Höhenmodell des USGS haben ergeben, daß die mit der Polyedermethode berechneten Reduktionen zu etwas größeren Reduktionsbeträgen führen, weil der Nahbereich- und Übergangsbereich wahrscheinlich besser erfaßt wird als bei der Methode von EHRISMANN & LETTAU (1971).

Es ist geplant, bei der Berechnung der topographischen Reduktion die Sphärizität der Erde zu berücksichtigen, was nur geringe Modifikationen am Rechenalgorithmus erfordert. Darüberhinaus sollen alle vorliegenden Informationen, die bei der topographischen Geländeaufnahme bei den Meßkampagnen angefallen sind, vom polaren, stationsbezogenen, Koordinatensystem in geographische Koordinaten umgerechnet und in das Höhenmodell integriert werden. Schließlich soll demnächst das bislang verwendete Verfahren von EHRISMANN & LETTAU (1971) durch die vorgestellte Polyedermethode abgelöst werden (s. Tabelle 2).

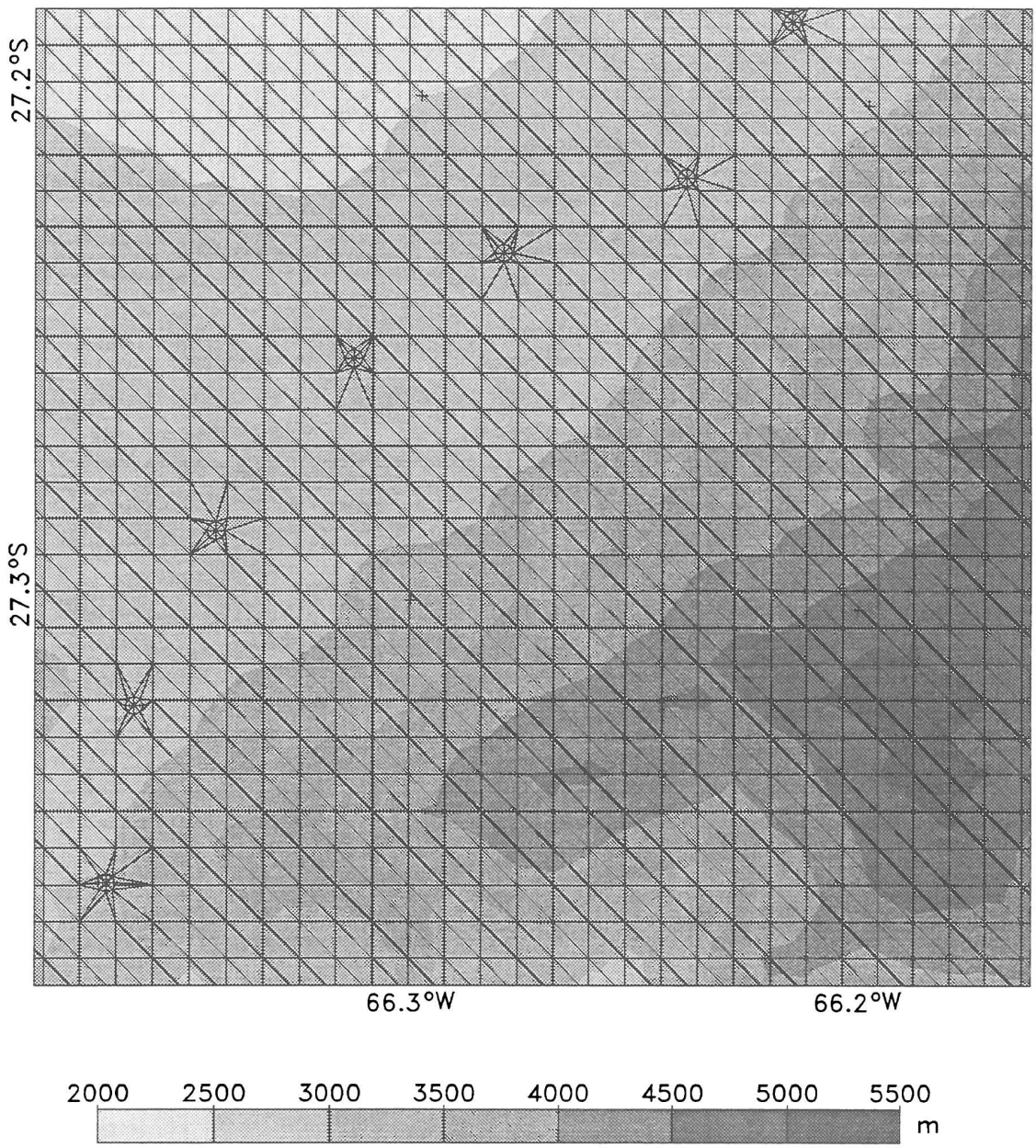

Abbildung 4: *Triangulierung der Höhenpunkte aus dem Geländemodell des USGS und sieben Schwerestationen bei der Berechnung der topographischen Reduktion mit der Polyedermethode.*

Anmerkung

Für die anregende Diskussion der hier behandelten Fragestellungen danken wir Herrn Dr. Bruno Meurers (Universität Wien) ganz herzlich. Die Untersuchungen sind entstanden im Rahmen der Teilprojekte D3 und B1B des Sonderforschungsbereichs 267, der von der Deutschen Forschungsgemeinschaft und der Freien Universität Berlin finanziert wird.

Literatur

DRAGICEVIC, M. (1970). Carta gravimetrica de los Andes meridionales e interpretacion de las anomalias de gravedad de Chile central. Publ. 93, Dep. de Geofis. y Geod., Univ de Chile, Santiago (Chile).

EHRISMANN, W. UND LETTAU, O. (1971). Topographische Reduktion von Schweremessungen in der näheren und weiteren Stationsumgebung mit Digitalrechnern. *Archiv für Meteorologie, Geophysik und Bioklimatologie*, **20**, 383–396. Serie A.

GÖTZE, H.-J. (1986). Schweremessungen und deren Interpretation im mittleren und östlichen Teil der Anden-Geotraverse. DFG Abschlußbericht (unveröffentlicht), Deutsche Forschungsgemeinschaft, Bonn.

GÖTZE, H.-J. (1995). Berechnung der Ableitungen des Schwerepotentials für einen Polyeder. Interner Bericht. FU Berlin, Berlin.

GÖTZE, H.-J. UND LAHMEYER, B. (1988). Application of three-dimensional interactive modeling in gravity and magnetics. *Geophysics*, **53**, 1096–1108.

GÖTZE, H.-J., LAHMEYER, B., SCHMIDT, S. UND STRUNK, S. (1990). A new gravity data base in the Central Andes (20° - 26°). *EOS*, **71**(16), 401–407.

GÖTZE, H.-J., ALVERS, M., GOLTZ, G., KIRCHNER, A., MÜLLER, A., SCHÄFER, U., SCHMIDT, S., ARANEDA, M., UGALDE, H., CHONG, G., BARRIO, L., LOPEZ, N. UND OMARINI, R. (1996). Group updates gravity database for the Central Andes. http://www.agu.org/eos_elec/95189e.html. American Geophysical Union.

GOLTZ, G. (1989). Zur Theorie und Anwendung der topographischen Reduktion nach Sideris in der Gravimetrie. Diplomarbeit, FU Berlin, Berlin.

GROW, J. A. UND BOWIN, C. O. (1975). Evidence for high - density crust and mantle beneath the Chile trench due to the descending lithosphere. *Journal of Geohysical Research*, **80**(11), 1449–1458.

HUTCHINSON, M. F. (1988). Calculation of hydrologically sound digital elevation models. In *Proc. Third Inter. Symp. Spatial Data Handling*, Columbus, Ohio. August 17-19., 1988.

HUTCHINSON, M. F. (1989). A new method for gridding elevation and stream line data with automatic removal of pits. *Journal of Hydrology*, **106**, 211–232.

HUTCHINSON, M. F. (1991). A continental hydrological assessment of a new grid-based digital elevation model of Australia. *Hydrological Processes*, **5**, 45–58.

ISACKS, B. L. (1988). Uplift of the Central Andes and bending of the Bolivian orocline. *Journal of Geophysical Research*, **93**, 3211–3231. B4.

JAMES, D. E. (1971). Plate tectonic model for the evolution of the Central Andes. *Geological Society of America Bulletin*, **82**, 3325–3346.

JENSON, S. UND BLISS, N. (1995). Preliminary release of the South American 30 arc-second DEM. ftp://edcftp.cr.usgs.gov/pub/data/30ASDCWDEM/SOUTH_AMERICA/README.txt. USGS.

MEURERS, B. (1992). Untersuchungen zur Bestimmung und Analyse des Schwerefeldes im Hochgebirge am Beispiel der Ostalpen. Habilitationsarbeit, Universität Wien, Wien.

PRINCE, R. A., SCHWELLER, W., COLBOURN, W., NESS, G. UND MASIAS, A. (1980). Bathymetry of the Peru-Chile continental margin and trench. Geol. Soc. Am. Map Chart Ser., MC-34, Geological Society of America.

RENKA, R. J. (1984). Algorithm 624: Triangulation and interpolation at arbitrarily distributed points in the plane. *ACM Transactions on Mathematical Software*, **10**(4), 440–442.

SCHMIDT, S. (1986). Die Verwendung von Altimetern zur Bestimmung von gravimetrischen Stationshöhen. Dissertation, TU Clausthal, Clausthal-Zellerfeld.

SIDERIS, M. G. (1984). Computation of gravimetric terrain corrections using Fast Fourier Transform techniques. Diplomarbeit, University of Calgary, Calgary. Department of Surveying Engineering, UCSE Reports 20007.

STRUNK, S. (1985). Auswertung gravimetrischer Messungen und deren 3D-Interpretation im Bereich der andinen Subduktionszone Nordchiles. Diplomarbeit, TU Clausthal, Clausthal-Zellerfeld.

STRUNK, S. (1990). Analyse und Interpretation des Schwerefelds des aktiven Kontinentalrandes der zentralen Anden (20° - 26° S). Dissertation, FU Berlin, Berlin.

3D SEISMIC VERSUS GRAVITY IN THE VIENNA BASIN

Harald Granser

OMV AG

Introduction

After a hiatus of several years OMV renewed its exploration efforts in the Vienna basin, especially in the Neogene Section which is the most important hydrocarbon region of Austria (Fig. 1). As the Vienna basin is a very mature exploration area, 3D Seismic was viewed as the most promising exploration method (e.g. Nestvold 1987). OMV's 3D campaign began in the southern Vienna basin in the area of Wienerherberg and Fischamend (Fig.1), the paper however is mainly concerned with the Matzen area in the northern Vienna basin where the acquisition of 3D seismic started in 1994 and is still ongoing.

Matzen is a giant field located about 30 km northeast of Vienna. It is the largest oilfield of onshore Central and Western Europe. Cumulative production since discovery in 1949 is about 500 MMbbl and almost 1 Tcf gas.

The interpretation of the newly acquired seismic obviously included reevaluation of existing data like 2D seismic lines, well logs, etc. and also gravity data.

Zych (1988) describes OMV's gravity data base in detail which was actually also very valuable in a slightly unconventional way. The very accurate elevation of the gravity stations was utilized to calculate the elevation static corrections in processing the 3D seismic data.

Geological Background

The Vienna basin is a Tertiary, rhomboidal pull-apart basin in the Alpine-Carpathian Overthrust belt superimposed on the allochthonous Flysch and Calcareous nappes which in turn overthrust the authochthonous Molasse and Mesozoic cover of the Bohemian massif. The up to 5 km deep Neogene sedimentary basin formed along a Miocene transform system which links the Eastern Alps and the Western Carpathians. To the east a number of NNE-trending basement highs (Leithagebirge, Male Karpaty) separates the Vienna basin and the Pannonian Basin. To the west, several major NE-striking faults delimit the basin from the Eastern Alps (Thermenlinie, Steinbergbruch). Subsidence commenced in Early Miocene (Burchfiel and Royden, 1982) and continued probably up to late Pannonian / Pontian with a possible inversion (Decker and Peresson 1996) at the Pannonian-Pontian boundary.

Most significant hydrocarbon pools in the Vienna basin are associated with fault controlled uplifted blocks forming structural highs where hydrocarbons accumulate in stacked reservoirs in Miocene beds (mostly lower Sarmatian and Baden). The most important of these oil and gasfields is the Matzen field which is described in detail by Kreutzer (1992).

Processing and Interpretation of Gravity Data

The Bouguer gravity data of the Vienna Basin were subject of a recent detailed investigation (Kröll et al. 1993). In short the main results may be summarised as follows. The "raw" Bouguer gravity data has a strong long wavelength overprint related to deep sources, pos-

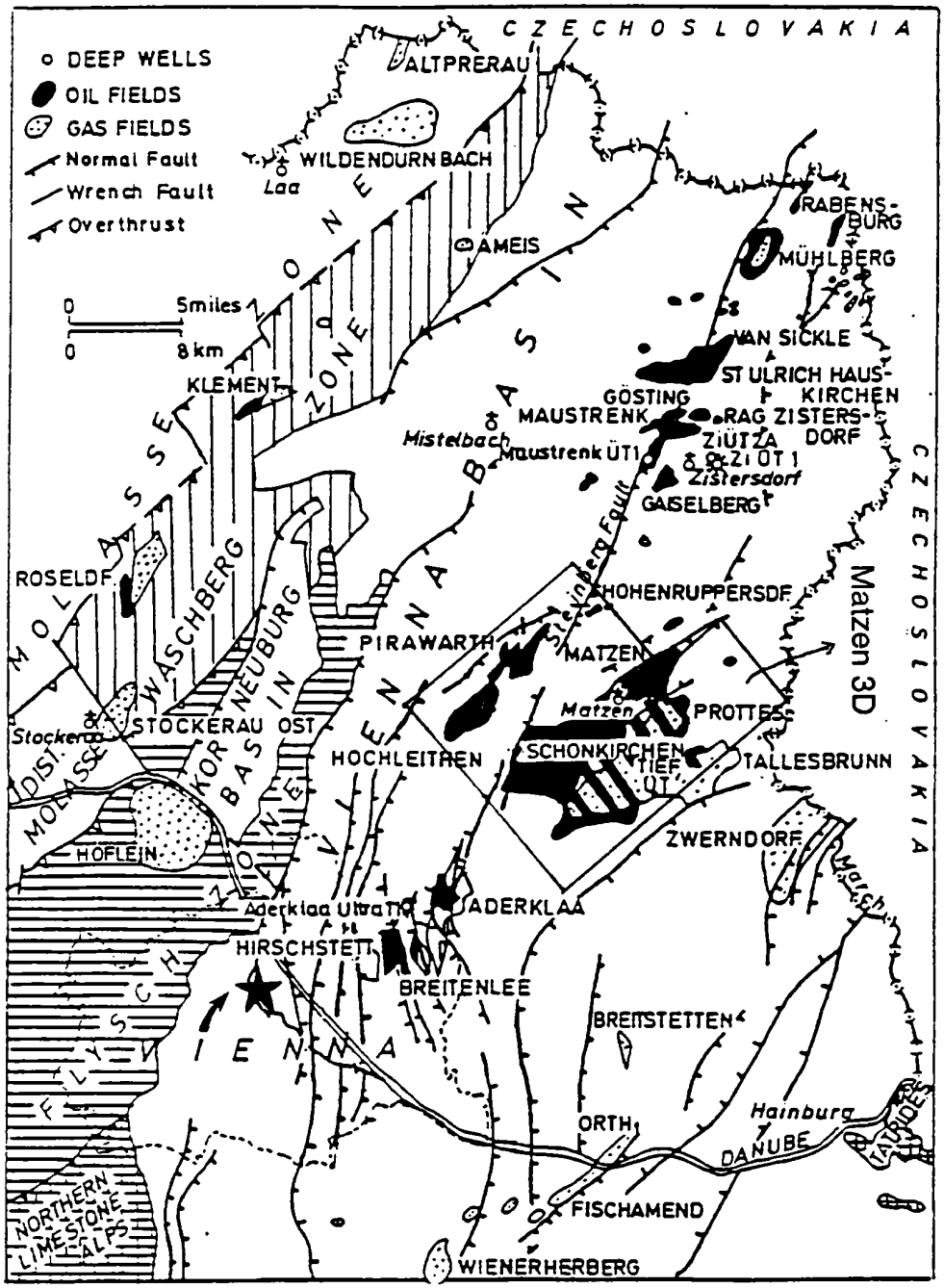

Figure 1: Main Elements of the Vienna Basin. Oil and gasfields in the Austrian part of the Vienna basin and surrounding regions. (According to Wessely, 1988).

sibly the Moho relief (see also Granser et. al 1989) which obscures the gravity image of shallower strata. Nevertheless major structural features are clearly discernible like the Anderklaa buried hill, an oilfield actually discovered by means of gravity, the St. Marx / Oberlaa uplifted block, etc.

A much improved resolution was achieved by horizontal gradient filtering of the Bouguer gravity grid. The main intrabasinal fault system like the Markgrafneusiedler fault, the Kopfstettener fault zone, the Leopoldsdorfer fault and many more are delineated. Furthermore the basin margins like the Steinberg fault are accurately mapped.

Additionally a system of NE-SW trending lineaments is delineated by the horizontal gradient filtering of the Bouguer gravity in the Matzen area. This previously unknown "structural feature" is approximately at right angle to the Steinberg fault which is tectonically difficult to explain. However, if interpreted as previously unknown fault trend it would obviously greatly influence the structural pattern of the central zone of the Vienna Basin and the area of the Matzen field.

For further investigation the gravity of the Vienna basin area was reprocessed using OMV's complete data set. Bouguer gravity data sets with reduction densities of 2.67 gcm^{-3} and 2.00 gcm^{-3} were gridded with a grid size of 250 × 250 meters.

The two Bouguer gravity grids were subsequently FFT filtered (Hildenbrand 1983) using a variety of options like bandpass filtering , horizontal, 1st and 2nd vertical derivative and the total gradient (analytic signal). The vertical gradient filtering probably produced the most interpretable results (Fig. 2) delineating the fault system in the Vienna basin as well as the intra-basinal topography.

Whereas most filtered maps of the 2.67 Bouguer gravity replicated the previously described NE-SW trending lineaments in the Matzen area (Kröll et al. 1993), these lineaments are completely absent in the processing products of the 2.00 Bouguer gravity. Comparison of the 2.67 maps with the topography in this area, mainly characterized by the drainage system of the Northern Vienna Basin, revealed a close correlation to the lineaments. Quite obviously the lineaments are caused by a Nettleton effect using a wrong reduction density of 2.67 gcm^{-3}; A reduction density of 2.00 gcm^{-3} is more appropriate for the Vienna basin.

In general a remarkable amount of structural detail is imaged in the vertical gradient map of the 2.00 Bouguer gravity. Many major intrabasinal faults are clearly delineated. However, additionally to the fault delineation which are also well shown in the horizontal gradient maps also the main structural highs within the Vienna basin are well imaged - and such the major HC accumulations as they are associated with them. These are in particular the Matzen-Anderklaa uplifted bock, the Enzersdorfer Hochzone associated with biogenic gasfields, the Zwerndorf horst associated with the Baumgarten gasfield, the Rabensburger Rücken sofar devoid of major HC finds and the very shallow uplifted Laxenburg-Oberlaa Hochzone which is also a prominent feature of the unfiltered Bouguer map. Closer inspection of the vertical gradient map on a different colourscheme than black and white of figure 2 shows that also secondary structural highs located on downthrown hangingwall blocks are delineated. HC accumulations associated with such structures are RAG's Gaiselberg oilfield and OMV's Moosbrunn Gasfield in the Southern Vienna basin.

Comparing the vertical gradient map with the Top Sarmat map published by Unterwelz (1980) based on well and seismic data shows a remarkably good correlation. Especially the fault positions are similar which is not straightforward as the dip of the faults is typically about 45 degrees and the Sarmat/Pannon boundary is an intrasedimentary timeline in the late Miocene (11.5 Ma) when the environment changed from brachyhaline to brackish.

Nevertheless the Sarmat/Pannon boundary is associated with a density contrast, otherwise the fault positions would not correlate that well with the top Sarmat map.

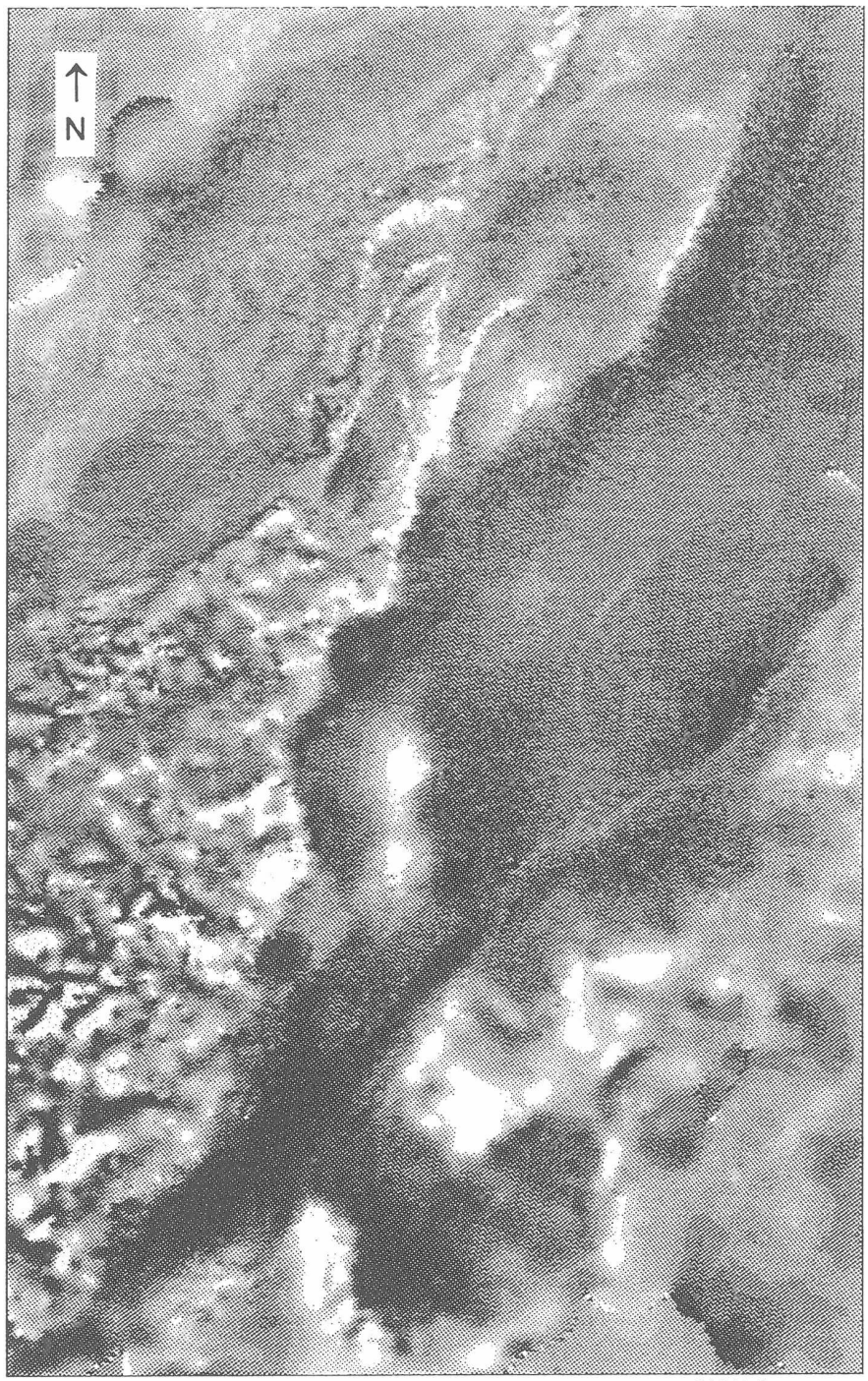

Figure 2: Vertical gradient of the 2.00 Bouguer gravity

Comparison with 3D Seismic

The 3D Großschweinbarth Seismic is situated in the northern Vienna basin and covers the oilfields of Hochleiten, Pirawarth and Matzen (Fig. 1). Sofar three swaths were acquired. The first swath designed for shallower targets with a geophone and shotlinespacing of 150 meters and Dynamite as a source.

The other swaths were acquired with a 300 meter spacing and Vibroseis as a source. A binsize of 25 × 25 meters was used and an average fold of 24 achieved. A standard 3D

processing scheme was applied with the static corrections being probably the most critical sequence.

Data quality is excellent for land 3D seismic standards. Figure 3 shows a typical seismic line running from the SW edge to the NE edge of the survey. The interpreted horizon is near the Sarmat/Pannon boundary and the little circles indicate faultplanes - The Hochleithen faults in the West then the Bockfliess faults and the North and South dipping Matzner Nordrandbrüche. The faultcuts with the near Top Sarmat seismic horizon are posted on top of the vertical gravity gradient in Figure 4. The correlation of the Bockfliess faultsystem as a continuation of the Steinberg fault is quite obvious. Also for the Hochleiten and the Hohenruppersdorf faultsystem a correlation between seismic faults and vertical gradient lineaments is present. Less clear but arguable is the correlation of the Matzner faultsystem. Again the position of the gravity lineaments is very near to the Top Sarmat faultcuts.

Conclusions

Gravity can be a very powerful exploration tool not only for mapping of structural highs but also for faultcorrelation in case of sparse 2D seismic. Filtering of potential field data sometimes helps.

Acknowledgements

The permission of OMV AG to publish this manuscript is appreciated.

References

Burchfiel, B.C., Royden, L.,1982. Carpathian Foreland Fold and Thrustbelt and its relation to the Pannonian and other basins. AAPG bull., 66, 1179-1192.

Decker, K., Peresson, H. 1996. Tertiary kinematics in the Alpine - Carpatian - Pannonian System: links between thrusting, transform faulting and crustal extension. in Wessely, G., Liebl, W. (eds): Oil and Gas in Alpidic Thrustbelts and Basins of Central and Eastern Europe, EAPG Spec. Pub. 5.

Granser, H., Meurers, B., Steinhauser, P., 1989. Apparent density mapping and 3D gravity inversion in the Eastern Alps. Geoph. Prosp., 37, 279-292.

Hildenbrand, T.G.,1983. A filtering program based on two-dimensional Fourier analysis. USGS Open File Rep. 83-237.

Kreutzer, N.,1992. Matzen Field - Austria. AAPG Treatise Atlas Structural Traps VII.

Kröll, A., Gnojek, I., Heinz, H., Jiricek, R., Meurers, B., Seiberl, W., Steinhauser, P., Wesseley, G., Zych, D.,1993. Erläuterungen zu den Karten über den Untergrund des Wiener Beckens und der angrenzenden Gebiete. GBA Wien.

Nestvold, E.O., 1987. The use of 3D seismic in exploration, appraisal and field development. Proc.12th World Petroleum Congress 2,125-132.

Wessely, G., 1988. Structure and development of the Vienna basin in Austria, in: Royden, L., Horvath, F., (eds.): The Pannonian basin, a study in basin evolution. AAPG Memoir, 45, 333-347.

Unterwelz, H., 1980. Wiener Becken Srukturkarte Oberkante Sarmat. In: Brix. F., Schultz, O., (eds.): Erdöl und Erdgas in Österreich. Verlag Naturhistorisches Museum Wien. Beilage 2.

Zych, D., 1988. 30 Jahre Gravimetermessungen der ÖMV AG in Österreich und ihre geologisch-geophysikalische Interpretation. Arch. f. Lagerst. forsch., GBA, 9, 155-175.

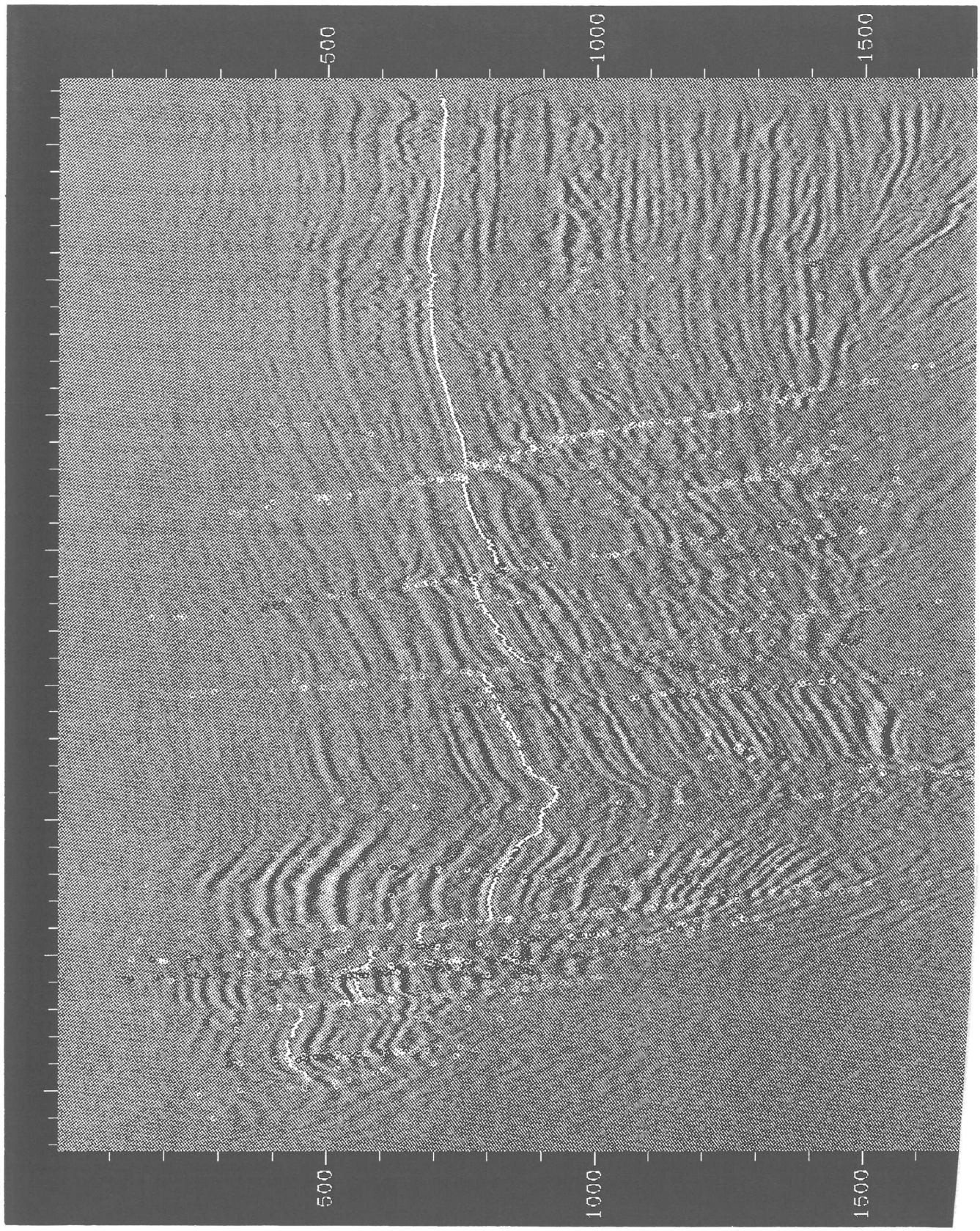

Figure 3: W-E Seismic line of the Matzen 3D volume. Interpreted seismic horizon near top Sarmat. Circles indicate faultcuts.

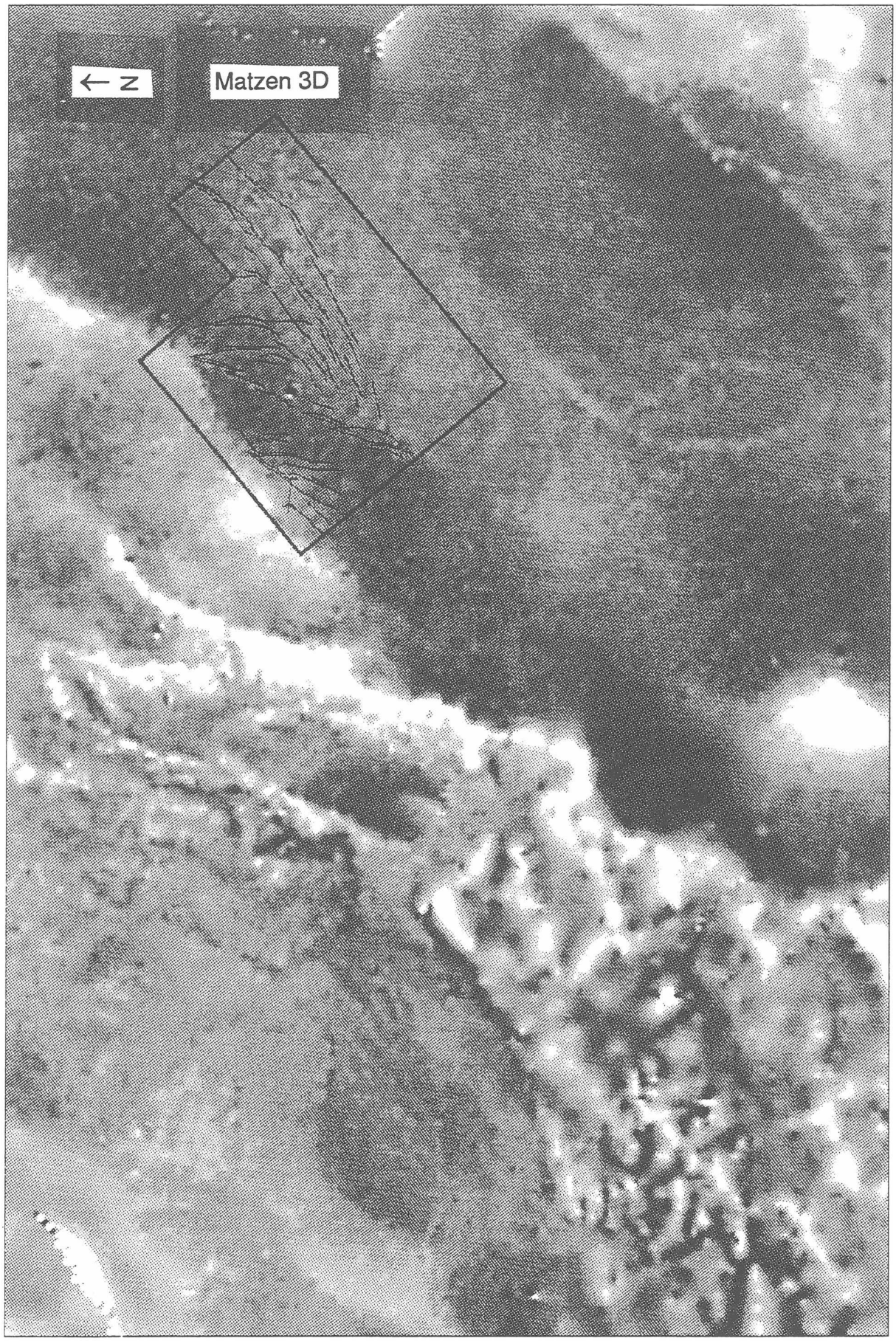

Figure 4: Vertical gradient map in the Matzen area with overposted seismic faultcuts of the near top Sarmat horizon.

ZUM EINSATZ VON GPS IN DER HOCHGEBIRGSGRAVIMETRIE

Herbert Lichtenegger[1] und Gerhard Kraiger[2]

[1] Institut für Angewandte Geodäsie
[2] Institut für Theoretische Geodäsie
Technische Universität Graz

Kurzfassung

Beim letzten Alpengravimetrie-Kolloquium wurde eine Studie über die Einmessung von Gravimeterstationen mit GPS vorgelegt. Mittlerweile wurden die dortigen Anregungen aufgegriffen und in insgesamt drei gravimetrischen Kampagnen im hochalpinen Bereich erfolgreich angewendet. In der vorliegenden Arbeit wird über die dabei gewonnenen Erfahrungen bezüglich Durchführung und Auswertung der GPS-Beobachtungen berichtet. Ferner werden Vorschläge zu einer weiteren Steigerung der Wirtschaftlichkeit des Verfahrens unterbreitet.

Abstract

A feasibility study for GPS-positioning in the context of gravimetric surveys was presented at the last „Alpengravimetrie-Kolloquium". Meanwhile, GPS was successfully applied during three gravimetric campaigns in high-mountain regions. The present paper reports on experiences obtained in performing and processing the GPS-observations. Also, possible further economic improvements are discussed.

1. Einleitung

Beim letzten Alpengravimetrie-Kolloquium in Leoben wurde eine Machbarkeitsstudie über die Einmessung von Gravimeterpunkten mittels GPS vorgelegt, vgl. Lichtenegger und Kraiger (1993). Danach ist es mit Einfrequenzgeräten und bei Beobachtungszeiten von maximal 30 Minuten möglich, für Basislinien bis 15 km Länge eine relative Höhengenauigkeit von ± 10 cm zu erzielen.

Die vorgeschlagene Methodik wurde vom Institut für Meteorologie und Geophysik der Universität Wien (Dr. Meurers) aufgegriffen und im Rahmen von insgesamt drei gravimetrischen Kampagnen (1993, 1994, 1995) im hochalpinen Bereich der Ötztaler Alpen praktisch erprobt. In der vorliegenden Arbeit wird über die dabei gewonnenen Erfahrungen hinsichtlich Durchführung und Auswertung der GPS-Beobachtungen sowie das Ergebnis berichtet.

Bezüglich theoretischer Details wird auf die bereits erwähnte Arbeit von Lichtenegger und Kraiger (1993) oder auf die Fachliteratur wie zum Beispiel Hofmann-Wellenhof et al. (1994a) oder Hofmann-Wellenhof et al. (1994b) verwiesen.

2. Beobachtungen

Für die Planung und Durchführung der Beobachtungen war der zweitgenannte Autor verantwortlich. Vor dem diesbezüglichen Erfahrungsbericht werden allerdings noch die Veränderungen mitgeteilt, die sich seit dem letzten Alpengravimetrie-Kolloquium im GPS-Status ergeben haben.

GPS-Status
Im Jahr 1993 wurden insgesamt sechs GPS-Satelliten in eine Umlaufbahn gebracht und es wurde somit gegen Ende des Jahres die volle Konstellation mit 24 Satelliten erreicht. Kurz danach, Ende Jänner 1994, erfolgte überraschenderweise die Aktivierung von Anti-Spoofing (A-S) und damit die Verschlüsselung des P-Codes auf dem Satellitensignal. Damit war für viele Empfänger die Phasenmessung auf dem Träger L2 entweder nicht mehr oder nur mit verminderter Genauigkeit möglich. Nach dem Test der vollen Konstellation mit 24 Block II Satelliten wurde schließlich im Juli 1995 offiziell die volle Verfügbarkeit des Systems erklärt.

Beschreibung des Meßgebietes
Das Meßgebiet, in dem vom Institut für Meteorologie und Geophysik der Universität in Wien in den letzten Jahren gravimetrische Kampagnen durchgeführt wurden, liegt im Bereich der Ötztaleralpen. Die Ausdehnung des jeweiligen Meßgebietes ist in der Tabelle 1 angegeben. Aus der Tabelle geht hervor, daß es sich um hochalpines Gelände mit Höhen bis über 3 000 m handelt. In dem Gebiet wurden insgesamt 138 Gravimeterpunkte mit einem mittleren Punktabstand von 3 km eingemessen. Die Bezeichnung der Punkte erfolgte durch eine vierstellige Zahl, wobei die beiden ersten Ziffern nach Addition von 100 die Blattnummer im österreichischen Kartenwerk 1:50 000 und die beiden letzten Ziffern die eigentliche Punktnummer darstellen. Dabei bezeichnen Nummern unter 10 die Referenzpunkte und jene über 10 die Neupunkte.

Jahr	Breite [Grad]	Länge [Grad]	Höhe [Meter]
1993	46.8 – 47.1	10.5 – 11.1	1 050 – 3 030
1994	46.8 – 47.1	10.5 – 11.1	1 270 – 3 230
1995	46.9 – 47.2	10.1 – 10.6	890 – 2 700

Tabelle 1: Ausdehnung der Meßgebiete

GPS-Beobachtungsmethodik
Die Bestimmung geodätischer Koordinaten im hochalpinen Bereich stellt durch den Einsatz von GPS prinzipiell kein Problem mehr dar. Für den angestrebten Genauigkeitsbereich und wegen der großräumigen Verteilung der Gravimeterpunkte kommen nur relativ statische Beobachtungsmethoden unter Verwendung der Trägerwellenphase in Betracht. Falls Zweifrequenzempfänger und die entsprechende Software verfügbar sind, kann vorteilhaft das Verfahren der statischen Schnellmessung („rapid static“) genutzt werden.

Die GPS-Empfänger wurden vom Institut für Angewandte Geodäsie der Technischen Universität in Graz angemietet. Es sind dies ehemalige P-Code Empfänger der Firma Ashtech, wobei die zweite Frequenz nach Aktivierung von A-S zunächst nicht genutzt werden konnte. Daher standen im Jahr 1994 nur L1-Beobachtungen zur Verfügung. Erst nach geeigneter Aufrüstung der Empfänger („Z-tracking") konnten in der Kampagne 1995 wieder die Phasen auf beiden Trägern beobachtet werden.

Die Planung der Beobachtungssessionen und die Auswahl der GPS-Punkte erfolgte nach den üblichen Richtlinien. Dabei ist zu beachten, daß sich seit der vollen Verfügbarkeit des Systems meist sechs Satelliten über dem Horizont befinden. Diese konnten im allgemeinen auch beobachtet werden, da Abschattungsprobleme seltener als erwartet aufgetreten sind.

Referenzpunkte
Zur Transformation der GPS-Ergebnisse in das Landessystem müssen im jeweiligen Meßgebiet mindestens drei Paßpunkte mit bekannten Koordinaten in beiden Systemen vorliegen. Diese Referenzpunkte wurden so gewählt, daß sie auch mit Landfahrzeugen leicht zugänglich waren. Somit konnte deren GPS-Einmessung auch während Schlechtwetterperioden erfolgen, ohne den Meßfortschritt der Gravimetrie zu beeinflussen.

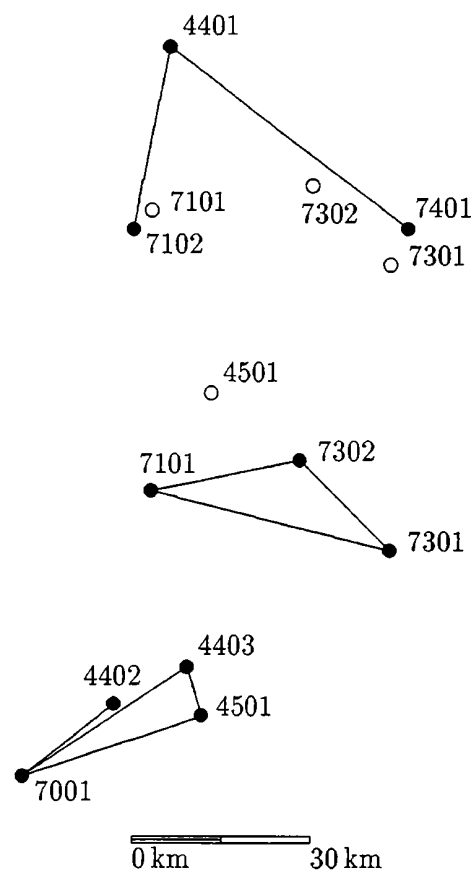

Abbildung 1: Verteilung der Referenzpunkte in den Jahren 1993 (oben), 1994 (Mitte) und 1995 (unten)

Die Konfiguration der Referenzpunkte ist in der Abbildung 1 dargestellt. Daraus ist ersichtlich, daß im Jahr 1993 das aus drei Punkten (oder zwei Basislinien) bestehende Paßpunktnetz (4401, 7102, 7401) nicht mit den Basispunkten für die gravimetrische Detailaufnahme (7101, 7301, 7302) verbunden war. Damit waren wohl die Landeskoordinaten der Paßpunkte, nicht aber jene der Basispunkte für die Detailaufnahme genügend genau kontrollierbar. So konnten beispielsweise fehlerhaft angegebene Landeskoordinaten für den Punkt 7401 korrigiert werden. Auch eine (grobe) Punktverwechslung im Punkt 7301 wurde über die GPS-Navigationslösung festgestellt. Hingegen blieb eine fehlerhafte Zentrierung im Punkt 7302 vorerst unentdeckt und konnte erst im Folgejahr richtiggestellt werden. In der Kampagne 1994 wurden die drei Basispunkte des Vorjahres (7101, 7301, 7302) durch drei Basislinien kontrolliert verbunden. Ein vierter Referenzpunkt (4501) konnte wegen fehlender Einbindung in das Paßpunktnetz nicht zur Datumstransformation herangezogen werden. Eine optimale Lösung stellt das Referenznetz der Kampagne 1995 dar. Sämtliche Referenzpunkte (4402, 4403, 4501, 7001) wurden über GPS eingemessen und konnten daher als Paßpunkte verwendet werden.

Wie aus der Tabelle 2 abgelesen werden kann, lagen die Längen der (primären) Basislinien zwischen den Referenzpunkten im Bereich von 20 bis 50 Kilometern und die Beobachtungszeiten schwankten zwischen einer und zwei Stunden. Erwähnenswert ist, daß hinsichtlich der Beobachtungszeiten für die Einmessung von Referenzpunkten noch ein Einsparungspotential vorhanden ist.

Jahr	Basislinie [von–nach]	Länge [km]	Beobachtungszeit [Minuten]	Beobachtete Satelliten
1993	4401–7102	28.9	120	6
	4401–7401	49.7	120	7
1994	7101–7302	27.0	78	6
	7101–7301	40.9	71	7
1995	7001–4402	22.3	67	7
	7001–4403	32.1	124	7
	7001–4501	33.8	128	7

Tabelle 2: Statistik für die Basislinien zwischen den Referenzpunkten

Neupunkte

Der Transport des Instrumentariums zu den Neupunkten wurde üblicherweise mittels Hubschrauber durchgeführt. Nur bei Schlechtwetter wurden für die Einmessung zufahrbarer Punkte auch Landfahrzeuge benutzt.

An den Neupunkten wurden neben den GPS-Beobachtungen die gravimetrischen Messungen und die tachymetrische Erfassung der Nahzone durchgeführt. Für die beiden letztgenannten Tätigkeiten wurde erfahrungsgemäß ein Zeitraum von etwa je 15 Minuten benötigt. Für die GPS-Beobachtungen an den Gravimeterpunkten wurden im Jahr 1993 und 1994 in Abhängigkeit von der Basislinienlänge Richtwerte von 25 bis 35 Minuten angesetzt. Diese Zeiten gelten unter Berücksichtigung der angestrebten Genauigkeit für

normale statische Einfrequenzbeobachtungen und für Basislinien bis etwa 15 km Länge. Die Sessionslängen können jedoch bei Anwendung des Verfahrens der statischen Schnellmessung wesentlich reduziert werden. Diesbezügliche Detailuntersuchungen wurden mit den Meßdaten der letztjährigen Meßkampagne durchgeführt.

Als Datenaufzeichnungsrate wurde in den Jahren 1993 und 1994 ein Intervall von 20 Sekunden gewählt. Im Jahr 1995 wurde die Datenrate wegen einer Verkürzung der Sessionslängen auf 10 Sekunden erhöht. In allen drei Kampagnen wurde die untere Schranke für die Satellitenelevation mit 15° und jene für den maximalen PDOP-Wert auf 5 gesetzt.

Die Tabelle 3 vermittelt einen statistischen Überblick über die Basislängen bei der Einmessung der Gravimeterpunkte. Es kann abgelesen werden, daß seit 1993 eine deutliche Zunahme von Basislinien über 10 km zu verzeichnen ist.

Jahr	Basislinienlänge			Minimum	Maximum	Mittel
	< 5 km	5–10 km	> 10 km	[km]	[km]	[km]
1993	11	27	17	2.1	17.2	8.3
1994	1	9	25	3.6	19.0	11.4
1995	7	16	25	1.7	17.4	9.9

Tabelle 3: Statistik der Basislinien zur Festlegung der Gravimeterpunkte

Wirtschaftliche Aspekte

In der Tabelle 4 sind Daten für eine Analyse der Wirtschaftlichkeit angeführt. Bei der Anzahl der Beobachtungstage gilt die erste Zahl für die Einmessung von Neupunkten, die zweite jene für die Einmessung der Referenzpunkte. Hierbei sind Tage nicht berücksichtigt, an denen wegen Schlechtwetter oder aus anderen Gründen ein Hubschraubereinsatz ganztägig nicht möglich war. Die höchste Zahl von Neupunkten pro Beobachtungstag wurde im Jahr 1993 erreicht. Diese Zahl täuscht allerdings, da in dieser Kampagne die Einmessung der Referenzpunkte vollständig von der Neupunktaufnahme getrennt war. In den Folgejahren hingegen wurde beides weitgehend gemeinsam durchgeführt. Dies drückt sich in der Gesamtanzahl von Punkten pro Tag aus, wo im Jahr 1995 eine deutliche Steigerung gegenüber den Vorjahren zu verzeichnen war. Dies ist eine Folge der verkürzten Sessionslängen in den Gravimeterpunkten.

Jahr	1993	1994	1995
Referenzpunkte	3	3	4
Neupunkte	55	35	48
Beobachtungstage	9+3	7+1	8+1
Neupunkte pro Tag	6.1	5.0	6.0
Punkte pro Tag	4.8	4.8	5.8

Tabelle 4: Wirtschaftliche Aspekte der GPS-Beobachtungen

3. Auswertungen

Die Auswertungen wurden vom Erstautor durchgeführt. Sie beinhalteten die Editierung und Bereinigung der Beobachtungsdaten, die Berechnung der Basisvektoren und die Transformation der GPS-Ergebnisse in das System der Landesaufnahme.

Dateneditierung
Wegen mangelnder Beobachtungserfahrung ergab sich für die Daten der Kampagne 1993 noch die Notwendigkeit einer umfangreichen Datenbereinigung. Dies gilt nicht mehr für die letztjährige Kampagne, bei der die auf Disketten gespeicherten Beobachtungsdaten mehr oder weniger direkt zur weiteren Auswertung übernommen werden konnten.

Basislinienauswertung
Es soll an dieser Stelle nicht im Detail auf die Auswertung von Basislinien eingegangen sondern vor allem das Problem der Lösung der Phasenmehrdeutigkeiten („Ambiguitäten") diskutiert werden.

Die ganzzahlige Lösung der Ambiguitäten ist ein wesentlicher Parameter für die Qualitätskontrolle. Eine diesbezügliche Statistik für die Basislinien zwischen den Neupunkten ist in der Tabelle 5 enthalten. Die Erfolgsquote wurde durch verschiedene Auswertestrategien, wie Wahl verschiedener Referenzsatelliten oder Elimination von schlechten Beobachtungsdaten, noch erhöht. Trotzdem konnten mit Einfrequenzdaten nicht alle Ambiguitäten eindeutig gelöst werden. Dabei muß jedoch festgestellt werden, daß die Nichtlösbarkeit nicht unbedingt mit der Basislinienlänge korreliert ist. Beispielsweise haben drei der problematischen Basislinien des Jahres 1993 eine Länge von unter 5 km während nur drei mehr als 10 km lang sind. Bemerkt wird, daß auch gute DOP-Faktoren noch keine Garantie für gute Ergebnisse sind. Zum Beispiel ist die optimale geometrische Konfiguration gegeben, wenn ein Satellit im Zenit beobachtet wird und sich die übrigen Satelliten in Horizontnähe befinden. Für letztere erhöht sich aber das Meßrauschen, wobei allerdings die Lage gegenüber der Höhe wesentlich stärker verfälscht wird.

Die nicht eindeutige Lösbarkeit der Ambiguitäten führt zu fehlerhaften Ergebnissen, die jedoch nicht wesentlich über dem angestrebten Genauigkeitsniveau liegen.

Jahr	Anzahl der Basislinien	Basislinien mit ganzzahliger Ambiguitätenlösung	Erfolg %
1993	55	48	87
1994	35	30	85
1995	48	41	85

Tabelle 5: Statistik für die Basislinienauswertung

Für die Kampagne im Jahr 1995 lagen Zweifrequenzdaten sowie Software für die Auswertung nach der statischen Schnellmessung vor. Damit konnte eine 100% Erfolgsquote erzielt werden. Darüber hinaus bietet dieses Verfahren aber auch die Möglichkeit, die notwendigen Beobachtungszeiten ganz wesentlich zu reduzieren. Als Faustregel kann eine Zeit von 10 Minuten vermehrt um eine Minute pro Kilometer Basislänge angesetzt wer-

den, solange mindestens fünf Satelliten unter guter Geometrie beobachtbar sind und die Basislinienlängen nicht mehr als 15 km betragen.

Abschließend sei angemerkt, daß für die Basislinien zwischen den Referenzpunkten durch die längeren Beobachtungszeiten sämtliche Ambigutäten eindeutig bestimmt wurden. Wiederholungsmessungen oder Schleifenschlußfehler in den Referenznetzen lassen auch eine Aussage über die mit GPS erreichte Genauigkeit zu, wobei diese erwartungsgemäß im allgemeinen bei ±1 ppm lag.

Datumstransformation

Für die Transformation des geodätischen Datums wurde das Modell der räumlichen Drehstreckung angesetzt. Dieses Modell beinhaltet insgesamt sieben unbekannte Parameter, nämlich die drei Komponenten eines Verschiebungsvektors, die Drehwinkel um die drei Achsen des Ausgangssystems und einen Maßstabsfaktor. Jeder Paßpunkt gibt Anlaß zu drei Bestimmungsgleichungen, daher liegt ab einer Anzahl von drei Paßpunkten eine Überbestimmung vor. Die optimale Lösung für die Transformationsparameter wird dann durch eine Ausgleichung gefunden.

In die Berechnung der räumlichen Drehstreckung müssen ellipsoidische Höhen eingeführt werden. Diese ergeben sich aus den Gebrauchshöhen der Landesvermessung durch Anbringen der Geoidhöhen. Das österreichische Geoid ist derzeit mit einer Genauigkeit von etwa 5 cm auf 100 km bekannt, vgl. Sünkel et al. (1987). Die Geoidhöhen bezogen auf das österreichische Datum standen in Form von Punktwerten eines 3×5 Bogenminuten Rasters zur Verfügung und konnten daraus für die GPS-Punkte interpoliert werden. Wie aus der Tabelle 6 abgelesen werden kann, schwanken die Geoidhöhen in den einzelnen Meßgebieten im Bereich von etwa 1.5 bis 3.0 Meter und sie sind daher für die geforderte Höhengenauigkeit von ±10 cm in Rechnung zu stellen.

	Geoidhöhen	
Jahr	Minimum [m]	Maximum [m]
1993	1.60	2.95
1994	1.77	2.93
1995	1.53	2.02

Tabelle 6: Statistik der Geoidhöhen in den Meßgebieten

Die in den einzelnen Jahren erhaltenen Parameter der Drehstreckung sind in der Tabelle 7 angeführt. Dabei wurde auf die Angabe der Komponenten des Verschiebungsvektors verzichtet, da diese für die Transformation der Basislinien nicht relevant sind. Aus der Tabelle kann abgelesen werden, daß die angegebenen Parameter in einem Bereich schwanken, der zu Basislinienänderungen von etwa 5 ppm führen kann. Dieser Wert liegt unter dem angestrebten Genauigkeitsniveau.

Eine Aussage über die Genauigkeit der Landeskoordinaten der Referenzpunkte kann nach der Transformation des geodätischen Datums aus den Restklaffungen getroffen werden. Diese betragen im allgemeinen nur wenige Zentimeter und beweisen die kleinräumige

Homogenität des österreichischen Festpunktfeldes.

Jahr	Maßstabsfaktor	Drehwinkel		
1993	0.999 9861	7″2	0″3	5″7
1994	0.999 9849	8″1	3″7	6″1
1995	0.999 9792	7″2	−0″6	5″7

Tabelle 7: Parameter für die Datumstransformation

Wirtschaftliche Aspekte
In der Tabelle 8 sind einige Kenndaten zur Abschätzung der Wirtschaftlichkeit bei der Auswertung der Ergebnisse angeführt. Daraus geht hervor, daß seit 1993 eine Reduzierung der Auswertekosten um 42% erzielt werden konnte. Dies ist in der nunmehrigen Verfügbarkeit geeigneter Software für alle Auswerteschritte begründet.

Jahr	1993	1994	1995
Neupunkte	55	35	48
Auswertekosten pro Punkt	520.–	510.–	300.–
Gesamtkosten pro Punkt	1 180.–	1 370.–	1 030.–

Tabelle 8: Wirtschaftliche Aspekte der GPS-Auswertungen

Der Vollständigkeit halber enthält die Tabelle 8 auch Angaben über die Gesamtkosten pro Neupunkt. Darin sind neben den Auswertekosten auch die Mietkosten für das Instrumentarium berücksichtigt. Im Vergleich zu den Auswertekosten konnten die Gesamtkosten nur um 13% reduziert werden. Daraus folgt, daß die Beobachtungen noch weiter rationalisiert werden müssen, um die Gesamtkosten auf etwa 600 Schilling pro Neupunkt zu senken.

4. Ausblick

Entgegen der ursprünglichen Zielsetzung werden in Zukunft grundsätzlich Zweifrequenzempfänger zur Verfügung stehen. Es können daher die Beobachtungszeiten reduziert werden. Die in der Tabelle 9 angegebenen Faustformeln berücksichtigen nur den Einfluß der Basislänge und gelten im Fall von fünf beobachteten Satelliten, einem PDOP-Faktor von unter 5, sowie bei normalen atmosphärischen Bedingungen. Ein beobachtbarer Satellit mehr oder weniger kann die notwendige Beobachtungszeit um bis zu 20% verändern.

Für die Einmessung des jeweiligen Referenznetzes ist das normale statische Verfahren anzuwenden, da die statische Schnellmessung derzeit auf Basislinien unter 15 km beschränkt ist.

Hingewiesen wird, daß eine weitere Verkürzung der Beobachtungszeiten durch verbesserte Auswertestrategien zur Fixierung der Phasenmehrdeutigkeiten möglich ist. Wird

jedoch die GPS-Beobachtung gleichzeitig mit der gravimetrischen Aufnahme und der Einmessung der Nahzone durchgeführt, ist eine weitere Reduktion der Sessionslängen nicht notwendig.

Träger	Normalmessung	Schnellmessung
L1	30 Minuten + 3 Minuten/km	20 Minuten + 2 Minuten/km
L1+L2	20 Minuten + 2 Minuten/km	10 Minuten + 1 Minute/km

Tabelle 9: Zeitaufwand für statische Beobachtungen

Bei Parallelbeobachtungen ist eine exzentrische Aufstellung der GPS-Antenne notwendig. Dabei können Exzentrizitäten von einigen Metern in der Lage mit Hilfe von Kompaß und Schrittmaß einfach berücksichtigt oder sogar vernachlässigt werden. Die Höhenübertragung kann unter anderem mit Hilfe des kinematischen GPS-Verfahrens erfolgen.

Die Wirtschaftlichkeit wird gesteigert, wenn gleichzeitig zwei Gravimetertrupps operieren, weil dadurch Personalkosten, Gerätemietkosten und Hubschrauberkosten gesenkt werden. Da die Betreuung der GPS-Empfänger keine spezielle Qualifikation erfordert, kann diese durch das Gravimeterpersonal erfolgen. Die Steuerung des GPS-Einsatzes hingegen soll durch einen Fachmann an der jeweiligen Referenzstation erfolgen, der im Feld auch eine vorläufige Basislinienauswertung durchführt.

Ein noch ungelöstes Problem stellt die Kommunikation zwischen dem Referenzpunkt und den Gravimeterpunkten dar. Eine solche ist aber notwendig, um auf unvorhergesehene Meßunterbrechungen, etwa infolge lokaler Gewitter, reagieren zu können.

In Zukunft wird jedenfalls der Einsatz von GPS bei der Hochgebirgsgravimetrie kein Problem mehr darstellen. Der Einsatz wird routinemäßig erfolgen und wird auch die eigentliche gravimetrische Aufnahme weder zeitlich noch personell behindern.

Literatur

Hofmann-Wellenhof B, Kienast G, Lichtenegger H (1994a): GPS in der Praxis. Springer-Verlag Wien New York.

Hofmann-Wellenhof B, Lichtenegger H, Collins J (1994b): GPS - Theory and Practice. Third, revised edition. Springer-Verlag Wien New York.

Lichtenegger H, Kraiger G (1993): Über die Einmessung von Gravimeterstationen mit GPS. In: Steinhauser P, Walach G (Hrsg): Tagungsbericht über das 6. Internationale Alpengravimetrie-Kolloquium in Leoben. Österreichische Beiträge zu Meteorologie und Geophysik, Heft 8, Zentralanstalt für Meteorologie und Geodynamik, Publikation Nr. 353, Wien

Sünkel H, Bartelme N, Fuchs H, Hanafy M, Schuh W-D, Wieser M (1987): The Gravity Field in Austria. In: Geodätische Arbeiten Österreichs für die Internationale Erdmessung, Neue Folge, Band IV, S. 47–76.

COMPARISON OF FEEDBACK CALIBRATION METHODS - RESULTS FROM LCR D-9

Bruno Meurers

Institute of Meteorology and Geophysics, University of Vienna

Abstract

During the last ten years the SRW feedback system of LCR D-9 has been regularly controlled on vertical calibration lines. The results are discussed and compared with different calibration methods which could be intensively performed in recent time. The feedback parameter obtained by adjusting the ten years' observations on different vertical calibration lines (Hannover, Vienna, Sevres) are in excellent agreement. Results from investigating the periodic errors of the LCR scale factor function fit very well to the vertical calibration line observations especially when regarding the quadratic term. The heavy mass experiment performed in the geophysical observatory near Budapest shows very high inner accuracy (0.1 - 0.2 µGal), but the linear term is too large (1 - 2.5 %) compared with the results obtained on calibration lines. Obviously systematic effects are present. This can be shown by comparing the differences between the adjusted and theoretical gravity signal. The periodic vertical movement calibration is in better agreement with calibration line observations, but also in this case the linear term is slightly too high (0.6 %).

1. Introduction

One of the most severe problems in high precise gravimetry is still the calibration of relative gravimeters. Today systematic errors introduced by non-linear scale factor functions and periodic errors of LCR gravimeters are eliminated by implementation of feedback systems. Nevertheless the calibration problem remains as the scale factor function of the feedback equipment may vary irregularly with time. The accuracy of relative gravity measurements during the absolute gravimeter intercomparison of 1989 and 1994 in Sevres/Paris (Becker et al. 1990, Becker et al. 1995) could not be essentially improved in comparison to earlier campaigns, although meanwhile all participating instruments had been equipped with feedback systems. Gravity net determination on the 1 µGal (10 nms^{-2}) accuracy level can still be achieved only by using a set of gravimeters. The results of individual gravimeters sometimes deviate by more than few µGal from the gravity obtained by a common adjustment of all instruments' data. Of course, this is not only due to imperfect calibration but mainly caused by phenomena systematically affecting the measuring device (instrumental drift, anelastic effects, atmospheric influences, magnetic fields, etc.). However, just these effects severely trouble the results of gravimeter calibrations too.

The most important and common calibration methods are summarized in Tab. 1. The possibility of temporal gravity variations at individual stations (e.g. due to aquifer level variations) is the fundamental problem of using vertical or horizontal calibration lines. It is impossible to distinguish between gravity and calibration factor variations, because the feedback parameters can not be assumed to be stable in every case. Therefore it is necessary to control the calibration factor of feedback systems regularly and to apply different calibration methods. However, mostly the different devices are not available at the measuring site. In that case combining calibration line observations with repeated non-linearity investigation at a specified scale position of the LCR gravimeter can be a very effective tool for feedback control (e.g. Meurers, 1995).

method	advantage	disadvantage
Vertical or horizontal calibration line	high amplitude reference full feedback range coverage	unstable reference due to unknown temporal gravity variations
Periodic vertical movement (Richter 1987, Van Ruymbeke 1989)	high amplitude reference wide feedback range coverage	transfer function required (Richter and Wenzel 1991, Wenzel 1994)
Heavy mass experiment (Varga et al. 1991, Varga et al. 1995, Csapó and Szatmari 1995)	stability of the reference high precise reference	low amplitude reference
Tidal monitoring at stations with well determined tidal parameters		low amplitude reference drift determination
Comparison with absolute gravimeters	absolute reference	low amplitude reference drift determination scatter of single drop results

Tab.1: Comparison of feedback calibration methods

In 1986 the LCR D-9 was equipped with a SRW-D electrostatic feedback system (Schnüll et al. 1984) and calibrated at the precise vertical calibration line in Hannover (Kanngieser et al. 1983). Using these results a vertical calibration line was established in Vienna to detect temporal variations of the feedback parameters. The gravity values at the six stations of this line cover almost regularly the full measuring range of the feedback system (≈ 5 mGal). Fortunately the feedback equipment is operating since the beginning without interruptions, therefore observations over a 10 years' interval are available.

In the last two years the opportunity of using further calibration methods could be utilized within short time intervals. The LCR D-9 participated in microgravimetric measurements at the 1994 international comparison of absolute gravimeters in Sevres. During this campaign a local calibration line was established by 18 gravimeters with different feedback types (14 LCR, type D or G and 4 Scintrex CG-3M), offering the linear feedback parameter determination in a common network adjustment (Becker et al. 1995). Most gravimeters could also apply the calibration method of periodic vertical acceleration on two different lift types (Richter et al. 1995, Van Ruymbeke et al. 1995). In 1994 and 1995 additional measurements have been performed using the heavy mass experiment in Budapest (Varga et al. 1995, Csapó and Szatmari 1995). They were combined with observations at the vertical calibration line in Hannover. In combination with additional feedback control performed in Vienna immediately before and after gravimeter transportation all these measurements contributed to a dense series of feedback calibrations. The main task of this paper is the comparison of different calibration methods by analyzing the results obtained from LCR D-9.

2. Vertical calibration line

Fig. 1 shows the temporal variation of the linear and quadratic term of the feedback calibration function calculated by adjusting the observations at the calibration lines in Vienna (squares) and Hannover (triangles) and by investigating the non-linearity of the LCR D-9 scale factor function (open circles). Both the gravity at the stations of the Vienna calibration line and the relative gravity corresponding to three equi-spaced scale positions of the LCR D-9 have been recalculated using the feedback parameters obtained in Hannover 1995. In this computation the temporal variation of the feedback parameters observed in Vienna immediately before and after the Hannover calibration was taken into account. Contrary to an earlier interpretation (Meurers, 1995) the Vienna calibration line was assumed to be stable for adjusting the feedback parameters. Fig. 2 shows the most recent part of the

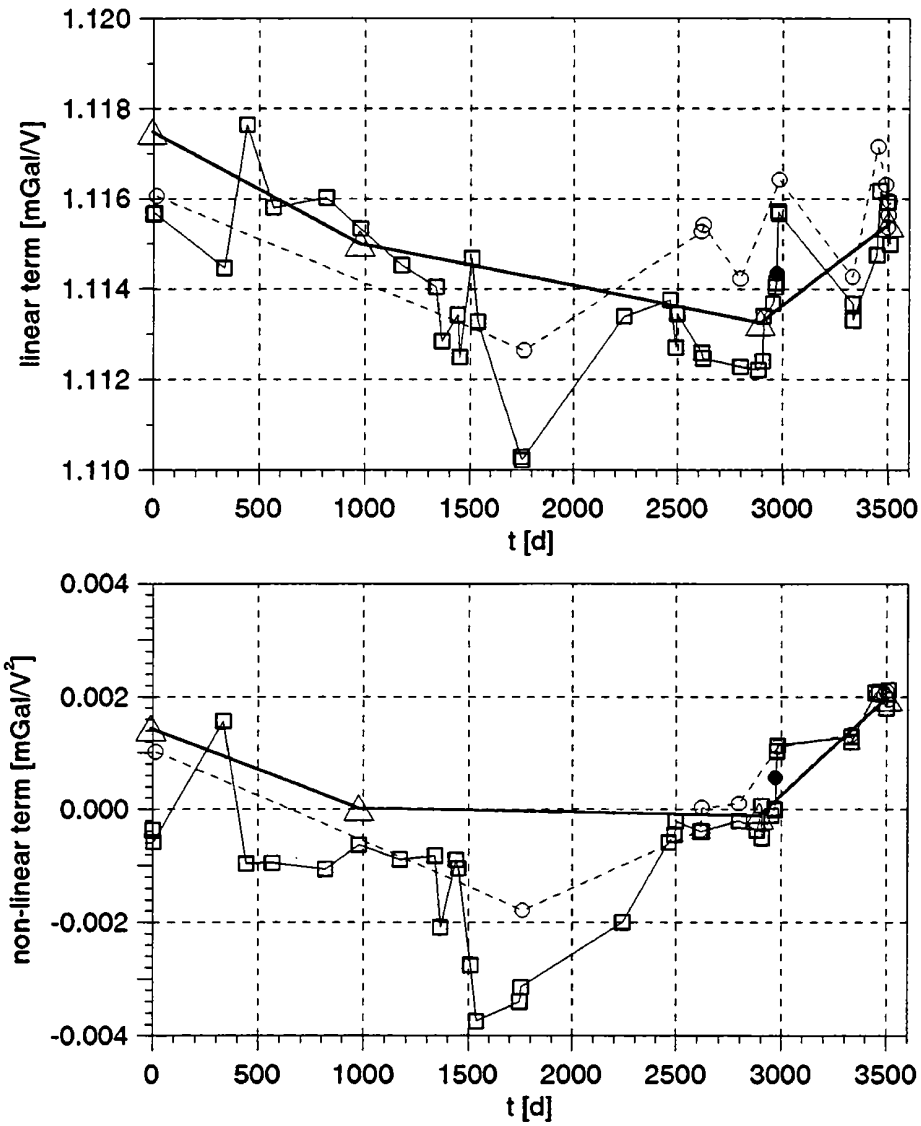

Fig. 1. Temporal variation of the linear and quadratic term of the feedback calibration function calculated by adjusting the observations at the calibration lines in Vienna (squares), Hannover (triangles), Sevres 1994 (dot) and by investigating the non-linearity of the LCR D-9 scale factor function (circles).

observation series in a higher time resolution. The black dot corresponds to the independent adjustment result obtained by using the gravity of the local calibration line in Sevres, which was established during the intercomparison 1994 (Becker et al. 1995).

When adjusting the linear term by using the relative gravity observed at different LCR scale positions (non-linearity experiment) the result is systematically affected due to anelastic spring behavior. Such effects occur because in this experiment the spring length varies due to the dial displacement. Considering this fact all results agree remarkably well and clearly prove the temporal variations to be significant. The linear calibration factor obtained for LCR D-9 in Sevres 1994 by common network adjustment is 1.1149. This figure fits also very well to the results presented in Fig. 2.

Just in the beginning of the observation series a great misfit occurs. The reason is not yet clear. One possible explanation could be a gravity variation at some stations of the Vienna calibration line. However, this is improbable, because a variation of up to 8 μGal would be required (Meurers, 1995). The more probable explanation is a rapid decrease of the linear

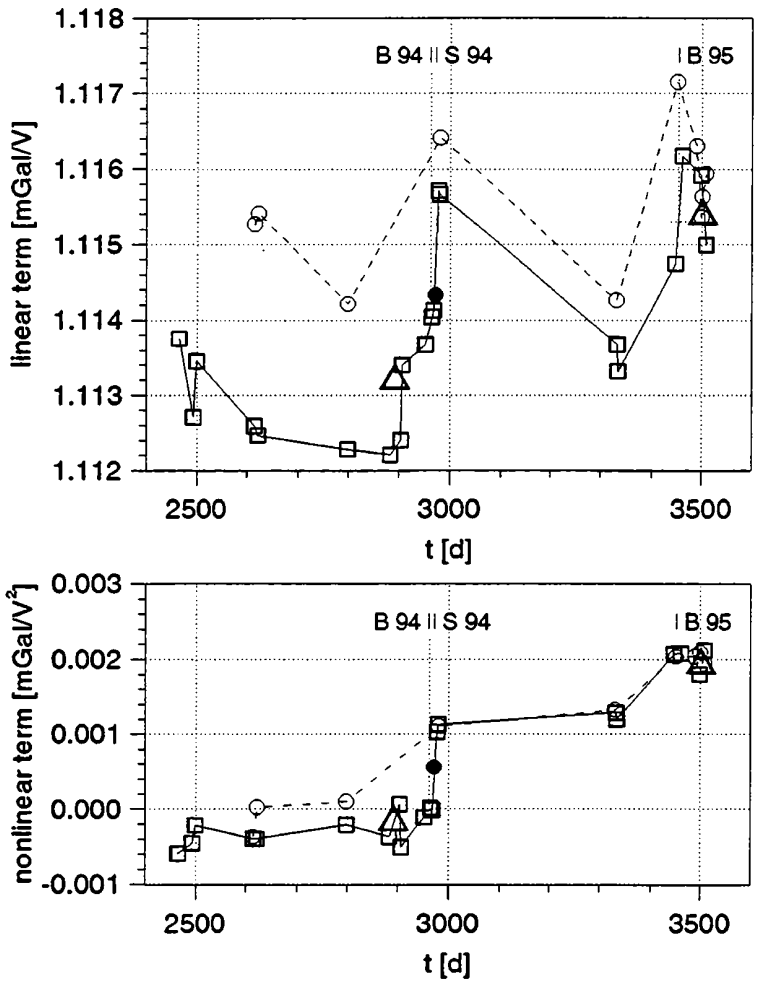

Fig. 2: Temporal variation of the linear and quadratic term of the feedback calibration function calculated by adjusting the observations at the calibration lines in Vienna (squares) and Hannover (triangles) and by investigating the non-linearity of the LCR D-9 scale factor function (circles). B: Heavy mass exp., Budapest 1994 resp. 1995, S: intercomparison, Sevres 1994 (dot)

and non-linear term between the initial calibration in Hannover and the first measurement at the Vienna vertical line. A similar discontinuous variation can be observed in 1994 too, which is significant. This is shown by repeated measurements immediately before and after the intercomparison campaign in Sevres and additionally confirmed by the combined non-linearity experiment (Fig. 2). Sudden variations are caused probably by a changing capacitor geometry due to transportation shocks. The occurrence of such discontinuous variations therefore requires in situ calibration during microgravimetric measurements. Beside using transportable platforms or local calibration lines, investigating the non-linearity of the LCR scale factor is very effective for controlling the feedback calibration function.

3. Moving mass calibration

In the Geophysical Laboratory of the Eötvös Lorand Geophysical Institute (ELGI) near Budapest a moving mass calibration device has been installed (Varga et al. 1995). A gravity signal of about 110 μGal is caused by a heavy cylinder ring, which slowly moves up and down while the gravimeter is fixed on an iron pillar coinciding with the cylinder ring axis. The mass movement is completely computer-controlled. The ring can be moved continuously or stepwise in user defined intervals. A data acquisition system samples the output voltage of

the feedback, the air pressure and the accurate position of the ring. Detailed information about technical design and accuracy investigations are given by Varga et al. (1995).

This experiment was performed for the first time with the LCR D-9 in May 1994 just before the gravimeter intercomparison in Sevres. In autumn 1995 the measurements were repeated again. During both campaigns four independent calibrations could be analyzed each with 3 cycles of stepwise up and down movement. Near the positions of the gravity signal extremes the mass was moved in 5 mm intervals. The feedback output voltage (resolution 0.1 mV) was sampled twice with one minute interval, the second sample is used for data analysis. The first sample was taken one minute after the mass came to rest. This procedure is sufficient to get accurate gravimeter readings. Fig. 3 shows the gravimeter response to a stepwise up and down movement after earth tidal correction. The drift function is undisturbed at least one minute after the mass has been stopped.

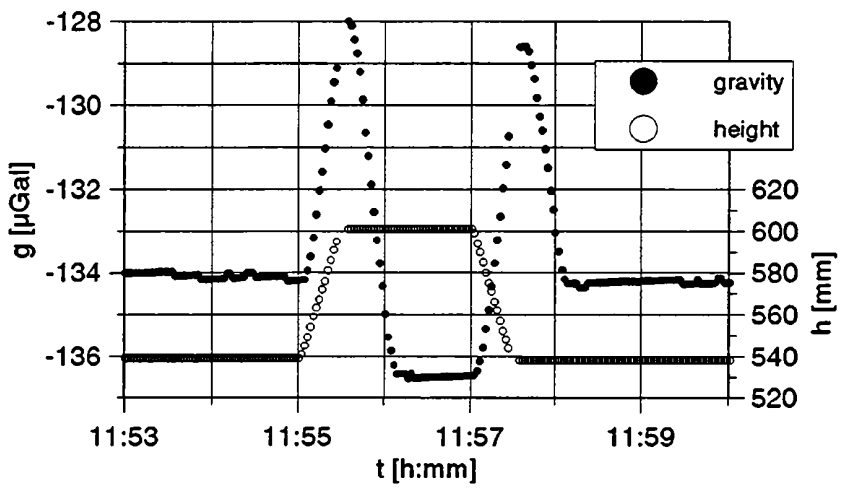

Fig. 3: Gravimeter response to cylinder ring movements (LCR D-9)

The first step of data processing consists of earth tidal correction and instrumental drift determination by adjusting polynomials up to third degree. The applied feedback parameters have been determined by linear interpolation of the results shown in Fig. 2. The earth tides were calculated very precisely by using the Tamura (1987) tidal potential and tidal parameters derived from the body tide model of Wahr-Dehant (Wahr 1981, Dehant 1987) and from Schwiderski's (1980) ocean tide model (Timmen and Wenzel 1995). Fig. 4 shows the results of drift and earth tide elimination for the observation series in 1995. The individual drift data does not represent simple noise as it does not irregularly scatter around the adjusted trend. On the contrary it is aligned to a continuous drift function which sometimes correlates with the mass position. This indicates the presence of systematic effects.

In a second processing step the difference between the extremes of the gravity signal is determined by fitting a 2nd degree polynomial to the gravity data close to the upper and lower extreme position respectively. The results are presented in Fig. 5 for the 1995 observations again. With except for the minimum position of the first measurement the adjusted parabolas are very similar proving the results to be reliable. The rms error is less than 0.05 µGal. In 1994 the observations were sometimes disturbed by smaller earthquakes, therefore not all up and down cycles could be evaluated. The polynomial adjustment in general shows greater rms errors than in 1995. Tab. 2 compares the results of the observations in 1994 and 1995. The maximum deviation from the mean are less than 0.4 µGal, the standard deviation is 0.2 µGal only for both calibrations.

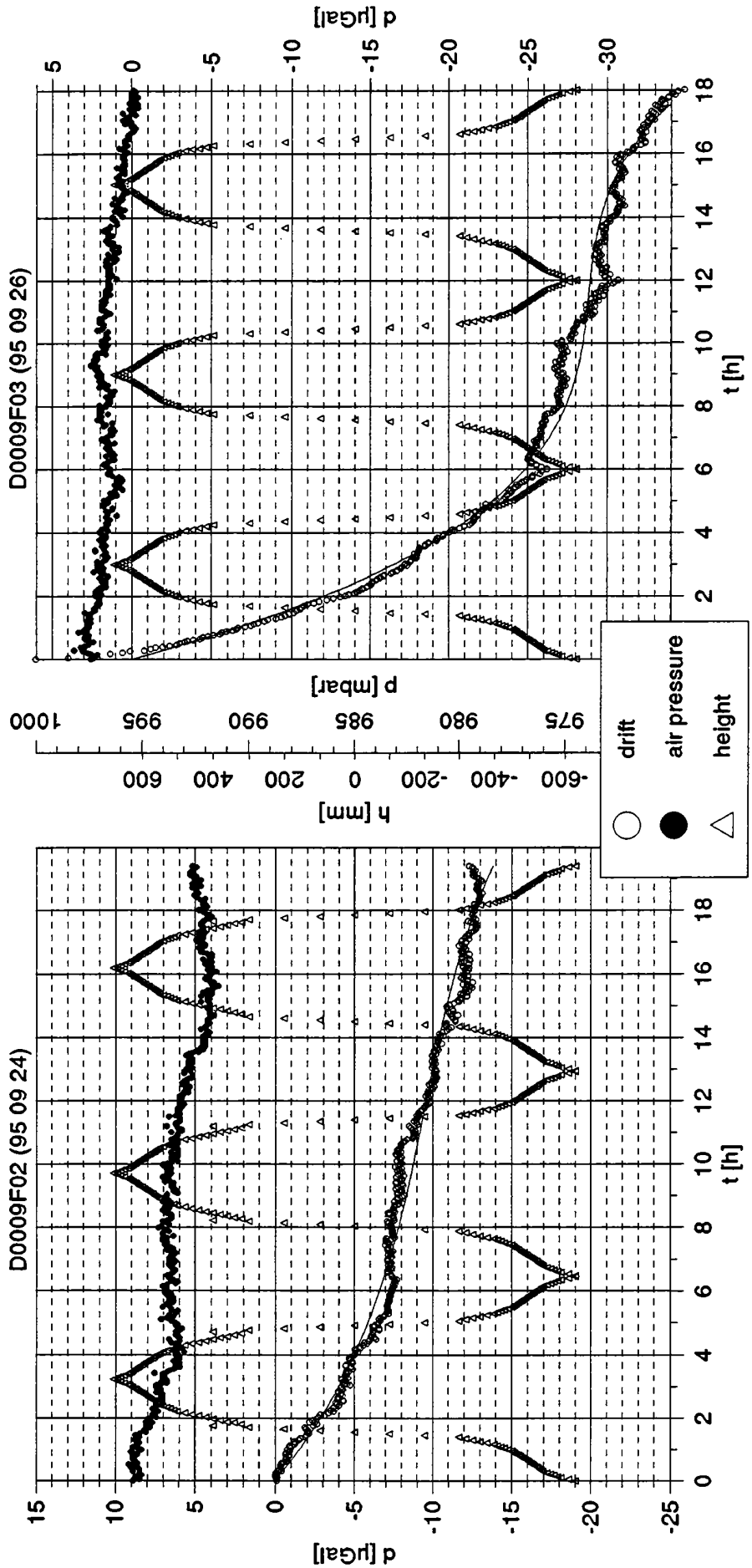

Fig. 4: Drift, air pressure and mass position. LCR D-9, Budapest, 1995.

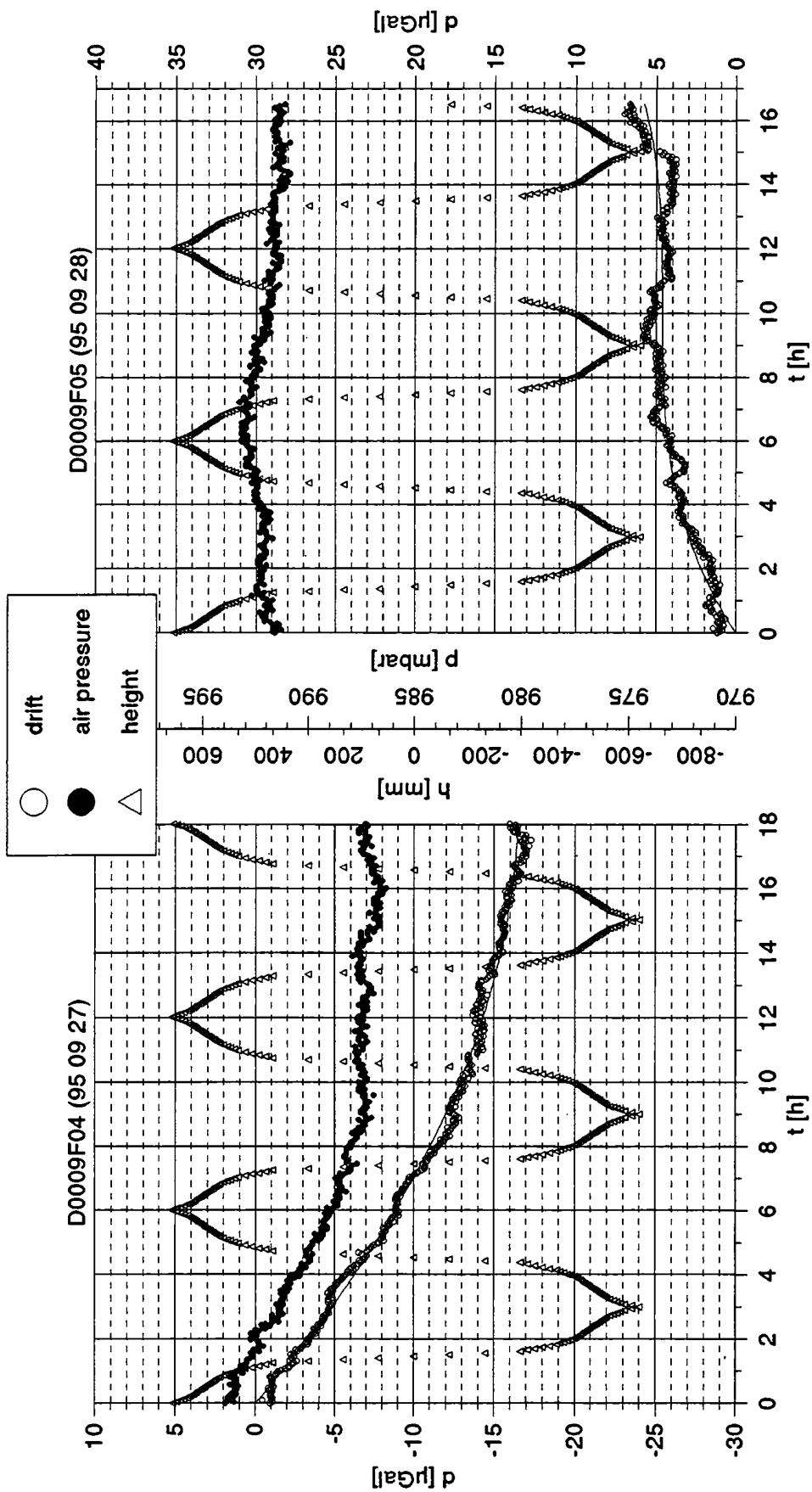

Fig. 4 (contd.): Drift, air pressure and mass position. LCR D-9, Budapest, 1995

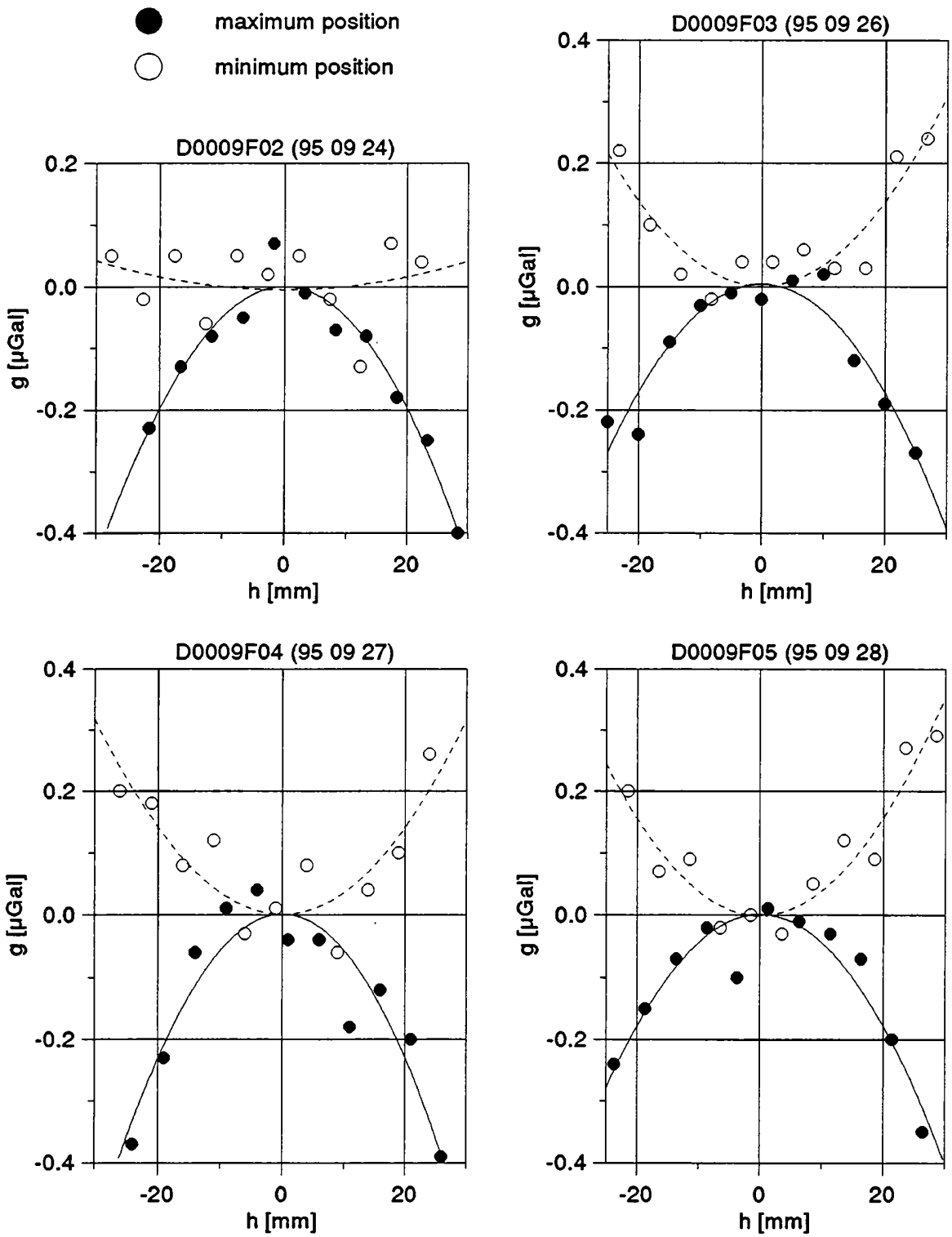

Fig. 5: Adjustment result at the mass positions of extreme gravity signal. LCR D-9. Budapest 1995.

It seems to be important to use such accurate tidal models as that mentioned above. The maximum deviations significantly increase to 0.8 µGal in 1994 and 0.7 µGal in 1995, when a simple model as Doodson's tidal potential development with constant amplitude factors is applied. A further improvement of the moving mass calibration result can probably be achieved by acquiring the sampling time with 1 second accuracy instead of recording the minute only. Besides a higher resolution of the gravity signal is desirable.

1994	maximum position			minimum position			
	g_{max} [µGal]	h_{max} [mm]	rms [µGal]	g_{min} [µGal]	h_{min} [mm]	rms [µGal]	δg [µGal]
D0009F03	-143.50	-507.9	±0.15	-252.46	586.1	±0.08	108.96
D0009F04	-138.94	-507.0	±0.15	-247.67	579.9	±0.14	108.73
D0009F05	-136.33	-507.1	±0.35	-245.00	586.4	±0.25	108.67
D0009F06	-134.76	-507.7	±0.16	-243.79	582.1	±0.17	109.03
mean: 108.86 µGal σ: ± 0.19 µGal							

1995	maximum position			minimum position			
	g_{max} [µGal]	h_{max} [mm]	rms [µGal]	g_{min} [µGal]	h_{min} [mm]	rms [µGal]	δg [µGal]
D0009F02	-35.46	-493.4	±0.03	-142.35	602.6	±0.06	106.90
D0009F03	-94.83	-495.0	±0.03	-202.12	598.2	±0.04	107.29
D0009F04	-19.95	-491.0	±0.05	-127.11	601.0	±0.05	107.16
D0009F05	-30.47	-491.4	±0.04	-137.60	596.4	±0.04	107.13
mean: 107.12 µGal σ: ± 0.16 µGal							

Tab. 2: Results of moving mass calibration in Budapest (LCR D-9)

Tab. 2 shows a rather big difference between the mean obtained in 1994 and 1995 respectively which can not be explained by the different linear eccentricity of the gravimeter sensor mass with regard to the cylinder axis. The theoretical gravity signal only slightly changes when the eccentricity increases. A comparison with the theoretical gravity signal requires a correction factor of more than 1% in 1994 and more than 2.5% in 1995. These factors are unrealistic because consequently in that case the gravity on vertical calibration lines would show errors of more than 100 µGal. Therefore systematic effects must be present. They are visible when comparing the observed relation between gravity and mass position with the theoretical one. These differences are shown in Fig. 6. They have been adjusted to zero at the maximum position to make them better comparable. Within each campaign the difference functions are almost identical, but they are clearly different between both campaigns

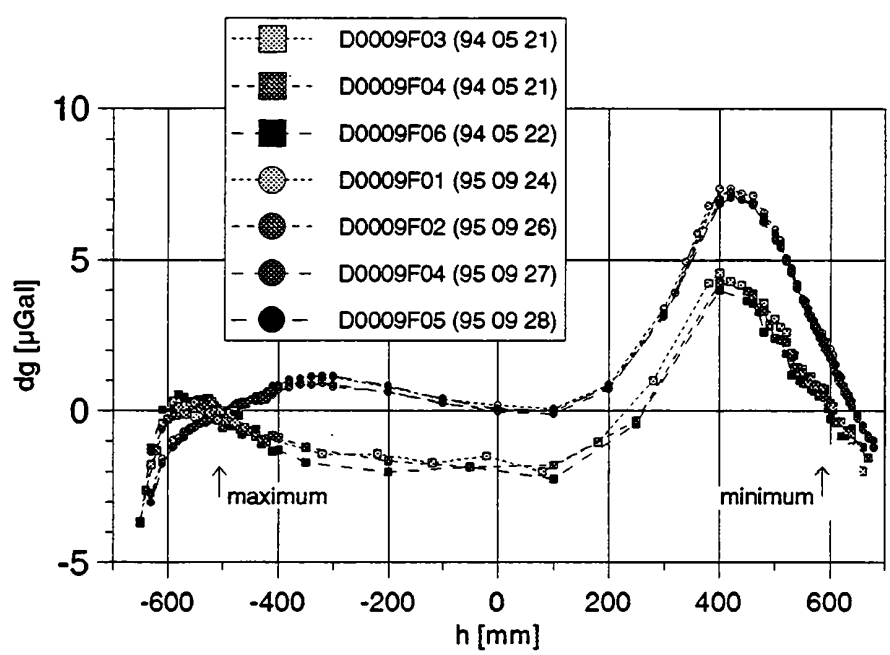

Fig. 6: Difference between observed and theoretical gravity signal vs. mass position

although possessing the same characteristics. In contrast to the theoretical gravity vs. position function the observed ones are asymmetric. That proves systematic effects to be present which can not yet be explained. Further investigations will be necessary.

4. Periodic vertical acceleration

During the intercomparison measurements in Sevres 1994 most of the relative instruments were additionally calibrated by evaluating the gravimeter's response to vertical accelerations. For this purpose the Frankfurt calibration system has been used (Richter et al. 1995). While at the mass moving calibration one up and down cycle lasts several hours in this experiment the periods of the vertical acceleration vary between 200 and 2400 s. Therefore the frequency transfer function resulting from the LCR mechanics and the filter characteristic of the feedback system must be determined too. This is done by observing the response function at different frequencies and adjusting a simple 2nd degree lowpass filter. In contrast to the mass moving calibration the non-linear term of the feedback factor must be well known as the signal amplitude reaches 1 mGal at the 200 s period. Introducing an erroneous non-linear feedback term can cause systematic errors especially when the signal is asymmetric with respect to zero voltage.

The following estimation shows that such effects do not contribute if the quadratic term b is some orders of magnitude less than the linear term a. Let $c(\omega)$ be the frequency dependent attenuation factor, g_0 the gravity corresponding to the feedback voltage at zero acceleration and v_0 the acceleration amplitude, then the following equation holds for the feedback output voltage U:

$$aU(t) + bU^2(t) = c(\omega) v_0 \cos(\omega t) + g_0 \tag{1}$$

The peak to peak voltage amplitude ΔU then results to:

$$\Delta U = U_{t=0} - U_{t=\pi/\omega} = \sqrt{\frac{a^2}{4b^2} + \frac{c v_0}{b} + \frac{g_0}{b}} - \sqrt{\frac{a^2}{4b^2} - \frac{c v_0}{b} + \frac{g_0}{b}} \tag{2}$$

If the non-linear term is completely disregarded, eq. (1) is reduced to:

$$\tilde{a} U(t) = c(\omega) v_0 \cos(\omega t) + g_0 \quad \Rightarrow \quad \Delta U = \frac{2 c v_0}{\tilde{a}} \tag{3}$$

Equating eqs. (2) and (3) leads after simple algebra to the estimate $\tilde{a}$ of the linear term:

$$\tilde{a} = \sqrt{a^2/4 + b(c v_0 + g_0)} + \sqrt{a^2/4 + b(g_0 - c v_0)} \tag{4}$$

Fig. 7 shows the estimated linear term as function of the acceleration amplitude and in dependence on the offset g_0 for three different feedback parameters b. Of course, this is an estimate for the maximum error, as commonly the non linear term is known at least roughly and therefore can be introduced into the analysis procedure. Mostly this term is of order 10^{-3} mGal/V^2. In this case the maximal error results only to few 0.1% only and therefore can be neglected also in the vertical acceleration experiment.

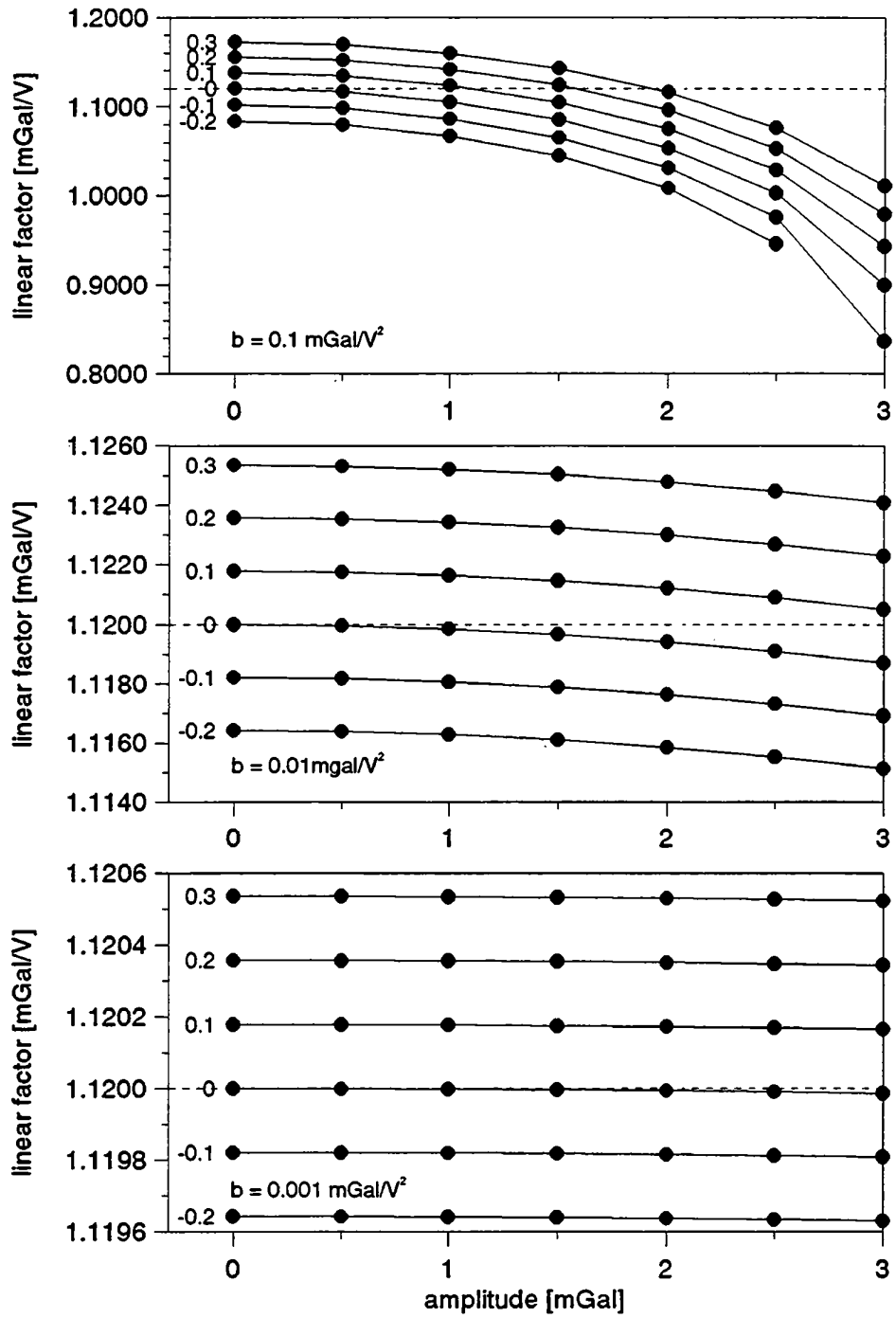

Fig. 7: Estimate of the linear feedback term obtained by neglecting the quadratic term b. Curve parameters indicate gravity offset in [mGal].

The linear feedback parameter of the LCR D-9 resulting from this calibration method was 1.1211 (Richter et al. 1995) which is too high by 0.6% compared with the value obtained on the Sevres calibration line. Similar differences have been observed with other LCR gravimeters too, only for three instruments both calibration methods agree well (Tab. 3).

LCR	owner	difference PVA - SCL [mGal/V]	%
D-6	GSC, Ottawa	+0.0136	+1.32
D-9	Inst.Geoph., Univ. Wien	+0.0062	+0.56
G-156	Geodetic Institute	+0.0036	+0.33
G-249	Univ. Karlsruhe	–0.0019	–0.17
G-258	Inst. Phys. Geod., Darmstadt	–0.0014	–0.13
G-298	Inst. Erdmessung	+0.0088	+0.82
G-709	Univ. Hannover	–0.0000	0
G-1919	ELGI Budapest	+0.0032	+0.27

Tab. 3: Comparison of calibration methods in Sevres 1994
PVA: Periodic vertical movement (Richter et al. 1995)
SCL: Sevres calibration line (Becker et al. 1995)

5. Conclusion

The results of feedback parameter determination obtained by adjusting the ten years' observations on different vertical calibration lines (Hannover, Vienna, Sevres) are in excellent agreement. Both the linear and quadratic term vary irregularly with time. This may be caused by a changing capacitor geometry due to transportation shocks and therefore makes in situ calibration necessary for microgravimetric applications besides regular feedback parameter control. Investigating the periodic errors of the LCR scale factor function is an effective tool for that purpose. The results from these experiments fit very well to the vertical calibration line observations especially when regarding the quadratic term.

The heavy mass experiment (cylinder ring) performed in the geophysical observatory near Budapest shows very high inner accuracy (0.1 - 0.2 μGal) but the linear term does not fit to the results obtained on calibration lines. The difference (1 - 2.5 %) is not constant in time and is too large to be explained by erroneous gravity determination on these lines. Obviously systematic effects are present. This can be shown by comparing the differences between the adjusted and theoretical gravity signal. In each set of observations these differences can be reproduced very exactly while their characteristics change significantly between 1994 and 1995 when the instrument was set up with different eccentricity regarding the cylinder axis. Of course this may be specific for the investigated LCR D-9 because similar phenomena are not reported from other instruments.

Applying the periodic vertical movement calibration also results to a linear term which is slightly too high compared with calibration line observations. It is not yet clear whether this is due to systematic effects or not, because three of eight gravimeters agreed very well.

It has to be mentioned that in all calibration methods the instruments are operating differently. The operation mode used on calibration lines corresponds exactly to that of microgravimetric net determination. During the heavy mass experiment the gravimeter remains unmoved without arresting the system between successive readings and is exposed to low frequency gravity variations. In the periodic vertical movement method the instrument is accelerated with relatively high frequencies. In this case therefore it is very important to determine the frequency transfer function of the sensor system. This may introduce an additional systematic error source.

Acknowledgement. Financial support from the Austrian Science Foundation FWF Project P9570-GEO is gratefully acknowledged.

6. References

Becker, B., Bernard, B., Boulanger, Y., Corrado, C., Faller, J., Fried, J., Groten, E., Hanada, H., Lindner, K., Meurers, B., Peter, C., Röder, R., Ruess, D., Timmen, L., Toro, S., Tsurata, S. and Zürn, W., 1990: Relative gravity measurements at the 3rd international comparison of absolute gravimeters. BGI, *Bulletin d'Information*, 67, 152-160.

Becker, B., Balestri, L., Bartell, R., Berrino, G., Bonvalot, S., Csapó, G., Diament, M., D'Errico, M., Gerstenecker, C., Gagnon, C., Jousset, P., Kopaev, A., Liard, J., Marson, I., Meurers, B., Nowak, I., Nakai, S., Rehren, F., Richter, B., Schnüll, M., Somerhausen, A., Spita, W., Szatmari, G., Van Ruymbeke, M., Wenzel, H.G., Wilmes, H., Zucchi, M., Zürn, W., 1995: Microgravimetric measurements at the 1994 international comparison of absolute gravimeters. Metrologia, 32, 145-152.

Csapó, G. and Szatmari, G.,1995: Apparatus for moving mass calibration of LaCoste-Romberg feedback gravimeters. Metrologia, 32, 225-230.

Dehant, V., 1987: Tidal parameters for an inelastic earth. Physic of the Earth and Planetary Interiors, 49, 97-116.

Kanngieser, E., Kummer, K., Torge, W. and Wenzel, H.G., 1983: Das Gravimeter-Eichsystem Hannover. Wiss. Arb. Fachrichtung Vermessungswesen, Univ. Hannover, 120.

Meurers, B., 1995: Problems of gravimeter calibration in high precision gravimetry. In: Sünkel, H., Marson, I., (eds): Gravity and Geoid. IAG Symposium 113, Springer Verlag, 19-26.

Richter, B., 1987: Das supraleitende Gravimeter. Deutsche Geod. Komm., Reihe C, Nr. 329.

Richter, B. and Wenzel, H.G., 1991: Precise instrumental phase lag determination by the step response method. *Bull. Inf. Marées Terr.*, 111, 8032-8052.

Richter, B., Wilmes, H. and Nowak, I., 1995: The Frankfurt calibration system for relative gravimeters. Metrologia, 32, 217-223.

Schnüll, M., Röder, R.H. and Wenzel, H.G., 1984: An improved electronic feedback system for LaCoste&Romberg gravity meters. BGI, *Bulletin d'Information*, 55, 27-36.

Schwiderski, E., 1980: Ocean tides. Part I: Global ocean tidal equations. Part II: A hydrodynamical interpolation model. Marine Geodesy, 161-255.

Timmen, L. and Wenzel, H.G., 1995: Worldwide synthetic gravity tide parameters. In: Sünkel, H., Marson, I., (eds): Gravity and Geoid. IAG Symposium 113, Springer Verlag, 92-101.

Van Ruymbeke, M., 1989: A calibration system for gravimeters using a sinusoidal acceleration resulting from a vertical periodic movement. *Bull. Géod.*, 63, 223-235.

Van Ruymbeke, M., Somerhausen, A. and Grammatica, N., 1995: Calibration of gravimeters with the VRR 8601 calibration platform. Metrologia, 32, 209-216.

Varga, P., Csapó, G., Becker, M. and Groten, E., 1991: Laboratory calibration of LCR type gravimeters. XXth General Assembly IUGG, Vienna 1991.

Varga, P., Hajósy, A., Csapó, G., 1995: Laboratory calibration of LaCoste-Romberg type gravimeters by using a heavy cylindrical ring. Geophys. J. Int., 120, 745-752.

Wahr, J.M., 1981: Body tides of an elliptical, rotating, elastic and oceanless Earth. Geoph. J. R. Astr. Soc., 64, 677-703.

Wenzel, H.G., 1994: Accurate instrumental phase lag determination for feedback gravimeters. *Bull. Inf. Marées Terr.*, 118, 8735-8752.

GRAVIMETRY FOR ENGINEERING APPLICATIONS

Georg Walach

Institute of Geophysics, University of Leoben

Abstract

In engineering geophysics gravity measurements are used mainly for the evaluation of ground stability. The tasks set include static risks such as unknown cavities, ground depressions and other inhomogeneities, as well as ecological risks such as investigation of hazardous waste deposits and monitoring of waste deposits. In the following four typical cases will be discussed.

Unknown underground cavities mostly occur in karst and mining areas but also in urban centres. Measurements above a tunnel situated 20 m below the surface show that a well defined anomaly appears only after collapse of the hanging wall, if the ratio between overburden and the height of the cavity goes below a critical value of 2,5.

Depressions of the surface caused by underground coal mining in sedimentary rocks generally are investigated using geodetic methods. An experiment with gravimetry shows that both methods in principle yield identical results. The advantage of geodesy lies in a precise description of the surface movements, whereas gravimetry records mass movements in deeper parts of the settlement cone.

In the investigation of hazardous waste deposits gravimetry will be used, if the surface above the waste deposit is not accessible for other geophysical methods (concrete or macadam cover; inside buildings). It can be shown that waste deposits possess a significant density contrast of -500 to -1500 kg/m^3 against natural rocks. Therefore, strong gravity minima can be recorded.

The compression respectively the determination of the waste density, is a problem in deposit management, as it determines the capacity of the facility. Using the method after NETTLETON the (time dependent) block density of the waste body can be determined from differential measurements with a precision of app. 5%.

The measurements, in the described cases were executed using a gravity meter LaCoste Romberg, G-type. Depending on the measuring conditions accuracies between 0,01 and 0,025 mGal were reached.

List of Authors

Name	Mail address	Country	Phone/Fax/Email	p.
ARNDT Rainier	Institut für Meteorologie und Geophysik, Universität Wien Abteilung für Montangeophysik Nordbergstraße 17 A - 1090 Wien	Austria	Phone: +43 1 31336 8413 Fax : +43 1 31336 775 E-mail: a8261gao@helios.edvz.univie.ac.at	175
BIELIK Miroslav	Geophysical Institute of the Slovak Academy of Sciences Dúbravská cesta 9 SQ - 84228 Bratislava	Slovakia	Phone: +42 7 378 2330 Fax : +42 7 375 278 E-mail: geofmiro@savba.sk	13
BRIMICH Ladislav	Geophysical Institute of the Slovak Academy of Sciences Dúbravská cesta 9 SQ - 84228 Bratislava	Slovakia	Phone: +42 7 378 2491 Fax : +42 7 375 278 E-mail: geofbrim@savba.sk	55
DYRELIUS Dan	Department of Geophysics University of Uppsala POB 556 S - 75122 Uppsala	Sweden	Phone: +46 18 182383 Fax : +46 18 501110	13
ERKER Erhard	Bundesamt für Eich- und Vermessungswesen Abt. K2 - Grundlagenvermessung Schiffamtsgasse 1-3 A - 1025 Wien	Austria	Phone: +43 1 21176 0 Fax : +43 1 2161062	97
GÖTZE Hans-Jürgen	Institut für Geologie, Geophysik und Geoinformatik Freie Universität Berlin Malteserstraße 74-100 D - 12249 Berlin	Germany	Phone: +49 30 779 2874 Fax : +49 30 775 3078 E-mail: hajo@zedat.fu-berlin.de	1 209
GOLTZ Georg	Institut für Geologie, Geophysik und Geoinformatik Freie Universität Berlin Malteserstraße 74-100 D - 12249 Berlin	Germany	Phone: +49 30 779 2877 Fax : +49 30 775 3078 E-mail: goltz@pollux.zedat.fu-berlin.de	209
GRAF Josef	Bundesamt für Eich- und Vermessungswesen Abt. K2 - Grundlagenvermessung Schiffamtsgasse 1-3 A - 1025 Wien	Austria	Phone: +43 1 21176 2312 Fax : +43 1 2161062	121
GRANSER Harald	OMV - AG Gerasdorfer Straße 151 A - 1210 Wien	Austria	Phone: +43 1 40440 3564 Fax : +43 1 40440 997 E-mail: harald.granser@omv.co.at	217
HOFMANN-WELLENHOF Bernhard	Institut für Angewandte Geodäsie und Photogrammetrie , TU Graz Abteilung für Landesvermessung und Landinformation Steyrergasse 30 A - 8010 Graz	Austria	Phone: +43 316 873 6830 Fax : +43 316 873 8888 E-mail: bhw@fphotsg01.tu-graz.ac.at	97
HVOZDARA Milan	Geophysical Institute of the Slovak Academy of Sciences Dúbravská cesta 9 SQ - 84228 Bratislava	Slovakia	Phone: +42 7 373 368 Fax : +42 7 375 278	55
KALMÁR János	Geodetic and Geophysical Research Institute of the Hungarian Academy of Sciences Csatkai Endre u. 6-8, POB 5 H - 9401 Sopron	Hungary	Phone: +36 99 314290 Fax : +36 99 313267	95
KIRCHNER Andreas	Institut für Geologie, Geophysik und Geoinformatik Freie Universität Berlin Malteserstraße 74-100 D - 12249 Berlin	Germany	Phone: +49 30 779 2393 Fax : +49 30 775 3078 E-mail: fu2444ra@zedat.fu-berlin.de	1

List of Authors (continued)

Name	Mail address	Country	Phone/Email	p.
KOVACSVOLGYI Sandor	Eötvös Lorand Geophysical Institute Columbus u. 17-23 H - 1145 Budapest	Hungary	Phone: +36 1 1637 438 Fax : +36 1 1637 256 E-mail: h7404leg@ella.hu	
KRAIGER Gerhard	Abteilung für Physikalische Geodäsie Technische Universität Graz Steyrergasse 30 A - 8010 Graz	Austria	Phone: +43 316 873 6353 Fax : +43 316 817909 E-mail: kraiger@fpgeods01.tu-graz.ac.at	225
KÜHTREIBER Norbert	Abteilung für Physikalische Geodäsie Technische Universität Graz Steyrergasse 30 A - 8010 Graz	Austria	Phone: +43 316 873 6352 Fax : +43 316 817909 E-mail: kueh@fpgeods02.tu-graz.ac.at	103
LICHTENEGGER Herbert	Institut für Angewandte Geodäsie und Photogrammetrie Abteilung für Landesvermessung und Landinformation Technische Universität Graz Steyrergasse 30 A - 8010 Graz	Austria	Phone: +43 316 873 6833 Fax : +43 316 873 8888 E-mail: lichteneg@ftug.tu-graz.ac.at	225
LILLIE Robert J.	Department of Geosciences Oregon State University Corvallis, Oregon 97331, USA	USA	Phone: +1 503 737 1242 Fax : +1 503 737 1200	13
MEURERS Bruno	Institut für Meteorologie und Geophysik, Universität Wien Abteilung für Angew. Geophysik Hohe Warte 38 A - 1190 Wien	Austria	Phone: +43 1 36026-3205 Fax : +43 1 3685612 E-mail: bruno.meurers@univie.ac.at	155 235
MORITZ Helmut	Abteilung für Physikalische Geodäsie Technische Universität Graz Steyrergasse 30 A - 8010 Graz	Austria	Phone: +43 316 873 6351 Fax : +43 316 817909 E-mail: moritz@fpgeods02. tu-graz.ac.at	97
MÜLLER Andreas	Institut für Geologie, Geophysik und Geoinformatik Freie Universität Berlin Malteserstraße 74-100 D - 12249 Berlin	Germany	Phone: +49 30 779 2396 Fax : +49 30 775 3078 E-mail: fu2444qa@zedat.fu-berlin.de	209
PAIL Roland	Institut für Experimentalphysik II Universitätsstraße 30 D -95440 Bayreuth	Germany	Phone: +49 921 552621	155
PAPP Gábor	Geodetic and Geophysical Research Institute of the Hungarian Academy of Sciences Csatkai Endre u. 6-8, POB 5 H - 9401 Sopron	Hungary	Phone: +36 99 314290 Fax : +36 99 313267 E-mail: papp@apollo.ggki.hu	95 145
PASTEKA Roman	Institut für Meteorologie und Geophysik, Universität Wien Nordbergstraße 17 A - 1090 Wien Department of Applied Geophysics Comenius University Bratislava Mlynská dolina SQ - 84215 Bratislava	Austria Slovakia	Fax : +43 1 31336 775	187
RADINGER Alexander	Joanneum Research Institut für Angewandte Geophysik Roseggerstraße 17 A - 8700 Leoben	Austria	Phone: +43 3842 47060 35 Fax : +43 3842 47060 32	73

List of Authors (continued)

Name	Mail address	Country	Phone/Fax/Email	p.
RAUTZ Konrad	Abteilung für Physikalische Geodäsie Technische Universität Graz Steyrergasse 30 A - 8010 Graz	Austria	Phone: +43 316 873 6354 Fax : +43 316 817909 E-mail: rautz@fpgeods02.tu-graz.ac.at	103
RÖMER Alexander	Institut für Meteorologie und Geophysik, Universität Wien Abteilung für Montangeophysik Nordbergstraße 17 A - 1090 Wien	Austria	Phone: +43 1 31336 8412 Fax : +43 1 31336 775 E-mail: a8261gam@helios.edvz.univie.ac.at	175
RUESS Diethard	Bundesamt für Eich- und Vermessungswesen Abt. K2 - Grundlagenvermessung Schiffamtsgasse 1-3 A - 1025 Wien	Austria	Phone: +43 1 21176 2312 Fax : +43 1 2161062 E-mail: diethard.ruess@univie.ac.at	91 113
SANTAVÝ Jaroslav	Geocomplex a.s. Geologická 21 SQ - 82207 Bratislava	Slovakia	Phone: +42 7 243 500 Fax : +42 7 243 428	39
SCHMIDT Sabine	Institut für Geologie, Geophysik und Geoinformatik Freie Universität Berlin Malteserstraße 74-100 D - 12249 Berlin	Germany	Phone: +49 30 779 2876 Fax : +49 30 775 3078 E-mail: sschmidt@zedat.fu-berlin.de	137 209
SCHÖNVISZKY László	EötvösLorand Geophysical Institute Columbus u. 17-23 H - 1145 Budapest	Hungary	Phone/Fax: +36 1 163 7231	
SEDLÁK Jiri	GEOFYZIKA a.s. Jecná 29a, POB 62 CZ - 61246 Brno	Czechia	Phone: +42 5 7264 284 Fax : +42 5 4122 5089 E-mail: root@ugfbr.cz	29 69
SEIBERL Wolfgang	Institut für Meteorologie und Geophysik, Universität Wien Abteilung für Montangeophysik Nordbergstraße 17 A - 1090 Wien	Austria	Phone: +43 1 31336 8419 Fax : +43 1 31336 775	175
SÜNKEL Hans	Abteilung für Mathematische Geodäsie und Geoinformatk Technische Universität Graz Steyrergasse 30 A - 8010 Graz	Austria	Phone: +43 316 873 6346 Fax : +43 316 813247 E-mail: suenkel@geomatics.tu-graz.ac.at	97
SZALAIOVÁ Viktória	Geocomplex a.s. Geologická 21 SQ - 82207 Bratislava	Slovakia	Phone: +42 7 243 500 Fax : +42 7 243 428	39
VARGA Peter	Geodetic and Geophysical Research Institute of the Hungarian Academy of Sciences Csatkai Endre u. 6-8, POB 5 H - 9401 Sopron	Hungary	Phone: +36 99 314290 Fax : +36 99 313267	79
VOZÁR Jozef	Geological Survey of Slovak Republic Mlynská dolina 1 SQ - 81704 Bratislava	Slovakia		39
WALACH Georg	Institut für Geophysik Montanuniversität Leoben Franz Josef Straße 18 A - 8700 Leoben	Austria	Phone: +43 3842 402 363 Fax : +43 3842 402 560	249

Table 2. Root mean square (rms) error values in μGal relative to the expected theoretical variation of the gravity.

Number of observations	rms errors
6	0.47 (0.40%)
12	0.41 (0.36%)
40	0.29 (0.25%)
50	0.25 (0.22%)
70	0.25 (0.22%)

Because of the need of very accurate determination of the extrema it is necessary to introduce adjustment calculations. This can be the least square method (the L_2 norm) in case of a Gaussian error (noise) distribution. In the observations of the gravity during the calibration procedure a number of outliers – possibly due to the long-periodic (1–5 minutes) beating of the microseisms – were detected which cannot be handled effectively with the commonly used least square method. For the adjustment calculations – on the basis values – possibly instead of least quares the robust estimation method must be used (Somogyi & Závoti, 1993).

On the basis of our experience with the calibration device equipped with a heavy cylindrical ring it can be concluded that it is one of the most reliable method of laboratory calibration of gravimeters. Its accuracy is at present 0.1–0.2 % and it can be further developed by using more sensitive instruments and more convenient annular masses.

3. SCALE AND TIME DEPENDENCE OF THE NEWTONIAN GRAVITATIONAL CONSTANT

There are several publications which report on the large-scale (10–1000 m) determination of gravity constants. G_∞ with numerical values significantly differing from the results of G_0 values determined in laboratories. A theoretical basis of this deviation can be given by introduction of the so called non-Newtonian gravity potential. This phenomenon can be given analytically in the following form (Stacey et al., 1987):

$$V = -\frac{G_\infty m_1 m_2}{r}\left(1 + \alpha \cdot e^{-\beta}\right) = V_N + V_Y \tag{2}$$

If $\alpha = 0$, $V = V_N$ where V_N is the Newtonian potential. If $\alpha \neq 0$, V_Y appears additionally which is called the Yukawa term. If $\beta \ll 1$ we get

$$G_0 = G_\infty(1 + \alpha) \tag{3}$$

On the basis of large scale Airy type experiments Stacey et al. (1987) got for G_∞ a value which is bigger than the G_0 value obtained in laboratories. The difference is $G_\infty - G_0 \sim 0.01$ what leads to $\alpha \sim 0.0075 \pm 0.0036$. To study this problem a special gravimeter calibration line was installed at the Geodynamical Observatory in Budapest

Arbeiten aus der Zentralanstalt für Meteorologie und Geodynamik

bisher erschienen:

Heft	Publ.Nr.	Fachgebiet	Autor	Titel und Umfang	Preis in öS
1	184	Geophysik	ECKEL, O.:	*Über die vertikale Temperaturverteilung im Traunsee.* Wien 1967, 42 S., 4 Tab., 24 Abb.	80,--
2	186	Meteorologie	STEINHAUSER, F.:	*Ergebnisse von Pilotballon - Höhenwindmessungen in Österreich,* Wien 1967, 44 S., 16 S. Tab., 28 Abb.	70,--
3	487	Geophysik	TOPERCZER, M.:	*Die Verteilung der erdmagnetischen Elemente in Österreich zur Epoche 1960.0.* Wien 1968, 18 S., 3 Tab., 10 Kartenbeilagen	vergriffen
4	190	Geophysik	BRÜCKL, E., G. GANGL und P. STEINHAUSER:	*Die Ergebnisse der seismischen Gletschermessungen am Dachstein im Jahre 1967.* Wien 1969, 24 S., 11 Abb.	50,--
5	191	Meteorologie	HADER, F.:	*Durchschnittliche extreme Niederschlagshöhen in Österreich. Wien 1969,* 19 S., 6 Tab., 1 Kartenbeilage	50,--
6	192	Meteorologie	STEINHAUSER, F.:	*Der Tagesgang der Bewölkung und Nebelhäufigkeit in Österreich.* Wien 1969, 22 S., 4 Tab., 16 Abb.	50,--
7	193	Geophysik	GANGL, G.:	*Die Erdbebentätigkeit in Österreich 1901-1968.* Wien 1970, 36 S., 11 Abb., 1 Kartenbeilage	vergriffen
8	195	Meteorologie	STEINHAUSER, F.:	*Die Windverhältnisse im Stadtgebiet von Wien.* Wien 1970, 17 S., 52 Tab., 47 Abb.	120,--
9	196	Geophysik	BRÜCKL, E., G. GANGL und P. STEINHAUSER:	*Die Ergebnisse der seismischen Gletschermessungen am Dachstein im Jahre 1968.* Wien 1971, 31 S., 7 Tab., 13 Abb.	vergriffen
10	198	Geophysik	BRÜCKL, E., G. GANGL:	*Die Ergebnisse der seismischen Gletschermessungen am Gefrorne Wand Kees im Jahre 1969.* Wien 1972, 13 S., 8 Abb., 3 Karten	50,--
11	201	Geophysik	BITTMANN, O., E. BRÜCKL, G. GANGL und F. J. WALLNER:	*Die Ergebnisse der seismischen Gletschermessungen am Obersten Pasterzenboden (Glocknergruppe) im Jahre 1970.* Wien 1973, 21 S., 9 Abb., 3 Karten	60,--
12	202	Meteorologie	STEINHAUSER, F.:	*Tages- und Jahresgang der Sonnenscheindauer in Österreich 1929-1968.* Wien 1973, 12 S., 98 Tab., 5 Abb.	110,--
13	203	Meteorologie		*Klimadaten des Neusiedlerseegebietes, I. Teil. Tabellen der Stundenwerte der Lufttemperatur, 1966-1970,* 105 Tab.	90,--
14	205	Geophysik	PÜHRINGER, A., W. SEIBERL, E. TRAPP und F. PAUSWEG:	*Die Verteilung der erdmagnetischen Elemente in Österreich zur Epoche 1970.0.* Wien 1975, 18 S., 3 Tab., 9 Kartenbeilagen	90,--
15	206	Meteorologie		*Klimadaten des Neusiedlerseegebietes, II. Teil. Tabellen der Stundenwerte der Relativen Feuchte, 1966-1970,* 105 Tab.	100,--
16	207	Meteorologie		*Hundert Jahre Meteorologische Weltorganisation und die Entwicklung der Meteorologie in Österreich.* Wien 1975, 50 S.	100,--

Heft	Publ.Nr.	Fachgebiet	Autor	Titel und Umfang	Preis in öS
17	208	Geophysik	TORPERCZER, M.:	*Die Geschichte der Geophysik an der Zentralanstalt für Meteorologie und Geodynamik.* Wien 1975, 24 S.	50,--
18	209	Meteorologie	CHALUPA, K.:	*Ergebnisse der Registrierung der Schwefeloxid-Immission in Wien - Hohe Warte, Okt. 1967-Dez. 1974.* Wien 1976, 62 S., 19 Tab., 24 Abb.	80,--
19	210	Geophysik	GUTDEUTSCH, R. und K. ARIC:	*Erdbeben im ostalpinen Raum.* Wien 1976, 23 S., 3 Karten	80,--
20	211	Meteorologie	TOLLNER, H., W. MAHRINGER und F. SÖBERL:	*Klima und Witterung der Stadt Salzburg.* Wien 1976, 176 S., 29 Abb.	220,--
21	214	Geophysik	SEIBERL, W.:	*Das Restfeld der erdmagnetischen Totalintensität in Österreich zur Epoche 1970.0.* Wien 1977, 8 S., 1 Kartenbeilage	vergriffen
22	216	Meteorologie	SABO, P.:	*Ein Vergleich deutscher und amerikanischer Höhenvorhersagekarten für den Alpenraum.* Wien 1977, 34 S., 11 Tab., 5 Abb.	60,--
23	217	Meteorologie	CEHAK, K.:	*Die Zahl der Tage mit Tau und Reif in Österreich.* Wien 1977, 17 S., 6 Tab., 1 Abb., 6 Karten	80,--
24	218	Meteorologie	CHALUPA, K.:	*Ergebnisse der Registrierung der Schwefeloxid- und Summenkohlenwasserstoff - Immission in Wien - Hohe Warte 1975.* Wien 1977, 40 S., 13 Tab., 12 Abb.	70,--
25	219	Geophysik	BRÜCKL, E. und O. BITTMANN:	*Die Ergebnisse der seismischen Gletschermessungen im Bereich der Goldberggruppe (Hohe Tauern) in den Jahren 1971 und 1972.* Wien 1977, 30 S., 2 Tab., 34 Abb., 2 Karten	80,--
26	222	Geophysik	FIEGWEIL, E.:	*Die Nachbebenserie der Friauler Beben vom 6. Mai und 15. September 1976.* Wien 1977, 20 S., 7 Tab., 5 Abb.	60,--
27	223	Meteorologie	MACHALEK, A.:	*Prognosenprüfung im Österreichischen Wetterdienst.* Wien 1977, 55 S., 4 Tab., 5 Abb.	80,--
28	224	Meteorologie	SKODA, G.:	*Kinematisch-Klimatologische Verlagerung von Kaltfronten und Troglinien.* Wien 1977, 32 S., 7 Tab., 10 Abb.	70,--
29	225	Geophysik	TRAPP, E. und D. ZYCH:	*Verteilung der Vertikalintensität im Raum Wien - Salzburg nach Meßergebnissen der Zentralanstalt und der ÖMV-AG.* Wien 1977, 15 S., 3 Tab., 1 Karte, 2 Kartenbeilagen	50,--
30	226	Meteorologie		*Klimadaten des Glocknergebietes, I. Teil: Tabellen und Stundenwerte der Lufttemperatur und der Relativen Luftfeuchte 1974-1976 (Wallack-Haus, Hochtor-Süd, Hochtor-Nord, Fuscher-Lacke).* 117 Tab.	150,--
31	227	Meteorologie		*Bericht über die 14. Internationale Tagung für Alpine Meteorologie vom 15.-17. Sept. 1976 in Rauris, Salzburg, 1. Teil.* Wien 1978, 323 S.	250,--
32	228	Meteorologie		*Bericht über die 14. Internationale Tagung für Alpine Meteorologie vom 15.-17. Sept. 1976 in Rauris, Salzburg, 2. Teil.* Wien 1978, 347 S.	250,--
33	229	Meteorologie	CHALUPA, K.:	*Ergebnisse der Registrierung der Schwefeloxid-, Summenkohlenwasserstoff- und Ozon-Immission in Wien - Hohe Warte, 1976.* Wien 1978, 53 S., 20 Tab., 17 Abb.	90,--

Heft	Publ.Nr.	Fachgebiet	Autor	Titel und Umfang	Preis in öS
34	231	Meteorologie		*Klimadaten des Glocknergebietes, II. Teil: Tabellen der Stundenwerte der Lufttemperatur und der Relativen Luftfeuchte 1974-1976 (Fusch, Ferleiten, Piffkaralm).* Wien 1978, 62 Tab.	80,--
35	233	Meteorologie		*Klimadaten des Glocknergebietes, III. Teil: Tabellen der Stundenwerte der Lufttemperatur und der relativen Luftfeuchte 1974-1976 (Guttal, Seppenbauer, Margaritze, Glocknerhaus, Schneetälchen, Polsterpflanzenstufe).* Wien 1978, 100 Tab.	130,--
36	234	Meteorologie	CHALUPA, K.:	*Ergebnisse der Registrierung der Immission von Stickoxiden, Summenkohlenwasserstoffen, Ozon und Schwefeldioxid in Wien - Hohe Warte, 1977.* Wien 1979, 74 S., 31 Tab., 24 Abb.	115,--
37	235	Meteorologie	MACHALEK, A.:	*Analyse von Fehlprognosen im Österreichischen Wetterdienst und Diskussion ihrer potentiellen Entstehungskriterien.* Wien 1979, 45 S., 2 Tab., 35 Abb.	100,--
38	236	Geophysik	DRIMMEL, J., E. FIEGWEIL und G. LUKESCHITZ:	*Die Auswirkung der Friauler Beben in Österreich. Makroseismische Bearbeitung der Starkbeben der Jahre 1976/77 samt historischem Rückblick.* Wien 1979, 83 S., 47 Abb., 3 Karten	150,--
39	238	Geophysik	FIEGWEIL, E.:	*Über die Vorkommen von Wiederholungsbeben in Mitteleuropa.* Wien 1979, 20 S., 9 Abb.	50,--
40	239	Meteorologie		*Klimadaten des Glocknergebietes, IV. Teil: Tabellen der Stundenwerte der Windgeschwindigkeit und der Windrichtung 1973-1976 (Fusch, Wallack-Haus, Guttal, Glocknerhaus, Margaritze, Fuscher-Lacke).* Wien 1979, 94 Tab.	120,--
41	242	Meteorologie	CHALUPA, K.:	*Ergebnisse der Registrierung der Immission von Stickoxiden, Ozon und Schwefeloxid in Wien - Hohe Warte, 1978.* Wien 1980, 58 S., 30 Tab., 15 Abb.	130,--
42	241	Meteorologie	CHALUPA, K.:	*Ergebnisse der Registrierung der Immission von Stickoxiden, Ozon und Schwefeloxid in Wien - Hohe Warte, 1979.* Wien 1980, 65 S., 32 Tab., 20 Abb.	130,--
43	246	Meteorologie	RAGETTE, G.:	*Methoden zur Berechnung großräumigen Niederschlages.* Wien 1980, 47 S., 1 Tab., 2 Abb.	70,--
44	247	Meteorologie		*Klimadaten des Glocknergebietes, V. Teil: Tabellen der Stundenwerte der Lufttemperatur und der Relativen Luftfeuchte, 1977-1979 (Wallack-Haus, Hochtor-Süd, Hochtor-Nord, Fuscher-Lacke).* Wien 1980, 135 Tab.	vergriffen
45	248	Geophysik	BRÜCKL, E., G. GANGL, W. SEIBERL und Chr. GNAM:	*Seismische Eisdickenmessungen auf dem Ober- und Untersulzbachkees in den Sommern der Jahre 1973 und 1974.* Wien 1980, 23 S., 2 Tab.	50,--
46	249	Meteorologie		*Klimadaten des Glocknergebietes, IV. Teil: Tabellen der Stundenwerte der Lufttemperatur und der Relativen Luftfeuchte, 1977-1979 (Fusch, Piffkaralm, Guttal, Seppenbauer, Margaritze, Glocknerhaus, Schneetälchen, Obere Grasheide, Polsterpflanzenstufe).* Wien 1981, 110 Tab.	120,--

Heft	Publ.Nr.	Fachgebiet	Autor	Titel und Umfang	Preis in öS
47	251	Meteorologie	CHALUPA, K.:	*Ergebnisse der Registrierung der Schwefeloxid-Immission in Wien - Stephansplatz, 1975-1979.* Wien 1981, 50 S., 13 Tab., 21 Abb.	vergriffen
48	252	Meteorologie	LAUSCHER, F.:	*Säkulare Schwankungen der Dezennienmittel und extreme Jahreswerte der Temperatur in allen Erdteilen.* Wien 1981, 42 S., 8 Tab.	50,--
49	254	Meteorologie	CHALUPA, K.:	*Ergebnisse der Registrierung der Schwefeloxid-Immission in Wien - Hohe Warte und in Wien - Stephansplatz, 1980.* Wien 1981, 46 S., 24 Tab., 13 Abb.	100,--
50	255	Geophysik	MELICHAR, P.:	*Ergebnisse der vergleichenden geomagnetischen Absolutmessungen an den Observatorien Tihany - Ungarn und Wien - Kobenzl.* Wien 1981, 35 S.	50,--
51	256	Geophysik	BRÜCKL, E. und K. ARIC:	*Die Ergebnisse der seismischen Gletschermessungen am Hornkees in den Zillertaler Alpen im Jahre 1975.* Wien 1981, 20 S., 5 Tab., 5 Abb., 1 Karte	vergriffen
52	257	Meteorologie		*Klimadaten des Glocknergebietes, VII. Teil: Tabellen der Stundenwerte der Windgeschwindigkeit und der Windrichtung 1977-1979 (Fusch, Fuscher Lacke, Wallack-Haus, Guttal).* Wien 1982, 82 Tab.	120,--
53	260	Meteorologie	STEINHAUSER, F.:	*Verteilung der Häufigkeiten der Windrichtungen und der Windstärken in Österreich zu verschiedenen Tages- und Jahreszeiten.* Wien 1982, 140 S., 131 Tab., 4 Kartenbeilagen	120,--
54	261	Meteorologie	DOBESCH, H. und F. NEUWIRTH:	*Wind in Niederösterreich, insbesondere im Wiener Becken und im Donautal.* Wien 1982, 212 S., 183 Abb.	vergriffen
55	266	Meteorologie		*Klimadaten des Glocknergebietes, VIII. Teil: Tabellen der Stundenwerte der Globalstrahlung 1975-1980 (Fuscher-Lacke und Wallack-Haus).* Wien 1983, 39 S.	50,--
56	268	Geophysik	WEBER, F. und R. WÜSTRICH:	*Ergebnisse der refraktionsseismischen Messungen am Hochkönigsgletscher.* Wien 1983, 50 S., 3 Tab., 7 Abb., 11 Beilagen	100,--
57	278	Meteorologie		*Klimadaten des Glocknergebietes, IX. Teil: Tabellen der Niederschlagsmeßergebnisse 1974-1980.* 48 S., 41 Tab.	70,--
59	283	Meteorologie	KAISER, A.:	*Inversionen in der bodennahen Atmosphäre über Klagenfurt.* Wien 1984, 79 S., 13 Tab., 22 Abb.	80,--
60	284	Meteorologie	LAUSCHER, F.:	*Ozonbeobachtungen in Wien von 1853-1981. Zusammenhänge zwischen Ozon und Wetterlagen.* Wien 1984, 29 S., 13 Tab. 3 Abb.	40,--
61	289	Meteorologie		*Klimadaten von Österreich Mittelwerte 1971-1980.* Teil I (Vorarlberg) und Teil II (Tirol). 71 S.	60,--
62	299	Geophysik	DRIMMEL, J.:	*Seismische Intensitätsskala 1985 (SIS-85).* Vorschlag einer Neufassung der Intensitätsskala MSK-64. 28 S., 8 Tab., 2 Abb.	40,--
63	300	Meteorologie		*Klimadaten von Österreich Mittelwerte 1971-1980.* Teil III (Salzburg) und Teil IV (Oberösterreich). 107 S.	80,--
64	302	Meteorologie	LAUSCHER, F.:	*Klimatologische Synoptik Österreichs mittels der ostalpinen Wetterklassifikation.* Wien 1985, 65 S., 32 Tab., 5 Abb.	90,--

Heft	Publ.Nr.	Fachgebiet	Autor	Titel und Umfang	Preis in öS
65	303	Geophysik	ZYCH, D.:	*Messungen der erdmagnetischen Vertikalintensität und Suszeptibilitätsuntersuchungen durch die ÖMV-AG als Beitrag zur Kohlenwasserstoffexploration in Österreich.* Wien 1985, 14 S., 2 Tab., 2 Abb., 3 Kartenbeilagen	60,--
66	304	Meteorologie	HOJESKY, H.:	*Langjährige Radiosonden- und Höhenwindmessungen über Wien 1952-1984.* Wien 1985, 219 S., 64 Tab., 13 Abb.	120,--
67	306	Geophysik		*Results of the Austrian Investigations in the International Lithosphere Program from 1981-1985.* Wien 1986, 79 S., 4 Tab., 28 Abb.	80,--
68	308	Hydrometeorologie	ECKEL, O. und H. DOBESCH:	*Mittelwerte der Wassertemperatur von Traunsee und Millstätter See nach mehrjährigen Registrierungen in verschiedenen Tiefen.* Wien 1986, 87 S., 74 Tab.	70,--
69	309	Meteorologie	KOLB, H., G. MAHRINGER, P. SEIBERT, W. SOBITSCHKA, P. STEINHAUSER und V. ZWATZ-MEISE:	*Diskussion meteorologischer Aspekte der radioaktiven Belastung in Österreich durch den Reaktorunfall in Tschernobyl.* Wien 1986, 63 S., 4 Tab., 20 Abb.	vergriffen
70	312	Geophysik	ARIC, K., E. BRÜCKL:	*Ergebnisse der seismischen Eisdickenmessungen im Gebiet der Stubaier Alpen (Daunkogelferner), der Venedigergruppe (Schlatenkees und Untersulzbachkees) und der Silvrettagruppe (Vermunt-Gletscher).* Wien 1987, 18 S., 4 Tab., 10 Abb., 4 Kartenbeilagen	80,--
71	314	Meteorologie	CHALUPA, K.:	*Ergebnisse der Registrierung der Schwefeloxid-Immission in Wien - Hohe Warte und in Wien - Stephansplatz, 1981.* Wien 1987, 67 S., 41 Tab., 11 Abb.	100,--
72	315	Meteorologie	CHALUPA, K.:	*Ergebnisse der Registrierung der Schwefeloxid-Immission in Wien - Hohe Warte und in Wien - Stephansplatz, 1982-1985.* Wien 1987, 76 S., 27 Tab., 15 Abb.	100,--
73	317	Geophysik	ARIC, K. et al:	*Structure of the Lithosphere in the Eastern Alps Derived from P-residual Analysis.* Wien 1988, 35 S., 3 Tab., 17 Abb.	60,--
74	322	Meteorologie	CHALUPA, K.:	*Ergebnisse der Registrierung der Schwefeloxid-Immission in Wien - Hohe Warte und in Wien - Stephansplatz 1986-1987 sowie eine Übersicht der 20jährigen Reihe 1968-1987.* Wien 1988, 80 S., 38 Tab., 20 Abb.	100,--

Berichte über den Tiefbau der Ostalpen

Herausgegeben von H. W. FLÜGEL und P. STEINHAUSER

bisher erschienen:

Heft	Publ.Nr.	Fachgebiet	Autor	Titel und Umfang	Preis in öS
1				*Jahresbericht 1973.* Verhandlungen der Geologischen Bundesanstalt. Jahrgang 1974, H. 4, S. A138-A148	
2				*Jahresbericht 1974.* Zentralanstalt für Meteorologie und Geodynamik, Wien 1975, 21 S., 5 Abb.	vergriffen
3				*Jahresbericht 1975.* Zentralanstalt für Meteorologie und Geodynamik, Wien 1976, 74 S., 14 Abb.	115,--
4	215		WALACH, G.:	*Geophysikalische Arbeiten im Gebiet des Nordsporns der Zentralalpen I: Magnetische Traverse 1 (Neunkirchen-Hochwechsel-Pöllauer Bucht).* Zentralanstalt für Meteorologie und Geodynamik, 22 S., 5 Abb., 4 Beilagen	40,--
5	221			*Jahresbericht 1976.* Zentralanstalt für Meteorologie und Geodynamik, Wien 1977, 101 S., 21 Abb.	130,--
6	230			*Jahresbericht 1977, Teil 1.* Zentralanstalt für Meteorologie und Geodynamik, Wien 1978, 54 S., 9 Abb.	85,--
7	240			*Jahresbericht 1977, Teil 2.* Zentralanstalt für Meteorologie und Geodynamik, Wien 1979, 60 S., 19 Abb.	90,--
8	244			*Tagungsbericht über das 1. Alpengravimetrie Kolloquium - Wien 1977.* Herausgeber: P. STEINHAUSER, Zentralanstalt für Meteorologie und Geodynamik, Wien 1980, 129 S., 35 Abb.	90,--
9	245		GÖTZE, H. J., O. ROSENBACH und P. STEINHAUSER:	*Die Bestimmung der mittleren Geländehöhen im Hochgebirge für die topographische Reduktion von Schweremessungen.* Zentralanstalt für Meteorologie und Geodynamik, Wien 1980, 16 S., 2 Tab., 5 Abb.	25,--
10	264		ROSENBACH, O., P. STEINHAUSER, W. EHRISMANN, H. J. GÖTZE, O. LETTAU, D. RUESS und W. SCHÖLER:	*Tabellen der mittleren Geländehöhen der Ostalpen und ihrer Umgebung für Rasterelemente $\Delta\varphi = 0.75'$. $\Delta\lambda = 1.25'$.* 1. Lieferung. Zentralanstalt für Meteorologie und Geodyna-mik, Wien 1982, 23 S., 20 Tab.	100,--
11	273			*Tagungsbericht über das 2. Internationale Alpengravimetrie Kolloquium - Wien 1980.* Herausgeber: B. MEURERS und P. STEINHAUSER, Zentralanstalt für Meteorologie und Geodynamik, Wien 1983, 168 S., 85 Abb.	200,--
12	288			*Tagungsbericht über das 3. Internationale Alpengravimetrie Kolloquium - Leoben 1983.* Herausgeber: B. MEURERS, P. STEINHAUSER und G. WALACH, Zentralanstalt für Meteorologie und Geodynamik, Wien 1985, 222 S.	270,--
13	323			*Tagungsbericht über das 4. Internationale Alpengravimetrie Kolloquium - Wien 1986.* Herausgeber: B. MEURERS und P. STEINHAUSER, Zentralanstalt für Meteorologie und Geodynamik, Wien 1988, 200 S., 77 Abb.	250,

Österreichische Beiträge zu Meteorologie und Geophysik

bisher erschienen:

Heft	Publ.Nr.	Fachgebiet	Autor	Titel und Umfang	Preis in öS
1	329	Meteorologie		*Tagungsbericht EURASAP, Wien, 14.-16. Nov. 1988, Evaluation of Atmospheric Dispersion Models Applied to the Release from Chernobyl.* Wien 1989, 20 Beiträge, 198 S., 100 Abb., 17 Tab.	200,--
2	332	Geophysik		*Tagungsbericht über das 5. Internationale Alpengravimetrie Kolloquium - Graz 1989.* Herausgeber: H. LICHTENEGGER, P. STEINHAUSER und H. SÜNKEL, Wien 1989, 256 S., 100 Abb., 17 Tab.	vergriffen
3	336	Geophysik		*Schwerpunktprojekt S47-GEO: Präalpidische Kruste in Österreich, Erster Bericht.* Herausgeber: V. HÖCK und P. STEINHAUSER, Wien 1990, 15 Beiträge, 257 S., 104 Abb., 17 Tab., 23 Fotos	280,--
4	338	Meteorologie	LANZINGER, A. et al:	*Alpex-Atlas.* FWF-Projekt P6302 GEO, Wien 1991, 234 S., 23 Abb., 2 Tab., 200 Karten	250,--
5	341	Meteorologie	BÖHM, R.:	*Lufttemperaturschwankungen in Österreich seit 1775.* Wien 1992, 95 S., 34 Abb., 24 Tab.	vergriffen
6	343	Geophysik	MEURERS, B.:	*Untersuchungen zur Bestimmung und Analyse des Schwerefeldes im Hochgebirge am Beispiel der Ostalpen.* Wien 1992, 146 S., 72 Abb., 9 Tab.	160,--
7	351	Meteorologie	AUER, I.:	*Niederschlagsschwankungen in Österreich seit Beginn der instrumentellen Beobachtungen durch die Zentralanstalt für Meteorologie und Geodynamik.* Wien 1993, 73 S., 18 Abb., 5 Tab., 6 Farbkarten	330,--
8	353	Meteorologie	STOHL, A., H. KROMP-KOLB:	*Analyse der Ozonsituation im Großraum Wien.* Wien 1994, 135 S., 73 Abb., 8 Tab.	330,--
9	356	Geophysik		*Tagungsbericht über das 6. Internationale Alpengravimetrie-Kolloquium, Leoben 1993.* Herausgeber: P. STEINHAUSER und G. WALACH, Wien 1993, 251 S., 146 Abb. [Korrektur der irrtümlichen Numerierung Heft 8/Publ. 353]	330,--
10	357	Meteorologie	ZWATZ-MEISE, V.:	*Contributions to Satellite and Radar Meteorology in Central Europe.* Wien 1994, 169 S., 25 Farbabb., 42 SW-Abb., 13 Tab.	330,--
11	359	Geophysik	LENHARDT W. A.:	*Induzierte Seismizität unter besonderer Berücksichtigung des tiefen Bergbaus.* Wien 1995, 91 S., 53 Abb.	330,--
12	361	Meteorologie	AUER, I., R. BÖHM, N. HAMMER †, W. SCHÖNER, WIESINGER W., WINIWARTER W.:	*Glaziologische Untersuchungen im Sonnblickgebiet: Forschungsprogramm Wurtenkees.* Wien 1995, 143 S., 59 SW-Abb., 13 Farbabb., 9 SW-Fotos, 47 Tab.	330,--
13	372	Umwelt	PIRINGER, M.:	*Results of the Sodar Intercomparison Experiment at Dürnrohr, Austria.* Wien 1996, 73 S., 19 Abb., 13 Tab.	330,--
14	373	Geophysik	MEURERS, B.:	*Proceedings of the 7th International Meeting on Alpine Gravimetry, Vienna 1996.* Wien 1996, 253 S., 128 Abb., 35 Tab.	330,--